Development of Palladium-Mediated Transannular C–H Functionalization Methods for Alicyclic Amines

by

Ellen Y. Aguilera

A dissertation submitted in partial fulfillment
of the requirements for the degree of
Doctor of Philosophy
(Chemistry)
in the University of Michigan
2021

Doctoral Committee:

Professor Melanie S. Sanford, Chair
Professor John Montgomery
Professor Peter J. H. Scott
Professor Nathaniel K. Szymczak

Ellen Y. Aguilera

eyaguil@umich.edu

ORCID iD: 0000-0002-2078-4311

Dedication

Para mi familia

Acknowledgements

First and foremost, I would like to thank my Ph.D. advisor, Professor Melanie Sanford. Thank you for the opportunity of a lifetime to work in your lab. I appreciate you always making time to meet with me constantly even in the middle of a pandemic! I admire your excitement about chemistry, and more so I admire your patience in explaining and teaching us about chemistry, which has made me feel so comfortable asking questions and learning during our discussions. Your ability to simplify challenging and complex problems is a trait that I aspire to achieve. Lastly, thank you for always believing in me when I doubted my capabilities in chemistry – You made me believe that I could, and so I did.

I would like to thank Professor Nathaniel Szymczak, Professor John Montgomery, and Professor Peter Scott for serving on my committee. Your comments and questions during my candidacy exam, data meeting, and thesis defense are greatly appreciated. Nate, thank you for allowing me to rotate in your lab and for your continuous support.

Next, I have to thank all my lab mates during my entire graduate career in the Sanford lab that made coming to lab each day a joy. I have enjoyed our many laughs, chemistry complaints and discussions, and most of all our endless Starbucks coffee breaks. In particular, I would like to thank my mentor, Dr. Pablo Cabrera, who guided me in my first year allowing me to establish my thesis project and challenging me to become a better graduate student. Also thank you to Dr. Melissa Lee and Dr. Devin Ferguson for providing chemistry suggestions and career advice even after you graduated. In addition, I would like to thank Dr. Elizabeth Meucci for our great memories in lab as well as for our fun time developing a class together! To María Morales and Geraldo

Camacho, thank you for your constant support and keeping me laughing in my latter years. Lastly, thanks to Pronay Roy for keeping lab fun during our five years in the Sanford lab!

Throughout my time in the Sanford lab, we've had so many post-docs and I thank all of them for providing feedback on my projects and guiding me through my job process. In particular, I thank Professor Courtney Roberts for being my forever mentor in chemistry, my career, and life. I can't forget Dr. Tolani Salvador who always made time to talk about chemistry and ensured I was having a great day.

I have also had the opportunity to collaborate with fantastic people in our lab. Thank you to Dr. Scott Thullen for bringing your great ideas to the project, and for your endless support, help, and advice during the job process. And thank you to Dr. Abebu Kassie for being such an easy person to collaborate with and being so supportive as I write my thesis.

Thank you to Dr. Michelle Ferrez for giving me the great chance to be a graduate student intern for University of Michigan's Undergraduate Research Program to learn more about the LSAMP. Thank you for always involving me in opportunities to share my journey in science as a women and minority with undergraduates. These events are what keep me going in STEM!

Also, a big thank you to my undergraduate advisor, Professor Jessica Hoover who guided me as a young scientist like deciding where to go for graduate school, and still after graduating making time to listen to me about my career choices. I appreciate your continuous advice and support!

Andrew, thank you for endlessly supporting me and my dreams, and being willing to follow them with me even when they make you move far away from home. You have brought so much light to my life and gave me the strength I needed to get through graduate school. To your family, thank you for your love and support when my family is so far away.

To Sammy and Renee, my American grandparents, thank you for seeing something so special in me and supporting me when I needed it the most, and never expecting anything in return. You gave me the opportunity of a lifetime to attend college, and I am so grateful. You are both dearly loved.

Last, but certainly not least, gracias a mi familia. Papá y Mamá, I will always carry the sacrifices you have made for me – You left all you knew in Bolivia for the opportunity to provide a better life for my sister and I. And I know those opportunities did not just come, but you fought for them. Thank you for working day and night to provide us with this wonderful life. I admire your resilience in life, and I thank you for teaching me that. You inspire me to be fearless in chasing my dreams whatever they may be, and to never let anything get in the way of reaching them. To my sister, Gisselle, thank you for being my role model. You have showed me that you have never taken the sacrifice our parents made lightly, and that has always inspired me to be better. I hope to be half the woman you are, so strong and driven from a young age.

And for all this support surrounding me throughout this journey, I thank you, God. You are the guiding light in my life, and when I did not know where to turn, I always turned to You, and You have guided me here, today.

Table of Contents

<h1 style="text-align:center">List of Tables</h1>

Abstract

Alicyclic amines are a prevalent motif present in a range of pharmaceutically relevant molecules. Conventional approaches for the synthesis of alicyclic amines require multi-step processes to build the alicyclic amine core. As such, accessing substituted derivatives requires laborious multi-step synthetic sequences. This thesis describes the research efforts centered on a complementary approach that utilizes late-stage $C(sp^3)$–H functionalization at remote sites of alicyclic amines. This enables rapid access to a wide variety of substituted alicyclic amines in a single step from the pre-assembled core structure.

Chapter 1 provides a detailed overview on the area of Pd-catalyzed $C(sp^3)$–H functionalization of alicyclic amines. This chapter covers the major challenges in accessing remote C–H bonds of alicyclic amines as well as the various approaches others have developed to achieve remote $C(sp^3)$–H functionalization of these motifs.

Chapter 2 focuses on probing the mechanism of our previously reported Pd-catalyzed transannular $C(sp^3)$–H arylation of alicyclic amines. The design, synthesis, characterization of Pd^{II} complexes that serve as models for catalytic intermediates in the reported methods is described in detail. With the synthesized Pd^{II} complexes, the transannular C–H activation step is investigated via H/D exchange studies. The mechanistic insights gained from these H/D exchange studies are reviewed.

Chapter 3 explores the reactivity of our synthesized Pd^{II} complex towards oxidation. Our efforts to achieve a variety of transannular functionalizations with a diverse set of oxidants is described. Also detailed is the development of a practical 2-step 1-pot approach for the *in situ*

assembly of the Pd^{II} complex followed by transannular functionalization. The translation of this stochiometric method to catalysis is also reported.

Chapter 4 covers our efforts to target multiple remote C–H sites of alicyclic amines core via our established Pd-catalyzed transannular C–H activation. The development of these catalytic transformations is described in detail. An in-depth investigation of this transformation is also conducted through the synthesis, isolation and study of reactive Pd intermediates.

Chapter 5 presents a new direction moving from Pd- to Ni-catalyzed methods. This chapter aims to understand the ligand effects present in recent methodologies that merge photoredox and Ni catalysis to achieve C–C cross-couplings. Several aminoquinoline derivatives are synthesized, characterized, and tested as viable ligands in the reported transformations. The synthesis, isolation, and characterization of reactive Ni^{II} aminoquinoline intermediates are also discussed. Preliminary results and future directions are presented in this chapter.

Chapter 1   Introduction

1.1 Importance of Late-Stage C−H Functionalization for Drug Discovery

The path to discovering a lead pharmaceutical drug candidate is a labor- and time- intensive process.[1] Identification of a lead compound typically involves synthesizing and characterizing a library of drug candidates. These candidates are then used for validation, optimization, screening

Figure 1.1 Number of Compounds Synthesized and Screened in Drug Development Process
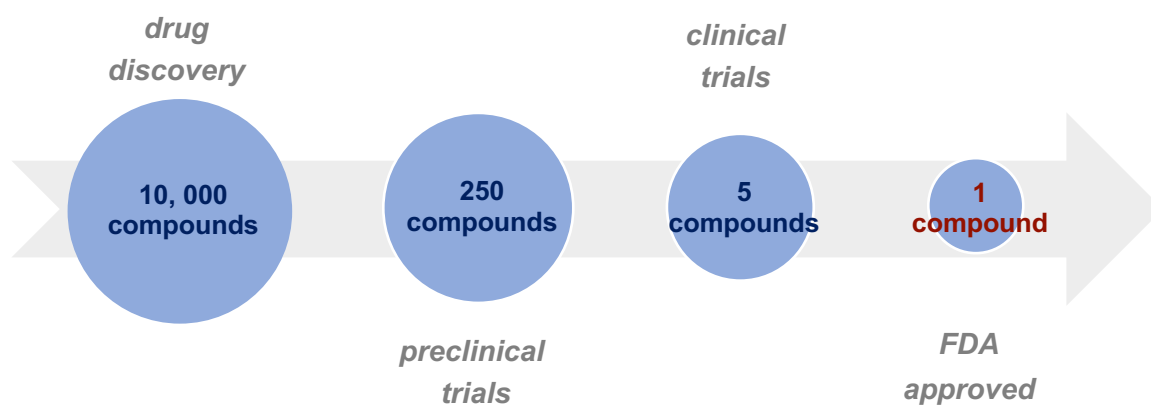
and assays for therapeutic efficacy (Figure 1.1). Automation for screening the candidates has largely accelerated the testing process; however, the timeline for the identification of a lead molecule can be prolonged by the lengthy syntheses required to make thousands of compounds and derivatives.[1,2] Further, accessing substituted derivatives of complex molecules can require multi-step processes to generate the core of the molecule.[3] As such, it is of high interest to develop synthetic methods that enable the rapid late-stage derivatization of pharmaceutically relevant motifs. A field dedicated to streamlining synthetic strategies is C−H bond functionalization.[4]

1.2 Pd-Catalyzed C(sp²)–H and C(sp³)–H Functionalization

C–H bond functionalization entails the development of reactions and transition metal catalyst systems that selectively transform a C–H bond of a complex molecule to a desired C–O, C–X (X = halide), C–N, C–S or C–C bond.[5] In the simplest terms, the C–H bond functionalization pathway involves a transition metal (*i.e.,* Ru, Rh, Ir, Pd) that can promote (*i*) C–H activation followed by (*ii*) functionalization of the resulting reactive intermediate.[6] The following discussion will focus on the use of divalent Pd as the metal catalyst for C–H functionalization, as it pertains to the work described in Chapters 2-4 of this thesis. In Pd systems, the C–H activation step entails the C–H bond reacting with Pd to form a reactive Pd–C bond. At Pd[II] centers this step is proposed to occur via a concerted-metalation deprotonation (CMD) pathway.[7,8] Scheme 1.1 demonstrates the CMD pathway from a Pd–carboxylate source proceeding through the 6-membered transition state, **1-A**, affording a concerted metalation and intramolecular deprotonation to generate a carboxylic acid (RCO_2H) and the reactive Pd–C bond. In the presence of an oxidant and/or nucleophile, this reactive Pd–C bond can undergo functionalization to produce the C–FG (FG = functional group) bond.

The key challenges associated with C–H bond functionalization reactions at Pd[II] relate to

Scheme 1.1 C–H Activation via CMD Pathway
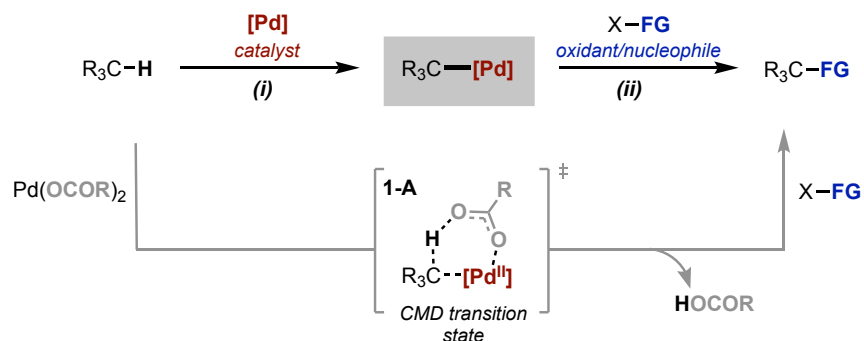
(a) the reactivity of the C–H bonds and (b) site selectivity.[6] Firstly, to compare the reactivity of

$C(sp^2)$–H and $C(sp^3)$–H bonds at Pd^{II} centers, we can explore their acidities, since the CMD

pathway fundamentally involves a deprotonation event. Generally, the pK_a of $C(sp^2)$–H bonds are

significantly more acidic (pK_a of benzene ~ 43) than unactivated $C(sp^3)$–H bonds ($pK_a > 50$).[9] The

more acidic $C(sp^2)$–H bond is thermodynamically preferred for C–H activation compared to less

acidic $C(sp^3)$–H bond. As such, less acidic substrates are typically more challenging to activate at

Pd^{II} centers via CMD pathways. Another challenge for C–H bond functionalization reactions is

site selectivity. As expected, for a simple substrate with one reactive C–H bond, site selectivity is

not a concern. However, the introduction of a highly decorated molecule with various $C(sp^2)$–H

and $C(sp^3)$–H bonds open the doors to unselective and promiscuous C–H functionalizations.

Scheme 1.2 Directed Pd-Catalyzed C–H Activation
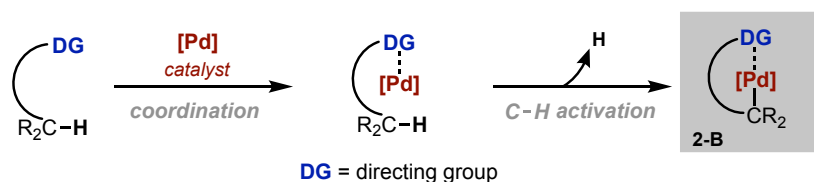
DG = directing group

A strategy that has been used to address challenges associated with both reactivity and site

selectivity challenges in C–H functionalization reactions since the mid-1990's is the utilization of

directing groups.[10] The directing group approach involves tethering a ligand (*i.e.,* directing group,

DG) to the C–H bond containing substrate. This ligand can then coordinate to Pd, bringing the

C–H bond of interest in close proximity to the catalyst center, thus promoting a selective C–H

activation and formation of palladacycle **2-B** (Scheme 1.2).[6,11] Common directing groups for Pd

typically consist of Lewis basic nitrogen and oxygen coordinating moieties. Specific examples of

directing groups include amides, imines, nitriles, ketones, carboxylic acids, and heterocycles.[12]

While these directing groups all are monodentate, there are also numerous examples of bidentate directing groups such as bipyridines and aminoquinolines.[11,13]

The utilization of directing groups for the development of Pd-catalyzed $C(sp^2)$–H functionalization reactions is well-established. Yu and coworkers from the Scripps Research Institute highlight the utility of directing groups by enabling carboxylic acids and amides as directing groups to lead Pd to the desired *ortho*-position, despite the possibility for electrophilic aromatic substitution reactivity and presence of similar $C(sp^2)$–H bonds (Scheme 1.3).[14] Hence, by harnessing the power of directing groups, selective *ortho*-$C(sp^2)$–H functionalizations of benzene derivatives can be achieved with various oxidants.

Scheme 1.3 Diverse $C(sp^2)$–H Functionalizations Enabled by Directed Pd-catalysis
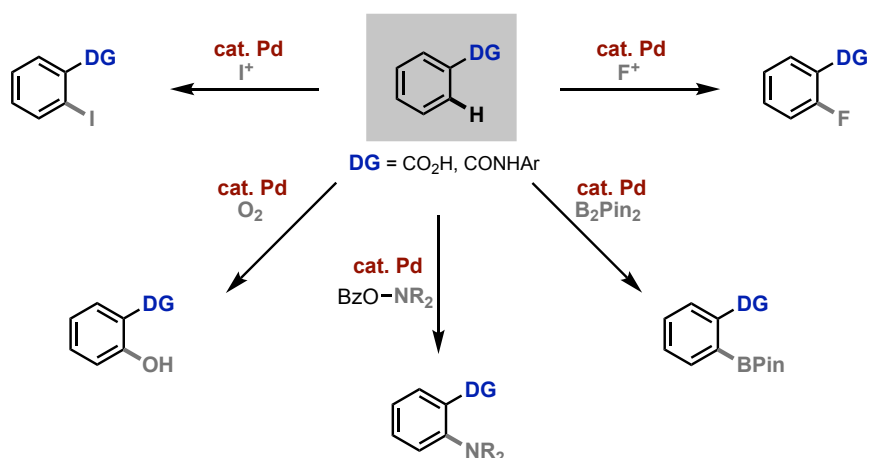
1.3 Directed Pd-Catalyzed $C(sp^3)$–H Functionalization of Alicyclic Amines

The aforementioned reports of directed Pd-catalyzed $C(sp^2)$–H functionalization have set the groundwork for moving to more challenging $C(sp^3)$–H substrates. One pharmaceutically relevant motif bearing $C(sp^3)$–H bonds is piperidine, a six-membered saturated nitrogen-containing heterocycle. Piperidine belongs to a class of alicyclic amine molecules that are among the most frequently encountered structures in pharmaceutical agents, with representative examples

shown in Figure 1.2.[15] A closer analysis of piperidine-containing pharmaceuticals shows that substitution is most common at the α-C(2) and γ-C(4) positions.[16] Due to the highly acidic nature of the C_α–H bond ($pK_a \sim 16$ when nitrogen is oxidized to a radical cation)[17] because of its' proximity to nitrogen, there is an exhaustive list of reports that selectively achieve C_α–H bond functionalization of alicyclic amines such as piperidine.[18] In contrast, the bonds further from nitrogen (*i.e.,* C_β–H and C_γ–H) are less acidic and thus, comparatively inert. As such, late-stage methods to selectively functionalize the remote C–H bonds of alicyclic amines remain limited.

Figure 1.2 Alicyclic Amine Core Motif Present in Pharmaceuticals
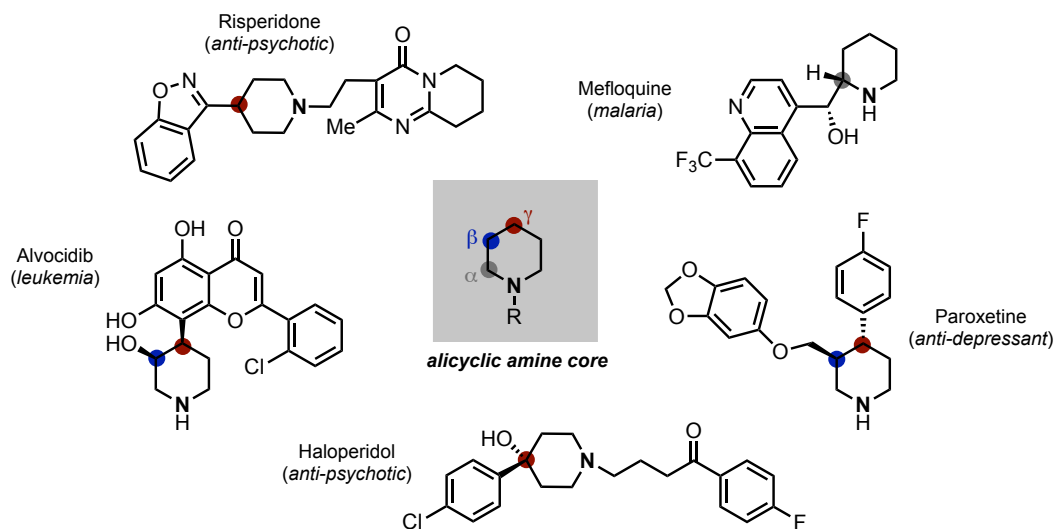
1.4 Challenges in Remote C(sp³)–H Functionalization of Alicyclic Amines

As alluded to previously, developing methods for remote C–H bond functionalization of alicyclic amines is highly challenging. In the presence of transition metals and/or oxidants (conditions required to promote C–H activation), alicyclic amines can readily undergo many other reactions as shown in Scheme 1.4. First, the highly acidic nature of the C_α–H bond, as mentioned earlier, can lead to α-oxidation (Scheme 1.4a).[19] Although this reactivity is useful when selectively targeting the α-site, it is problematic when targeting the inert remote C–H sites in terms of relative

Scheme 1.4 Side Reactions Preventing Remote C–H Functionalization
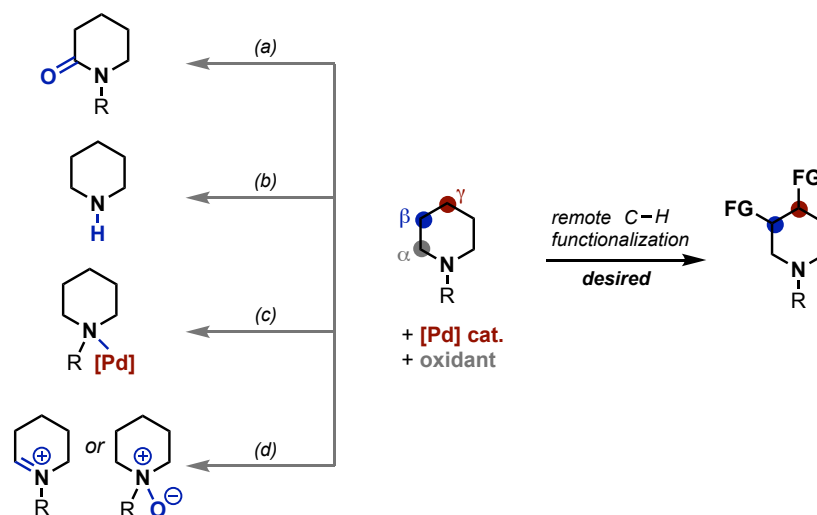
rates. In other words, the rate of C_α–H functionalization can outcompete the rate of C_β–H/C_γ–H functionalization. Additionally, the nitrogen of the amine can promote a number of other deleterious side reactions, including dealkylation (Scheme 1.4b), binding of Pd (Scheme 1.4c), and *N*-oxidation (Scheme 1.4d).[19] It is evident that in order to achieve *selective* remote functionalization of alicyclic amines, the rate of remote C_β–H/C_γ–H functionalization has to outcompete undesired C_α–H oxidation/*N*-oxidation.

1.5 Directing Groups for Selective Remote Pd-Catalyzed C–H Functionalization of Alicyclic Amines

The concept of directing groups as employed in Pd-catalyzed $C(sp^2)$–H functionalization reactions has been revisited for selective functionalization of remote $C(sp^3)$–H bonds of alicyclic amines. Other strategies to achieve this include the blocking the C_α–H sites[20] as well as protonation of the amine nitrogen[21] to deactivate proximal C–H sites. As it relates to this thesis, we will focus on the utilization of directing group strategies to achieve C_β–H/C_γ–H functionalization. The

directing group approach is essential in this case as it can guide Pd to the remote C–H sites to yield

selective remote C–H functionalization over C_α–H oxidation/*N*-oxidation.

Scheme 1.5 Examples of Directed Pd-Catalyzed Remote C–H Functionalization

(a) Free Amine as Directing Group

(b) Amide Directing Group

(c) Bidentate Directing Group: Amine and Amide (*Our Group*)
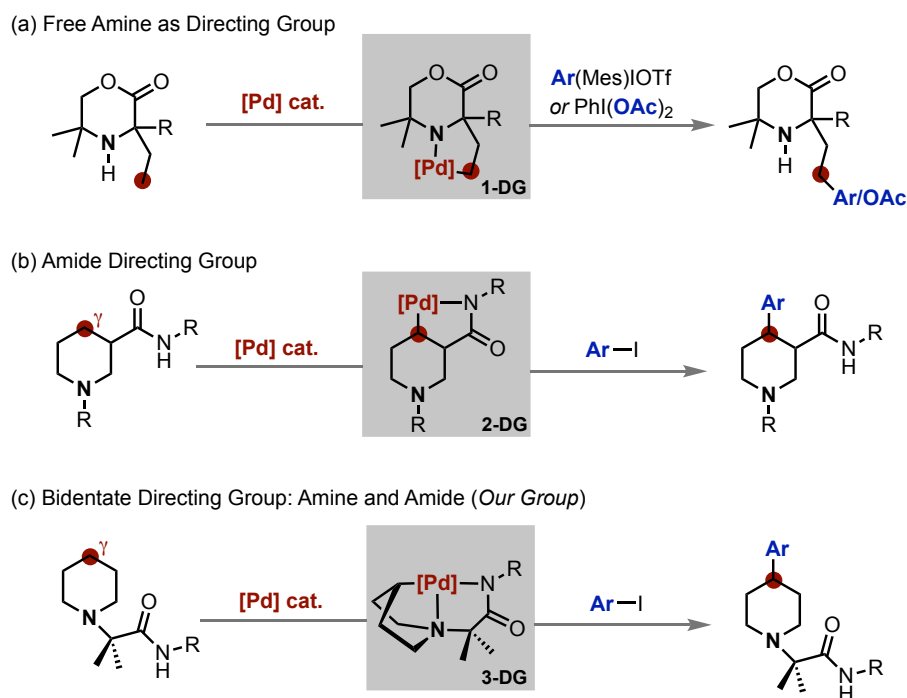
In 2015, Gaunt and coworkers from University of Cambridge demonstrated the ability of

the amine ring nitrogen to act as a directing group to activate the remote $C(sp^3)$–H bonds. These

reactions proceed via palladacycle **1-DG**, and form selectively arylated and acetoxylated products

(Scheme 1.5a).[22] Although this method does not functionalize the amine ring directly, it highlights

how the native amine nitrogen can be harnessed as a directing group for remote functionalization.

Following this report, Yu and Bull showed that installing an amide directing group directly on the

alicyclic amine core could enable Cγ–H arylation via a 5-membered palladacycle **2-DG** (Scheme

1.5b).[23a,b] Expanding on this method, others have shown that by moving the directing group to

different positions of the alicyclic amine core, the Cβ–H bond can also be targeted.[23c] Inspired by

the incorporation of both these directing groups, our lab assembled a bidentate directing group by

tethering an amide to the amine nitrogen.[24] This bidentate directing group enabled Pd-catalyzed remote C_γ–H arylation via a transannular C–H activation, which similar to the other examples, forms a 5-membered palladacycle **3-DG** (Scheme 1.5c) that then undergoes functionalization. This method is attractive in that it allows for the further functionalization of the alicyclic amines, as all sites are open due to the directing group on the nitrogen amine.

Chapters 2, 3, and 4 are centered on understanding and expanding upon our group's previously reported Pd-catalyzed transannular C–H arylation methodology (Scheme 1.6a). Specifically, Chapter 2 describes the design and development of Pd^{II}–amine complexes to investigate the proposed transannular C–H activation intermediate **3-DG** via hydrogen/deuterium exchange (Scheme 1.6b). Chapter 3 leverages these Pd^{II}–amine complexes to achieve diverse transannular C(sp^3)–H functionalizations (Scheme 1.6c). Finally, Chapter 4 exploits the transannular C–H activation palladacycle **3-DG** to develop a Pd-catalyzed C_β–H/C_γ–H multi-functionalization of bicyclic amines (Scheme 1.6d).

Scheme 1.6 Summary of Thesis Chapters 2, 3, and 4
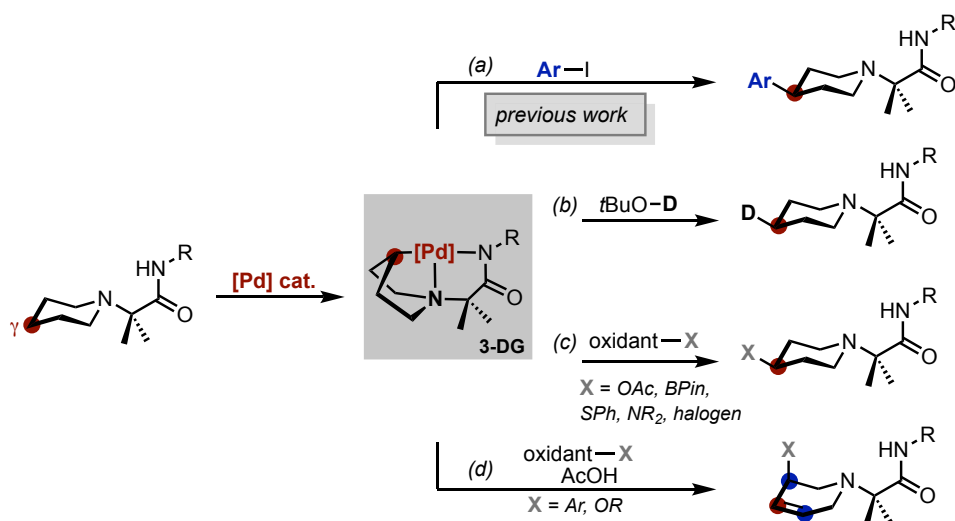
1.6 Recent Advances in Ni-Catalyzed Cross-Couplings

This section entails the topic to be discussed in Chapter 5 of this thesis, which takes a leap on the periodic table from Pd, the central theme of the previous Chapters 2-4, to Ni. Throughout the years, Ni has shown the ability to serve as a valuable transition metal catalyst for numerous transformations.[25] Moreover, as the cost of Pd increases, Ni remains inexpensive and shows high sustainability making it an attractive catalyst.[26,27] However, the differences between Pd and Ni does not only lie in their monetary values, but more importantly on their reactivity differences. In general, Pd catalysis is limited to two-electron redox events, where the oxidation state of Pd ranges from +0, +II, and +IV. However, Ni has the ability to undergo one- or two-electron redox events creating numerous possible intermediates in the +0, +I, +II, +III, and +IV oxidation states. This redox flexibility provides Ni the ability to uniquely engage in different and often more challenging bond forming reactions than Pd.[28] Notable examples include C–C cross-couplings reactions and more recently, metallaphotoredox enabled cross-couplings.[29,30]

Figure 1.3 Ni Catalysis Mechanistic Manifolds
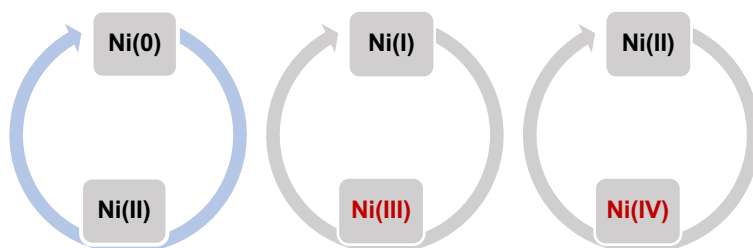
With an increase in Ni-mediated reactions, there is a range of mechanistic manifolds that are proposed due the unique one- and two- electron redox events of Ni. The mechanistic manifolds most commonly proposed for Ni-catalyzed cross-couplings is the Ni^0/Ni^{II} catalytic cycle, in which Ni species in both oxidation states are well-characterized (Figure 1.3).[31] However, recently, a number of groups have developed Ni-catalyzed methods that invoke a Ni^{II}/Ni^{IV} and $Ni^{II}/Ni^{III}/Ni^{IV}$ catalytic cycle (Figure 1.3).[32,33] However, these high-valent Ni intermediates are poorly

characterized and, as such, their reactivities and roles in catalysis are less well understood. This is an underexplored area in the field of transition-metal cross-couplings and, as such, the putative high-valent Ni^{III} and Ni^{IV} intermediates as well as the role of additives (*i.e.*, ligands, oxidants) in the reactions has not been well-studied.

The importance of understanding the complicated Ni catalytic manifolds is highlighted by the strong ligand effects observed in dual Ni photoredox reactions (Scheme 1.7). Fu, MacMillan, and Molander showcase successful C–C cross-coupling enabled by the merger of Ni and photoredox catalysis through a proposed Ni^{III} intermediate.[34,35] They observe that the reaction yields are dramatically altered based on the selection of ligand for Ni. In the presence of L_2-donor ligands, trace yields are obtained while LX-donor ligands afford much higher yields. Due to the insufficient fundamental mechanistic understanding at high-valent Ni centers and how ligands can affect the Ni center, these effects are not understood and remain a question throughout the chemistry community.

Scheme 1.7 Ligand Effects in Dual Ni Photoredox Catalysis Examples
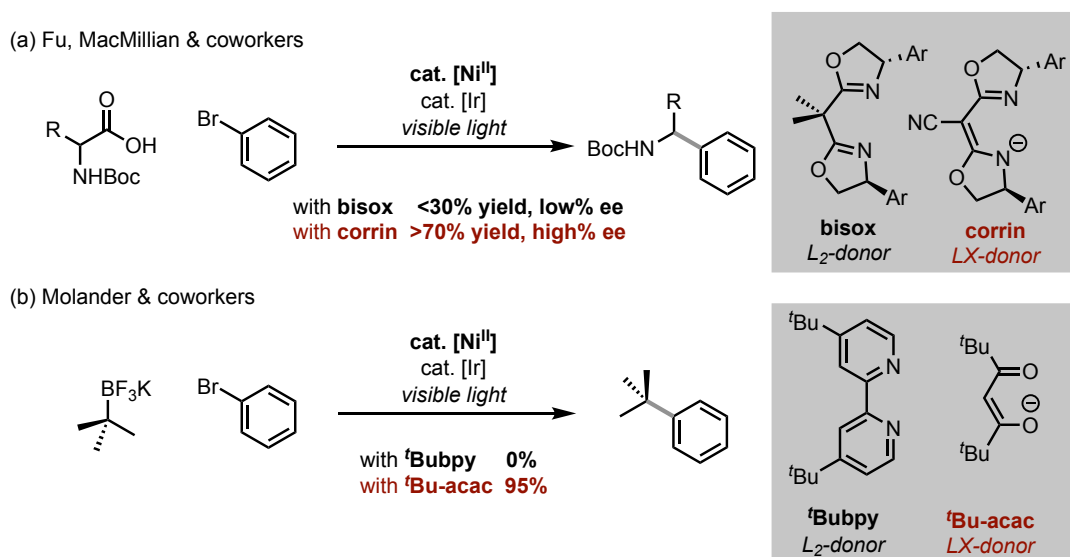
Chapter 5 will describe our approach to investigate the strong LX-type ligand effects reported in the aforementioned photoredox and Ni-catalyzed reactions. Additionally, this chapter will provide preliminary results on the path to mechanistic elucidation of the high-valent Ni intermediates.

1.7 References

(1) (a) Hughes, J.; Rees, S.; Kalindjian, S.; Philpott, K. Principles of Early Drug Discovery: Principles of Early Drug Discovery. *British Journal of Pharmacology* **2011**, *162*, 1239–1249 (b) Mohs, R. C.; Greig, N. H. Drug Discovery and Development: Role of Basic Biological Research. *Alzheimer's & Dementia: Translational Research & Clinical Interventions* **2017**, *3*, 651–657. (c) Lansdowne, L. E. Exploring the Drug Development Process. https://www.technologynetworks.com/drug-discovery/articles/exploring-the-drug-development-process-331894 (accessed Feb 4, 2021).
(2) Hertzberg, R. P.; Pope, A. J. High-Throughput Screening: New Technology for the 21st Century. *Current Opinion in Chemical Biology* **2000**, *4*, 445–451.
(3) (a) Blakemore, D. C.; Castro, L.; Churcher, I.; Rees, D. C.; Thomas, A. W.; Wilson, D. M.; Wood, A. Organic Synthesis Provides Opportunities to Transform Drug Discovery. *Nature Chem* **2018**, *10*, 383–394. (b) Moir, M.; Danon, J. J.; Reekie, T. A.; Kassiou, M. An Overview of Late-Stage Functionalization in Today's Drug Discovery. *Expert Opinion on Drug Discovery* **2019**, *14*, 1137–1149. (c) Börgel, J.; Ritter, T. Late-Stage Functionalization. *Chem* **2020**, *6*, 1877–1887.
(4) (a) Wencel-Delord, J.; Glorius, F. C–H Bond Activation Enables the Rapid Construction and Late-Stage Diversification of Functional Molecules. *Nature Chem* **2013**, *5*, 369–375. (b) Cernak, T.; Dykstra, K. D.; Tyagarajan, S.; Vachal, P.; Krska, S. W. The Medicinal Chemist's Toolbox for Late Stage Functionalization of Drug-like Molecules. *Chem. Soc. Rev.* **2016**, *45,* 546–576.
(5) Bergman, R. G. C–H Activation. *Nature* **2007**, *446*, 391–393.
(6) Lyons, T. W.; Sanford, M. S. Palladium-Catalyzed Ligand-Directed C−H Functionalization Reactions. *Chem. Rev.* **2010**, *110*, 1147–1169.
(7) (a) Gallego, D.; Baquero, E. A. Recent Advances on Mechanistic Studies on C–H Activation Catalyzed by Base Metals. *Open Chemistry* **2018**, *16*, 1001–1058. (b) Yang, Y.-F.; She, Y. Computational Exploration of Pd-Catalyzed C-H Bond Activation Reactions. *Int J Quantum Chem* **2018**, *118*, e25723.
(8) (a) Lapointe, D.; Fagnou, K. Overview of the Mechanistic Work on the Concerted Metallation–Deprotonation Pathway. *Chem. Lett.* **2010**, *39*, 1118–1126. (b) Ackermann, L. Carboxylate-Assisted Transition-Metal-Catalyzed C−H Bond Functionalizations: Mechanism and Scope. *Chem. Rev.* **2011**, *111*, 1315-1345. (c) Gorelsky, S. I.; Lapointe, D.; Fagnou, K. Analysis of the Palladium-Catalyzed (Aromatic)C–H Bond Metalation-Deprotonation Mechanism Spanning the Entire Spectrum of Arenes. *J. Org. Chem.* **2012**, *77*, 658-668. (d) Gorelsky, S. I. Origins of Regioselectivity of the Palladium-Catalyzed (Aromatic)C–H Bond Metalation-Deprotonation. *Coordination Chemistry Reviews* **2013**, *257*, 153-164.
(9) (a) Bordwell, F. G. Equilibrium Acidities in Dimethyl Sulfoxide Solution. *Acc. Chem. Res.* **1988**,*21* (12), 456–463. (b) Anslyn, E. V.; Dougherty, D. A. Luo, *Modern Physical Organic Chemistry*; University Science Books, 2006.

(10) Murai, S.; Kakiuchi, F.; Sekine, S.; Tanaka, Y.; Kamatani, A.; Sonoda, M.; Chatani, N. Efficient Catalytic Addition of Aromatic Carbon-Hydrogen Bonds to Olefins. *Nature* **1993**, *366*, 529–531.

(11) Sambiagio, C.; Schönbauer, D.; Blieck, R.; Dao-Huy, T.; Pototschnig, G.; Schaaf, P.; Wiesinger, T.; Zia, M. F.; Wencel-Delord, J.; Besset, T.; Maes, B. U. W.; Schnürch, M. A Comprehensive Overview of Directing Groups Applied in Metal-Catalysed C–H Functionalisation Chemistry. *Chem. Soc. Rev.* **2018**, *47*, 6603–6743.

(12) Zhang, M.; Zhang, Y.; Jie, X.; Zhao, H.; Li, G.; Su, W. Recent Advances in Directed C–H Functionalizations Using Monodentate Nitrogen-Based Directing Groups. *Org. Chem. Front.* **2014**, *1*, 843.

(13) Rej, S.; Ano, Y.; Chatani, N. Bidentate Directing Groups: An Efficient Tool in C–H Bond Functionalization Chemistry for the Expedient Construction of C–C Bonds. *Chem. Rev.* **2020**, *120*, 1788–1887.

(14) Engle, K. M.; Yu, J.-Q. Developing Ligands for Palladium (II)-Catalyzed C–H Functionalization: Intimate Dialogue between Ligand and Substrate. *J. Org. Chem.* **2013**, *78*, 8927–8955.

(15) Baumann, M.; Baxendale, I. R. An Overview of the Synthetic Routes to the Best Selling Drugs Containing 6-Membered Heterocycles. *Beilstein J. Org. Chem.* **2013**, *9*, 2265–2319.

(16) Vitaku, E.; Smith, D. T.; Njardarson, J. T. Analysis of the Structural Diversity, Substitution Patterns, and Frequency of Nitrogen Heterocycles among U.S. FDA Approved Pharmaceuticals: Miniperspective. *J. Med. Chem.* **2014**, *57* (24), 10257–10274.

(17) Chu, J. C. K.; Rovis, T. Complementary Strategies for Directed C(sp^3)−H Functionalization: A Comparison of Transition-Metal-Catalyzed Activation, Hydrogen Atom Transfer, and Carbene/Nitrene Transfer. *Angew. Chem. Int. Ed*. **2018**, *57*, 62-101

(18) (a) Pastine, S. J.; Gribkov, D. V.; Sames, D. sp^3 C−H Bond Arylation Directed by Amidine Protecting Groups: α-Arylation of Pyrrolidines and Piperidines. *J. Am. Chem. Soc*. **2006**, *128*, 14220−14221. (b) Campos, K. R. Direct sp^3 C−H Bond Activation Adjacent to Nitrogen in Heterocycles. *Chem. Soc. Rev*. **2007**, *36*, 1069−1084. (c) Mitchell, E. A.; Peschiulli, A.; Lefevre, N.; Meerpoel, L.; Maes, B. U. W. Direct α-Functionalization of Saturated Cyclic Amines. *Chem. - Eur. J*. **2012**, *18*, 10092−10142. (d) Shi, L.; Xia, W. Photoredox functionalization of C−H Bonds Adjacent to a Nitrogen Atom. *Chem. Soc. Rev*. **2012**, *41*, 7687−7697. (e) He, J.; Hamann, L. G.; Davies, H. M. L.; Beckwith, R. E. J. Late-Stage C−H Functionalization of Complex Alkaloids and Drugs Molecules via Intermolecular Rhodium-Carbenoid Insertion. *Nat. Commun.* **2015**, *6*, 5943. (f) Spangler, J. E.; Kobayashi, Y.; Verma, P.; Wang, D.-H.; Yu, J.-Q. α-Arylation of Saturated Azacycles and N-methylamines via Palladium(II)-Catalyzed C(sp3) − H Coupling. *J. Am. Chem. Soc*. **2015**, *137*, 11876−11879. (g) Chen, W.; Ma, L.; Paul, A.; Seidel, D. Direct α-C−H Bond Functionalization of Unprotected Cyclic Amines. *Nat. Chem.* **2017**, *10*, 165−169.

(19) For examples of amines undergoing side reactions in presence of metal catalysts and oxidants, see: (a) Murahashi, S.; Naota, T.; Yonemura, K. Ruthenium-Catalyzed Cytochrome P450-Type Oxidation of Tertiary Amines with Alkyl Hydroperoxides. *J. Am. Chem. Soc.* **1988**, *110*, 8256-8258. (b) Venkataramanan, N. S.; Kuppuraj, G.; Rajagopal, S. Metal-Salen Complexes as Efficient Catalysts for the Oxygenation of Heteroatom Containing Organic Compounds–Synthetic and Mechanistic Aspects. *Coord. Chem. Rev*. **2005**, *249*, 1249-1268. (c) Park, J.; Morimoto, Y.; Lee, Y.-M.; You, Y.; Nam, W.; Fukuzumi, S. Scandium Ion-Enhanced Oxidative Dimerization and N-Demethylation of *N,N*-Dimethylanilines by a Non-Heme Iron(IV)-Oxo Complex. *Inorg. Chem*. **2011**, *50*, 11612-11622. (d) Liu, P.; Liu, Y.; Wong, E. L.-M.; Xiang, S.; Che, C.-M. Iron

Oligopyridine Complexes as Efficient Catalysts for Practical Oxidation of Arenes, Alkanes, Tertiary Amines and *N*-Acyl Cyclic Amines with Oxone. *Chem. Sci*. **2011**, *2*, 2187-2195. (e) Cai, X. W.; Sha, M.; Guo, C. P.; Pan, R. M. Synthesis of Tertiary Amine *N*-Oxides–A Review. *Asian J. Chem.* **2012**, *24*, 3781-3784. (f) Genovino, J.; Lütz, S.; Sames, D.; Touré, B. B. Complementation of Biotransformations with Chemical C–H Oxidation: Copper-Catalyzed Oxidation of Tertiary Amines in Complex Pharmaceuticals. *J. Am. Chem. Soc.* **2013**, *135*, 12346-12352. (g) Ling, Z.; Yun, L.; Liu, L.; Fu, X. Aerobic Oxidative N-Dealkylation of Tertiary Amines in Aqueous Solution Catalyzed by Rhodium Porphyrins. *Chem. Commun.* **2013**, *49*, 4214-4216. (h) Malik, H. A.; Taylor, B. L. H.; Kerrigan, J. R.; Grob, J. E.; Houk, K. N.; Du Bois, J.; Hamann, L. G.; Patterson, A. W. Non-Directed Allylic C–H Acetoxylation in the Presence of Lewis Basic Heterocycles. *Chem. Sci.* **2014**, *5*, 2352-2361. (i) Kim, S.; Ginsbach, J. W.; Lee, J. Y.; Peterson, R. L.; Liu, J. J.; Siegler, M. A.; Sarjeant, A. A.; Solomon, E. I.; Karlin, K. D. Amine Oxidative *N*-Dealkylation Via Cupric Hydroperoxide Cu-OOH Homolytic Cleavage Followed by Site-Specific Fenton Chemistry. *J. Am. Chem. Soc.* **2015**, *137*, 2867-2874.

(20) For remote C–H functionalization blocking C_α–H sites on alicyclic amines, see: (a) McNally, A.; Haffemayer, B.; Collins, B. S.; Gaunt, M. J. Palladium-Catalysed C−H activation of Aliphatic Amines to Give Strained Nitrogen Heterocycles. *Nature* **2014**, *510*, 129-133. (b) Calleja, J.; Pla, D.; Gorman, T. W.; Domingo, V.; Haffemayer, B.; Gaunt, M. J. A Steric Tethering Approach Enables Palladium-Catalysed C−H activation of primary amino alcohols. *Nature Chemistry* **2015**, *7*, 1009-1016.

(21) For remote C−H functionalization protonating nitrogen on alicyclic amines, see: (a) Annese, C.; D'Accolti, L.; De Zotti, M.; Fusco, C.; Toniolo, C.; Williard, P. G.; Curcu, R. Concerning Selectivity in the Oxidation of Peptides by Dioxiranes. Further Insight in the Effect of Carbamate Protecting Groups. *J. Org. Chem*. **2010**, *75*, 4812-4816. (b) Mbofana, C. T.; Chong, E.; Lawniczak, J.; Sanford, M. S. Iron-Catalyzed Oxyfunctionalization of Aliphatic Amines at Remote Benzylic C−H Sites. *Org. Lett*. **2016**, *18*, 4258-4261. (c) Schultz, D. M.; Lévesque, F.; DiRocco, D. A.; Reibarkh, M; Ji, Y.; Joyce, L. A.; Dropinski, J. F.; Sheng, H.; Sherry, B. D.; Davies, I. W. Oxyfunctionalization of the Remote C−H Bonds of Aliphatic Amines by Decatungstate Photocatalysis. *Angew. Chem. Int. Ed.* **2017**, *56*, 15274-15278. (d) Lee, M.; Sanford, M. S. Remote C(sp³)−H Oxygenation of Protonated Aliphatic Amines with Potassium Persulfate. *Org. Lett.* **2017**, *19*, 572-575. (e) White, C. M.; Zhao, J. Aliphatic C−H Oxidations for Late-Stage Functionalization. *J. Am. Chem. Soc*. **2018**, *140*, 13988-14009.

(22) McNally, A.; Haffemayer, B.; Collins, B. S. L.; Gaunt, M. J. Palladium-Catalysed C–H Activation of Aliphatic Amines to Give Strained Nitrogen Heterocycles. *Nature* **2014**, *510*, 129–133.

(23) (a) Ye, S.; Yang, W.; Coon, T.; Fanning, D.; Neubert, T.; Stamos, D.; Yu, J.-Q. N-Heterocyclic Carbene Ligand-Enabled C(sp³)−H Arylation of Piperidine and Tetrahydropyran Derivatives. *Chem. Eur. J.* **2016**, *22*, 4748–4752. (b) Affron, D. P.; Bull, J. A. Palladium-Catalyzed Directed C(sp³)-H Arylation of Saturated Heterocycles at C-3 Using a Concise Optimization Approach: Pd-Catalyzed Directed C(sp³)-H Arylation. *Eur. J. Org. Chem.* **2016**, *2016*, 139–149. (c) Van Steijvoort, B. F.; Kaval, N.; Kulago, A. A.; Maes, B. U. W. Remote Functionalization: Palladium-Catalyzed C5(sp³)-H Arylation of 1-Boc-3-Aminopiperidine through the Use of a Bidentate Directing Group. *ACS Catal.* **2016**, *6*, 4486–4490.

(24) Topczewski, J. J.; Cabrera, P. J.; Saper, N. I.; Sanford, M. S. Palladium-Catalysed Transannular C–H Functionalization of Alicyclic Amines. *Nature* **2016**, *531*, 220–224.

(25) (a) Tasker, S. Z.; Standley, E. A.; Jamison, T. F. Recent Advances in Homogeneous Nickel Catalysis. *Nature* **2014**, *509*, 299–309. (b) Ananikov, V. P. Nickel: The "spirited horse" of transition metal catalysis. *ACS Catalysis* **2015**, *5*, 1964–1971. (c) Harry, N. A.; Saranya, S.; Ujwaldev, S. M.; Anilkumar, G. Recent Advances and Prospects in Nickel-Catalyzed C–H Activation. *Catal. Sci. Technol.* **2019**, *9*, 1726–1743.

(26) Daily Metal Spot Prices for Ni and Pd. https://www.dailymetalprice.com/metalprices.php?c=ni&u=lb&d=20 (accessed Feb 4, 2021).

(27) Emsley, J. *Nature's Building Blocks: An A-Z Guide to the Elements*; Oxford University Press: New York, 2002.

(28) (a) Tobisu, M.; Xu, T.; Shimasaki, T.; Chatani, N. Nickel-Catalyzed Suzuki–Miyaura Reaction of Aryl Fluorides. *J. Am. Chem. Soc.* **2011**, *133*, 19505–19511. (b) Mesganaw, T.; Garg, N. K. Ni- and Fe-Catalyzed Cross-Coupling Reactions of Phenol Derivatives. *Org. Process Res. Dev.* **2013**, *17*, 29–39.

(29) (a) Richmond, E.; Moran, J. Recent Advances in Nickel Catalysis Enabled by Stoichiometric Metallic Reducing Agents. *Synthesis* **2018**, *50*, 499–513.

(30) Zhu, C.; Yue, H.; Chu, L.; Rueping, M. Recent Advances in Photoredox and Nickel Dual-Catalyzed Cascade Reactions: Pushing the Boundaries of Complexity. *Chem. Sci.* **2020**, *11*, 4051–4064.

(31) (a) Tsou, T. T.; Kochi, J. K. Mechanism of Biaryl Synthesis with Nickel Complexes. *J. Am. Chem. Soc.* **1979**, *101*, 7547–7560. (b) Laskowski, C. A.; Bungum, D. J.; Baldwin, S. M.; Del Ciello, S. A.; Iluc, V. M.; Hillhouse, G. L. Synthesis and Reactivity of Two-Coordinate Ni(I) Alkyl and Aryl Complexes. *J. Am. Chem. Soc.* **2013**, *135*, 18272–18275. (c) Cornella, J.; Gomez-Bengoa, E; Martin, R. Combined Experimental and Theoretical Study on the Reductive Cleavage of Inert C–O Bonds with Silanes: Ruling out a Classical Ni(0)/Ni(II) Catalytic Couple and Evidence for Ni(I) Intermediates. *J. Am. Chem. Soc.* **2013**, 135, 1997–2009. (d) Montgomery, J. "Organonickel Chemistry" in *Organometallics in Synthesis: Fourth Manual* Lipshutz, B. H. (Ed.) Wiley, Hoboken, N.J., **2013**, pp. 319-428. (e) Rosen, B. M.; Quasdorf, K. W.; Wilson, D. A.; Zhang, N.; Resmerita, A-M.; Garg, N. K.; Percec, V. Nickel-Catalyzed Cross-Couplings Involving Carbon–Oxygen Bonds. *Chem Rev.* **2011**, *111*, 1346.

(32) (a) Jones, G. D.; Martin, J. L.; McFarland, C.; Allen, O. R.; Hall, R. E.; Haley, A. D.; Brandon, R. J.; Konovalova, T.; Desrochers, P. J.; Pulay, P.; Vicic, D. A. Ligand Redox Effects in the Synthesis, Electronic Structure, and Reactivity of an Alkyl−Alkyl Cross-Coupling Catalyst. *J. Am. Chem. Soc.* **2006**, *128*, 13175–13183. (b) Zultanski, S. L.; Fu, G. C. Catalytic Asymmetric γ-Alkylation of Carbonyl Compounds via Stereoconvergent Suzuki Cross-Couplings. *J. Am. Chem. Soc.* **2011**, *133*, 15362–15364. (c) Hu, X. Nickel-Catalyzed Cross Coupling of Non-Activated Alkyl Halides: A Mechanistic Perspective. *Chem. Sci.* **2011**, *2*, 1867. (d) Joshi-Pangu, A.; Wang, C.-Y.; Biscoe, M. R. Nickel-Catalyzed Kumada Cross-Coupling Reactions of Tertiary Alkylmagnesium Halides and Aryl Bromides/Triflates. *J. Am. Chem. Soc.* **2011**, *133*, 8478–8481. (e) Dudnik, A. S.; Fu, G. C. Nickel-Catalyzed Coupling Reactions of Alkyl Electrophiles, Including Unactivated Tertiary Halides, To Generate Carbon–Boron Bonds. *J. Am. Chem. Soc.* **2012**, *134*, 10693–10697. (f) Dai, Y. Wu, F.; Zang, Z. H.; You, H. Z.; Gong, H. G. Ni-Catalyzed Reductive Allylation of Unactivated Alkyl Halides with Allylic Carbonates. *Chem. Eur. J.* **2012** *18*, 808–812. (g) Schley, N. D.; Fu, G. C. Nickel-Catalyzed Negishi Arylations of Propargylic Bromides: A Mechanistic Investigation. *J. Am. Chem. Soc.* **2014**, *136*, 16588–16593. (h) Aihara, Y.; Tobisu, M.; Fukumoto, Y.; Chatani, N. Ni(II)-Catalyzed Oxidative Coupling between C(sp^2)–H in Benzamides and C(sp^3)–H in Toluene Derivatives. *J. Am. Chem. Soc.* **2014**, *136*, 15509–

15512. (i) Wu, X.; Zhao, Y.; Ge, H. Nickel-Catalyzed Site-Selective Alkylation of Unactivated C(sp^3)–H Bonds. *J. Am. Chem. Soc.* **2014**, *136*, 1789–1792. (j) Tellis, J. C.; Primer, D. N.; Molander, G. A. Single-Electron Transmetalation in Organoboron Cross-Coupling by Photoredox/Nickel Dual Catalysis. *Science* **2014**, *345*, 433–436. (k) Zuo, Z.; Ahneman, D. T.; Chu, L.; Terrett, J. A.; Doyle, A. G.; MacMillan, D. W. C. Merging Photoredox with Nickel Catalysis: Coupling of -Carboxyl sp^3-Carbons with Aryl Halides. *Science* **2014**, *345*, 437–440. (l) Cornella, J.; Edwards, J. T.; Qin, T.; Kawamura, S.; Wang, J.; Pan, C.-M.; Gianatassio, R.; Schmidt, M.; Eastgate, M. D.; Baran, P. S. Practical Ni-Catalyzed Aryl–Alkyl Cross-Coupling of Secondary Redox-Active Esters. *J. Am. Chem. Soc.* **2016**, *138*, 2174–2177.

(33) (a) Semmelhack, M. F.; Helquist, P. M.; Jones, L. D. Synthesis with Zerovalent Nickel. Coupling of Aryl Halides with Bis(1,5-Cyclooctadiene)Nickel(0). *J. Am. Chem. Soc.* **1971**, *93*, 5908–5910. (b) Terao, J.; Kambe, N. Cross-Coupling Reaction of Alkyl Halides with Grignard Reagents Catalyzed by Ni, Pd, or Cu Complexes with π-Carbon Ligand(s). *Acc. Chem. Res.* **2008**, *41*, 1545–1554. (c) Aihara, Y.; Chatani, N. Nickel-Catalyzed Direct Alkylation of C–H Bonds in Benzamides and Acrylamides with Functionalized Alkyl Halides via Bidentate-Chelation Assistance. *J. Am. Chem. Soc.* **2013**, *135*, 5308–5311. (d) Aihara, Y.; Chatani, N. Nickel-Catalyzed Direct Arylation of C(sp^3)–H Bonds in Aliphatic Amides via Bidentate-Chelation Assistance. *J. Am. Chem. Soc.* **2014**, *136*, 898–901. (e) Iyanaga, M.; Aihara, Y.; Chatani, N. Direct Arylation of C(sp^3)–H Bonds in Aliphatic Amides with Diaryliodonium Salts in the Presence of a Nickel Catalyst. *J. Org. Chem.* **2014**, *79*, 11933–11939. (f) Castro, L. C. M.; Chatani, N. Nickel Catalysts/ *N*, *N* ′-Bidentate Directing Groups: An Excellent Partnership in Directed C–H Activation Reactions. *Chem. Lett.* **2015**, *44*, 410–421. (g) Yan, S.-Y.; Liu, Y.-J.; Liu, B.; Liu, Y.-H.; Zhang, Z.-Z.; Shi, B.-F. Nickel-Catalyzed Direct Thiolation of Unactivated C(sp^3)–H Bonds with Disulfides. *Chem. Commun.* **2015**, *51*, 7341–7344. (h) Yang, X.; Shan, G.; Wang, L.; Rao, Y. Recent Advances in Transition Metal (Pd, Ni)-Catalyzed C(sp^3)−H Bond Activation with Bidentate Directing Groups. *Tetrahedron Letters* **2016**, *57*, 819–836. (i) Ruan, Z.; Lackner, S.; Ackermann, L. A General Strategy for the Nickel-Catalyzed C−H Alkylation of Anilines. *Angew. Chem. Int. Ed.* **2016**, *55*, 3153–3157.

(34) Zuo, Z.; Cong, H.; Li, W.; Choi, J.; Fu, G. C.; MacMillan, D. W. C. Enantioselective Decarboxylative Arylation of α-Amino Acids via the Merger of Photoredox and Nickel Catalysis. *J. Am. Chem. Soc.* **2016**, *138*, 1832–1835.

(35) Primer, D. N.; Molander, G. A. Enabling the Cross-Coupling of Tertiary Organoboron Nucleophiles through Radical-Mediated Alkyl Transfer. *J. Am. Chem. Soc.* **2017**, *139*, 9847–9850.

Chapter 2   Model Complexes for the Palladium-Catalyzed Transannular C$_\gamma$–H Functionalization of Alicyclic Amines

Note: This Chapter is based on work published in Aguilera, E. Y.; Sanford, M. S.* "Model Complexes for the Palladium-Catalyzed Transannular C–H Functionalization of Alicyclic Amines" *Organometallics* **2019**, *38*, 138–142.

2.1 Introduction

Alicyclic amines appear in a wide variety of biologically active molecules.[1] As such, there is great interest in developing synthetic methods for the late-stage functionalization of these motifs.[2] In 2016, our group reported the transannular C$_\gamma$–H arylation of piperidines and other alicyclic amines (Scheme 2.1).[3a] This transformation is unusual in that it enables highly selective functionalization of the C$_\gamma$–H bond in lieu of the more activated C$_\alpha$–H bonds at the 2-position.[4] In our original report,[3a] we proposed that this selectivity derives from bidentate coordination of the amine nitrogen and the tethered amide[5] of substrate **I** at Pd^{II} to form an intermediate of general structure **II** (Scheme 2.1, step i).[3a] Subsequent isomerization to the boat conformer then positions

Scheme 2.1 Proposed Mechanism for the Transannular C$_\gamma$–H Arylation of Alicyclic Amines
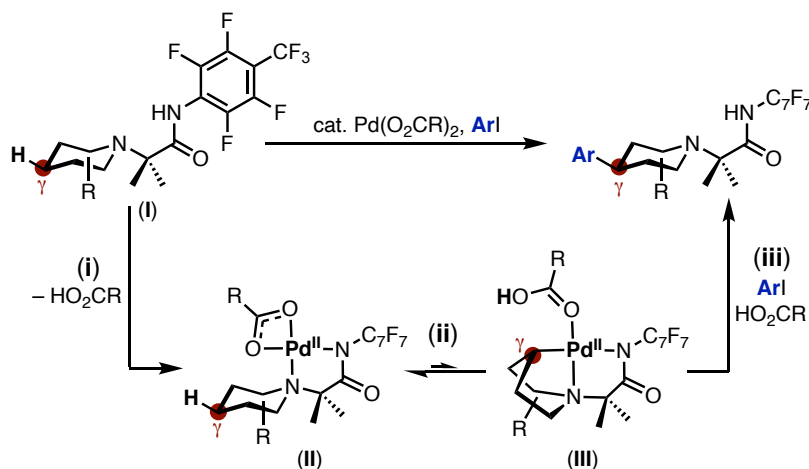
the C_γ–H bond proximal to the Pd^{II} center for C(sp^3)–H activation to form **III** (step ii), followed by functionalization with ArI and ligand exchange to release the product (step iii).

The proposed transannular C(sp^3)–H activation (step ii) is unusual in that it forms a strained bicyclo[2.2.1]palladacyclic intermediate (**III**). Only one example of this type of structure has been generated and characterized from a C–H activation reaction.[6] Recent DFT calculations suggest that complex **III** is approximately 20 kcal/mol uphill from **II**,[7] indicating that this transannular C(sp^3)–H activation at Pd^{II} is highly thermodynamically unfavorable. This stands in contrast to the vast majority of reported C(sp^3)–H cyclopalladation reactions, which generally produce isolable 5-membered palladacycles under relatively mild conditions.[8,9]

We sought to interrogate the C–H activation step of the proposed catalytic cycle by isolating and studying key intermediates along this pathway. Herein we demonstrate that amines of general structure **I** bind to Pd in a bidentate fashion to form isolable intermediates in which the C_γ–H bond is in close proximity to both the Pd center and the carboxylate ligand. Furthermore, we show that these complexes react stoichiometrically with aryl iodides to afford C–H arylation products. Finally, we demonstrate that these synthesized Pd^{II} complexes participate in H/D exchange with d_{10}-*tert*-butanol at temperatures as low as 40 ºC. Overall these studies support the mechanism proposed in Scheme 2.1 and provide new insights into the transannular C(sp^3)–H activation step of this catalytic cycle.

2.2 Results and Discussion

Part A. *Studying Pd-catalyzed Transannular C–H Arylation/Activation*

Design and Synthesis of Pd^{II} Complexes

We initially focused on synthesizing the putative catalytic intermediate **I**. Two different alicyclic amine cores were selected for these studies, 3-azabicyclo[3.1.0]hexane (**A**) and 2,3,4,5-

tetrahydro-1H-1,5-methano-3-benzazepine (**B**), as both are effective substrates for the catalytic C–H arylation reaction.[3a] Under a variety of conditions, the reaction between **A/B** and various Pd[II] sources yielded complex mixtures of products that could not be definitively isolated or characterized (Scheme 2.2). We hypothesized that complex **II** might be stabilized by the incorporation of a monodentate pyridine ligand to generate the pyridine adduct **2**.

Scheme 2.2 Attempted Synthesis of **II** and Hypothesis for Stabilization with Pyridine
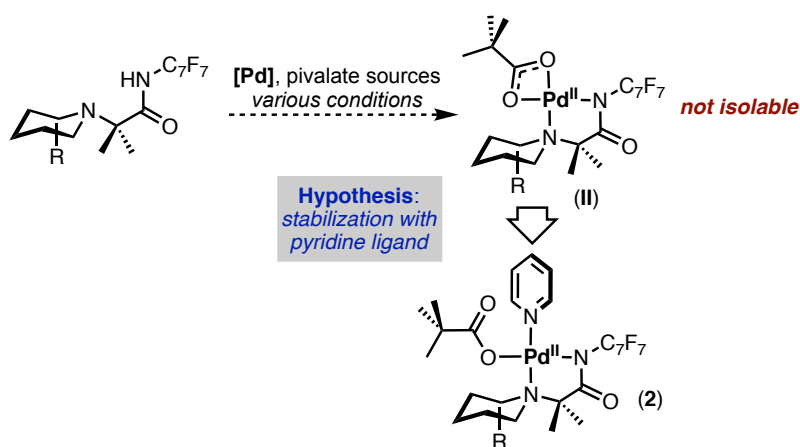
The reaction of **A** with Pd(OAc)$_2$, CsOPiv, and pyridine in *tert*-amyl alcohol at 100 °C for 2 h afforded product **1-A** in 85% isolated yield (Scheme 2.3). ^{1}H NMR spectroscopic analysis of **1-A** in CDCl$_3$ at room temperature showed the presence of two isomers (**1-A^1** and **1-A^2**) in an approximately 1:1 ratio (see Figure 2.3 in Experimental Procedures).[10] Yellow crystals of **1-A^1** and **1-A^2** were obtained in the same unit cell by vapor diffusion of hexanes into a dichloromethane solution at 25 °C. The solid-state structure shows that **1-A^1** and **1-A^2** are square planar Pd[II] complexes in which **A** is bound through both the amine and amide nitrogen atoms (Figure 2.1). The key difference between these complexes is the orientation of the cyclopropane ring relative to the Pd[II] center. In **1-A^2**, this ring points away from Pd, while in **1-A^1** the ring is oriented towards the Pd and pivalate ligand. Notably, isomer **1-A^1** is the conformation from which transannular C–

H activation is expected to take place. The reactive $C(sp^3)$–H (H1) is 3.411 Å from the C=O of the pivalate ligand and 4.421 Å from the Pd center in complex **1-A^1** (Table 2.1).

Scheme 2.3 Synthesis of Complex Isomers **1-A^1** and **1-A^2**
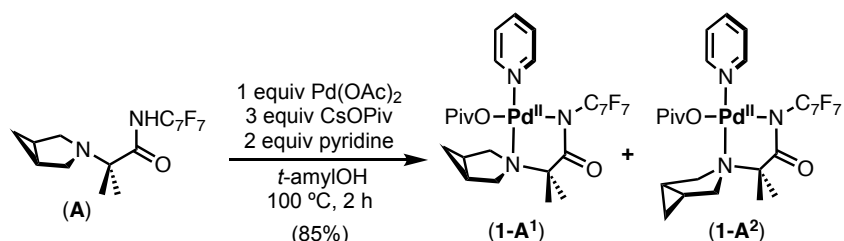
Figure 2.1 X-Ray Crystal Structures of **1-A^1**, **1-A^2** and **1-B**
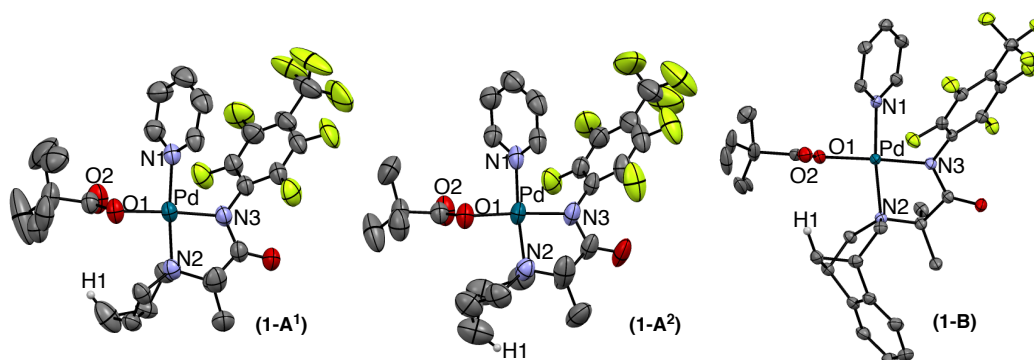
Table 2.1 Comparison of Bond Distances for Complexes **1-A^1**, **1-A^2** and **1-B**

	Pd–N1	*Pd–N2*	*Pd–N3*	*Pd–O1*	*Pd–H1*	*O2–H1*
1-A^1	2.037 Å	2.060 Å	2.007Å	2.033 Å	4.421 Å	3.411 Å
1-A^2	2.023 Å	2.058 Å	2.003 Å	2.023 Å	5.173 Å	5.293 Å
1-B	2.031 Å	2.094 Å	2.002 Å	2.039 Å	3.694 Å	2.711 Å

An analogous complex was formed in 40% isolated yield from the reaction of **B** with Pd(OAc)$_2$, CsOPiv, and pyridine in *tert*-amyl alcohol at 100 °C for 2 h (Scheme 2.4). Both ^{1}H NMR spectroscopic analysis and X-ray crystallography show that **1-B** is a single isomer, with the

transannular C–H bond (H1) pointing towards the Pd center and pivalate ligand (Figure 2.1). In

this case the Pd–H1 and O2–H1 distances are even shorter at 3.694 Å, and 2.711 Å, respectively

(Table 2.1).

Scheme 2.4 Synthesis of Complex **1-B**
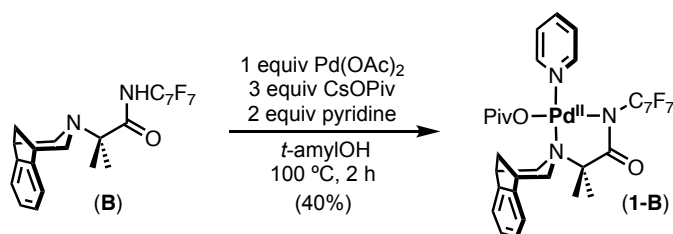
Reactivity of Pd^{II} Complexes Towards Arylation

We next explored the reactivity of complexes **1-A** and **1-B** towards C–H activation and

functionalization with PhI (Scheme 2.1, steps *ii* and *iii*). A key question for these studies is whether

1 serves as a viable model system for catalytic intermediate **II**, or whether the presence of the

pyridine impedes C–H activation and/or functionalization. To test this, each complex was treated

with PhI under catalytically relevant conditions (3 equiv of CsOPiv, 3 equiv of PhI in *t*-amyl

alcohol at 100 ºC for 18 h).[3b] The reactions were then cooled to room temperature, quenched with

hydrazine to cleave the ligands and precipitate palladium black, and analyzed by GC to quantify

the C$_\gamma$–H arylation products (Scheme 2.5). The reactions of **1-A** and **1-B** afforded the C–H arylat-

Scheme 2.5 Complexes **1-A** and **1-B** under Arylation Conditions

20
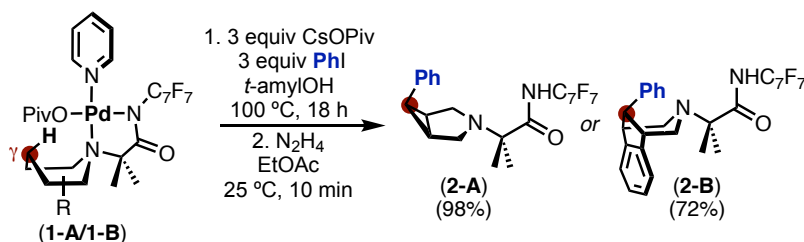
ion products **2-A** and **2-B** in 98% and 72% yield, respectively, confirming that these model complexes are competent for the C–H activation/arylation sequence.

H/D Exchange Studies with Pd[II] Complexes

As discussed above, DFT calculations suggest that transannular $C(sp^3)$–H activation at **II** to form σ-alkyl complex **III** is highly thermodynamically unfavorable.[7] Consistent with these calculations, attempts to observe or isolate palladacyclic analogues of **III** under a variety of conditions (with and without added base) were unsuccessful. Thus, we turned to hydrogen/deuterium (H/D) exchange experiments[11] as a method to interrogate C–H activation at **1-A** and **1-B**. H/D exchange studies were carried out using the solvent d_{10}-*tert*-butanol (C_4D_9OD) as the source of deuterium. Complexes **1-A** and **1-B** were initially heated at 100 ºC for 18 h in C_4D_9OD in the presence of 3 equiv of CsOPiv. The reactions were then cooled to room temperature, quenched with hydrazine, and analyzed by GCMS as well as ^1H and ^2H NMR spectroscopy. Both **1-A** and **1-B** reacted under these conditions to form mono-deuterated amine products with 65% and 81% deuterium incorporation, respectively (Table 2.2, entries 1 and 7). NMR spectroscopic analysis of the products showed that the deuterium is site- and stereoselectively incorporated at the expected transannular site on the amine core to form **A-*d*** and **B-*d***. These results demonstrate that transannular C–H activation is reversible and that it occurs in the absence of the aryl iodide oxidant.

We next probed the role of CsOPiv in this H/D exchange process. Literature studies suggest that C–H activation at Pd[II]–carboxylate complexes proceeds via a concerted-metalation deprotonation (CMD) pathway, in which the carboxylate ligand acts as an intramolecular base (**TS-I** in Figure 2.2).[6,12] As such, we hypothesized that the added carboxylate should not be

required for the H/D exchange. Indeed, nearly identical yields of **A-*d*** and **B-*d*** were obtained under otherwise identical conditions, but in the absence of CsOPiv (Table 2.2, entries 2 and 8).

Table 2.2 H/D Exchange at Complexes **1-A** and **1-B**
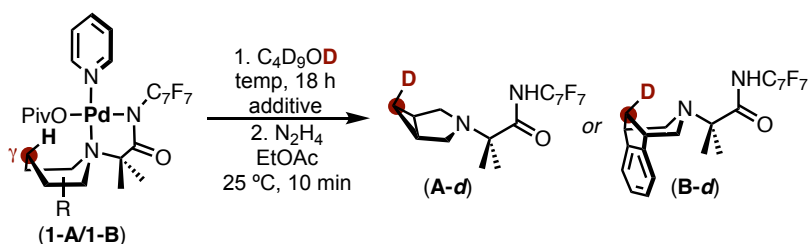
entry	complex	temp	additive	% deuteration
1	1-A	100 ºC	3 equiv CsOPiv	65%
2	1-A	100 ºC	none	58%
3	1-A	100 ºC	2 equiv pyridine-d_5	31%
4	1-A	80 ºC	none	40%
5	1-A	60 ºC	none	16%
6	1-A	40 ºC	none	2%
7	1-B	100 ºC	3 equiv CsOPiv	81%
8	1-B	100 ºC	none	80%
9	1-B	100 ºC	2 equiv pyridine-d_5	64%
10	1-B	80 ºC	none	78%
11	1-B	60 ºC	none	74%
12	1-B	40 ºC	none	18%

The CMD transition state **TS-I** requires an open coordination site for interaction between the Cγ–H bond and the Pd center. As such, this pathway is expected to require pyridine dissociation from complexes **1** prior to C–H activation. To test for this possibility, we next examined whether the addition of exogeneous pyridine inhibits H/D exchange in these systems. Consistent with this proposal, the addition of 2 equiv of pyridine resulted in a significant decrease in the % deuterium incorporation for both amines (Table 2.2, compare entries 2 and 8 to entries 3 and 9, respectively).

Figure 2.2 Proposed Transition State for C–H Activation via CMD Mechanism
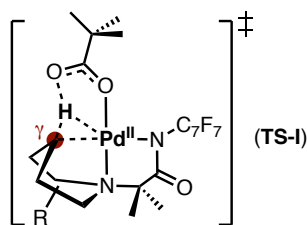
Next, we investigated the temperature required for transannular C–H activation in these systems. As shown in Table 2.2, H/D exchange was observed after 18 h at temperatures as low as 60 ºC for **1-A** (entry 5) and 40 ºC for **1-B** (entry 12). These results suggest that C–H functionalization reactions of substrates **A** and **B**, which are typically conducted at temperatures >100 ºC,[3] can potentially be optimized to proceed under much milder conditions. In addition, the observation that **1-B** is significantly more reactive than **1-A** is consistent with the observation that this complex is formed as a single isomer with the transannular C–H bond in close proximity to the Pd center and the reactive carboxylate oxygen.

Finally, catalytic H/D exchange was also studied for the Pd-catalyzed transannular C–H activation step. Under similar arylation conditions except for the aryl iodide oxidant, substrate **A** with 10 mol% Pd(OAc)$_2$ yielded low H/D exchange. Through optimization, it was found that the addition of deuterated acetic acid led to an increase in deuterium incorporation (Scheme 2.6).

Scheme 2.6 Pd-Catalyzed H/D Exchange
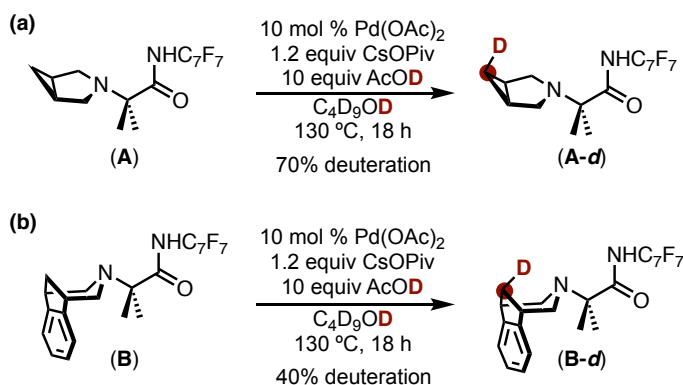
Part B. *Exploring Ligand Effects in Pd-Catalyzed Transannular C–H Arylation/Activation*

In 2018 our lab reported significant increases in the rate and yield of transannular $C(sp^3)$–H arylation with substrate **B**, in the presence of picolinic acid as a ligand.[3b] As such, we sought to develop a Pd^{II} complex where the role of picolinic acid in C–H arylation/activation could be directly studied.

Design and Synthesis of Pd^{II}–Picolinic Acid Complex

We envisioned that the ideal Pd^{II} complex to study the role of picolinic acid would contain substrate **B** bound to the Pd^{II} center via the amine nitrogen and the tethered amide, and picolinic acid bound as an LX-type ligand. With complex **1-B** in hand, we anticipated that performing a ligand exchange between **1-B** and picolinic acid would result in the desired complex. Indeed, treating complex **1-B** with picolinic acid in MeCN at 25 °C for 1 h yielded **1-C** in 30% isolated yield (Scheme 2.7). **1-C** was characterized by X-ray crystallography, which shows a single isomer, with the nitrogen of the picolinic acid trans to the amine nitrogen of **B**. Notably, the O2-H1 distance in this system is 4.555 Å, which is significantly longer distance that of **1-B** (2.711 Å). This increased distance is due to the coordination of the pyridine nitrogen.

Scheme 2.7 Synthesis of Complex **1-C** via Ligand Exchange
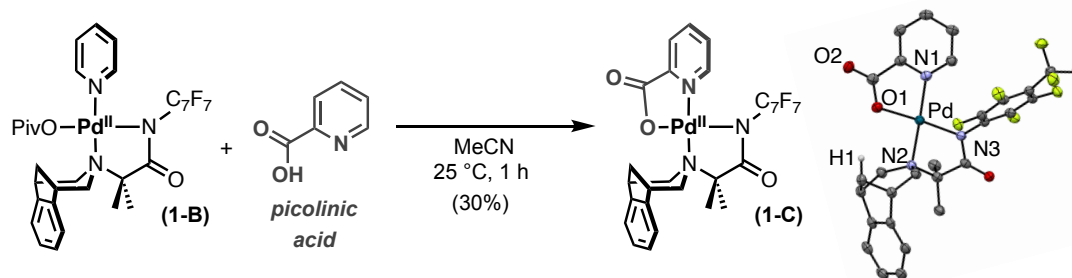
Future Work for Probing the Role of Picolinic Acid

We propose that complex **1-C** can be used to interrogate the role of picolinic acid in C–H arylation/activation. Firstly, similar to Part A, complex **1-C** could be exposed to arylation conditions to verify that it is competent for this transformation. Next, **1-C** could be utilized in both stoichiometric and catalytic H/D exchange reactions as described above. Significant changes in % deuterium incorporation at C–H$_\gamma$ could suggest picolinic acid participates in the C–H activation step. Moreover, we could also diversify picolinic acid bound to Pd during the H/D exchange/arylation reaction to monitor its role in the reaction.

2.3 Conclusions

In summary, we designed, synthesized, and characterized Pd^{II} complexes that serve as models for catalytic intermediates in the Pd-catalyzed transannular C(sp^3)–H arylation of alicyclic amines. While the transannular C(sp^3)–H activation intermediate appears to be thermodynamically uphill, the C–H cleavage step was directly interrogated via H/D exchange. These studies show that transannular C(sp^3)–H activation in these systems occurs with high selectivity at temperatures as low as 40 °C. Furthermore, the results are consistent with C$_\gamma$–H cleavage occurring via a CMD mechanism the Pd^{II} oxidation state. Overall, we anticipate that these investigations will inform the

development of new, mild methods for the late-stage functionalization of alicyclic amine substrates.

2.4 Experimental Procedures and Characterization of Compounds

2.4.1 General Procedures, Materials and Methods

General Procedures

NMR spectra were obtained on a Varian VNMR 700 (699.76 MHz for ^{1}H and ^{2}H; 175.95 MHz for ^{13}C) or a Varian VNMR 500 (500.09 MHz for ^{1}H; 470.56 MHz for ^{19}F) spectrometer. ^{1}H, ^{2}H and, ^{13}C chemical shifts are reported in parts per million (ppm) relative to TMS, with the residual solvent peak used as an internal reference. ^{19}F chemical shifts are reported in ppm and are referenced on a unified scale to the frequency of the residual solvent peak in the ^{1}H NMR spectrum. Abbreviations used in the NMR data: s, singlet; d, doublet; t, triplet; q, quartet; dt, doublet of triplets; bq, broad quartet. Elemental analyses were conducted by Midwest Microlabs. X-ray crystallographic data were collected on a Bruker SMART APEX-I CCD-based X-ray diffractometer. Flash chromatography was conducted using a Biotage Isolera One system with cartridges containing high performance silica gel. Melting points were conducted on a OptiMelt automated melting point system.

Materials and Methods

Pd(OAc)$_2$ was purchased from Pressure Chemical Company. Cesium pivalate and iodobenzene were purchased from Aldrich. *tert*-Amyl alcohol and 4-iodoanisole were purchased from Acros Organics. Pyridine, dichloromethane, and hexane were obtained from Fisher. Deuterated solvents were purchased from Cambridge Isotope Laboratories. Hydrazine monohydrate was purchased from Alfa Aesar. All commercial reagents were stored under ambient conditions unless otherwise stated. All commercial reagents were used without further

purification/drying unless explicitly stated in the experimental section. All reactions were performed in air unless stated in experimental section. Reaction vessels were sealed with either a septum (flask) or a Teflon-lined cap (4 mL, 10 mL or 20 mL vial) with Teflon tape wrapped around the cap.

2.4.2 Synthesis and Characterization of Starting Material

(S1)   (S2)   toluene, 140 °C, 18 h   (S3)
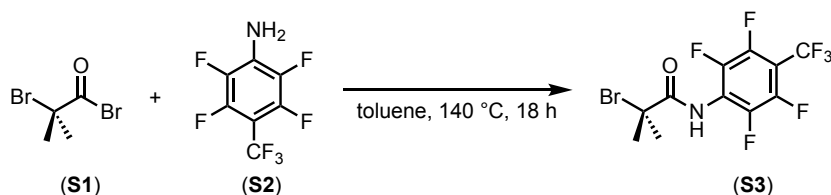
Synthesis of S3: A round bottomed flask was charged with 2,3,5,6-tetrafluoro-4-(trifluoromethyl)aniline **S2** (2.50 g, 10.7 mmol, 1.0 equiv) and anhydrous toluene (30 mL). To this flask, 2-bromoisobutyryl bromide **S1** (1.32 mL, 10.7 mmol, 1.0 equiv) was added. A reflux condenser was attached and capped with a drying tube packed with cotton and K_2CO_3. The reaction mixture was heated at 140 °C for 18 h. The resulting mixture was allowed to cool to room temperature and then concentrated under reduced pressure. The solid was recrystallized from hot hexanes. The crystalline product (**S3**) was collected, washed with cold hexanes, and dried to obtain light tan crystals (3.70 g, 90% yield). The NMR data for the product match those reported in the literature.[3]

(S4)   (S3) K_2CO_3, NaI / MeCN, 60 °C, 18 h   (A)
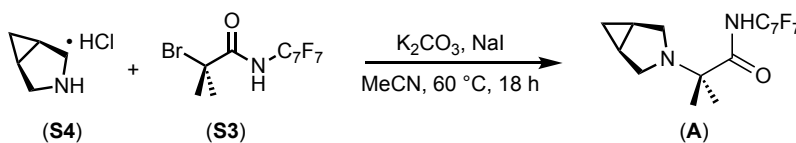
Synthesis of A: A 20 mL vial was charged with 3-azabicyclo[3.1.0]hexane hydrochloride **S4** (300 mg, 2.55 mmol, 1 equiv), α-bromopropanamide **S3** (1.0 g, 2.55 mmol, 1.0 equiv), K_2CO_3 (1.16 g, 8.16 mmol, 3.2 equiv), and NaI (200 mg, 1.27 mmol, 0.5 equiv), followed by the addition of

anhydrous acetonitrile (13 mL). The vial was capped and heated at 60 °C. After 18 h, the reaction was cooled to room temperature and filtered through silica gel, and the silica gel was washed with ethyl acetate. The filtrate was concentrated under reduced pressure. The crude material was purified by flash chromatography on silica gel (gradient elution from 0% to 20% EtOAc in hexanes). The product (**A**) was obtained as a white solid (700 mg, 72% yield). The NMR data for the product match those reported in the literature.[3a]
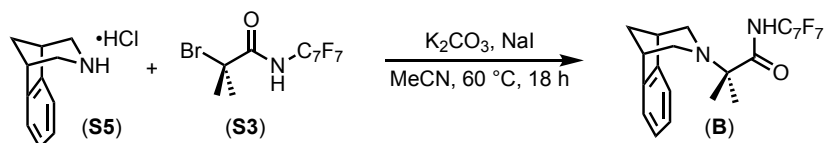
Synthesis of B: A 20 mL vial was charged with **S5** (500 mg, 2.62 mmol, 1 equiv), α-bromopropanamide **S3** (980 mg, 2.62 mmol, 1.0 equiv), K_2CO_3 (1.16 g, 8.38 mmol, 3.2 equiv), and NaI (196 mg, 1.31 mmol, 0.5 equiv), followed by the addition of anhydrous acetonitrile (13 mL). The vial was capped, and heated at 60 °C. After 18 h, the reaction was cooled to room temperature and filtered through silica gel, and the silica gel was washed with ethyl acetate. The filtrate was concentrated under reduced pressure. The crude material was purified by flash chromatography on silica gel (gradient elution from 0% to 20% EtOAc in hexanes). The product (**B**) was obtained as a white solid (840 mg, 70% yield). The NMR data for the product match those reported in the literature.[3]

2.4.3 Synthesis and Characterization of Pd Complexes
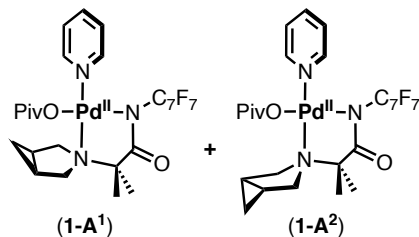
Synthesis of 1-A: A 20 mL vial was charged with **A** (100 mg, 0.26 mmol, 1.0 equiv), Pd(OAc)$_2$ (58.5 mg, 0.26 mmol, 1.0 equiv), and cesium pivalate (182 mg, 0.78 mmol, 3.0 equiv) followed by the addition of *tert*-amyl alcohol (~4 mL). The vial was capped, and the mixture was stirred at room temperature to allow for the cesium pivalate to solubilize. After 5 min, the vial was opened and pyridine (42 μL, 0.52 mmol, 2.0 equiv) was added. The vial was sealed and heated at 100 °C. After 2 h, the reaction was cooled to room temperature, and the solvent was removed under vacuum. The resulting solid was dissolved in dichloromethane (~10 mL), and the solution was filtered through a plug of Celite. The filtrate was concentrated under vacuum, the resulting solid was dissolved in a minimum quantity of dichloromethane, and hexane (~15 mL) was added. This solution was filtered through a plug of Celite, and the solvent was removed under vacuum (repeat twice). The resulting dark yellow solid was washed with cold hexanes to yield 1-A as a light yellow solid (148 mg, 85% yield). The product was obtained as a 1:1 mixture of two isomers: **1-A^1** and **1-A^2**. The ^{1}H NMR spectrum of this mixture of isomers is in **Figure 2.3**. COSY and HSQC experiments were conducted to identify the protons corresponding to each of the two isomers, and these are labelled C and D in the NMR spectrum above. However, the specific isomer associated with each set of peaks could not be definitively identified by NMR spectroscopy.

Figure 2.3 ^{1}H NMR Spectrum of Complex **1-A**[1] and **1-A**[2] in CDCl$_3$ (500 MHz)
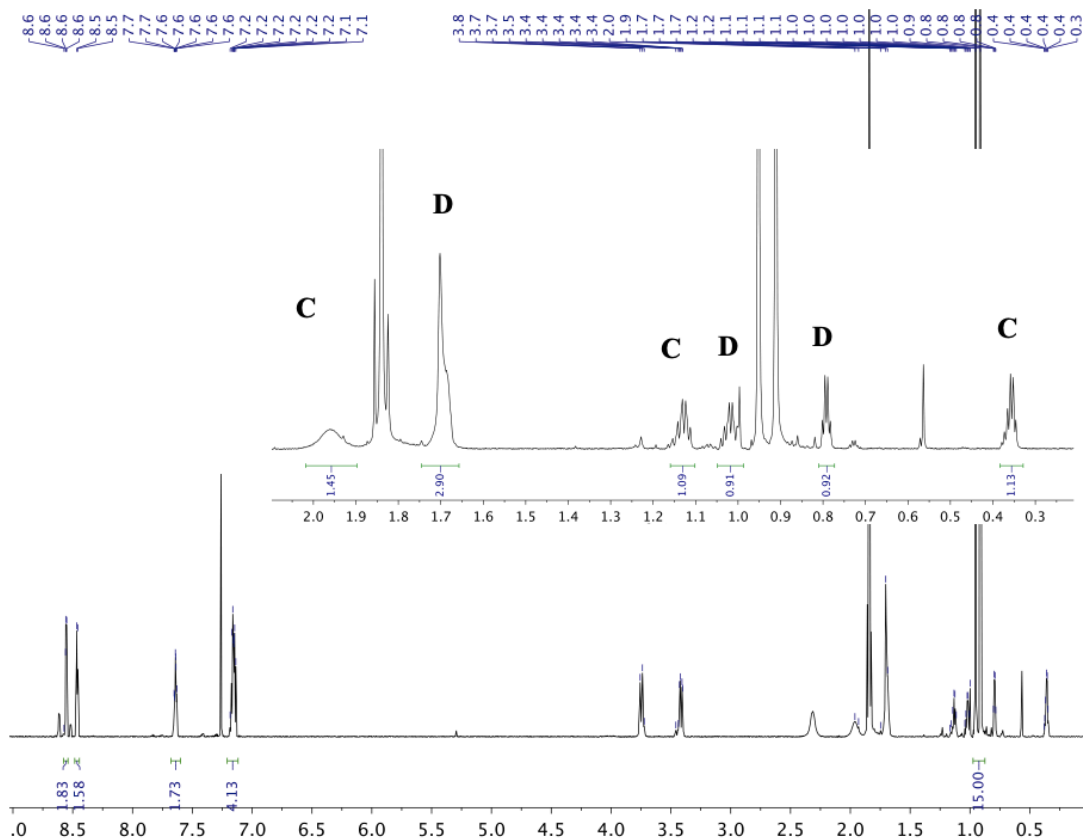
^{1}H NMR (500 MHz, CDCl$_3$, 23 °C): δ 8.54 (d, J_{HH} = 5.2 Hz, 2H), 8.44 (d, J_{HH} = 5.2 Hz, 2H), 7.62 (t, J_{HH} = 7.1 Hz, 2H), 7.13 (q, J_{HH} = 7.1 Hz, 4H), 3.73 (d, J_{HH} = 14.1 Hz, 2H), 3.40 (dd, J_{HH} = 14.1, 3.0 Hz, 2H), 1.97 (app s, 2H, **C**), 1.67 (dt, J_{HH} = 10.2, 3.0, 2H, **D**), 1.11 (q, J_{HH} = 7.6 Hz, 1H, **C**), 1.00 (q, J_{HH} = 7.6 Hz, 1H, **D**), 0.93 (s, 6H), 0.89 (s, 9H), 0.78 (q, J_{HH} = 4.4 Hz, 1H, **D**), 0.34 (q, J_{HH} = 4.4 Hz, 1H, **C**).

^{13}C NMR (176 MHz, CDCl$_3$, 23 °C, mixture of isomers): δ 185.4, 185.0, 179.4, 152.0, 138.5, 124.6, 73.6, 70.3, 58.3, 39.0, 28.0, 24.8, 21.9, 20.8, 18.9.

^{19}F NMR (470 MHz, CDCl$_3$, 23 °C): δ –56.1 (t, 3H), –143.5 (m, 2H), –143.6 (m, 2H).

HRMS-electrospray (m/z): [M]$^+$ calcd. for C$_{21}$H$_{19}$F$_7$N$_3$O$_2$Pd (**1-A** minus pivalate ligand), 568.0451; found, 568.0452.

Elemental Analysis calcd for $C_{26}H_{28}F_7N_3O_3Pd$, C: 46.61; H: 4.21; N: 6.27; found, C: 46.52; H: 4.12; N: 6.03.

(1-B)
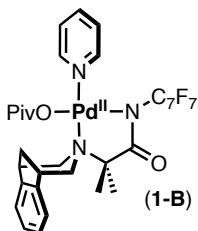
Synthesis of 1-B: A 20 mL vial was charged with **B** (100 mg, 0.22 mmol, 1.0 equiv), Pd(OAc)₂ (50.0 mg, 0.22 mmol, 1.0 equiv), and cesium pivalate (155 mg, 0.66 mmol, 3.0 equiv) followed by the addition of *tert*-amyl alcohol (~4 mL). The vial was capped, and the mixture was stirred at room temperature to allow for the cesium pivalate to solubilize. After 5 min, the vial was opened and pyridine (36 μL, 0.44 mmol, 2.0 equiv) was added. The reaction vial was sealed and heated at 100 °C. After 2 h, the reaction was cooled, and solvent was removed under vacuum. The resulting solid was dissolved in dichloromethane (~10 mL), and this solution was filtered through a plug of Celite. The filtrate was concentrated under vacuum. The resulting solid was then dissolved in a minimum quantity of dichloromethane, and hexane (~15 mL) was added. This solution was filtered through a plug of Celite and then through a plug of silica gel that was further washed with ethyl acetate (50 mL). The solvent was removed under vacuum, and the resulting yellow solid was washed with cold hexanes to yield **1-B** as a light yellow solid (63 mg, 40% yield). NMR spectroscopic analysis at room temperature shows a single isomer (Figure 2.4).

Figure 2.4 ^{1}H NMR Spectrum of Complex **1-B** in CDCl$_3$ (700 MHz)
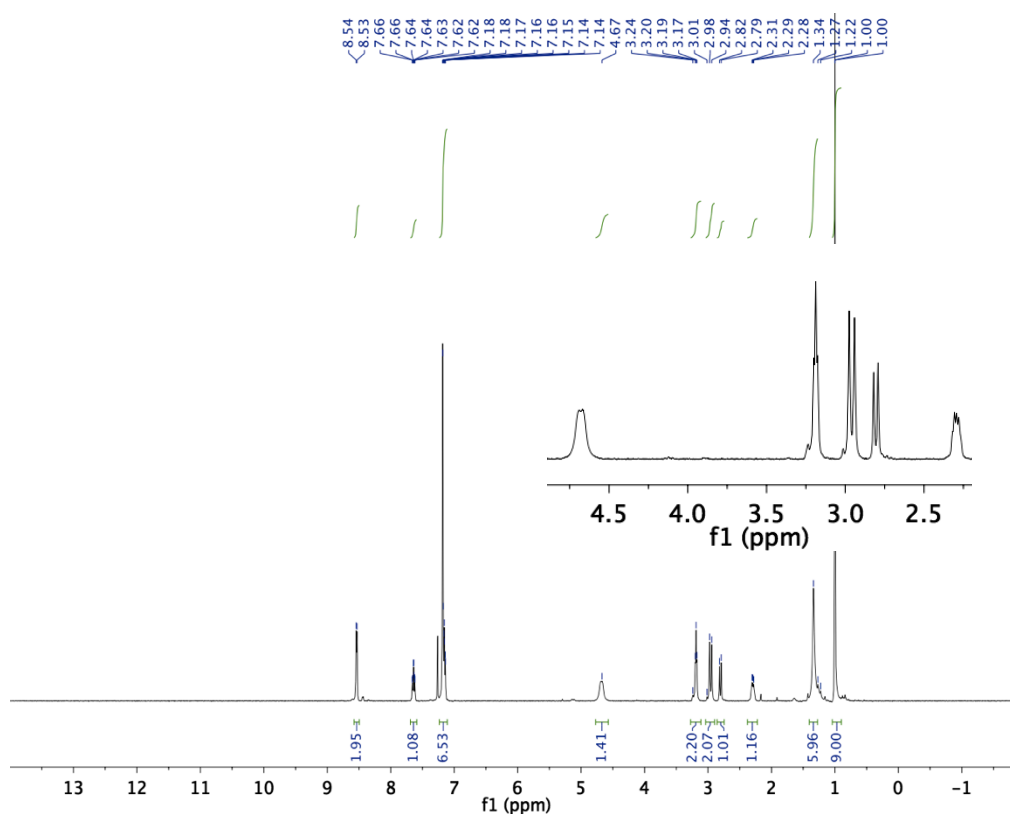
^{1}H NMR (700 MHz, DCl$_3$, 23 °C): δ 8.53 (d, J_{HH} = 5.7 Hz, 2H), 7.63 (t, J_{HH} = 7.7 Hz, 1H), 7.17 (app s, 6H), 4.67 (app s, 1H), 3.18 (t, J_{HH} = 5.0 Hz, 2H), 2.95 (d, J_{HH} = 13.4 Hz, 2H), 2.80 (d, J_{HH} = 10.5 Hz, 2H), 2.28 (dt, J_{HH} = 10.5, 5.0 Hz, 1H), 1.33 (s, 6H), 0.99 (s, 9H).

^{13}C NMR (176 MHz, CDCl$_3$, 23 °C): δ 185.2, 179.4, 152.2, 146.4, 138.5, 127.9, 124.8, 123.0, 75.7, 56.9, 39.9, 39.1, 35.3, 28.0.

^{19}F NMR (470 MHz, CDCl$_3$, 23 °C): δ –56.1 (t, 3H), –143.4 (m, 2H), –143.6 (m, 2H).

HRMS-electrospray (m/z): [M]$^+$ calcd. for C$_{27}$H$_{23}$F$_7$N$_3$OPd (1-B minus pivalate ligand), 644.0764; found, 644.0774.

Elemental Analysis calcd for C$_{32}$H$_{32}$F$_7$N$_3$O$_3$Pd, C: 51.52; H: 4.32; N: 5.63; found, C: 51.22; H: 4.11; N: 5.45.

2.4.4 Arylation Reactions with Pd Complexes
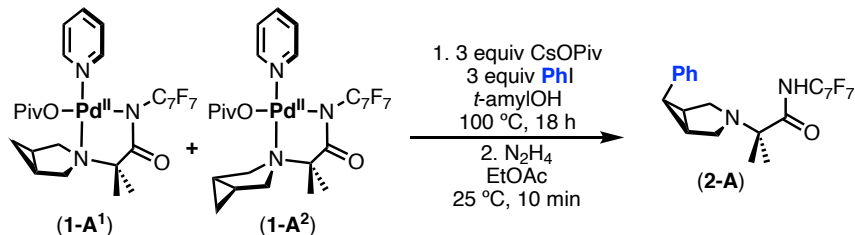
A 4 mL vial was charged with **1-A** (10 mg, 0.015 mmol, 1.0 equiv), cesium pivalate (10.5 mg, 0.045 mmol, 3.0 equiv), aryl iodide (5.0 µL, 0.045 mmol, 3.0 equiv), and *tert*-amyl alcohol (0.30 mL). The vial was sealed with a Teflon-lined cap and heated at 100 °C. After 18 h, the reaction was cooled, diluted with EtOAc, and quenched with hydrazine (6 drops). The reaction was stirred at room temperature for 10 min. The resulting suspension was filtered through a plug of Celite and concentrated under vacuum. The product (**2-A**) was obtained in 98% yield as determined by gas chromatography with 1,3,5-trimethoxybenzene added as a standard.
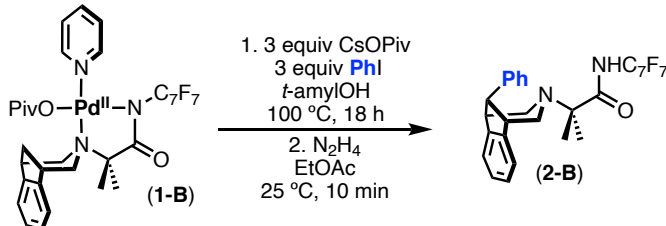
A 4 mL vial was charged with **1-B** (10.0 mg, 0.0134 mmol, 1.0 equiv), cesium pivalate (9.4 mg, 0.402 mmol, 3.0 equiv), aryl iodide (4.5 µL, 0.0402 mmol, 3.0 equiv), and *tert*-amyl alcohol (0.30 mL). The vial was sealed with a Teflon-lined cap and heated at 100 °C. After 18 h, the reaction was cooled, diluted with EtOAc, and quenched with hydrazine (6 drops). This mixture was stirred at room temperature for 10 min. The resulting suspension was filtered through a plug of Celite and concentrated under vacuum. The product (**2-B**) was obtained in 72% yield as determined by gas chromatography with 1,3,5-trimethoxybenzene added as a standard.

2.4.5 Hydrogen/Deuterium Exchange with Pd Complexes
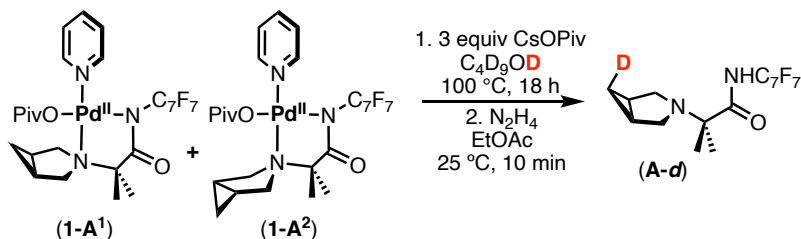
A 10 mL vial was charged with **1-A** (10 mg, 0.015 mmol, 1.0 equiv), cesium pivalate (9.4 mg, 0.0402 mmol, 3.0 equiv), and C_4D_9OD (0.30 mL). The vial was sealed with a Teflon-lined cap and heated at 100 °C (or the appropriate temperature listed in Table 2.2). After 18 h, the reaction was cooled, diluted with EtOAc, and quenched with hydrazine (6 drops). This mixture was stirred at room temperature for 10 min. The resulting suspension was filtered through a plug of Celite and concentrated under vacuum. The product (**A-d**) was obtained without further purification as a white solid (65% deuterium incorporation at 100 ºC with CsOPiv added). The ^{1}H and ^{2}H NMR spectra are shown in **Figure 2.5** (the star indicates the deuteration site).

Figure 2.5 From Bottom to Top Spectra: ^{1}H NMR Spectrum of **A** in CDCl$_3$ (700 MHz). ^{1}H NMR spectrum of **A-d** in CDCl$_3$ (700 MHz). ^{2}H NMR Spectrum of **A-d** in CHCl$_3$ with 1 drop of CDCl$_3$ (700 MHz)

HRMS-electrospray (m/z): [M]$^+$ calcd. for $C_{16}H_{13}D_2F_7N_2O$, 386.1198; found, 386.1217
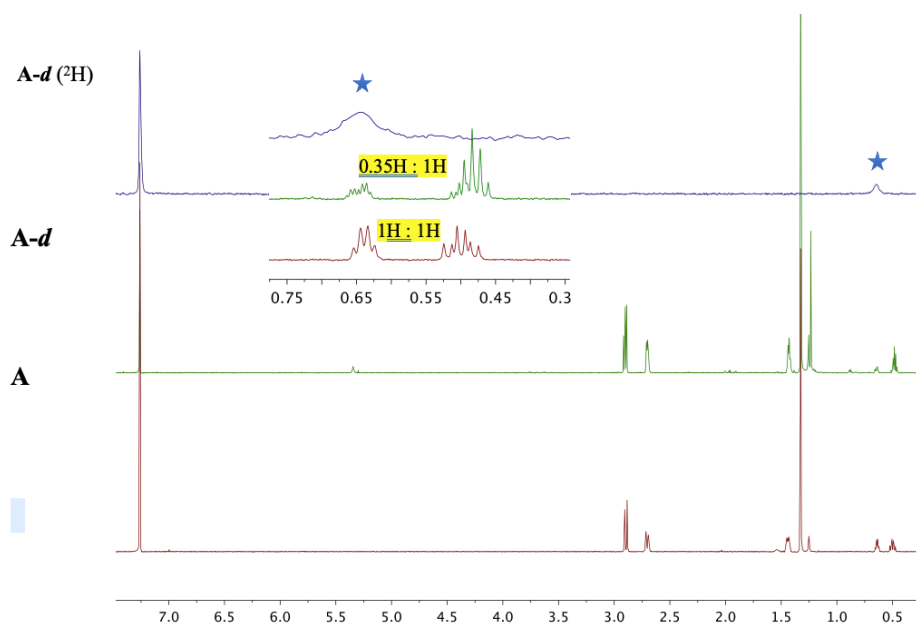
Melting point: 103-105 °C.

A 10 mL vial was charged with **1-B** (10.0 mg, 0.0134 mmol, 1.0 equiv), cesium pivalate (9.4 mg, 0.0402 mmol, 3.0 equiv) an C_4D_9OD (0.30 mL). The vial was sealed with a Teflon-lined cap and heated at 100 °C. After 18 h, the reaction was cooled, diluted with EtOAc, and quenched with hydrazine (6 drops). This mixture was stirred at room temperature for 10 min. The resulting suspension was filtered through a plug of Celite and concentrated under vacuum. The product (**B-d**) was obtained without further purification as a white solid (81% deuterium incorporation). ^{1}H and ^{2}H NMR spectrum shown in **Figure 2.6** (star indicates deuteration site).

Figure 2.6 From Bottom to Top Spectra: ^{1}H NMR Spectrum of **B** in CDCl$_3$ (700 MHz). ^{1}H NMR Spectrum of **B-d** in CDCl$_3$ (700 MHz). ^{2}H NMR Spectrum of **B-d** in CHCl$_3$ with 1 drop of CDCl$_3$ (700 MHz)

HRMS-electrospray (m/z): [M]$^+$ calcd. for C$_{22}$H$_{17}$D$_2$F$_7$N$_2$O, 462.1511; found, 462.1522.

Melting point: 115-117 °C

2.4.6 X-Ray Crystallography Data

X-Ray Crystallography Experimental Data of 1-A

Figure 2.7 X-Ray Crystal Structure of Complex **1-A^1** and **1-A^2**. Hydrogen Atoms expect H1 are Omitted for Clarity

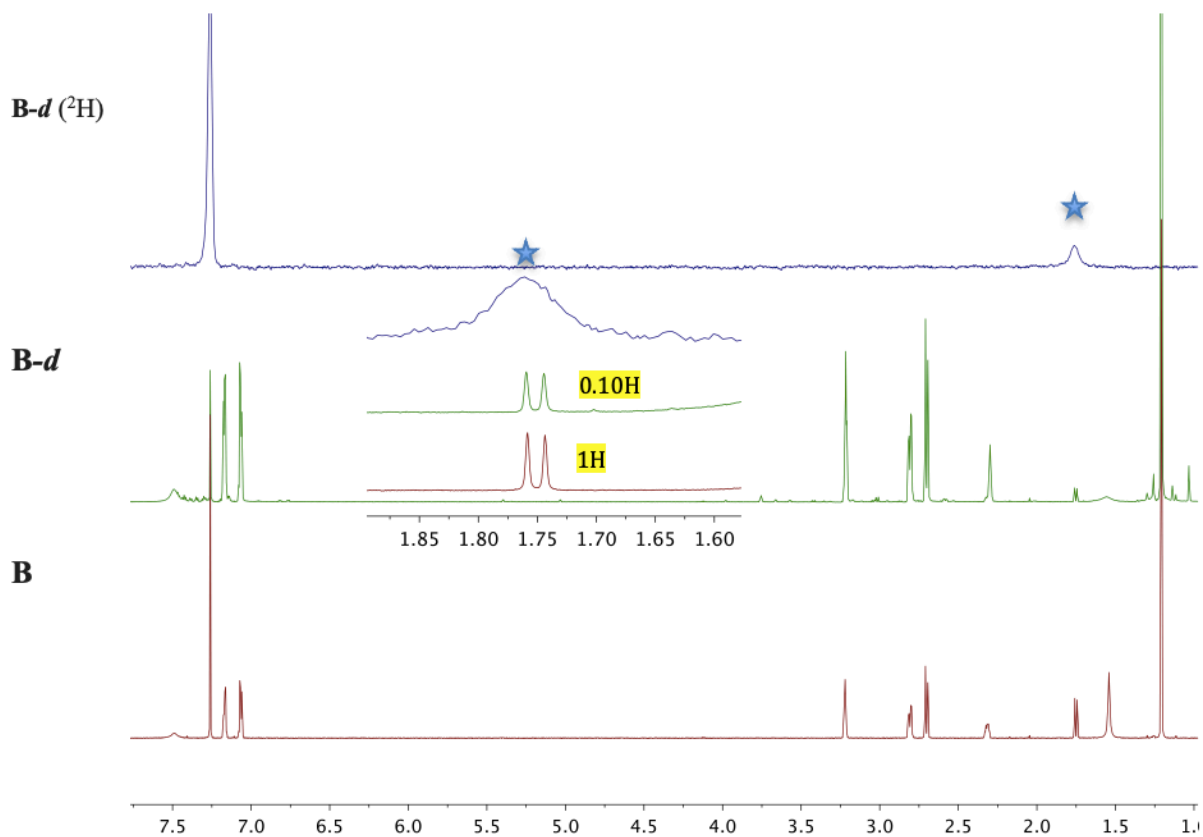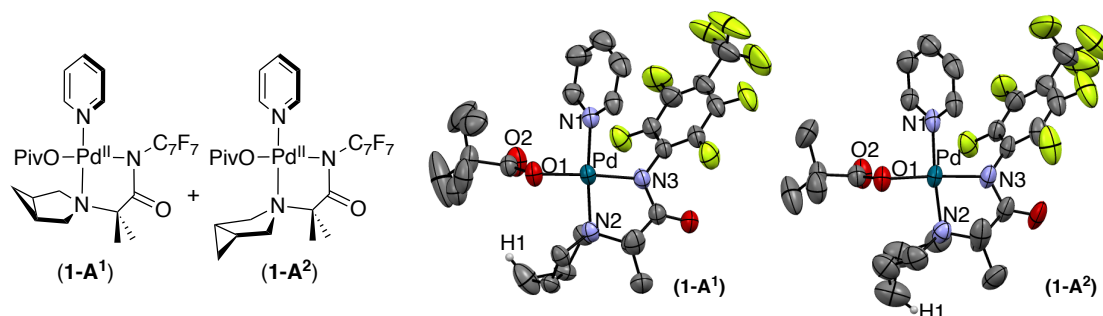Yellow blocks of **1-A** were grown by vapor diffusion of a dichloromethane/hexanes solution of the compound at 25 deg. C. A crystal of dimensions 0.15 x 0.14 x 0.13 mm was mounted on a Rigaku AFC10K Saturn 944+ CCD-based X-ray diffractometer equipped with a low temperature device and Micromax-007HF Cu-target micro-focus rotating anode (λ = 1.54187 A) operated at 1.2 kW power (40 kV, 30 mA). The X-ray intensities were measured at 225(1) K with the detector placed at a distance 42.00 mm from the crystal. A total of 2028 images were collected with an oscillation width of 1.0° in ω. The exposure times were 1 sec. for the low angle images, 5 sec. for high angle. Rigaku d*trek images were exported to CrysAlisPro for processing and corrected for absorption. The integration of the data yielded a total of 41954 reflections to a maximum 2θ value of 138.61° of which 10145 were independent and 9929 were greater than 2σ(I). The final cell constants (Table 2.3) were based on the xyz centroids of 26720 reflections above 10σ(I). Analysis of the data showed negligible decay during data collection. The structure was solved and refined with the Bruker SHELXTL (version 2016/6) software package, using the space group P1bar with Z = 4 for the formula $C_{26}H_{28}N_3O_3F_7Pd$. All non-hydrogen atoms were refined anisotropically with the hydrogen atoms placed in idealized positions. Full matrix least-squares refinement based on F^2 converged at R1 = 0.0449 and wR2 = 0.1193 [based on I > 2sigma(I)], R1 = 0.0457 and wR2 = 0.1198 for all data. Additional details are presented in Table 2.3 and are given as

G.M. Sheldrick (2015) "Crystal structure refinement with SHELXL", Acta Cryst., C71, 3-8 (Open Access).

CrystalClear Expert 2.0 r16, Rigaku Americas and Rigaku Corporation (2014), Rigaku Americas, 9009, TX, USA 77381-5209, Rigaku Tokyo, 196-8666, Japan.

CrysAlisPro 1.171.38.41 (Rigaku Oxford Diffraction, 2015).

Table 2.3 Crystal Data and Structural Refinement for **1-A**

Empirical Formula	$C_{26}H_{28}F_7N_3O_3Pd$
Formula Weight	669.91
Temperature	225 (2) K
Wavelength	1.54184 A
Crystal System	triclinic
Space Group	P-1
Unit Cell Dimensions	a = 11.9284(2) Å, α = 90.6890(10)°
	b = 15.2060(3) Å, β = 91.8040(10)°
	c = 16.0712(2) Å, γ = 106.135(2)°
Volume	2798.18(8) A^3
Z	4
Calculated Density	1.590 Mg/m^3
Absorption Coefficient	6.071 mm^{-1}
F(000)	1352
Crystal Size	0.15x0.14x0.13 mm
Theta Range for Data Collection	2.751 to 69.303
Limiting Indices	-14≤h≤14, -17≤k≤18, -19≤l≤19
Reflections Collected	41954
Independent Reflections	10145
Completeness to Theta	97.9%

Absorption Correction	Semi-empirical from equivalents
Max and Min Transmission	1.00000 to 0.58322
Refinement Method	Full-matrix least-squares on F^2
Data / Restraints / Parameters	10145 / 280 / 852
Goodness-of-Fit on F^2	1.076
Final R Indices [$l>2\sigma(l)$]	R1 = 0.0449, wR2 = 0.1193
R indices (all data)	R1 = 0.0457, wR2 = 0.1198
Extinction Coefficient	0.00559(19)
Largest Difference Peak and Hole	0.707 and -1.106 A^{-3}

X-Ray Crystallography Experimental Data of 1-B

Figure 2.8 X-Ray Crystal Structure of Complex **1-B**. Hydrogen Atoms expect H1 are Omitted for Clarity
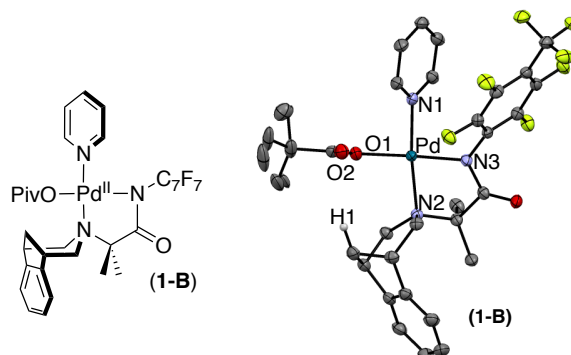
Yellow plates of **1-B** were grown from a dichloromethane/pentane solution of the compound at 22 deg. C. A crystal of dimensions 0.17 x 0.13 x 0.10 mm was mounted on a Rigaku AFC10K Saturn 944+ CCD-based X-ray diffractometer equipped with a low temperature device and Micromax-007HF Cu-target micro-focus rotating anode (λ = 1.54187 A) operated at 1.2 kW power (40 kV, 30 mA). The X-ray intensities were measured at 85(1) K with the detector placed at a distance 42.00 mm from the crystal. A total of 2028 images were collected with an oscillation width of 1.0° in ω. The exposure times were 1 sec. for the low angle images, 5 sec. for high angle. Rigaku d*trek images were exported to CrysAlisPro for processing and corrected for absorption. The

integration of the data yielded a total of 46436 reflections to a maximum 2θ value of 138.75° of which 5754 were independent and 5746 were greater than $2\sigma(I)$. The final cell constants (Table 2.4) were based on the xyz centroids 36972 reflections above $10\sigma(I)$. Analysis of the data showed negligible decay during data collection. The structure was solved and refined with the Bruker SHELXTL (version 2014/6) software package, using the space group P2(1)/c with Z = 4 for the formula $C_{32}H_{32}N_3O_3F_7Pd$. All non-hydrogen atoms were refined anisotropically with the hydrogen atoms placed in idealized positions. The carbons of the t-butyl portion of the pivalate ligand are rotationally disordered. Full matrix least-squares refinement based on F^2 converged at R1 = 0.0255 and wR2 = 0.0255 [based on I > 2sigma(I)], R1 = 0.0678 and wR2 = 0.0678 for all data. Additional details are presented in Table 2.4 and are given as Supporting Information in a CIF file. Acknowledgement is made for funding from NSF grant CHE-0840456 for X-ray instrumentation.

Sheldrick, G.M. SHELXTL, v. 2014/6; Bruker Analytical X-ray, Madison, WI, 2014.

CrystalClear Expert 2.0 r16, Rigaku Americas and Rigaku Corporation (2014), Rigaku Americas, 9009, TX, USA 77381-5209, Rigaku Tokyo, 196-8666, Japan.

CrysAlisPro 1.171.38.41 (Rigaku Oxford Diffraction, 2015).

Table 2.4 Crystal Data and Structural Refinement for **1-B**

Empirical Formula	$C_{32}H_{32}F_7N_3O_3Pd$
Formula Weight	746.00
Temperature	85 (2) K
Wavelength	1.54184 A
Crystal System	Monoclinic
Space Group	P2(1)/c

Unit Cell Dimensions	a = 11.93742(6) Å, α = 90 °
	b = 17.17739(10) Å, β = 99.4512(5) °
	c = 15.29186(8) Å, γ = 90 °
Volume	3093.09(3) A^3
Z	4
Calculated Density	1.602 Mg/m^3
Absorption Coefficient	5.563 mm^{-1}
F(000)	1512
Crystal Size	0.170 x 0.130 x 0.100 mm
Theta Range for Data Collection	4.553 to 69.377 °
Limiting Indices	-14≤h≤14, -20≤k≤20, -18≤l≤18
Reflections Collected	46436
Independent Reflections	5754
Completeness to Theta	99.9%
Absorption Correction	Semi-empirical from equivalents
Max and Min Transmission	1.00000 to 0.64683
Refinement Method	Full-matrix least-squares on F^2
Data / Restraints / Parameters	5754 / 42 / 451
Goodness-of-Fit on F^2	1.094
Final R Indices [l>2σ(l)]	R1 = 0.0255, wR2 = 0.0678
R indices (all data)	R1 = 0.0255, wR2 = 0.0678
Extinction coefficient	0.00103(8)
Largest Difference Peak and Hole	0.590 and -0.757 A^{-3}

2.5 References

(1) (a) Vitaku, E.; Smith, D. T.; Njardarson, J. T. Analysis of the Structural Diversity, Substitution Patterns, and Frequency of Nitrogen Heterocycles among U.S. FDA Approved Pharmaceuticals. *J. Med. Chem.* **2014**, *57*, 10257. (b) Taylor, R. D.; MacCoss, M.; Lawson, A. D. G. Rings in Drugs. *J. Med. Chem.* **2014**, *57*, 5845-5859.

(2) (a) Godula, K.; Sames, D. C–H Bond Functionalization in Complex Organic Synthesis. *Science* **2006**, *312*, 67-72. (b) Campos, K. R. Direct sp^3 C–H Bond Activation Adjacent to Nitrogen in Heterocycles. *Chem. Soc. Rev.* **2007**, *36*, 1069-1084. (c) Mitchell, E. A.; Peschiulli, A.; Lefevre, N.; Meerpoel, L.; Maes, B. U. W. Direct α-Functionalization of Saturated Cyclic Amines. *Chem. Eur. J.* **2012**, *18*, 10092-10142. (d) Shi, L.; Xia, W. Photoredox Functionalization of C–H Bonds Adjacent to a Nitrogen Atom. *Chem. Soc. Rev.* **2012**, *41*, 7687-7697. (e) Noisier, A. F.; Brimble, M. A. C–H Functionalization in the Synthesis of Amino Acids and Peptides. *Chem. Rev.* **2014**, *114*, 8775-8806. (f) Seidel, D. The Azomethine Ylide Route to Amine C–H Functionalization: Redox-Versions of Classic Reactions and a Pathway to New Transformation. *Acc. Chem. Res.* **2015**, *48*, 317-328.

(3) (a) Topczewski, J. J.; Cabrera, P. J.; Saper, N. I.; Sanford, M. S. Palladium-Catalysed Transannular C–H Functionalization of Alicyclic Amines. *Nature*, **2016**, *531*, 220-224. (b) Cabrera, P. J.; Lee, M.; Sanford, M. S. Second-Generation Palladium Catalyst System for Transannular C–H Functionalization of Azabicycloalkanes. *J. Am. Chem. Soc.* **2018**, *140*, 5599-5605.

(4) Examples of C–H functionalization at C-2 of alicyclic amines, see: (a) Pastine, S. J.; Gribkov, D. V.; Sames, D. sp^3 C–H Bond Arylation Directed by Amidine Protecting Groups: α-Arylation of Pyrrolidines and Piperidines. *J. Am. Chem. Soc.* **2006**, *128*, 14220-14221. (b) Mitchell, E. A.; Peschiulli, A.; Lefevre, N.; Meerpoel, L.; Maes, B. U. W. Direct α-Functionalization of Saturated Cyclic Amines. *Chemistry*, **2012**, *18*, 10092-10142. (c) Shi, L.; Xia, W. Photoredox functionalization of C–H Bonds Adjacent to a Nitrogen Atom. *Chem. Soc. Rev.* **2012**, *41*, 7687-7697. (d) He, J.; Hamann, L.G., Davies, H. M. L.; Beckwith, R. E. J. Late-Stage C–H Functionalization of Complex Alkaloids and Drugs Molecules via Intermolecular Rhodium-Carbenoid Insertion. *Nature Commun.* **2015**, *6*, 5943. (e) Spangler, J. E.; Kobayashi, Y.; Verma, P.; Wang, D.-H.; Yu, J.-Q. α-Arylation of Saturated Azacycles and N-methylamines via Palladium(II)-Catalyzed C(sp^3) –H Coupling. *J. Am. Chem. Soc.* **2015**, *137*, 11876-11879. (f) Chen, W.; Ma, L.; Paul, A.; Seidel, D. Direct α-C–H Bond Functionalization of Unprotected Cyclic Amines. *Nature Chem.* **2018**, *10*, 165-169.

(5) Examples of fluoroamide directing groups in Pd-catalyzed C–H functionalization: (a) Chen, X.; Engle, K. M.; Wang, D.-H.; Yu, J.-Q. *Angew. Chem. Int. Ed.* **2009**, *48*, 5094-5115. (b) Lyons, T.; Sanford, M. S. Palladium-Catalyzed Ligand-Directed C–H Functionalization Reactions. *Chem. Rev.* **2010**, *110*, 1147-1169. (c) He, J.; Wasa, M.; Chan, L. S. K.; Shao, Q. Yu, J.-Q. Palladium-Catalyzed Transformations of Alkyl C–H Bonds. *Chem. Rev.* **2017**, *117*, 8754-8786.

(6) Bercaw, J. E.; Day, M. W.; Golisz, S. R.; Hazari, N.; Henling, L. M.; Labinger, J. A.; Schofer, S. J.; Virgil, S. Robotic Lepidoptery: Structural Characterization of (mostly) Unexpected Palladium Complexes Obtained from High-Throughput Catalyst Screening. *Organometallics* **2009**, *28*, 5017-5024.

(7) Dewyer, A. L.; Zimmerman, P. M. Simulated Mechanism for Palladium-Catalyzed Directed γ-Arylation of Piperidine. *ACS Catal.* **2017**, *7*, 5466-5477.

(8) Reviews on C(sp)^3–H cyclopalladation: (a) Ryabov, A. D. Mechanisms of Intramolecular Activation of C–H Bonds in Transistion-Metal Complexes. *Chem. Rev*. **1990**, *90*, 403-424. (b) Baudoin, O. Transistion Metal-Catalyzed Arylation of Unactivated C(sp^3)–H Bonds. *Chem. Soc. Rev.* **2011**, *40*, 4902-4911. (c) Rouquet, G.; Chatani, N. Catalytic Functionalization of C(sp^2)–H and C(sp^3)–H Bonds by Using Bidentate Directing Groups. *Angew. Chem. Int. Ed.* **2013**, *52*, 11726-11743. (d) Tran, L. D.; Roane, J.; Daugulis, O. Bidentate, Monoanionic Auxiliary-Directed Functionalization of Carbon-Hydrogen Bonds. *Acc. Chem. Res*. **2015**, *48*, 1053-1064.

(9) Examples of amine or amide-directed C(sp^3)–H activation to form stable palladacycles: (a) Shabashov, D.; Daugulis, O. Auxiliary-Assisted Palladium-Catalyzed Arylation and Alkylation of sp^2 and sp^3 Carbon-Hydrogen Bonds. *J. Am. Chem. Soc.* **2010**, *132*, 3965-3972. (b) Calleja, J.; Pla, D.; Gorman, T. W.; Domingo, V.; Haffemayer, B.; Gaunt, M. J. A Steric Tethering Approach Enables Palladium- Catalysed C–H Activation of Primary Amino Alcohols. *Nature Chem.* **2015**, *7*, 1009-1016. (c) Xu, Y.; Young, M. C.; Wang, C.; Magness, D. M.; Dong, G. Catalytic C(sp^3)–H Arylation of Free Primary Amines with an *exo* Directing Group Generated In-Situ. *Angew. Chem. Int. Ed.* **2016**, *55*, 9084-9087. (d) Ren, Z.; Dong, G. Direct Observation of C–H Cyclopalladation at Tertiary Positions Enabled by an Exo-Directing Group. O*rganometallics* **2016**, *35*, 1057-1059. (e) Cabrera-Pardo, J. R.; Trowbridge, A.; Nappi, M.; Ozaki, K.; Gaunt, M. J. Selective Palladium(II)-Catalyzed Aliphatic Carbonylation of Methylene b-C–H Bonds in Aliphatic Amines. *Angew. Chem. Int. Ed.* **2017**, *56*, 11958-11962. (f) Coomber, C. E.; Benhamou, L.; Bucar, D.-K.; Smith, P. D.; Porter, M. J.; Sheppard, T. D. Silver-Free Palladium-Catalyzed C(sp^3)–H Arylation of Saturated Bicyclic Amines Scaffolds. *J. Org. Chem.* **2018**, *83*, 2495-2503.

(10) The arylation reactions can also be performed at 60 °C, yielding 4% of **2-A** and 55% of **2-B**.

(11) (a) Jones, W. D. Isotope Effects in C–H Bond Activation Reactions by Transition Metals. *Acc. Chem. Res.* **2003**, *36*, 140. (b) Blum, S. A.; Tan, K. L. Bergman, R. G. Application of Physical Organic Methods to the Investigation of Organometallic Reaction Mechanisms. *J. Org. Chem.* **2003**, *68*, 4127. (c) Lloyd-Jones, G.; Muñoz, M. P. Isotopic Labelling in the Study of Organic and Organometallic Mechanism and Structure: An Account. *J. Labelled Compd. Radiopharm*. **2007**, *50*, 1072. (d) Evans, L. A.; Fey, N.; Lloyd-Jones, G. C.; Muñoz, M. P.; Slatford, P. A. Cryptocatalytic 1,2-Alkene Migration in a σ-Alkyl Palladium Diene Complex. *Angew. Chem. Int. Ed.* **2009**, *48*, 6262-6265. (e) Gómez-Gallego, M.; Sierra, M. A. *Chem. Rev.* **2011**, *111*, 4857-4963. (f) Simmons, E. M.; Hartwig, J. F. *Angew. Chem. Int. Ed*. **2012**, *51*, 3066-3072. (g) Ma, S.; Villa, G.; Thuy-Boun, P. S.; Homs, A.; Yu, J.-Q. Palladium-Catalyzed ortho-Selective C–H Deuteration of Arenes: Evidence for Superior Reactivity of Weakly Coordinated Palladacycles. *Angew. Chem*. **2014**, *126*, 753-756. (h) Zhao, D.; Luo, H.; Chen, B.; Chen, W.; Zhang, G.; Yu, Y. Palladium-Catalyzed H/D Exchange Reaction with 8-aminoquinoline as the Directing Group: Access to *ortho*-Selective Deuterated Aromatic Acids and *beta*-Selective Deuterated Aliphatic Acids. *J. Org. Chem.* **2018**, 83, *15*, 7860-7866.

(12) As expected, D incorporation at the NH of the directing group is also observed.

(13) (a) Lapointe, D.; Fagnou, K. Overview of the Mechanistic Work on the Concerted Metallation-Deprotonation Pathway. *Chem. Lett*. **2010**, *39*, 1118-1126. (b) Livendahl, M.; Echavarren, A. M. Palladium-Catalyzed Arylation Reactions: A Mechanistic Perspective. *Isr. J. Chem.* **2010**, *50*, 630-651. (c) Gary, J. B.; Sanford, M. S. Participation of Carbonyl Oxygen in Carbon-Carboxylate Bond-Forming Reductive Elimination from Palladium. *Organometallics* **2011**, *30*, 6143-6149. (d) Ackermann, L. Carboxylate-Assisted Transistion-Metal-Catalyzed C–H Bond Functionalizations: Mechanism and Scope. *Chem. Rev.* **2011**, *111*, 1315-1345. (e) Gorelsky, S. I.; Lapointe, D.; Fagnou, K. Analysis of the Palladium-Catalyzed (Aromatic)C–H Bond

Metalation-Deprotonation Mechanism Spanning the Entire Spectrum of Arenes. *J. Org. Chem.* **2012**, *77*, 658-668. (f) Gorelsky, S. I. Origins of Regioselectivity of the Palladium-Catalyzed (Aromatic)C–H Bond Metalation-Deprotonation. *Coordination Chemistry Reviews* **2013**, *257*, 153-164.

Chapter 3   Investigating Diverse Oxidants for Pd-Mediated Transannular
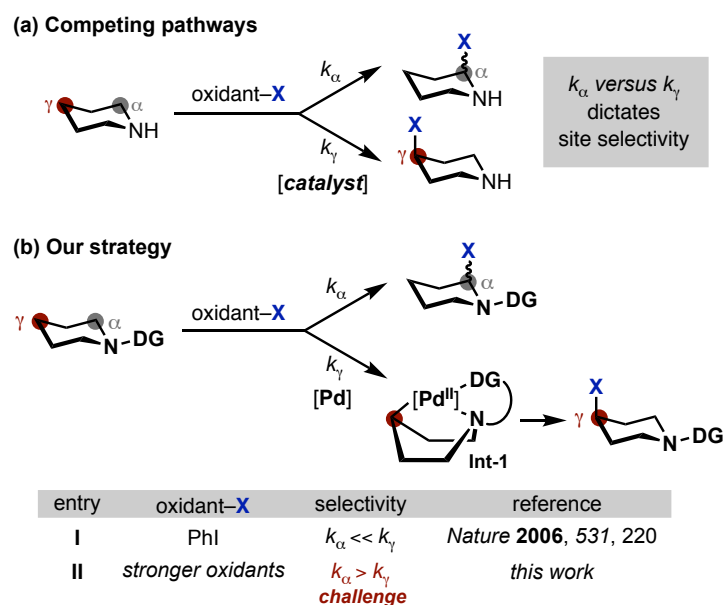**Functionalization of Alicyclic Amines**

Note: This Chapter is based on work published in Aguilera, E. Y.; Sanford, M. S.* "Palladium-Mediated Cγ–H Functionalization of Alicyclic Amines" *Angew. Chem. Int. Ed*. **2021**, 10.1002/anie.202101782.

3.1 Introduction

Alicyclic amines bearing various substitution patterns are common structural motifs in bioactive molecules.[1] Conventional synthetic routes to these structures require multi-step sequences to assemble the appropriately functionalized alicyclic amine cores.[2] Approaches involving the late-stage C–H functionalization of pre-assembled alicyclic amines would complement existing synthetic routes and thus streamline the diversification of these motifs. Over the past several decades, numerous methods have been developed for functionalization at the activated C_α–H position of alicyclic amines (Scheme 3.1a, k_α).[3] These studies have shown that the proximity of the C_α–H bond to nitrogen greatly enhances its reactivity towards oxidative functionalization.[4] For example, $C(sp^3)$–H bonds α to nitrogen have relatively low bond dissociation energies (~90 kcal/mol).[5] Furthermore, oxidation of nitrogen to a radical cation renders the C_α–H site highly acidic ($pK_a \sim 16$) relative to unactivated $C(sp^3)$–H bonds ($pK_a > 50$).[6] In contrast, the $C(sp^3)$–H bonds that are remote from nitrogen (for example, C_γ–H) are typically much less reactive than C_α–H, making it significantly more challenging to selectively target these sites.

Conceptually, the selective γ-functionalization of alicyclic amines requires controlling the relative reactivity of the C_α–H (Scheme 3.1a, k_α) versus C_γ–H sites (Scheme 3.1a, k_γ). To date, most successful efforts have achieved selectivity through modification of the substrate. Common strategies involve (a) blocking the C_α–H sites with other substituents (thus decreasing k_α),[7] (b) protonating the amine nitrogen to electronically deactivate C_α–H (thus decreasing k_α),[8] or (c) employing a directing group to accelerate C_γ–H functionalization (increasing k_γ).[9] In an example of the latter, our group recently demonstrated that installing a directing group on the amine nitrogen can enable transannular C_γ–H activation via a boat-like intermediate (**Int-1**, Scheme 3.1b).[10] When the Pd catalyst for this transformation is paired with a mild aryl iodide (ArI) oxidant, k_γ is significantly greater than k_α. As such, directed transannular C–H arylation outcompetes background α-functionalization (Scheme 3.1b, entry **I**).

Scheme 3.1 (a) Competing C_α–H versus C_γ–H (b) Our Strategy

| entry	oxidant–**X**	selectivity	reference
I	PhI	$k_\alpha \ll k_\gamma$	*Nature* **2006**, *531*, 220
II	*stronger oxidants*	$k_\alpha > k_\gamma$ *challenge*	*this work*

An important goal for enhancing the utility of this transformation is to broaden the scope of functional groups that can be selectively introduced at C_γ. In principle, this can be achieved by

replacing the aryl iodide with an alternative oxidant (oxidant–X) that is designed to transfer the functional group of interest (X). However, in practice, changing to alternative, more kinetically reactive oxidants (for example, *N*-halosuccinimides, hypervalent iodine reagents, electrophilic fluorinating reagents) results in a dramatic increase in k_α, such that the background α-functionalization pathway predominates (Scheme 3.1b, entry **II**; *vide infra* for examples). In this chapter, we present a strategy to address this challenge that leverages the stoichiometric *in situ* formation of Pd(II) amine complexes to enable selective transannular C_γ–H functionalization with a wide range of oxidants.

3.2 Results and Discussion

Initial studies targeted the Pd-catalyzed transannular C_γ–H bromination of **1-A** with *N*-bromosuccinimide (NBS). Notably, NBS has been successfully employed in related Pd-catalyzed ligand-directed $C(sp^3)$–H bromination reactions (of non-amine containing substrates),[11] while **1-A** was shown to be an effective substrate for transannular C–H arylation with PhI. At 100 °C in *tert*-amyl alcohol, **1-A** reacts with PhI to afford the C_γ–H phenylation product in 30% yield, with *no detectable background α-functionalization products* ($k_\alpha \ll k_\gamma$). However, when NBS was used in place of PhI under otherwise analogous catalytic conditions, none of the C_γ–H bromination product **γ-Br** was detected (Scheme 3.2). Instead, α-oxidation products **α-N** and **α-O** were formed in 30%
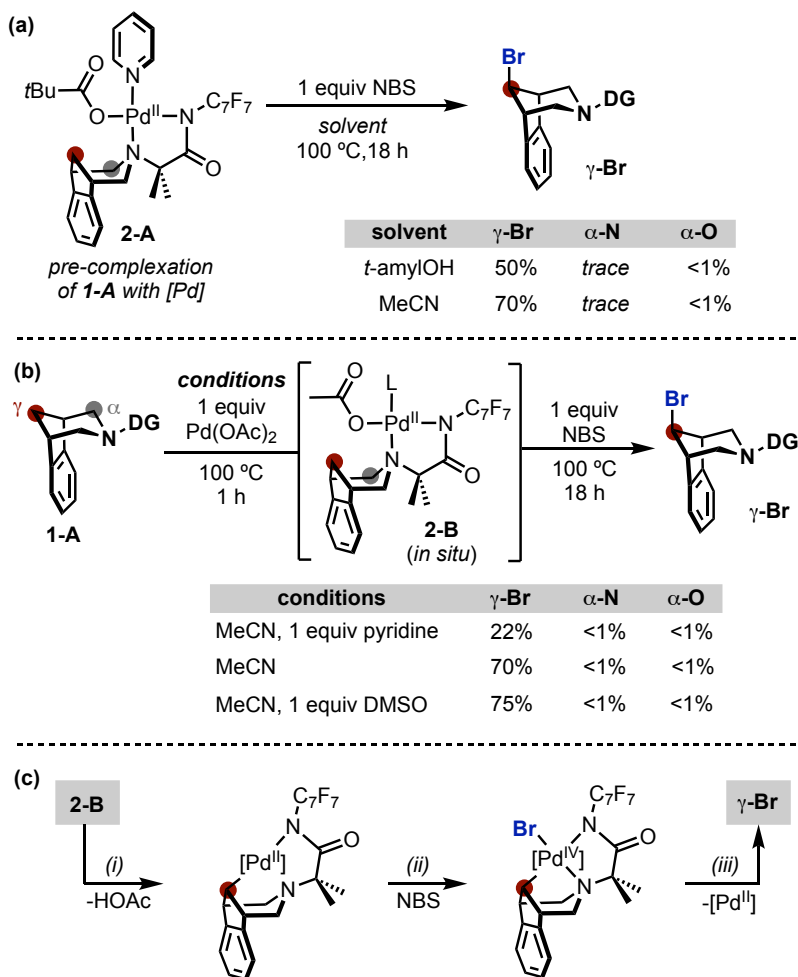
Scheme 3.2 Pd-Catalyzed Bromination with NBS

conditions	γ-Br	α-N	α-O
with [Pd]	>1%	30%	30%
without [Pd]	>1%	25%	31%
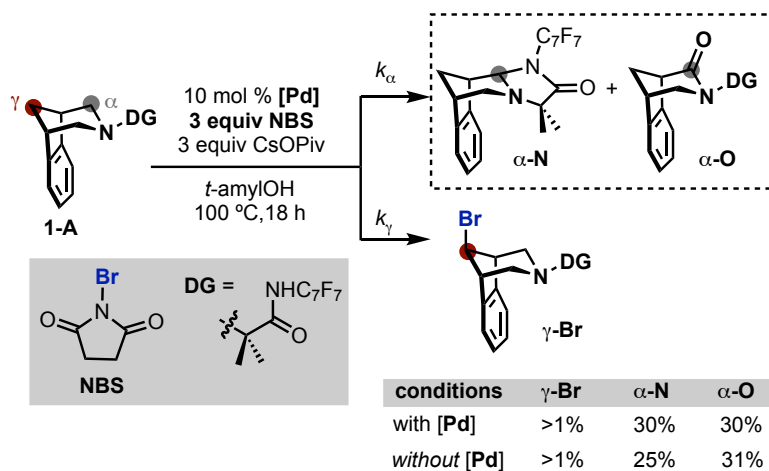
and 30% yield, respectively (Scheme 3.2). When this reaction was conducted in the absence of Pd

catalyst, **α-N** and **α-O** were obtained in nearly identical yields of 25% and 31%, respectively.

These results demonstrate that with NBS, the rate of background α-oxidation (k_α) is significantly

greater than that of Pd-catalyzed γ-oxidation (k_γ).

We hypothesized that these relative rates might be reversed by pre-assembling a complex

between substrate **1-A** and Pd (Scheme 3.3a).[12] This proposal was predicated on our previous work

(Chapter 2) showing that γ-H/D exchange is fast at the isolable Pd-complex **2-A** (occurring at

temperatures as low as 40 °C).[12] This suggests that pre-complexation to Pd could enhance k_γ versus

k_α in the NBS reactions. Indeed, the treatment of 1 equiv of complex **2-A** with 1 equiv of NBS in

tert-amyl alcohol at 100 °C for 18 h led to the selective formation of **γ-Br** in 50% yield (Scheme

3.3a). Only traces (<1%) of **α-N/α-O** were detected in this stoichiometric reaction. **γ-Br** was

formed as a single regio- and stereoisomer, as determined by NMR spectroscopy. As discussed

below, this stereochemistry suggests that C$_\gamma$–Br bond formation occurs via an inner sphere process

with retention of configuration. Changing the solvent to MeCN led to a higher (70%) yield of **γ-**

Br, again with <1% of **α-N/α-O**.

To render this approach more practical, we next pursued a 2-step 1-pot approach to the *in situ* assembly/γ-functionalization of a **1-A**/Pd complex. First, 1 equiv of **1-A**, 1 equiv of Pd(OAc)$_2$, and 1 equiv of pyridine were stirred at 100 °C for 1 h in MeCN. NBS (1 equiv) was then added and the mixture was heated at 100 °C for an additional 18 h. This afforded a modest 22% yield of γ-**Br** with <1% of α-**N**/α-**O** (Scheme 3.3b). A control reaction without added pyridine gave 70% yield of γ-**Br**, and the addition of 1 equiv of DMSO further improved the yield to 75% while maintaining high selectivity (<1% of α-**N**/α-**O**).[13]

Scheme 3.3 (a) γ-**Br** with Complex **2-A** (b) *In situ* Method for γ-**Br** (c) Proposed Pathway

solvent	γ-**Br**	α-**N**	α-**O**
t-amylOH	50%	*trace*	<1%
MeCN	70%	*trace*	<1%

| conditions	γ-**Br**	α-**N**	α-**O**
MeCN, 1 equiv pyridine	22%	<1%	<1%
MeCN	70%	<1%	<1%
MeCN, 1 equiv DMSO	75%	<1%	<1%

A proposed pathway for this sequence based on literature precedent for the individual steps is shown in Scheme 3.3c. Initial coordination of **1-A** to Pd(OAc)$_2$ affords **2-B** with L = MeCN or DMSO.[12] Acetate-assisted transannular C$_\gamma$–H activation[10c, 14] (Scheme 3.3c, *i*) is followed by oxidation of this σ-alkyl Pd^{II} intermediate to Pd^{IV} with NBS (Scheme 3.3c, *ii*).[15] C(sp^3)–Br bond-forming reductive elimination from this highly reactive Pd^{IV} center[16] then proceeds via an inner sphere mechanism with retention of configuration at carbon[17] to afford the product **γ-Br** (Scheme 3.3c, *iii*).

Figure 3.1 γ-Functionalizations with *in situ* Method
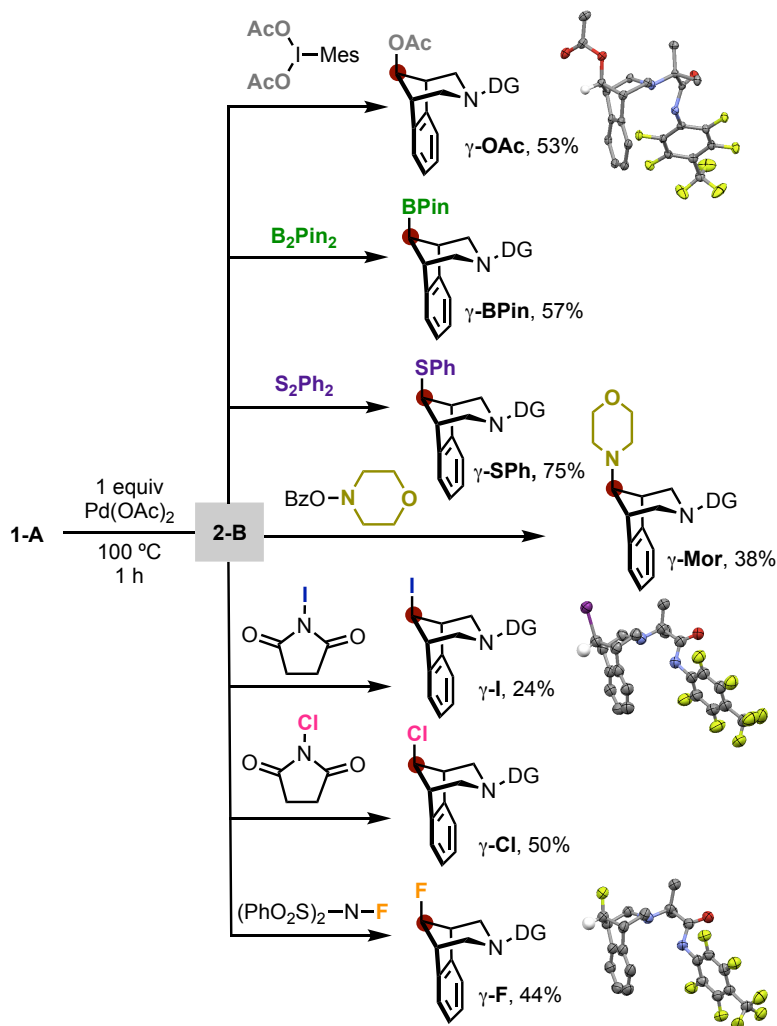
We next explored the use of a series of different oxidants in this 2-step, 1-pot protocol in order to install diverse functional groups at the γ-position. As shown in Figure 3.1, this approach enabled the formation of C–O, C–S, C–N, C–F, C–Cl, C–I, and C–B bonds in high γ-selectivity and modest to good isolated yield. The site- and stereoselectivity of each functionalization was established via ^{1}H NMR spectroscopy (all products) as well as X-ray crystallography (for **γ-I, γ-F, γ-OAc**). In all cases, the major product derived from C_γ–H functionalization.[18]

Scheme 3.4 Scope of C_γ-BPin Functionalization
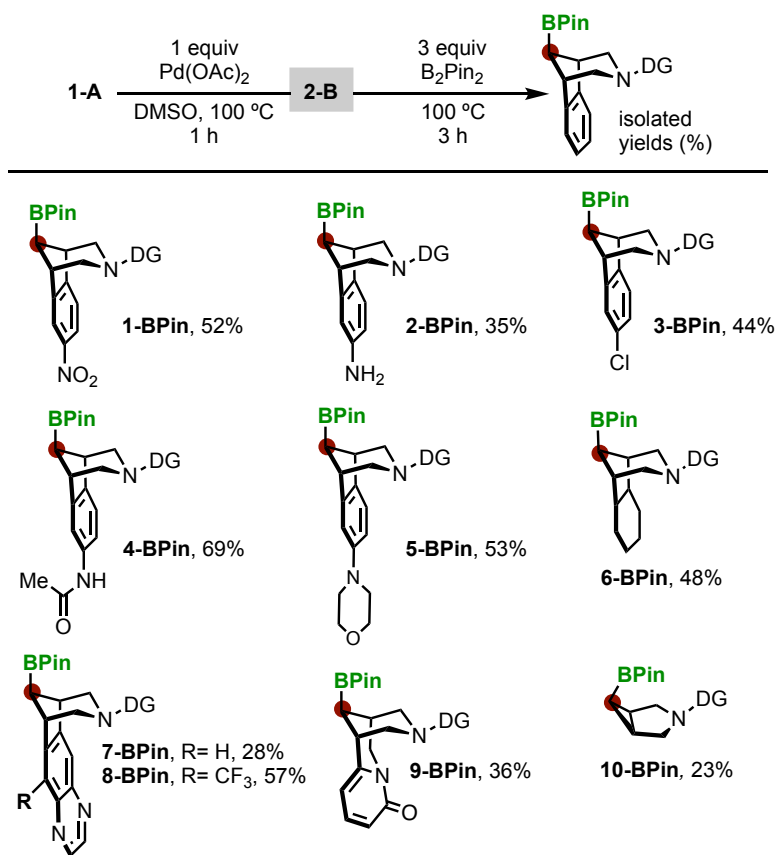
Then, we evaluated the scope of C_γ–H functionalization with respect to alicyclic amine substrates. The borylation reaction with B_2Pin_2 was selected for this study based on the versatility of the boronate ester products (which are readily transformed into amines, alcohols, or C–C

bonds).[19] As shown in Scheme 3.4, substrates bearing electron deficient (**1-BPin**) and halide containing compounds (**3-BPin**) were tolerant under these conditions. Of note, free and protected amines (**2-BPin** and **4-BPin,** respectively) provided sufficient yields of the borylated product. More complex functionalities, such as morpholine groups (**5-BPin**) and bicyclic compounds (**6-BPin**) were also suitable for this transformation. Varenicline (**7-BPin**) and its CF_3-substituted derivative (**8-BPin**) were well tolerated in 28% and 57% yield, respectively. Cytisine (**9-BPin**) also worked yielding 36%. In addition, the amitifadine core (**10-BPin**) was tolerated, albeit in low yields. In cases with simple piperidines as the substrate, only starting material and α-functionalization was observed.

Finally, we aimed to translate our stoichiometric γ-borylation studies to a catalytic approach. Altering the Pd loading from 1 equiv to 10 mol % under otherwise identical conditions afforded **γ-BPin** in 15% yield with the remaining mass balance as **1-A** (Table 3.1). This result reveals that catalyst turnover is a key challenge under these conditions. As such, we hypothesized that since the reaction undergoes a concerted-metalation deprotonation mechanism adding a base should facilitate more turnovers. Carbonate and carboxylate bases were therefore investigated (see Table 3.2 in Experimental Procedures) with Li_2CO_3 providing an improved yield of 50% (Table 3.1). Lastly, increasing the reaction temperature to 100 to 130 °C gave an optimized yield of 60% for **γ-BPin.** Substrates from Scheme 3.4 were performed under the catalytic conditions and low yields were observed with unreacted starting material remaining in all cases. While this method did not translate well to a broader substrate scope, it serves as a proof-of-concept of rapidly translating a stoichiometric approach to catalysis.

Table 3.1 Pd-Catalyzed γ-Borylation
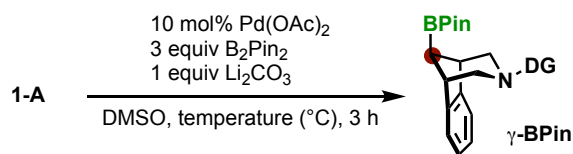
| additive	temperature (°C)	γ–BPin
none	100	15%
Li$_2$CO$_3$	100	50%
Li$_2$CO$_3$	130	55%

3.3 Conclusions

In summary, this chapter describes a strategy for the selective C$_\gamma$–H oxidation of alicyclic amine substrates via pre-formation of amine-Pd complexes. This pre-complexation increases the relative rate of the desired C$_\gamma$–H activation versus competing background C$_\alpha$–H oxidation. This work adds to a growing suite of methods in which the use of stoichiometric Pd enables selective late-stage diversification of complex organic molecules.[20] While catalytic processes are often favored by the organic chemistry community, this stoichiometric approach provides rapid and selective access to numerous challenging-to-synthesize alicyclic amine derivatives. In the context of, for example, medicinal chemistry, the speed, selectivity, and diversity of products generated via this approach counterbalance the cost of the Pd. Ultimately, we anticipate that pre-complexation could prove valuable for tuning selectivity in other reactions of alicyclic amines as well as in metal-mediated C–H functionalizations of more diverse substrates.

3.4 Outlook

We are interested in developing Pd-catalyzed γ-functionalization methods from select stoichiometric functionalizations described above. Initial attempts focused on Pd-catalyzed γ-fluorination due to its' importance in pharmaceuticals and positron emission tomography (PET) imaging. Our preliminary optimization results show that by pre-stirring substrate **1-A**, 20 mol % Pd(OAc)₂, 20 mol% of **ligand 1**, and NaOAc in MeCN for 1 h followed by sequential addition of NSFI, **γ-F** was achieved in 40% yield with unreacted **1-A** remaining (Scheme 3.5). Further optimization will attempt to lower the loading of Pd to 10 mol %. Additionally, we are currently investigating this catalytic method towards pharmaceutical drugs such as Chantix.

Scheme 3.5 Pd-Catalyzed γ-Fluorination
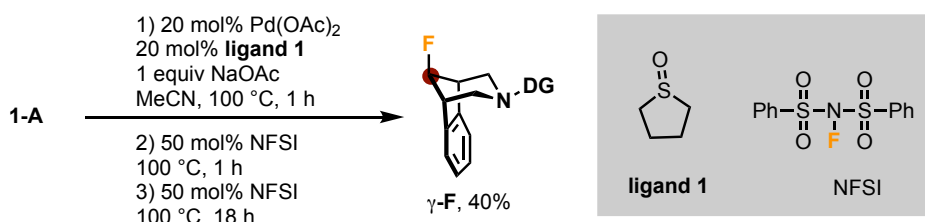
With this method in hand, we investigated additional oxidants that were successful in our stoichiometric work. We observed *N*-chlorosuccinimide afforded **γ-Cl** in 20% yield while *N*-bromosuccinimide and *N*-iodosuccinimide gave 0% and trace yields of their corresponding products, respectively. Additionally, using iodomesitylene diacetate as the oxidant afforded **γ-OAc** in trace yields (see Section 3.5.7). These preliminary catalysis results provide a starting point for further optimization to improve upon these methodologies.

3.5 Experimental Procedures

### 3.5.1 General Procedures, Materials and Methods

General Procedures

NMR spectra were obtained on a Varian VNMR 700 (699.76 MHz for ^{1}H; 175.95 MHz for ^{13}C) or a Varian VNMR 500 (500.09 MHz for ^{1}H; 470.56 MHz for ^{19}F) or a Varian NMR 400 (128.38 MHz for ^{11}B NMR) spectrometer. ^{1}H and ^{13}C chemical shifts are reported in parts per million (ppm) relative to TMS, with the residual solvent peak (most commonly CDCl$_3$) used as an internal reference. ^{19}F chemical shifts are reported in ppm and are referenced on a unified scale to the frequency of the residual solvent peak in the ^{1}H NMR spectrum. ^{1}H and ^{19}F multiplicities are reported as follows: singlet (s), doublet (d), doublet of doublets (dd), doublet of doublets of doublets (ddd), doublet of triplets (dt), triplet (t), quartet (q), and multiplet (m). High resolution mass spectra were obtained at the University of Michigan core facility. X-ray crystallographic data were collected on a Bruker SMART APEX-I CCD-based X-ray diffractometer conducted by Midwest Microlab, Indianapolis, IN. Flash chromatography was conducted on a Biotage Isolera One chromatography system using preloaded high-performance silica gel columns (10 g, 25 g, 50 g, or 100 g as appropriate). GC-FID was conducted on a Shimadzu CG-17A system. Melting points were obtained on a OptiMelt automated melting point system.

Materials and Methods

All reagents were obtained from a commercial vendor (Aldrich, CombiBlocks, Oakwood, Synthonix, Enamine, Carbosynth, Pressure Chemicals, Matrix, SantaCruz Biotech, or Ontario Chemicals). Pd(OAc)$_2$ was purchased from Pressure Chemical. Acetronitrile and dimethylsulfoxide were purchased from Sigma-Aldrich. Hydrazine monohydrate was purchased from Alfa Aesar. All commercial reagents were used without further purification/drying unless explicitly stated in the experimental section. All reactions were performed under ambient atmosphere unless stated in experimental section. The manipulation of solid reagents was

conducted on the benchtop unless otherwise stated. Reactions were conducted under ambient

atmosphere unless otherwise stated. Reaction vessels were sealed with either a septum (flask) or a

Teflon-lined cap (4 mL or 20 mL vial) with Teflon tape wrapped around the cap. Reactions

conducted at elevated temperatures were heated on a hot plate using an aluminum block.

Temperature was regulated using an external thermocouple

3.5.2 Synthesis of Starting Materials
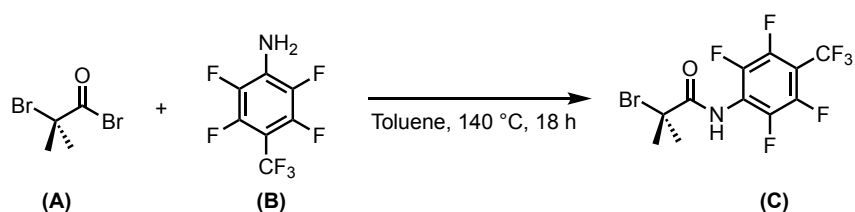
Synthesis of C: α-Bromo propanamide **C** was synthesized following a literature procedure[10a]

from starting materials **A** and **B**.

Amine Starting Material Syntheses (D-2 *through* D-8)

*Amine starting materials without experimental procedures were purchased from commercial*

vendors.
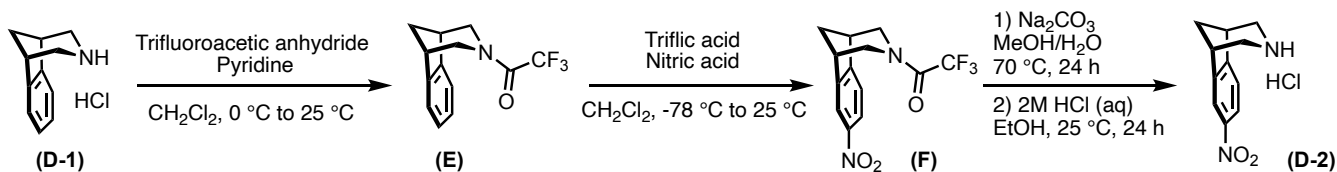
Synthesis of D-2: Using a patented procedure,[21] compound **D-2** was obtained as a white solid. The

^{1}H NMR spectrum matched that reported in the literature.[21] **D-2** was used as the starting material

to prepare substrate **1-B**.
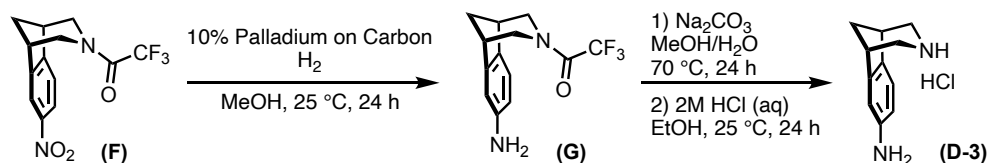
Synthesis of D-3: Using a patented procedure,[21] compound **D-3** was obtained as a white solid. The

^{1}H NMR spectrum matched that reported in the literature.[21] **D-3** was used as the starting material

to prepare substrate **1-C**.
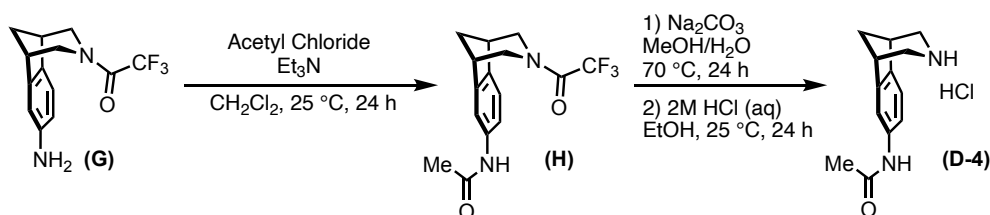
Synthesis of D-4: Using a patented procedure,[21] compound **D-4** was obtained as a white solid.

The ^{1}H NMR spectrum matched that reported in the literature.[21] **D-4** was used as the starting
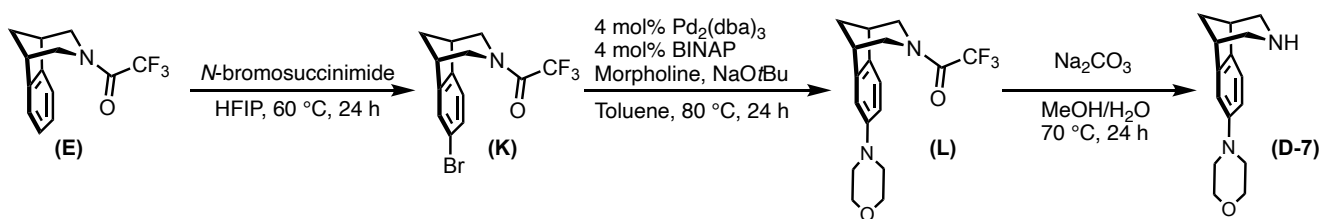
material to prepare substrate **1-E.**
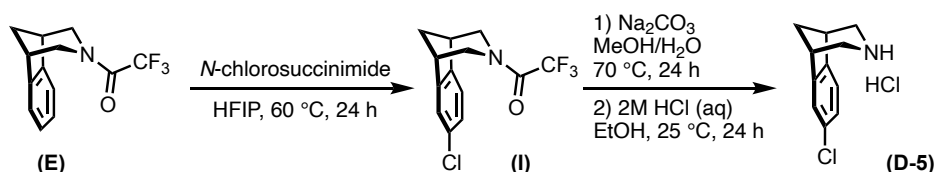
Synthesis of D-5: **D-5** was prepared using a modified literature procedure.[22] In a 20 mL

scintillation vial, **E** (2.0 g, 0.0078 mol, 1.0 equiv) was dissolved in hexafluoro-2-propanol (HFIP,

10 mL). To this stirred solution, *N*-chlorosuccinimide (1.0 g, 0.0078 mol, 1.0 equiv) was added,

and the reaction vial was sealed. The reaction mixture was stirred at 60 °C for 24 h. The reaction

was allowed to cool to rt and was then concentrated under reduced pressure. Purification via

column chromatography (gradient elution of 50% EtOAc in hexanes) afforded **I** as a white solid

(1.5 g, 67% yield). The ^{1}H NMR spectrum of **I** matched that reported in the literature.[21] Compound **D-5** was prepared from **I** using a literature procedure.[21] Product **D-5** was obtained as a white solid (1.1 g, 92% yield), and the ^{1}H NMR spectrum matched that reported in the literature.[21] **D-5** was used as the starting material to prepare substrate **1-D**.
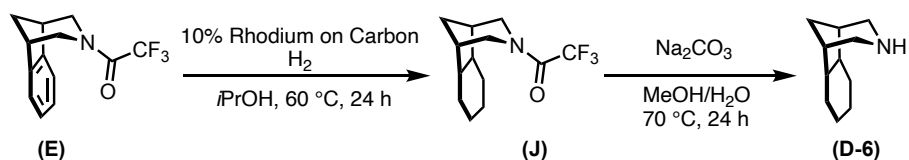

Synthesis of D-6: **D-6** was prepared using a modified literature procedure.[23] Under ambient atmosphere, a 20 mL vial was charged with **E** (1.0 g, 3.9 mmol, 1.0 equiv), rhodium on carbon (39.7 mg, 0.39 mmol, 10%), and *i*PrOH (12 mL). The 20 mL vial was placed in a Parr Reactor, where the reaction was pressurized under 5 atm of hydrogen. The reaction was stirred in the Parr Reactor for 24 h at 60 °C. The reaction was allowed cool to rt and was then removed from the Parr Reactor. The solution was filtered through a pad of Celite, and the filtrate was concentrated under reduced pressure. The crude material was purified by silica gel chromatography (gradient elution of 15% to 30% EtOAc in hexanes), which afforded **J** as a white solid (800 mg, 78% yield). Compound **J** (800 mg, 3.0 mmol, 1.0 equiv) and Na_2CO_3 (650 mg, 6.0 mmol, 2.0 equiv) were added to a 20 mL vial followed by a 2:1 MeOH (10 mL)/H_2O (5 mL) mixture. The reaction was stirred at 70 °C for 24 h and then concentrated under reduced pressure. The solid was dissolved in CH_2Cl_2, and an aqueous extraction was performed. The organic layers were combined and

concentrated. Product **D-6** was obtained as a colorless oil without further purification (480 mg, 97% yield). **D-6** was used as the starting material to prepare substrate **1-G**.


Synthesis of D-7: **D-7** was prepared using a modified literature procedure.[22,24] In a 20 mL scintillation vial, **E** (1.0 g, 3.9 mmol, 1.0 equiv) was dissolved in HFIP (10 mL). To this stirred solution, *N*-bromosuccinimide (69.5 mg, 3.9 mmol, 1.0 equiv) was added, and the reaction vial was sealed. The reaction mixture was stirred at 60 °C for 24 h. The reaction was allowed to cool to rt and then concentrated under reduced pressure. Final purification via column chromatography (gradient elution of 50% EtOAc in hexanes) afforded **K** as a white solid (700 mg, 54% yield). Under a nitrogen atmosphere, a 20 mL scintillation vial was charged with **K** (700 mg, 2.1 mmol, 1.0 equiv), Pd$_2$(dba)$_3$ (38.4 mg, 0.042 mmol, 4 mol%), BINAP (52.2 mg, 0.084 mmol, 4 mol%), and NaO*t*Bu (282 mg, 2.9 mmol, 1.4 equiv). The solids in the vial were dissolved in toluene (15 mL) and then morpholine (217 μL, 2.5 mmol, 1.2 equiv) was added. The vial was sealed, and the reaction mixture was stirred at 80 °C for 24 h. The reaction was allowed to warm to rt and then diluted with diethyl ether. An aqueous extraction was performed, and the organic layers were collected and concentrated under reduced pressure. The crude material was purified via silica gel chromatography (gradient elution of 50% EtOAc in hexanes), and compound **L** was obtained as a white solid (500 mg, 70% yield). Compound **L** (500 mg, 1.5 mmol, 1.0 equiv) and Na$_2$CO$_3$ (350 mg, 3.0 mmol, 2.0 equiv) were dissolved in a 2:1 MeOH (10 mL)/H$_2$O (5 mL) mixture in a 20 mL vial. The reaction was stirred at 70 °C for 24 h. The reaction solution was then concentrated under reduced pressure. The resulting solids was dissolved in CH$_2$Cl$_2$, and an aqueous extraction was

performed. The organic layers were combined and concentrated. Product **D-7** was obtained as a colorless oil and was used without further purification to prepare substrate **1-F**.


(M) → (D-8)

Reagents: NaSO$_2$CF$_3$, tBuOOH, CH$_2$Cl$_2$, 0 °C to 25 °C
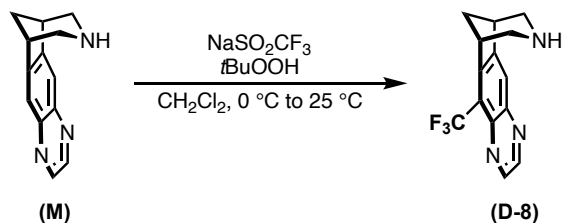
Synthesis of D-8: **D-8** was prepared from compound **M** using a literature procedure.[25] ^{1}H and ^{19}F NMR spectra of **D-8** matched that reported in the literature.[25] **D-8** was used as the starting material to prepare substrate **1-I**.

Directing Group Installation Procedure[10a]

(D-1) + (C) → (1-A)

Reagents: K$_2$CO$_3$, NaI, MeCN, 60 °C, 18 h
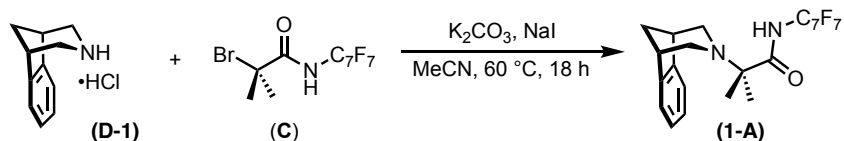
A 20 mL scintillation vial was charged with **D-1** (254 mg, 1.30 mmol, 1.0 equiv), α-bromo propanamide **C** (497 mg, 1.30 mmol, 1.0 equiv), K$_2$CO$_3$ (574 mg, 4.16 mmol, 3.2 equiv), and NaI (96.2 mg, 0.65 mmol, 0.5 equiv). Anhydrous acetonitrile (15 mL) was then added. The vial was sealed, and the vial was heated to an external temperature of 60 °C. After 18 h, the reaction was cooled to rt, diluted with EtOAc (~5 mL), and filtered through silica gel. The filtrate was concentrated under reduced pressure. Final purification via column chromatography (gradient elution from 0% to 20% EtOAc in hexanes) afforded product **1-A** (447 mg, 75% yield) as a white solid.[1] Amine derivatives **1-B** through **1-K** were prepared in an analogous manner using the appropriate amine starting material (**D-2** through **D-8**). Substrate-specific are included below.

Characterization of Directing Group Installation Products (1-B *through* 1-K)
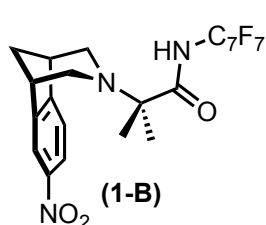
1-B: Isolated yield: 950 mg, 54% (white solid)

^{1}H NMR (700 MHz, CDCl$_3$, 23 ºC): δ 8.08-8.04 (multiple peaks, 2H), 7.44 (br s, 1H), 7.36 (d, J = 8.1 Hz, 1H), 3.36 (t, J = 7.2 Hz, 2H), 2.89 (t, J = 10.9 Hz, 2H), 2.78 (t, J = 10.3 Hz, 2H), 2.40 (app s, 1H), 1.87 (d, J = 10.9 Hz, 1H), 1.25 (s, 6H).

^{13}C NMR (176 MHz, CDCl$_3$, 23 ºC): δ 175.2, 153.5, 147.7, 147.6, 123.1, 122.2, 116.9, 64.2, 50.6, 50.2, 44.0, 41.2, 41.1, 22.2, 20.7. *Carbon resonances associated with perfluoroaryl group are not observed.*[10]

^{19}F NMR (470 MHz, CDCl$_3$, 23 ºC): δ –56.1 (t, 3F), –140.8 (app. s, 2F), –143.7 (app. s, 2F).

HRMS-electrospray (m/z): [M]$^+$ calcd. for C$_{22}$H$_{18}$F$_7$N$_3$O$_3$, 506.1309; found, 506.1316. Melting point: 125-127 °C

Chromatography conditions: 10% EtOAc in hexanes
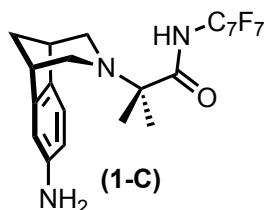
1-C: Isolated yield: 580 mg, 26% (off-white solid)

^{1}H NMR (700 MHz, CDCl$_3$, 23 ºC): δ 7.80 (br s, *NH of amide*, variable integrations), 6.92 (d, J = 7.7 Hz, 1H), 6.52 (d, J = 2.2 Hz, 1H), 6.36 (dd, J = 7.7, 2.2 Hz, 1H), 3.46 (s, 2H), 3.10 (dt, J = 13.6, 4.5 Hz, 2H), 2.81-2.72 (multiple peaks, 2H), 2.69-2.61 (multiple peaks, 2H), 2.26 (m, 1H), 1.70 (d, J = 10.3 Hz, 1H), 1.22 (s, 3H), 1.21 (s, 3H).
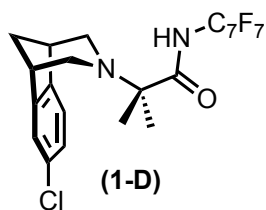
^{13}C NMR (176 MHz, CDCl$_3$, 23 ºC): δ 176.5, 147.0, 145.7, 135.4, 122.3, 112.9, 109.5, 63.8, 50.8, 50.7, 43.8, 41.4, 40.4, 21.9, 21.7. *Carbon resonances associated with perfluoroaryl group are not observed.*[10]

^{19}F NMR (470 MHz, CDCl$_3$, 23 ºC): δ –56.1 (t, 3F), –141.9 (m, 2F), –143.0 (m, 2F).

HRMS-electrospray (m/z): [M]$^+$ calcd. for C$_{22}$H$_{20}$F$_7$N$_3$O, 476.1567; found, 476.1577.

Melting point: 114-115 °C

Chromatography conditions: 5% EtOAc in hexanes

1-D: Isolated yield: 550 mg, 22% (white solid)

^{1}H NMR (700 MHz, CDCl$_3$, 23 ºC): δ 7.56 (br s, 1H), 7.15-7.07 (multiple peaks, 3H), 3.21 (dd, J = 11.7, 7.2 Hz, 2H), 2.84 (dd, J = 10.5, 4.0 Hz, 1H), 2.76 (dd, J = 10.5, 4.0 Hz, 1H), 2.73-2.67 (multiple peaks, 2H), 2.32 (m, 1H), 1.76 (d, J = 10.6 Hz, 1H), 1.23 (s, 3H), 1.21 (s, 3H).
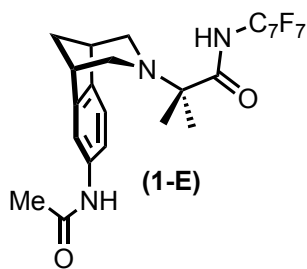
^{13}C NMR (176 MHz, CDCl$_3$, 23 ºC): δ 179.9, 147.7, 144.2, 132.4, 126.9, 122.9, 122.3, 63.9, 50.8, 50.2, 43.8, 41.2, 40.7, 22.5, 20.9. *Carbon resonances associated with perfluoroaryl group are not observed.*[10]

^{19}F NMR (470 MHz, CDCl$_3$, 23 ºC): δ –56.1 (t, 3F), –141.4 (m, 2F), –143.3 (m, 2F).

HRMS-electrospray (m/z): [M]$^+$ calcd. for C$_{22}$H$_{18}$ClF$_7$N$_2$O, 495.1069; found, 495.1083.

Melting point: 90-92 °C

Chromatography conditions: 5% EtOAc in hexanes

1-E: Isolated yield: 660 mg, 69% (white solid)

^{1}H NMR (700 MHz, CD$_3$OD, 23 ºC): δ 7.53 (br s, 1H), 7.19 (app. t, 2H), 3.22 (s, 1H), 3.17 (s, 1H), 2.93 (d, J = 10.6 Hz, 1H), 2.79 (d, J = 10.6 Hz, 1H), 2.75 (d, J = 10.5 Hz, 2H), 2.28 (m, 1H), 1.98 (s, 3H), 1.82 (d, J = 10.5 Hz, 1H), 1.24 (s, 3H), 1.19 (s, 3H).

Note in CD$_3$OD, amide H's are not observed.

^{13}C NMR (176 MHz, CD$_3$OD, 23 ºC): δ 178.5, 170.9, 147.5, 142.7, 138.9, 122.9, 119.2, 114.6, 64.8, 52.3, 50.7, 44.5, 42.7, 42.2, 24.4, 23.5, 19.8. *Carbon resonances associated with perfluoroaryl group are not observed.*[10]

^{19}F NMR (470 MHz, CDCl$_3$, 23 ºC): δ –56.0 (t, 3F), –141.8 (m, 2F), –143.1 (m, 2F).

HRMS-electrospray (m/z): [M]$^+$ calcd. for C$_{24}$H$_{22}$F$_7$N$_3$O$_2$, 518.1673; found, 518.1676. Melting point: 145-151°C

Chromatography conditions: 10% EtOAc in hexanes
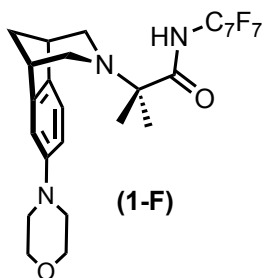
1-F: Isolated yield: 406 mg, 55% (white solid)

^{1}H NMR (700 MHz, CDCl$_3$, 23 ºC): δ 7.06 (d, J = 8.0 Hz, 1H), 6.76 (d, J = 2.3 Hz, 1H), 6.58 (dd, J = 8.0, 2.3 Hz, 1H), 3.75 (dd, J = 5.4, 4.2 Hz, 4H), 3.15 (d, J = 6.2 Hz, 2H), 2.95 (q, J = 4.3 Hz, 4H), 2.83-2.73 (multiple peaks, 2H), 2.68 (t, J = 10.0 Hz, 2H), 2.29 (m, 1H), 1.73 (d, J = 10.5 Hz, 1H), 1.22 (s, 3H), 1.21 (s, 3H). *Note in this spectrum, amide H is not observed.*

^{13}C NMR (176 MHz, CDCl$_3$, 23 ºC): δ 176.4, 150.9, 146.8, 137.1, 122.1, 113.6, 110.3, 67.0, 63.8, 51.0, 50.5, 49.9, 43.9, 41.7, 40.5, 22.6, 21.1. *Carbon resonances associated with perfluoroaryl group are not observed.*[10]

^{19}F NMR (470 MHz, CDCl$_3$, 23 ºC): δ –56.0 (t, 3F), –141.6 (m, 2F), –142.7 (m, 2F).

HRMS-electrospray (m/z): [M]$^+$ calcd. for C$_{26}$H$_{26}$F$_7$N$_3$O$_2$, 546.1986; found, 546.1989. Melting point: 142-145 °C

Chromatography conditions: 10% EtOAc in hexanes
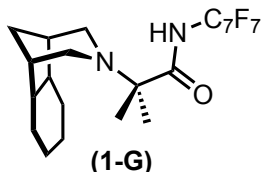
1-G: Isolated yield: 615 mg, 33% (white solid)

^{1}H NMR (700 MHz, CD$_3$OD, 23 ºC): δ 2.90 (d, J = 10.5 Hz, 2H), 2.48 (dd, J = 10.5, 2.0 Hz, 2H), 2.10 (s, 2H), 2.00-1.94 (multiple peaks, 4H), 1.79 (d, J = 8.5 Hz, 2H), 1.62-1.54 (multiple peaks, 2H), 1.43-1.35 (multiple peaks, 8H), 1.31 (d, J = 10.5 Hz, 2H). *Note in CD$_3$OD, amide H is not observed.*

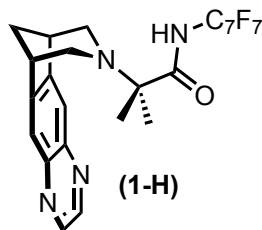^{13}C NMR (176 MHz, CDCl$_3$, 23 ºC): δ 175.2, 64.9, 48.4, 39.6, 38.5, 37.5, 20.6, 20.4, 20.1. *Carbon resonances associated with perfluoroaryl group are not observed.*[10]

^{19}F NMR (470 MHz, CDCl$_3$, 23 ºC): δ –56.1 (t, 3F), –141.0 (m, 2F), –143.2 (m, 2F).

HRMS-electrospray (m/z): [M]$^+$ calcd. for C$_{22}$H$_{25}$F$_7$N$_2$O, 467.1928; found, 467.1941.

Melting point: 78-83°C

Chromatography conditions: 5% EtOAc in hexanes

1-H: The ^{1}H, ^{13}C, and ^{19}F NMR spectral data for **1-H** matched that reported in the literature.[10a]

(1-H)
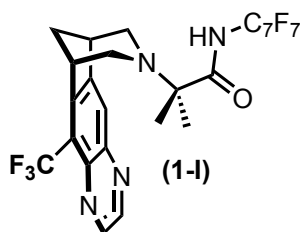
1-I: Isolated yield: 405 mg, 20% (off-white solid)

^{1}H NMR (700 MHz, CDCl$_3$, 23 ºC): δ 8.88 (d, J = 1.8 Hz, 1H), 8.83 (d, J = 1.8 Hz, 1H), 8.01 (s, 1H), 7.38 (s, 1H), 3.98 (app s, 1H), 3.56 (app. s, 1H), 3.14 (m, 1H), 3.01 (d, J = 10.6 Hz, 1H), 2.89 (d, J = 10.6 Hz, 2H), 2.41 (d, J = 11.0 Hz, 1H), 2.00 (d, J = 11.0 Hz, 1H), 1.24 (s, 3H), 1.21 (s, 3H).

(1-I)

^{13}C NMR (176 MHz, CDCl$_3$, 23 ºC): δ 174.4, 150.1, 149.1, 145.0, 144.1, 143.0, 140.3, 124.9, 124.5 (q, J = 276.0 Hz), 121.1 (q, J = 30.1 Hz), 64.2, 51.9, 51.6, 42.2, 41.4, 40.8, 21.5, 21.5. *Carbon resonances associated with perfluoroaryl group are not observed.*[10]

^{19}F NMR (470 MHz, CDCl$_3$, 23 ºC): δ –55.4 (app. s, 3F), –56.1 (t, 3F), –141.5 (m, 2F), –144.9 (m, 2F).

HRMS-electrospray (m/z): [M]$^+$ calcd. for C$_{25}$H$_{18}$F$_{10}$N$_4$O, 581.1394; found, 581.1384.

Melting point: 178-184 °C

Chromatography conditions: 20% EtOAc in hexanes
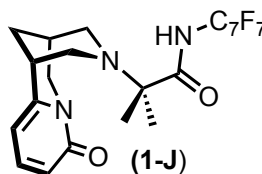
1-J: The ^{1}H, ^{13}C, and ^{19}F NMR spectral data for **1-J** matched those reported in the literature.[10a]

(1-J)
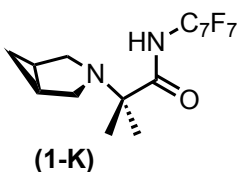
1-K: The ^{1}H, ^{13}C, and ^{19}F NMR spectral data for **1-K** matched those reported in the literature.[10a]

(1-K)

Synthesis of 2-A: Pd complex **2-A** was synthesized from **1-A** and Pd(OAc)$_2$ following a

literature procedure.[12]

(1-A) → **(2-A)**

Reagents and conditions above the arrow:
1 equiv Pd(OAc)$_2$
3 equiv CsOPiv
2 equiv pyridine
t-amylOH, 60 °C, 24 h
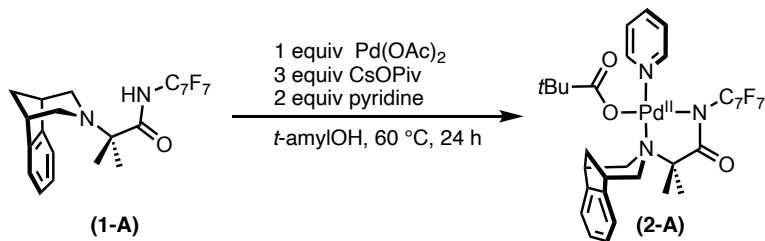
3.5.3 Pd-Catalyzed γ-Functionalization Attempts

General Procedure A (adapted from reference 10): A 4 mL vial was charged with substrate **1-A** (10.1 mg, 0.022 mmol, 1.0 equiv), Pd(OAc)$_2$ (0.50 mg, 0.0022 mmol, 10 mol %), and CsOPiv (15.4 mg, 0.066 mmol, 3.0 equiv) followed by the addition of the desired oxidant (0.066 mmol, 3.0 equiv). With a syringe, *t*-amylOH (0.3 mL) was added. The vial was sealed, and the mixture was stirred at 100 °C. After 18 h at this temperature, the reaction was cooled, diluted with EtOAc, and quenched with hydrazine (3 drops). The resulting mixture was stirred at rt for 10 min. The suspension was then filtered through a plug of Celite, concentrated under vacuum, and analyzed via GC-FID analysis using 1,3,5-trimethoxybenzene as internal standard (0.022 mmol, 1.0 equiv).

Table 3.2 Attempts at Pd-Catalyzed γ-Functionalization
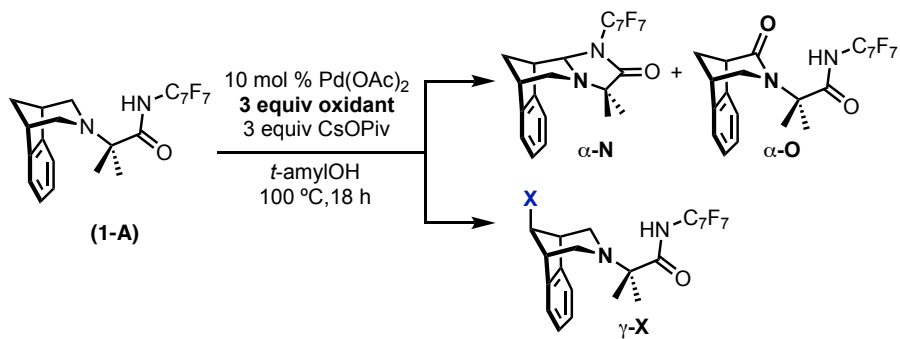
oxidant	X	γ-X	α-N	α-O
PhI	Ph	30%	0%	0%
(N-bromosuccinimide)	Br	0%	30%	30%
(N-chlorosuccinimide)	Cl	0%	10%	0%
(N-iodosuccinimide)	I	0%	15%	15%
Mes–I(OAc)$_2$	OAc	0%	10%	30%
B$_2$Pin$_2$	BPin	0%	<1%	0%
S$_2$Ph$_2$	SPh	0%	0%	0%

Table 3.3 Controls Reactions with No Pd
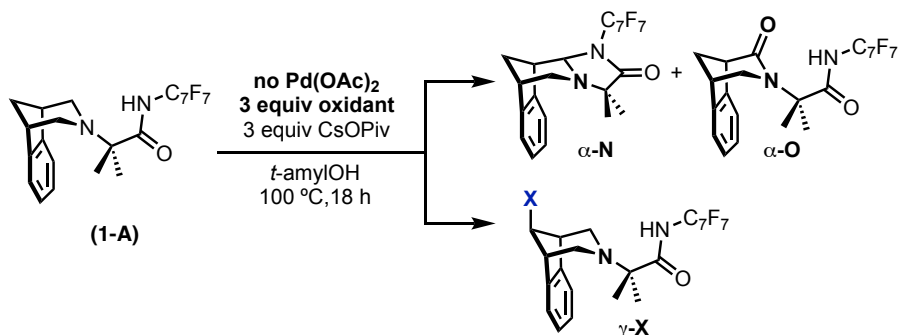
oxidant	X	γ-X	α-N	α-O
PhI	Ph	0%	<1%	0%
(N-bromosuccinimide)	Br	0%	25%	31%
(N-chlorosuccinimide)	Cl	0%	10%	0%
(N-iodosuccinimide)	I	0%	20%	0%
Mes—I(OAc)$_2$	OAc	0%	10%	15%
B$_2$Pin$_2$	BPin	0%	<1%	0%
S$_2$Ph$_2$	SPh	0%	10%	0%
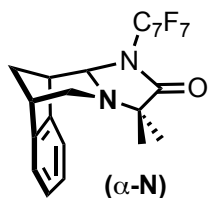
α-N: General Procedure A was followed using *N*-bromosuccinimide as the oxidant and Pd(OAc)$_2$.

Isolated yield: 2.0 mg, 20% (colorless oil)

^{1}H NMR (700 MHz, CDCl$_3$, 23 ºC): δ 7.19 (dd, *J* = 6.9, 1.3 Hz, 2H), 7.14 (td, *J* = 6.9, 2.2 Hz, 1H), 6.76 (d, *J* = 7.3 Hz, 1H), 5.03 (s, 1H), 3.17 (s, 1H), 3.07-3.02 (m, 1H), 2.95 (d, *J* = 5.7 Hz, 1H), 2.90-2.84 (m, 1H), 2.55 (ddd, *J* = 11.5, 5.5, 3.8 Hz, 1H), 1.93 (d, *J* = 11.5 Hz, 1H), 1.14 (s, 3H), 0.70 (s, 3H).

^{13}C NMR (176 MHz, CDCl$_3$, 23 ºC): δ 175.7, 146.7, 141.1, 127.56, 126.8, 123.5, 122.0, 60.0, 45.7, 43.0, 42.0, 40.8, 29.9, 22.8, 19.3. *Carbon resonances associated with perfluoroaryl group are not observed.*[10]

^{19}F NMR (470 MHz, CDCl$_3$, 23 °C): δ –56.2 (t, 3F), –136.3 (m, 1F), –139.1 (m, 1F), –140.5 (m, 1F), –143.2 (m, 1F).

HRMS-electrospray (m/z): [M]$^+$ calcd. for C$_{22}$H$_{17}$F$_7$N$_2$O, 459.1302; found, 459.1303.

Chromatography conditions: 7% EtOAc in hexanes

α-O: General Procedure A was followed using *N*-bromosuccinimide as the oxidant and Pd(OAc)$_2$.
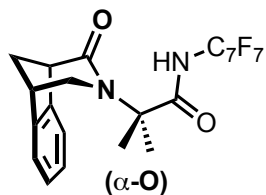
Isolated yield: 2.5 mg, 24% (off-white solid)

^{1}H NMR (700 MHz, CDCl$_3$, 23 °C): δ 7.38 (dd, *J* = 11.7, 7.3 Hz, 2H), 7.25 (dd, *J* = 7.3, 1.2 Hz, 1H), 7.20 (td, *J* = 7.5, 1.2 Hz, 1H), 6.56 (br s, 1H), 3.71 (d, *J* = 4.0 Hz, 1H), 3.66 (dd, *J* = 10.9, 4.0 Hz, 1H), 3.58 (t, *J* = 4.4 Hz, 1H), 3.31 (dt, *J* = 10.9, 1.5 Hz, 1H), 2.53 (ddd, *J* = 11.8, 7.1, 2.9 Hz, 1H), 2.28 (d, *J* = 11.1 Hz, 1H), 1.54 (s, 3H), 1.33 (s, 3H).

^{13}C NMR (176 MHz, CDCl$_3$, 23 °C): δ 172.5, 172.1, 144.0, 143.7, 128.4, 127.8, 122.9, 122.9, 61.9, 49.9, 49.5, 39.9, 37.9, 24.1, 21.5. *Carbon resonances associated with perfluoroaryl group are not observed.*[10]

^{19}F NMR (470 MHz, CDCl$_3$, 23 °C): δ –56.0 (t, 3F), –141.5 (m, 2F), –143.8 (m, 2F).

HRMS-electrospray (m/z): [M]$^+$ calcd. for C$_{22}$H$_{17}$F$_7$N$_2$O$_2$, 475.1251; found, 475.1237.

Melting point: 199-202 °C

Chromatography conditions: 35% EtOAc in hexanes

3.5.4 γ-Functionalization with Pre-Formed Pd(II) Complex
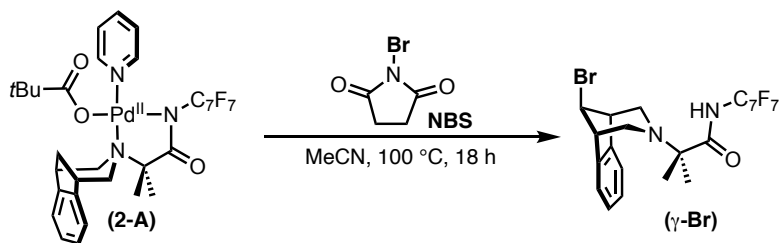
A 4 mL vial was charged with **2-A** (20.0 mg, 0.026 mmol, 1.0 equiv) and *N*-bromosuccinimide (NBS) (4.6 mg, 0.026 mmol, 1.0 equiv) followed by the addition of MeCN (0.5 mL). The vial was sealed, and the mixture was stirred at 100 °C. After 18 h at this temperature, the reaction was cooled, diluted with EtOAc, and quenched with hydrazine (6 drops). This mixture was stirred at rt for 10 min. The resulting suspension was filtered through a plug of Celite and concentrated under

vacuum. The product (**γ-Br**) was purified via silica gel column chromatography. Characterization and yield for **γ-Br** is shown below.

3.5.5 *In-situ* Generation of Pd(II) Complex for γ-Functionalization
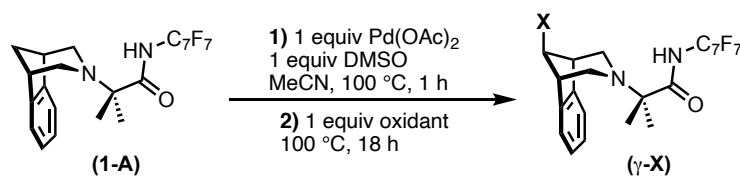
Procedure A: A 4 mL vial was charged with substrate **1-A** (20.0 mg, 0.0435 mmol, 1.0 equiv), Pd(OAc)$_2$ (10.0 mg, 0.0435 mmol, 1.0 equiv), and acetonitrile (0.6 mL). With a syringe, dimethyl sulfoxide (3.0 μL, 0.0435 mmol, 1.0 equiv) was added. The vial was sealed wih a Teflon-lined cap, and the mixture was stirred at 100 °C. After 1 h at this temperature, the vial was allowed to cool, the cap was removed, and the corresponding oxidant (0.0435 mmol, 1.0 equiv) was added. The vial was re-sealed, and the mixture was heated to 100 °C. After 18 h at this temperature, the reaction was cooled, diluted with EtOAc, and quenched with hydrazine (6 drops). This mixture was stirred at rt for 10 min. The resulting suspension was filtered through a plug of Celite and concentrated under vacuum. The crude material was purified via silica gel column chromatography.

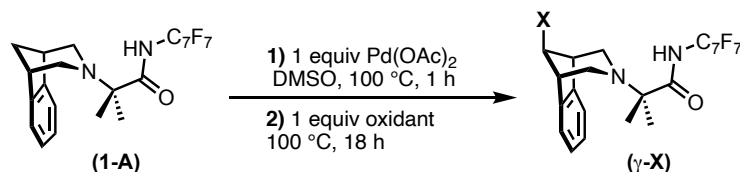**Procedure B:** A 4 mL vial was charged with substrate **1-A** (20.0 mg, 0.0435 mmol, 1.0 equiv), Pd(OAc)$_2$ (10.0 mg, 0.0435 mmol, 1.0 equiv), and acetonitrile (0.6 mL). With a syringe, dimethyl sulfoxide (9.3 μL, 0.13 mmol, 3.0 equiv) was added. The vial was sealed with a Teflon-lined cap, and the mixture was stirred at 100 °C. After 1 h at this temperature, the vial was allowed to cool, the cap was removed, and the corresponding oxidant (0.0435 mmol, 1.0 equiv) was added. The

vial was re-sealed, and the mixture was stirred and heated to 100 °C. After 18 h at this temperature, the reaction was cooled, diluted with EtOAc, and quenched with hydrazine (6 drops). This mixture was stirred at rt for 10 min. The resulting suspension was filtered through a plug of Celite and concentrated under vacuum. The crude material was purified via silica gel column chromatography.


Procedure C: A 4 mL vial was charged with substrate **1-A** (20.0 mg, 0.0435 mmol, 1.0 equiv), Pd(OAc)$_2$ (10.0 mg, 0.0435 mmol, 1.0 equiv), and dimethyl sulfoxide (0.6 mL). The vial was sealed with a Teflon-lined cap, and the mixture was stirred at 100 °C. After 1 h at this temperature, the vial was allowed to cool, the cap was removed, and the corresponding oxidant (0.13 mmol, 3.0 equiv) was added. The vial was re-sealed, and the mixture was stirred and heated to 100 °C. After 18 h at this temperature, the reaction was cooled, diluted with EtOAc, filtered through a plug of Celite, and concentrated under vacuum. The crude material was purified via silica gel column chromatography.
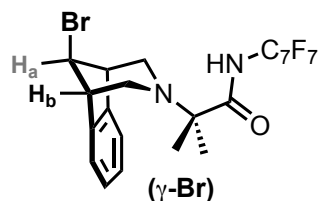
γ-Br: Procedure B was followed using *N*-bromosuccinimide as the oxidant.
Isolated yield: 15.5 mg, 66% (off-white solid)
^{1}H NMR (700 MHz, CDCl$_3$, 23 °C): δ 7.46 (br s, 1H), 7.23-7.20 (multiple peaks, 2H), 7.16 (dd, J = 5.4, 3.2 Hz, 2H), 4.57 (t, J_{ab} = 4.5 Hz, 1H), 3.30 (d, J = 11.0 Hz, 2H), 3.26 (t, J = 4.5 Hz, 2H), 2.69 (dd, J = 11.0, 3.7 Hz, 2H), 1.27 (s, 6H).
Note: J_{ab} value matches the expected J value of ~ 4 Hz in a 5- and 6-membered ring where H$_a$ and H$_b$ are equatorial and trans to each other.[26]
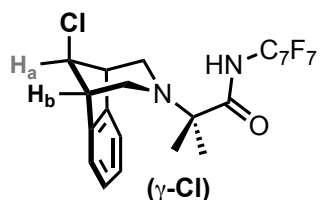^{13}C NMR (176 MHz, CDCl$_3$, 23 °C): δ 175.8, 142.8, 127.8, 122.0, 64.0, 55.5, 45.2, 44.3, 21.8. *Carbon resonances associated with perfluoroaryl group are not observed.*[10]
^{19}F NMR (470 MHz, CDCl$_3$, 23 °C): δ –56.1 (t, 3F), –141.3 (m, 2F), –143.1 (m, 2F).
HRMS-electrospray (m/z): [M]$^+$ calcd. for C$_{22}$H$_{18}$BrF$_7$N$_2$O, 539.0491; found, 539.0560.

Melting point: 99-101 °C
Chromatography conditions: 5% EtOAc in hexanes

γ-Cl: Procedure B was followed using *N*-chlorosuccinimide as the oxidant.
Isolated yield: 10.8 mg, 50% (white solid)
^{1}H NMR (700 MHz, CDCl3, 23 ºC): δ 7.46 (br s, 1H), 7.23 (dd, *J* = 5.4, 3.1 Hz, 2H), 7.17 (dd, *J* = 5.4, 3.1 Hz, 2H), 4.45 (t, *J*ab = 4.6 Hz, 1H), 3.27 (d, *J* = 12.1 Hz, 2H), 3.24 (t, *J* = 4.6 Hz, 2H), 2.64 (dd, *J* = 11.1, 3.7 Hz, 2H), 1.27 (s, 6H).
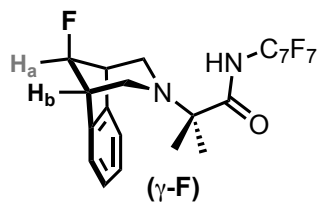^{13}C NMR (176 MHz, CDCl3, 23 ºC): δ 175.9, 142.6, 127.8, 122.3, 64.0, 62.1, 45.3, 43.3, 21.8. *Carbon resonances associated with perfluoroaryl group are not observed.*[10]
^{19}F NMR (470 MHz, CDCl3, 23 ºC): δ –56.1 (t, 3F), –141.4 (m, 2F), –143.1 (m, 2F).
HRMS-electrospray (m/z): [M]+ calcd. for $C_{22}H_{18}ClF_7N_2O$, 495.0996; found, 495.1065.
Melting point: 112-114 °C
Chromatography conditions: 5% EtOAc in hexanes

γ-F: Procedure A was followed using *N*-fluorobenzenesulfonimide (NFSI) as the oxidant.
Isolated yield: 9.2 mg, 44% (white solid)
^{1}H NMR (700 MHz, CDCl3, 23 ºC): δ 7.53 (br s, 1H), 7.23 (dd, *J* = 5.4, 3.3 Hz, 2H), 7.19 (dd, *J* = 5.4, 3.3 Hz, 2H), 4.97 (dt, *J*H,F = 56.0, *J*ab = 5.1 Hz, 1H), 3.32 (t, *J* = 4.4 Hz, 2H), 3.08 (dd, *J* = 11.0, 3.3 Hz, 2H), 2.65 (dt, *J* = 11.0, 3.7 Hz, 2H), 1.25 (s, 6H).
^{13}C NMR (176 MHz, CDCl3, 23 ºC): δ 175.9, 140.5, 128.1, 123.0, 91.0 (d, *J* = 201.4 Hz), 63.9, 43.5 (d, *J* = 17.4 Hz), 43.4 (d, *J* = 2.5 Hz), 21.8. *Carbon resonances associated with perfluoroaryl group are not observed.*[10]
^{19}F NMR (470 MHz, CDCl3, 23 ºC): δ –63.7 (t, 3F), –149.1 (m, 2F), –150.7 (m, 2F), –198.4 (dt, *J* = 56.0, 3.8, 1F).
HRMS-electrospray (m/z): [M]+ calcd. for $C_{22}H_{18}F_8N_2O$, 479.1291; found, 479.1364.
Melting point: 125-127 °C
Chromatography conditions: 3% EtOAc in hexanes
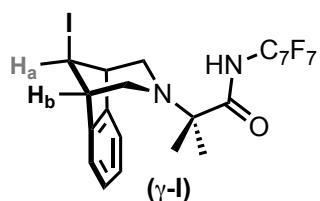
γ-I: Procedure B was followed using *N*-iodosuccinimide as the oxidant.
Isolated yield: 6.0 mg, 24% (off-white solid)
^{1}H NMR (700 MHz, CDCl3, 23 ºC): δ 7.44 (br s, 1H), 7.21 (dd, *J* = 5.3, 3.1 Hz, 2H), 7.13 (dd, *J* = 5.3, 3.1 Hz, 2H), 4.68 (t, *J*ab = 4.4 Hz, 1H), 3.27 (d, *J* = 10.7 Hz, 2H), 3.21 (t, *J* = 3.8 Hz, 2H), 2.77 (dd, *J* = 11.4, 3.8 Hz, 2H), 1.28 (s, 6H).
^{13}C NMR (176 MHz, CDCl3, 23 ºC): δ 175.8, 142.7, 127.6, 121.6, 63.9, 46.2, 45.4, 37.1, 21.9. *Carbon resonances associated with perfluoroaryl group are not observed.*[10]

^{19}F NMR (470 MHz, CDCl$_3$, 23 ºC): δ –56.1 (t, 3F), –141.4 (m, 2F), –143.1 (m, 2F).

HRMS-electrospray (m/z): [M]$^+$ calcd. for C$_{22}$H$_{18}$F$_7$IN$_2$O, 587.0352; found, 587.0423.

Melting point: 107-110 °C

Chromatography conditions: 5% EtOAc in hexanes
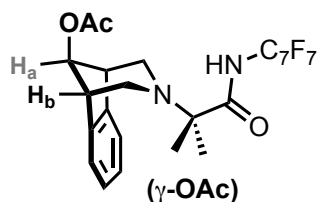
γ-OAc: Procedure A was followed using iodomesitylene diacetate as the oxidant.

Isolated yield: 11.9 mg, 53% (off-white solid)

^{1}H NMR (700 MHz, CDCl$_3$, 23 ºC): δ 7.49 (br s, *NH of amide*, variable integrations), 7.22 (dd, *J* = 5.4, 3.1 Hz, 2H), 7.16 (dd, *J* = 5.4, 3.1 Hz, 2H), 5.03 (t, *J*$_{ab}$ = 4.8 Hz, 1H), 3.34 (t, *J* = 4.1 Hz, 2H), 2.99 (d, *J* = 10.7 Hz, 2H), 2.63 (dd, *J* = 10.7, 3.7 Hz, 2H), 2.20 (s, 3H), 1.25 (s, 6H).

^{13}C NMR (176 MHz, CDCl$_3$, 23 ºC): δ 176.0, 170.3, 141.7, 127.8, 122.6, 74.6, 63.9, 43.7, 42.7, 29.9, 21.7, 21.3. *Carbon resonances associated with perfluoroaryl group are not observed.*[10]

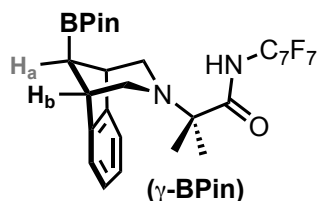^{19}F NMR (470 MHz, CDCl$_3$, 23 ºC): δ –56.1 (t, 3F), –141.4 (m, 2F), –143.1 (m, 2F).

HRMS-electrospray (m/z): [M]$^+$ calcd. for C$_{24}$H$_{21}$F$_7$N$_2$O$_3$, 519.1440; found, 519.1509.

Melting point: 110-112 °C

Chromatography conditions: 10% EtOAc in hexanes

γ-BPin: Procedure C was followed using bis(pinacolato) diboron as the oxidant.

Isolated yield: 14.7 mg, 57% (off-white solid)

^{1}H NMR (401 MHz, CDCl$_3$, 23 ºC): δ 7.52 (br s, *NH of amide*, variable integrations), 7.15 (dd, *J* = 5.3, 3.1 Hz, 2H), 7.03 (dd, *J* = 5.3, 3.1 Hz, 2H), 3.36 (t, *J* = 4.0 Hz, 2H), 2.89 (d, *J* = 10.5 Hz, 2H), 2.69 (dd, *J* = 10.5, 2.8 Hz, 2H), 1.94 (t, *J*$_{ab}$ = 4.0 Hz, 1H), 1.32 (s, 12H), 1.19 (s, 6H).

^{13}C NMR (176 MHz, CDCl$_3$, 23 ºC): δ 176.4, 147.4, 126.5, 121.2, 83.6, 63.9, 48.6, 42.8, 29.9, 25.1, 21.7. *Carbon resonances associated with perfluoroaryl group are not observed.*[10]

^{19}F NMR (470 MHz, CDCl$_3$, 23 ºC): δ –56.1 (t, 3F), –141.6 (m, 2F), –143.0 (m, 2F).

^{11}B NMR (128 MHz, CDCl$_3$, 23 °C): δ 32.8.

HRMS-electrospray (m/z): [M]$^+$ calcd. for C$_{28}$H$_{30}$BF$_7$N$_2$O$_3$, 587.2238; found, 587.2310.

Melting point: 149-153 °C

Chromatography conditions: 5% EtOAc in hexanes
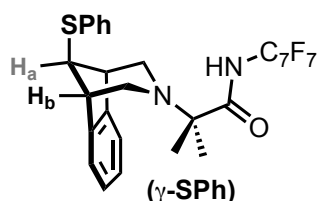
γ-SPh: Procedure C was followed with phenyl disulfide as the oxidant.

Isolated yield: 18.7 mg, 75% (off-white solid)

^{1}H NMR (700 MHz, CDCl$_3$, 23 ºC): δ 7.49 (br s, 1H), 7.44 (d, *J* = 7.5 Hz, 2H), 7.31 (t, *J* = 7.5 Hz, 2H), 7.25 (d, *J* = 8.1 Hz, 1H), 7.20 (multiple peaks, 2H), 7.12 (d, *J* = 10.1 Hz, 2H), 3.86 (t, *J*$_{ab}$ = 3.5 Hz, 1H), 3.28 (d, *J* = 10.0 Hz, 4H), 2.66 (d, *J* = 10.9 Hz, 2H), 1.28 (s, 6H).

^{13}C NMR (176 MHz, CDCl$_3$, 23 ºC): δ 176.0, 144.7, 131.1, 129.3, 127.3, 127.1, 122.0, 64.0, 56.6, 44.6, 44.5, 29.9, 21.9. *Carbon resonances associated with perfluoroaryl group are not observed.*[10]

^{19}F NMR (470 MHz, CDCl$_3$, 23 ºC): δ –56.7 (t, 3F), –142.0 (m, 2F), –143.7 (m, 2F).

HRMS-electrospray (m/z): [M]$^+$ calcd. for C$_{28}$H$_{23}$F$_7$N$_2$OS, 569.1419; found, 569.1492.

Melting point: 70-75 °C

Chromatography conditions: 5% EtOAc in hexanes
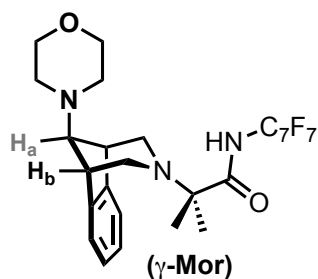
γ-Mor: Procedure C was followed with morpholino benzoate as the oxidant.

Isolated yield: 8.9 mg, 38% (white solid)

^{1}H NMR (700 MHz, CDCl$_3$, 23 ºC): δ 7.53 (br s, *NH of amide*, variable integrations), 7.19 (dd, *J* = 5.3, 3.1 Hz, 2H), 7.12 (dd, *J* = 5.3, 3.1 Hz, 2H), 3.79 (t, *J* = 4.3 Hz, 4H), 3.24 (t, *J* = 4.0 Hz, 2H), 3.15 (d, *J* = 10.0 Hz, 2H), 2.60 (t, *J*$_{ab}$ = 4.3 Hz, 1H), 2.53 (s, 4H), 2.48 (dd, *J* = 10.0, 3.8 Hz, 2H), 1.24 (s, 6H).

^{13}C NMR (176 MHz, CDCl$_3$, 23 ºC): δ 176.3, 144.2, 127.2, 122.4, 70.3, 67.1, 63.9, 50.9, 43.3, 41.8, 21.7. *Carbon resonances associated with perfluoroaryl group are not observed.*[10]

^{19}F NMR (470 MHz, CDCl$_3$, 23 ºC): δ –56.1 (t, 3F), –141.6 (m, 2F), –143.1 (m, 2F).

HRMS-electrospray (m/z): [M]$^+$ calcd. for C$_{26}$H$_{26}$F$_7$N$_3$O$_2$, 546.1913; found, 546.1989.

Melting point: 107-109 °C

Chromatography conditions: 75% EtOAc in hexanes

3.5.6 Scope of Pd-Mediated γ-Borylation Reaction
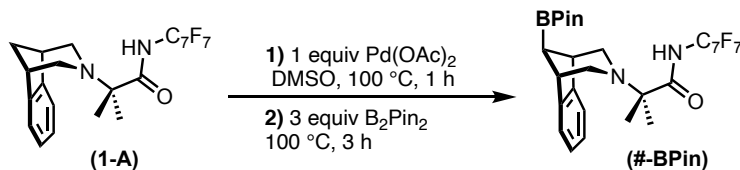
General Procedure: A 4 mL vial was charged with the **corresponding substrate** (1.0 equiv) and Pd(OAc)$_2$ (1.0 equiv). Dimethyl sulfoxide (0.6 mL) was added with a syringe. The vial was sealed with a Teflon-lined cap, and the mixture was stirred at 100 °C. After 1 h at this temperature, the vial was allowed to cool, the cap was removed, and B$_2$Pin$_2$ (3.0 equiv) was added. The vial was re-sealed, and the mixture was stirred and heated at 100 °C. After 3 h at this temperature, the reaction was cooled, diluted with dichloromethane, and stirred at rt for 10 min. The resulting suspension was filtered through a plug of Celite and concentrated under vacuum overnight. The

crude material was purified via silica gel column chromatography. See substrate-specific notes below.
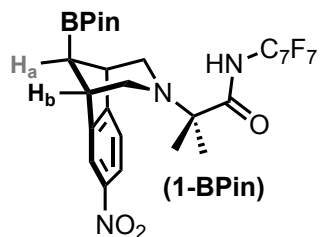
1-BPin: The general procedure was followed using substrate **1-B** (20.0 mg, 0.040 mmol, 1.0 equiv), Pd(OAc)$_2$ (9.0 mg, 0.040 mmol, 1.0 equiv), and B$_2$Pin$_2$ (30.5 mg, 0.120 mmol, 3.0 equiv) as starting materials.

Isolated yield: 12.9 mg, 52% (white solid)

^{1}H NMR (700 MHz, CDCl$_3$, 23 ºC): δ 8.03 (dd, J = 7.9, 2.1 Hz, 1H), 8.00 (d, J = 2.1 Hz, 1H), 7.47 (br s, 1H), 7.32 (d, J = 8.0 Hz, 1H), 3.47 (dt, J = 14.7, 4.1 Hz, 2H), 3.01-2.93 (multiple peaks, 2H), 2.77 (ddd, J = 21.7, 9.9, 4.1 Hz, 2H), 2.01 (t, J_{ab} = 4.8 Hz, 1H), 1.33 (s, 12H), 1.22 (s, 3H), 1.21 (s, 3H).

^{13}C NMR (176 MHz, CDCl$_3$, 23 ºC): δ 175.3, 155.3, 149.4, 147.3, 122.8, 121.6, 116.3, 83.9, 64.2, 48.5, 48.1, 42.8, 42.7, 25.1, 22.2, 20.6. *Carbon resonances associated with perfluoroaryl group are not observed.*[10]

^{19}F NMR (470 MHz, CDCl$_3$, 23 ºC): δ –56.1 (t, 3F), –140.8 (m, 2F), –143.7 (m, 2F).

^{11}B NMR (128 MHz, CDCl$_3$, 23 °C): 32.7.

HRMS-electrospray (m/z): [M]$^+$ calcd. for C$_{28}$H$_{29}$BF$_7$N$_3$O$_5$, 632.2161; found, 632.2155.

Melting point: 115-120 °C

Chromatography conditions: 15% EtOAc in hexanes
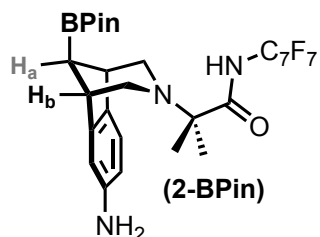
2-BPin: The general procedure was followed using substrate **1-C** (20.0 mg, 0.042 mmol, 1.0 equiv), Pd(OAc)$_2$ (9.5 mg, 0.042 mmol, 1.0 equiv), and B$_2$Pin$_2$ (32.0 mg, 0.126 mmol, 3.0 equiv) as starting materials.

Isolated yield: 8.8 mg, 35% (white solid)

^{1}H NMR (700 MHz, CDCl$_3$, 23 ºC): δ 7.81 (br s, 1H), 6.91 (d, J = 7.7 Hz, 1H), 6.51 (d, J = 2.1 Hz, 1H), 6.33 (dd, J = 7.7, 2.1 Hz, 1H), 3.44 (app. s, 2H), 3.24 (dt, J = 12.0, 4.2 Hz, 2H), 2.84 (dd, J = 15.2, 10.6 Hz, 2H), 2.70-2.59 (multiple peaks, 2H), 1.89 (t, J_{ab} = 4.1 Hz, 1H), 1.31 (s, 12H), 1.19 (s, 3H), 1.19 (s, 3H).

^{13}C NMR (176 MHz, CDCl$_3$, 23 ºC): δ 176.5, 148.8, 145.3, 137.2, 121.7, 112.4, 109.2, 83.5, 63.9, 48.7, 48.6, 43.0, 42.0, 25.1, 21.9, 21.6. *Carbon resonances associated with perfluoroaryl group are not observed.*[10]

^{19}F NMR (470 MHz, CDCl$_3$, 23 ºC): δ –56.0 (t, 3F), –141.9 (m, 2F), –143.1 (m, 2F).

^{11}B NMR (128 MHz, CDCl$_3$, 23 °C): 33.9.

HRMS-electrospray (m/z): [M]$^+$ calcd. for C$_{28}$H$_{31}$BF$_7$N$_3$O$_3$, 602.2419; found, 602.2417.

Melting point: 107-110 °C

Chromatography conditions: 20% EtOAc in hexanes
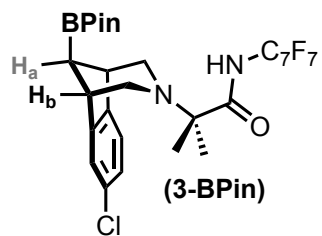
(3-BPin)

3-BPin: The general procedure was followed using substrate **1-D** (20.0 mg, 0.040 mmol, 1.0 equiv), Pd(OAc)$_2$ (9.0 mg, 0.040 mmol, 1.0 equiv), and B$_2$Pin$_2$ (30.5 mg, 0.120 mmol, 3.0 equiv) as starting materials.

Isolated yield: 10.8 mg, 44% (clear oil)

^{1}H NMR (700 MHz, CDCl$_3$, 23 ºC): δ 7.59 (br s, 1H), 7.10 (d, J = 7.8 Hz, 2H), 7.06 (dd, J = 7.8, 2.0 Hz, 1H), 3.34 (dt, J = 13.7, 4.2 Hz, 2H), 2.89 (t, J = 11.4 Hz, 2H), 2.72 (dd, J = 10.7, 4.2 Hz, 1H), 2.65 (dd, J = 10.7, 4.2 Hz, 1H), 1.94 (t, J_{ab} = 4.2 Hz, 1H), 1.32 (s, 12H), 1.21 (s, 3H), 1.19 (s, 3H).

^{13}C NMR (176 MHz, CDCl$_3$, 23 ºC): δ 175.9, 149.5, 146.0, 132.0, 126.5, 122.3, 121.8, 83.7, 64.0, 48.7, 48.1, 42.9, 42.4, 25.1, 25.0, 22.4, 20.8. *Carbon resonances associated with perfluoroaryl group are not observed.*[10]

^{19}F NMR (470 MHz, CDCl$_3$, 23 ºC): δ –56.1 (t, 3F), –141.4 (m, 2F), –143.3 (m, 2F).

^{11}B NMR (128 MHz, CDCl$_3$, 23 °C): 33.6.

HRMS-electrospray (m/z): [M]$^+$ calcd. for C$_{28}$H$_{29}$BClF$_7$N$_2$O$_3$, 621.1921; found, 621.1920.

Chromatography conditions: 10% EtOAc in hexanes
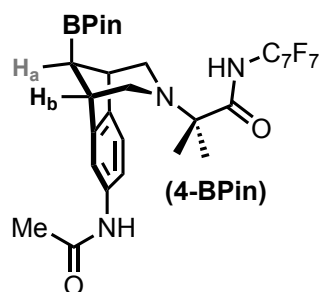
(4-BPin)

4-BPin: The general procedure was followed using substrate **1-E** (20.0 mg, 0.039 mmol, 1.0 equiv), Pd(OAc)$_2$ (8.8 mg, 0.039 mmol, 1.0 equiv), and B$_2$Pin$_2$ (29.7 mg, 0.117 mmol, 3.0 equiv) as starting materials.

Isolated yield: 17.3 mg, 69% (white solid)

^{1}H NMR (700 MHz, CDCl$_3$, 23 ºC): δ 7.68 (br s, 1H), 7.48 (d, J = 2.0 Hz, 1H), 7.12-7.04 (multiple peaks, 2H), 7.00 (dd, J = 7.8, 2.0 Hz, 1H), 3.34-3.30 (multiple peaks, 2H), 2.87 (dd, J = 13.0, 11.0 Hz, 2H), 2.74-2.62 (multiple peaks, 2H), 2.04 (s, 3H), 1.92 (t, J_{ab} = 4.3 Hz, 1H), 1.31 (s, 12H), 1.20 (s, 3H), 1.17 (s, 3H).

^{13}C NMR (176 MHz, CDCl$_3$, 23 ºC): δ 176.1, 167.9, 148.3, 143.3, 136.6, 121.4, 117.5, 113.5, 83.6, 63.9, 48.8, 48.2, 43.0, 42.4, 25.1, 25.0, 24.3, 22.7, 20.7. *Carbon resonances associated with perfluoroaryl group are not observed.*[10]

^{19}F NMR (470 MHz, CDCl$_3$, 23 ºC): δ –56.0 (t, 3F), –141.9 (m, 2F), –143.1 (m, 2F).

^{11}B NMR (128 MHz, CDCl$_3$, 23 °C): 31.7.

HRMS-electrospray (m/z): [M]$^+$ calcd. for C$_{30}$H$_{33}$BF$_7$N$_3$O$_4$, 644.2525; found, 644.2519.

Melting point: 60-65 °C

Chromatography conditions: 25% EtOAc in hexanes
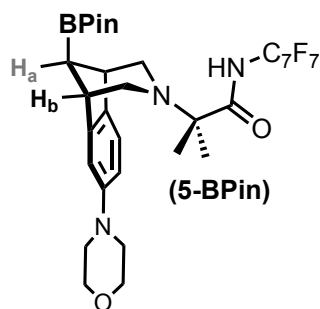
5-BPin: The general procedure was followed using substrate **1-F** (20.0 mg, 0.037 mmol, 1.0 equiv), Pd(OAc)$_2$ (8.3 mg, 0.037 mmol, 1.0 equiv), and B$_2$Pin$_2$ (28.2 mg, 0.111 mmol, 3.0 equiv) as starting materials.

Isolated yield: 13.1 mg, 53% (white solid)

^{1}H NMR (700 MHz, CDCl$_3$, 23 ºC): δ 7.75 (br s, *NH of amide*, variable integrations), 7.04 (d, *J* = 8.0 Hz, 1H), 6.74 (d, *J* = 2.3 Hz, 1H), 6.54 (dd, *J* = 8.0, 2.3 Hz, 1H), 3.75 (ddd, *J* = 5.8, 3.8, 2.1 Hz, 4H), 3.29 (dt, *J* = 15.1, 3.8 Hz, 2H), 2.95 (dddd, *J* = 17.5, 11.7, 9.5, 4.7 Hz, 4H), 2.91-2.84 (multiple peaks, 2H), 2.67 (ddd, *J* = 30.5, 10.7, 4.1 Hz, 2H), 1.91 (t, *J*$_{ab}$ = 4.0, 1H), 1.32 (s, 12H), 1.19 (s, 3H), 1.18 (s, 3H).

^{13}C NMR (176 MHz, CDCl$_3$, 23 ºC): δ 176.4, 150.6, 148.5, 139.0, 121.6, 113.0, 110.0, 83.6, 67.0, 63.8, 49.9, 48.9, 48.4, 43.3, 42.1, 25.1, 22.4, 21.1. *Carbon resonances associated with perfluoroaryl group are not observed.*[10]

^{19}F NMR (470 MHz, CDCl$_3$, 23 ºC): δ –56.0 (t, 3F), –141.6 (m, 2F), –142.7 (m, 2F).

^{11}B NMR (128 MHz, CDCl$_3$, 23 °C): 33.2.

HRMS-electrospray (m/z): [M]$^+$ calcd. for C$_{32}$H$_{37}$BF$_7$N$_3$O$_4$, 672.2838; found, 672.2829.

Melting point: 168-171 °C

Chromatography conditions: 15% EtOAc in hexanes
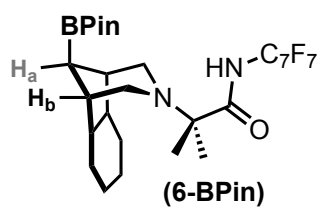
6-BPin: The general procedure was followed using substrate **1-G** (20.0 mg, 0.043 mmol, 1.0 equiv), Pd(OAc)$_2$ (9.7 mg, 0.043 mmol, 1.0 equiv), and B$_2$Pin$_2$ (32.8 mg, 0.129 mmol, 3.0 equiv) as starting materials.

Isolated yield: 12.3 mg, 48% (white solid)

^{1}H NMR (700 MHz, CD$_3$OD, 23 ºC): δ 2.74 (dt, *J* = 10.7, 2.2 Hz, 2H), 2.70 (dd, *J* = 10.7, 1.9 Hz, 2H), 2.20 (s, 2H), 2.02-1.88 (multiple peaks, 5H), 1.77 (d, *J* = 8.3 Hz, 2H), 1.38 (s, 6H), 1.29 (d, *J* = 1.0 Hz, 15H), 1.13 (t, *J*$_{ab}$ = 4.1 Hz, 1H). *Note in CD$_3$OD, amide H is not observed.*

^{13}C NMR (176 MHz, CDCl$_3$, 23 ºC): δ 175.4, 83.2, 65.1, 46.1, 41.4, 40.4, 25.2, 20.6, 20.6, 20.4. *Carbon resonances associated with perfluoroaryl group are not observed.*[10]

^{19}F NMR (470 MHz, CDCl$_3$, 23 ºC): δ –56.1 (t, 3F), –141.1 (m, 2F), –143.2 (m, 2F).

^{11}B NMR (128 MHz, CDCl$_3$, 23 °C): 31.7.

HRMS-electrospray (m/z): [M]$^+$ calcd. for C$_{28}$H$_{36}$BF$_7$N$_2$O$_3$, 593.2780; found, 593.2774.

Melting point: 50-53 °C

Chromatography conditions: 5% EtOAc in hexanes
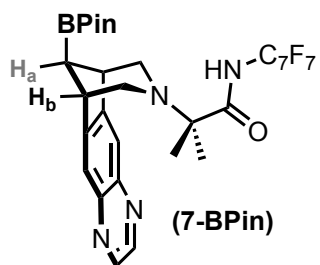
7-BPin: The general procedure was followed using substrate **1-H** (20.0 mg, 0.039 mmol, 1.0 equiv), Pd(OAc)$_2$ (8.8 mg, 0.039 mmol, 1.0 equiv), and B$_2$Pin$_2$ (29.7 mg, 0.117 mmol, 3.0 equiv) as starting materials.

Isolated yield: 7.0 mg, 28% (white solid)

^{1}H NMR (700 MHz, CDCl$_3$, 23 ºC): δ 8.71 (app. s, 2H), 7.77 (app. s, 2H), 7.46 (br s, 1H), 3.63 (t, J = 4.0 Hz, 2H), 3.06 (d, J = 11.0 Hz, 2H), 2.89 (dd, J = 11.0, 4.0 Hz, 2H), 2.05 (t, J_{ab} = 4.0 Hz, 1H), 1.35 (s, 12H), 1.19 (s, 6H).

^{13}C NMR (176 MHz, CDCl$_3$, 23 ºC): δ 175.2, 151.5, 144.0, 143.2, 120.4, 83.9, 64.1, 49.7, 42.8, 25.1, 21.5. *Carbon resonances associated with perfluoroaryl group are not observed.*[10]

^{19}F NMR (470 MHz, CDCl$_3$, 23 ºC): δ –56.1 (s, 3F), –141.4 (m, 2F), –144.3 (m, 2F).

^{11}B NMR (128 MHz, CDCl$_3$, 23 °C): 32.7.

HRMS-electrospray (m/z): [M]$^+$ calcd. for C$_{30}$H$_{30}$BF$_7$N$_4$O$_3$, 639.2372; found, 639.2355.

Melting point: 110-115 °C

Chromatography conditions: 30% EtOAc in pentanes
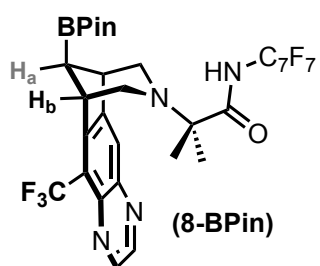
8-BPin: The general procedure was followed using substrate **1-I** (20.0 mg, 0.035 mmol, 1.0 equiv), Pd(OAc)$_2$ (7.9 mg, 0.035 mmol, 1.0 equiv), and B$_2$Pin$_2$ (26.7 mg, 0.105 mmol, 3.0 equiv) as starting materials.

Isolated yield: 14.1 mg, 57% (colorless oil)

^{1}H NMR (700 MHz, CDCl$_3$, 23 ºC): δ 8.86 (d, J = 1.8 Hz, 1H), 8.82 (d, J = 1.8 Hz, 1H), 7.97 (s, 1H), 7.43 (s, 1H), 4.11 (m, 1H), 3.66 (m, 1H), 3.11-2.99 (multiple peaks, 3H), 2.89 (dd, J = 11.0, 4.5 Hz, 1H), 2.02 (t, J_{ab} = 4.0 Hz 1H), 1.35 (s, 12H), 1.21 (s, 3H), 1.19 (s, 3H).

^{13}C NMR (176 MHz, CDCl$_3$, 23 ºC): δ 174.5, 151.8, 150.8, 144.8, 144.1, 142.8, 140.1, 125.2 (q, J = 276.3 Hz), 124.1, 120.6 (q, J = 29.7 Hz), 84.1, 64.2, 49.7, 49.4, 43.1, 42.4, 25.1, 25.1, 21.41, 21.4. *Carbon resonances associated with perfluoroaryl group are not observed.*[10]

^{19}F NMR (470 MHz, CDCl$_3$, 23 ºC): δ –55.4 (app. s, 3F), –56.0 (t, 3F), –141.6 (m, 2F), –144.8 (m, 2F).

^{11}B NMR (128 MHz, CDCl$_3$, 23 °C): 35.5.

HRMS-electrospray (m/z): [M]$^+$ calcd. for C$_{31}$H$_{29}$BF$_{10}$N$_4$O$_3$, 707.2246; found, 707.2246.

Chromatography conditions: 25% EtOAc in hexanes
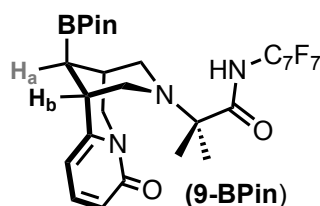
9-BPin: The general procedure was followed using substrate **1-J** (20.0 mg, 0.041 mmol, 1.0 equiv), Pd(OAc)$_2$ (9.2 mg, 0.041 mmol, 1.0 equiv), and B$_2$Pin$_2$ (31.2 mg, 0.123 mmol, 3.0 equiv) as starting materials.

Isolated yield: 9.1 mg, 36% (light yellow solid)

^{1}H NMR (700 MHz, CDCl$_3$, 23 ºC): δ 7.71 (s, 1H), 7.03 (dd, J = 9.2, 6.8 Hz, 1H), 6.33 (dd, J = 9.2, 1.4 Hz, 1H), 5.95 (d, J = 7.1 Hz, 1H), 4.18 (d, J = 15.4 Hz, 1H), 3.91 (dd, J = 15.4, 6.4 Hz, 1H), 3.24 (m, 1H), 3.02 (d, J = 11.3 Hz, 1H), 2.79 (d, J = 10.8 Hz, 1H), 2.77 – 2.70 (multiple peaks, 2H), 2.66 (d, J = 11.3 Hz, 1H), 1.31 (s, 12H), 1.28 (s, 3H), 1.26 (app. d, J_{ab} = 4.9 Hz, 1H), 1.18 (s, 3H).

^{13}C NMR (176 MHz, CDCl$_3$, 23 ºC): δ 175.0, 163.3, 151.3, 138.4, 117.1, 104.6, 84.4, 64.6, 54.4, 51.8, 51.2, 36.9, 29.9, 29.6, 25.0, 25.0, 23.8, 17.4. *Carbon resonances associated with perfluoroaryl group are not observed.*[10]

^{19}F NMR (470 MHz, CDCl$_3$, 23 ºC): δ –56.1 (t, 3F), –141.0 (m, 2F), –142.8 (m, 2F).

^{11}B NMR (128 MHz, CDCl$_3$, 23 °C): 31.7.

HRMS-electrospray (m/z): [M]$^+$ calcd. for C$_{28}$H$_{31}$BF$_7$N$_3$O$_4$, 618.2369; found, 618.2370.

Melting point: 67-72 °C

Chromatography conditions: 60% EtOAc in hexanes
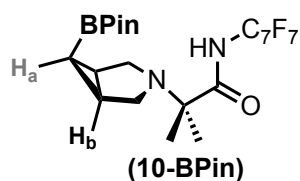
10-BPin: The general procedure was followed using substrate **1-K** (20.0 mg, 0.052 mmol, 1.0 equiv), Pd(OAc)$_2$ (11.7 mg, 0.052 mmol, 1.0 equiv), and B$_2$Pin$_2$ (40.0 mg, 0.156 mmol, 3.0 equiv) as starting materials.

Isolated yield: 5.2 mg, 20% (colorless oil)

^{1}H NMR (700 MHz, CDCl$_3$, 23 ºC): δ 9.92 (br s, 1H), 3.04 (d, J = 8.5 Hz, 2H), 2.70 (dt, J = 8.5, 2.1 Hz, 2H), 1.74-1.70 (multiple peaks, 2H), 1.31 (s, 6H), 1.13 (s, 12H), 0.02 (t, J_{ab} = 8.5 Hz, 1H).

^{13}C NMR (176 MHz, CDCl$_3$, 23 ºC): δ 176.3, 83.3, 61.8, 47.0, 25.5, 24.7, 20.9, 19.9. *Carbon resonances associated with perfluoroaryl group are not observed.*[10]

^{19}F NMR (470 MHz, CDCl$_3$, 23 ºC): δ –56.0 (t, 3F), –141.5 (m, 2F), –142.8 (m, 2F).

^{11}B NMR (128 MHz, CDCl$_3$, 23 °C): 33.8.

HRMS-electrospray (m/z): [M]$^+$ calcd. for C$_{22}$H$_{26}$BF$_7$N$_2$O$_3$, 511.1997; found, 511.1995.

Chromatography conditions: 5% EtOAc in pentanes. Performed on water-deactivated silica gel.

Table 3.4 Substrates that did not undergo Pd-Mediated γ-Borylation under these conditions

11-BPin, 0%   **12-BPin**, 10%   **13-BPin**, 10%

14-BPin, 0%   **15-BPin**, 0%   **16-BPin**, 0%   **17-BPin**, <5%

3.5.7 Pd-Catalyzed γ-Functionalizations

Pd-Catalyzed γ-Borylation

1-A → (10 mol% Pd(OAc)$_2$, 3 equiv B$_2$Pin$_2$, **1 equiv Base**, DMSO, 100 °C, 3 h) → **γ-BPin**
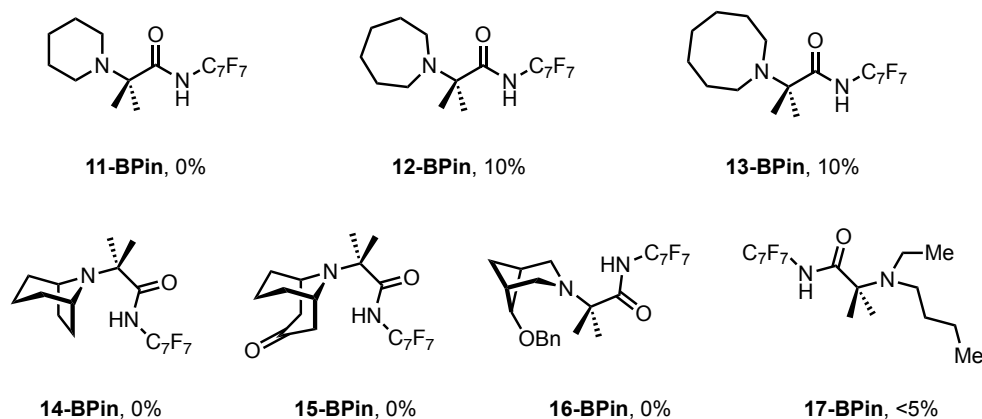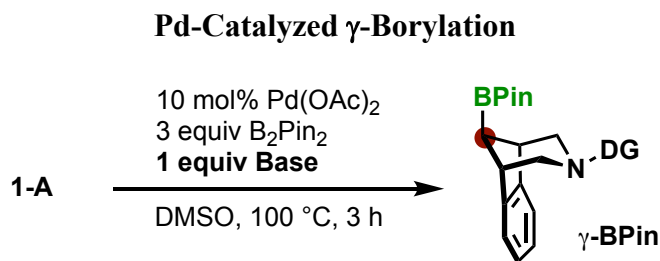
General Procedure A: A 4 mL vial was charged with substrate **1-A** (10.1 mg, 0.022 mmol, 1.0 equiv), Pd(OAc)$_2$ (0.50 mg, 0.0022 mmol, 10 mol%), and base (0.022 mmol, 1.0 equiv) followed by the addition of B$_2$Pin$_2$ (16.8 mg, 0.066 mmol, 3.0 equiv). With a syringe, DMSO (0.3 mL) was added. The vial was sealed, and the mixture was stirred at 100 °C. After 3 h at this temperature, the reaction was cooled, diluted with EtOAc, and the resulting suspension was filtered through a plug of Celite and concentrated under vacuum and analyzed via GC-FID analysis using trimethoxybenzene as internal standard (0.022 mmol, 1.0 equiv).

Table 3.5 Evaluation of carboxylate and carbonate bases

Base	γ–BPin
CsOPiv	20%
CsOAc	35%
Cs$_2$CO$_3$	10%
K$_2$CO$_3$	5%
KOAc	25%
NaOAc	35%
LiOAc	40%

Li$_2$CO$_3$	50%

Pd-Catalyzed γ-Fluorination

1-A

1) 20 mol% Pd(OAc)$_2$
20 mol% **ligand 1**
1 equiv NaOAc
MeCN, 100 °C, 1 h

2) 50 mol% NFSI
100 °C, 1 h
3) 50 mol% NFSI
100 °C, 18 h

→ γ-**F**, 40%

ligand 1   NFSI
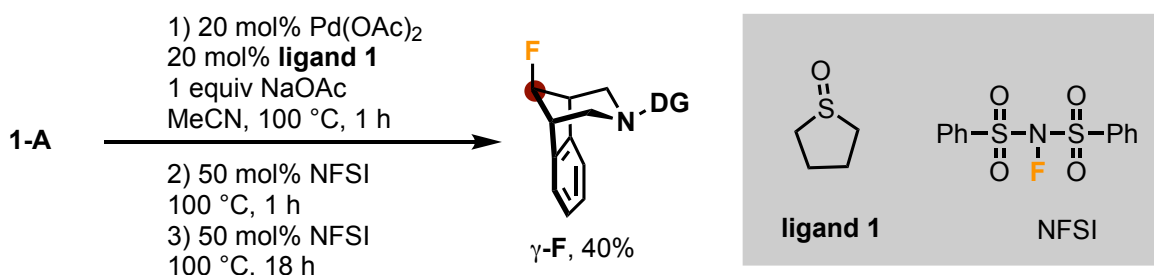
General Procedure B: A 4 mL vial was charged with substrate **1-A** (10.1 mg, 0.022 mmol, 1.0 equiv), Pd(OAc)$_2$ (1.0 mg, 0.0044 mmol, 20 mol%), and NaOAc (1.8 mg, 0.022 mmol, 1.0 equiv) followed by MeCN (0.3 mL). With a syringe, **ligand 1** (0.5 µL, 0.0044 mmol, 20 mol%) was added. The vial was sealed, and the mixture was stirred at 100 °C. After 1 h at this temperature, the reaction was cooled. Once cooled, the vial was open and NFSI (3.5 mg, 0.011 mmol, 50 mol%) was added. Again, the vial was sealed, and the mixture was stirred at 100 °C. After 1 h at this temperature, the reaction was cooled and then the vial was open and NFSI (3.5 mg, 0.011 mmol, 50 mol%) was added. The vial was sealed, and the mixture was stirred at 100 °C for 18 h. After 18 h, the reaction was cooled, diluted with EtOAc, and quenched with hydrazine (3 drops). This mixture was stirred at rt for 10 min. The resulting suspension was filtered through a plug of Celite and concentrated under vacuum and analyzed via ^{19}F NMR using 1,3,5-trifluorobenzene as internal standard (0.022 mmol, 1.0 equiv) to afford 40% yield.

Additional Pd-Catalyzed γ-Functionalizations

Results shown in Table 3.3 for oxidants evaluated in General Procedures A and B.

Table 3.6 Oxidant Screen in our Pd-catalyzed γ-Functionalization Procedures

oxidant	General Procedure A	General Procedure B
N-bromosuccinimide	**γ-Br**, trace	**γ-Br**, 0%
N- chlorosuccinimide	**γ-Cl**, 0%	**γ-Cl**, 20%
N-iodosuccinimide	**γ-I**, 0%	**γ-I**, trace
MesI(OAc)₂	**γ-OAc**, 0%	**γ-OAc**, trace

3.5.8 X-Ray Crystallography Data

X-Ray Crystallography Experimental Data of γ-F
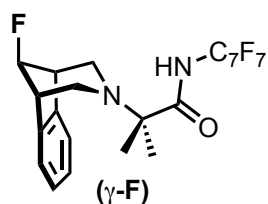
Colorless needles of **γ-F** were grown from a hexane solution of the compound at 23 ºC. A crystal of dimensions 0.10 x 0.02 x 0.02 mm was mounted on a Rigaku AFC10K Saturn 944+ CCD-based X-ray diffractometer equipped with a low temperature device and Micromax-007HF Cu-target micro-focus rotating anode (λ = 1.54187 A) operated at 1.2 kW power (40 kV, 30 mA). The X-ray intensities were measured at 85(1) K with the detector placed at a distance 42.00 mm from the crystal. A total of 2028 images were collected with an oscillation width of 1.0° in ω. The exposure times were 7 s for the low angle images, 40 s for high angle. Rigaku d*trek images were exported to CrysAlisPro for processing and corrected for absorption. The integration of the data yielded a total of 30204 reflections to a maximum 2θ value of 141.14° of which 3836 were independent and 2148 were greater than 2θ(I). The final cell constants (Table 3.1) were based on the xyz centroids of 2665 reflections above 10σ(I). Analysis of the data showed negligible decay during data collection. The structure was solved and refined with the Bruker SHELXTL (version 2016/6) software package, using the space group P2(1)/n with Z = 4 for the formula $C_{22}H_{18}F_8N_2O$. All non-

hydrogen atoms were refined anisotropically with the hydrogen atoms placed in a combination of idealized and refined positions. Full matrix least-squares refinement based on F^2 converged at R1 = 0.0911 and wR2 = 0.2445 [based on I > 2sigma(I)], R1 = 0.1491 and wR2 = 0.3127 for all data. Additional details are presented in Table 3.1 and are given as Supporting Information in a CIF file.

Table 3.7 Crystal Data and Structural Refinement for γ-F

Empirical Formula	$C_{22}H_{18}F_8N_2O$
Formula Weight	478.38
Temperature	85 (2) K
Wavelength	1.54184 Å
Crystal System	monoclinic
Space Group	P2(1)/n
Unit Cell Dimensions	a = 6.6001(7) Å, α = 90°
	b = 18.5833(15) Å, β = 94.564(9)°
	c = 16.9595(13) Å, γ = 90°
Volume	2073.5(3) Å^3
Z	4
Calculated Density	1.532 Mg/m^3
Absorption Coefficient	1.278 mm^{-1}

F(000)	976
Crystal Size	0.100 x 0.020 x 0.020 mm
Theta Range for Data Collection	3.534 to 70.712
Limiting Indices	$-7 \leq h \leq 7$, $-22 \leq k \leq 22$, $-20 \leq l \leq 20$
Reflections Collected	30204
Independent Reflections	3836
Completeness to Theta	99.5%
Absorption Correction	Semi-empirical from equivalents
Max and Min Transmission	1.00000 to 0.42936
Refinement Method	Full-matrix least-squares on F^2
Data / Restraints / Parameters	3836 / 0 / 304
Goodness-of-Fit on F^2	1.046
Final R Indices [$l>2\sigma(l)$]	R1 = 0.0911, wR2 = 0.2445
R indices (all data)	R1 = 0.1491, wR2 = 0.3127
Extinction Coefficient	N/A
Largest Difference Peak and Hole	0.349 and -0.406 Å^{-3}

X-Ray Crystallography Experimental Data of γ-OAc

(γ-OAc)
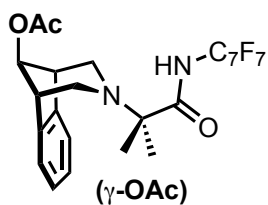
Colorless needles of **γ -OAc** were grown from an acetone solution of the compound at 23 °C. A crystal of dimensions 0.20 x 0.12 x 0.10 mm was mounted on a Rigaku AFC10K Saturn 944+ CCD-based X-ray diffractometer equipped with a low temperature device and Micromax-007HF Cu-target micro-focus rotating anode (λ = 1.54187 A) operated at 1.2 kW power (40 kV, 30 mA). The X-ray

intensities were measured at 85(1) K with the detector placed at a distance 42.00 mm from the crystal. A total of 2028 images were collected with an oscillation width of 1.0° in ω. The exposure times were 1 sec. for the low angle images, 4 sec. for high angle. Rigaku d*trek images were exported to CrysAlisPro for processing and corrected for absorption. The integration of the data yielded a total of 33169 reflections to a maximum 2θ value of 138.49° of which 4179 were independent and 4103 were greater than 2σ(I). The final cell constants (Table 3.2) were based on the xyz centroids of 19361 reflections above 10σ(I). Analysis of the data showed negligible decay during data collection. The structure was solved and refined with the Bruker SHELXTL (version 2016/6) software package, using the space group P2(1)/n with Z = 4 for the formula $C_{24}H_{21}F_7N_2O_3$. All non-hydrogen atoms were refined anisotropically with the hydrogen atoms placed in a combination of idealized and refined positions. Full matrix least-squares refinement based on F^2 converged at R1 = 0.0503 and wR2 = 0.1307 [based on I > 2sigma(I)], R1 = 0.0508 and wR2 = 0.1311 for all data. Additional details are presented in Table 3.2 and are given as Supporting Information in a CIF file. Acknowledgement is made for funding from NSF grant CHE-0840456 for X-ray instrumentation.

G.M. Sheldrick (2015) "Crystal structure refinement with SHELXL", Acta Cryst., C71, 3-8 (Open Access).

CrystalClear Expert 2.0 r16, Rigaku Americas and Rigaku Corporation (2014), Rigaku Americas, 9009, TX, USA 77381-5209, Rigaku Tokyo, 196-8666, Japan.

CrysAlisPro 1.171.38.41 (Rigaku Oxford Diffraction, 2015)

Table 3.8 Crystal Data and Structural Refinement for γ-OAc

Empirical Formula	$C_{24}H_{21}F_7N_2O_3$
Formula Weight	518.43

Temperature	85 (2) K
Wavelength	1.54184 A
Crystal System	monoclinic
Space Group	P2(1)/n
Unit Cell Dimensions	a = 13.6948(2) Å, α = 90 ° b = 9.15070(10) Å, β = 102.8070(10)° c = 18.4622(2) Å, γ = 90 °
Volume	2256.07(5) Å^3
Z	4
Calculated Density	1.526 Mg/m^3
Absorption Coefficient	1.226 mm^{-1}
F(000)	1064
Crystal Size	0.200 x 0.120 x 0.100 mm
Theta Range for Data Collection	3.658 to 69.245 °
Limiting Indices	$-16 \leq h \leq 16$, $-11 \leq k \leq 11$, $-22 \leq l \leq 22$
Reflections Collected	33169
Independent Reflections	4179
Completeness to Theta	99.9%
Absorption Correction	Semi-empirical from equivalents
Max and Min Transmission	1.00000 to 0.77789
Refinement Method	Full-matrix least-squares on F^2
Data / Restraints / Parameters	4179 / 0 / 333
Goodness-of-Fit on F^2	1.064

Final R Indices [l>2σ(l)]	R1 = 0.0503, wR2 = 0.1307
R indices (all data)	R1 = 0.0508, wR2 = 0.1311
Extinction Coefficient	0.0036(3)
Largest Difference Peak and Hole	0.851 and -0.545 Å^{-3}

X-Ray Crystallography Experimental Data of γ-I
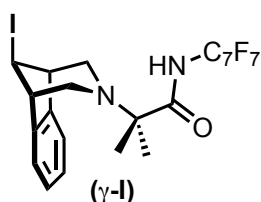
Colorless needles of **γ-I** were grown from a hexanes solution of the compound at 23 deg. C. A crystal of dimensions 0.18 x 0.05 x 0.02 mm was mounted on a Rigaku AFC10K Saturn 944+ CCD-based X-ray diffractometer equipped with a low temperature device and Micromax-007HF Cu-target micro-focus rotating anode (λ = 1.54187 A) operated at 1.2 kW power (40 kV, 30 mA). The X-ray intensities were measured at 85(1) K with the detector placed at a distance 42.00 mm from the crystal. A total of 2028 images were collected with an oscillation width of 1.0° in ω. The exposure times were 1 sec. for the low angle images, 3 sec. for high angle. Rigaku d*trek images were exported to CrysAlisPro for processing and corrected for absorption. The integration of the data yielded a total of 32312 reflections to a maximum 2θ value of 138.72° of which 4126 were independent and 3860 were greater than 2σ(I). The final cell constants (Table 3.3) were based on the xyz centroids of 14962 reflections above 10σ(I). Analysis of the data showed negligible decay during data collection. The structure was solved and refined with the Bruker SHELXTL (version 2016/6) software package, using the space group P2(1)/c with Z = 4 for the formula $C_{22}H_{18}N_2OF_7I$. All non-hydrogen atoms were refined anisotropically with the hydrogen atoms placed in idealized positions. Full matrix least-squares refinement based on F^2 converged at R1 = 0.0769 and wR2 = 0.2065 [based on I > 2sigma(I)], R1 = 0.0795 and wR2 =

0.2238 for all data. Additional details are presented in Table 3.3 and are given as Supporting Information in a CIF file. Acknowledgement is made for funding from NSF grant CHE-0840456 for X-ray instrumentation.

G.M. Sheldrick (2015) "Crystal structure refinement with SHELXL", Acta Cryst., C71, 3-8 (Open Access).

CrystalClear Expert 2.0 r16, Rigaku Americas and Rigaku Corporation (2014), Rigaku Americas, 9009, TX, USA 77381-5209, Rigaku Tokyo, 196-8666, Japan.

CrysAlisPro 1.171.38.41 (Rigaku Oxford Diffraction, 2015).

Table 3.9 Crystal Data and Structural Refinement for γ-**I**

Empirical Formula	$C_{22}H_{18}F_7IN_2O$
Formula Weight	586.28
Temperature	85 (2) K
Wavelength	1.54184 A
Crystal System	monoclinic
Space Group	P2(1)/c
Unit Cell Dimensions	a = 20.9907(7) Å, α = 90 °
	b = 6.6416(2) Å, β = 108.394(4)°
	c = 16.8750(8) Å, γ = 90 °
Volume	2232.38(15) Å^3
Z	4
Calculated Density	1.744 Mg/m^3
Absorption Coefficient	11.974 mm^{-1}
F(000)	1152

Crystal Size	0.180 x 0.050 x 0.020 mm
Theta Range for Data Collection	5.264 to 69.362 °
Limiting Indices	-25≤h≤25, -8≤k≤7, -20≤l≤18
Reflections Collected	32312
Independent Reflections	4126
Completeness to Theta	99.7%
Absorption Correction	Semi-empirical from equivalents
Max and Min Transmission	1.00000 to 0.31704
Refinement Method	Full-matrix least-squares on F^2
Data / Restraints / Parameters	4126 / 0 / 300
Goodness-of-Fit on F^2	1.152
Final R Indices [l>2σ(l)]	R1 = 0.0769, wR2 = 0.2065
R indices (all data)	R1 = 0.0795, wR2 = 0.2238
Extinction Coefficient	n/a
Largest Difference Peak and Hole	2.541 and -0.477 $Å^{-3}$

3.6 References

(1) (a) Vitaku, E.; Smith, D. T.; Njardarson, J. T. Analysis of the Structural Diversity, Substitution Patterns, and Frequency of Nitrogen Heterocycles among U.S. FDA Approved Pharmaceuticals. *J. Med. Chem.* **2014**, *57*, 10257-10274. (b) Taylor, R. D.; MacCoss, M.; Lawson, A. D. G. Rings in Drugs. *J. Med. Chem.* **2014**, *57,* 5845−5859. (c) Top 200 Pharmaceutical Products by Prescription in 2016; University of Arizona, **2016**. http://njardarson.lab.arizona.edu/sites/njardarson.lab.arizona.edu/files/ 2016Top200PharmaceuticalPrescriptionSalesPosterLowResV2.pdf (accessed September 25, 2020).
(2) Källström, S.; Leino, R. Synthesis of Pharmaceutically Active Compounds Containing a Disubstituted Piperidine Framework. *Bioorg. Med. Chem*. **2008**, *16*, 601-635.

(3) For examples of C$_\alpha$–H of alicyclic amines, see: (a) Pastine, S. J.; Gribkov, D. V.; Sames, D. sp^3 C−H Bond Arylation Directed by Amidine Protecting Groups: α-Arylation of Pyrrolidines and Piperidines. *J. Am. Chem. Soc*. **2006**, *128*, 14220−14221. (b) Campos, K. R. Direct sp^3 C−H Bond Activation Adjacent to Nitrogen in Heterocycles. *Chem. Soc. Rev*. **2007**, *36*, 1069−1084.(c) Mitchell, E. A.; Peschiulli, A.; Lefevre, N.; Meerpoel, L.; Maes, B. U. W. Direct α-Functionalization of Saturated Cyclic Amines. *Chem. - Eur. J*. **2012**, *18*, 10092−10142. (d) Shi, L.; Xia, W. Photoredox functionalization of C−H Bonds Adjacent to a Nitrogen Atom. *Chem. Soc. Rev*. **2012**, *41*, 7687−7697. (e) He, J.; Hamann, L. G.; Davies, H. M. L.; Beckwith, R. E. J. Late-Stage C−H Functionalization of Complex Alkaloids and Drugs Molecules via Intermolecular Rhodium-Carbenoid Insertion. *Nat. Commun.* **2015**, *6*, 5943. (f) Spangler, J. E.; Kobayashi, Y.; Verma, P.; Wang, D.-H.; Yu, J.-Q. α-Arylation of Saturated Azacycles and N-methylamines via Palladium(II)-Catalyzed C(sp3) − H Coupling. *J. Am. Chem. Soc*. **2015**, *137*, 11876−11879. (g) Chen, W.; Ma, L.; Paul, A.; Seidel, D. Direct α-C−H Bond Functionalization of Unprotected Cyclic Amines. *Nat. Chem.* **2017**, *10*, 165−169.

(4) For examples of amines undergoing side reactions in presence of metal catalysts and oxidants, see: (a) Murahashi, S.; Naota, T.; Yonemura, K. Ruthenium-Catalyzed Cytochrome P450-Type Oxidation of Tertiary Amines with Alkyl Hydroperoxides. *J. Am. Chem. Soc.* **1988**, *110*, 8256-8258. (b) Venkataramanan, N. S.; Kuppuraj, G.; Rajagopal, S. Metal-Salen Complexes as Efficient Catalysts for the Oxygenation of Heteroatom Containing Organic Compounds–Synthetic and Mechanistic Aspects. *Coord. Chem. Rev*. **2005**, *249*, 1249-1268. (c) Park, J.; Morimoto, Y.; Lee, Y.-M.; You, Y.; Nam, W.; Fukuzumi, S. Scandium Ion-Enhanced Oxidative Dimerization and N-Demethylation of *N,N*-Dimethylanilines by a Non-Heme Iron(IV)-Oxo Complex. *Inorg. Chem*. **2011**, *50*, 11612-11622. (d) Liu, P.; Liu, Y.; Wong, E. L.-M.; Xiang, S.; Che, C.-M. Iron Oligopyridine Complexes as Efficient Catalysts for Practical Oxidation of Arenes, Alkanes, Tertiary Amines and *N*-Acyl Cyclic Amines with Oxone. *Chem. Sci*. **2011**, *2*, 2187-2195. (e) Cai, X. W.; Sha, M.; Guo, C. P.; Pan, R. M. Synthesis of Tertiary Amine *N*-Oxides–A Review. *Asian J. Chem.* **2012**, *24*, 3781-3784. (f) Genovino, J.; Lütz, S.; Sames, D.; Touré, B. B. Complementation of Biotransformations with Chemical C–H Oxidation: Copper-Catalyzed Oxidation of Tertiary Amines in Complex Pharmaceuticals. *J. Am. Chem. Soc.* **2013**, *135*, 12346-12352. (g) Ling, Z.; Yun, L.; Liu, L.; Fu, X. Aerobic Oxidative N-Dealkylation of Tertiary Amines in Aqueous Solution Catalyzed by Rhodium Porphyrins. *Chem. Commun.* **2013**, *49*, 4214-4216. (h) Malik, H. A.; Taylor, B. L. H.; Kerrigan, J. R.; Grob, J. E.; Houk, K. N.; Du Bois, J.; Hamann, L. G.; Patterson, A. W. Non-Directed Allylic C–H Acetoxylation in the Presence of Lewis Basic Heterocycles. *Chem. Sci.* **2014**, *5*, 2352-2361. (i) Kim, S.; Ginsbach, J. W.; Lee, J. Y.; Peterson, R. L.; Liu, J. J.; Siegler, M. A.; Sarjeant, A. A.; Solomon, E. I.; Karlin, K. D. Amine Oxidative *N*-Dealkylation Via Cupric Hydroperoxide Cu–OOH Homolytic Cleavage Followed by Site-Specific Fenton Chemistry. *J. Am. Chem. Soc.* **2015**, *137*, 2867-2874.

(5) Wayner, D. D. M.; Clark, K. B.; Rauk, A.; Yu, D.; Armstrong, D. A. C−H Bond Dissociation Energies of Alkyl Amines: Radical Structures and Stabilization Energies. *J. Am. Chem. Soc.* **1997**, *119*, 8925-8932.

(6) Chu, J. C. K.; Rovis, T. Complementary Strategies for Directed C(sp^3)−H Functionalization: A Comparison of Transition-Metal-Catalyzed Activation, Hydrogen Atom Transfer, and Carbene/Nitrene Transfer. *Angew. Chem. Int. Ed*. **2018**, *57*, 62-101.

(7) For remote C–H functionalization blocking C$_\alpha$–H sites on alicyclic amines, see: (a) McNally, A.; Haffemayer, B.; Collins, B. S.; Gaunt, M. J. Palladium-Catalysed C−H activation of Aliphatic Amines to Give Strained Nitrogen Heterocycles. *Nature* **2014**, *510*, 129-133. (b) Calleja, J.; Pla,

D.; Gorman, T. W.; Domingo, V.; Haffemayer, B.; Gaunt, M. J. A Steric Tethering Approach Enables Palladium-Catalysed C−H activation of primary amino alcohols. *Nature Chemistry* **2015**, *7*, 1009-1016.

(8) For remote C−H functionalization protonating nitrogen on alicyclic amines, see: (a) Annese, C.; D'Accolti, L.; De Zotti, M.; Fusco, C.; Toniolo, C.; Williard, P. G.; Curcu, R. Concerning Selectivity in the Oxidation of Peptides by Dioxiranes. Further Insight in the Effect of Carbamate Protecting Groups. *J. Org. Chem*. **2010**, *75*, 4812-4816. (b) Mbofana, C. T.; Chong, E.; Lawniczak, J.; Sanford, M. S. Iron-Catalyzed Oxyfunctionalization of Aliphatic Amines at Remote Benzylic C−H Sites. *Org. Lett*. **2016**, *18*, 4258-4261. (c) Schultz, D. M.; Lévesque, F.; DiRocco, D. A.; Reibarkh, M; Ji, Y.; Joyce, L. A.; Dropinski, J. F.; Sheng, H.; Sherry, B. D.; Davies, I. W. Oxyfunctionalization of the Remote C−H Bonds of Aliphatic Amines by Decatungstate Photocatalysis. *Angew. Chem. Int. Ed*. **2017**, *56*, 15274-15278. (d) Lee, M.; Sanford, M. S. Remote C(sp^3)−H Oxygenation of Protonated Aliphatic Amines with Potassium Persulfate. *Org. Lett.* **2017**, *19*, 572-575. (e) White, C. M.; Zhao, J. Aliphatic C−H Oxidations for Late-Stage Functionalization. *J. Am. Chem. Soc*. **2018**, *140*, 13988-14009.

(9) For remote C−H functionalization using directing groups, see: (a) Antermite, D.; Bull, J. A. Transition Metal-Catalyzed Directed C(sp^3)−H Functionalization of Saturated Heterocycles. *Synthesis* **2019**, *51*, 3171-3204. (b) He, C.; Whitehurst, W. G.; Gaunt, M. J. Palladium-Catalyzed C(sp^3)−H Bond Functionalization of Aliphatic Amines. *Chem* **2019**, *5*, 1031-1058. (c) Li, Z.; Dechantsreiter, M.; Dandapani, S. A Systematic investigation of the Scope of Transannular C−H Heteroarylation of Cyclic Secondary Amines for Synthetic Application in Medicinal Chemistry. *J. Org. Chem*. **2020**, *85*, 6747-6760.

(10) (a)Topczewski, J. J.; Cabrera, P. J.; Saper, N. I.; Sanford, M. S. Palladium-Catalysed Transannular C−H Functionalization of Alicyclic Amines. *Nature* **2016**, *531*, 220−224. (b) Cabrera, P. J.; Lee, M.; Sanford, M. S. Second-Generation Palladium Catalyst System for Transannular C−H Functionalization of Azabicycloalkanes. *J. Am. Chem. Soc*. **2018**, *140*, 5599-5606. (c) Dewyer, A. L.; Zimmerman, P. M. Simulated Mechanism for Palladium-Catalyzed Directed γ-Arylation of Piperidine. *ACS Catal*. **2017**, *7*, 5466-5477.

(11) Zhu, R.-Y.; Saint-Denis, T. G.; Shao, Y.; He, J.; Sieber, J. D.; Senanayake, C. H.; Yu, J.-Q. Ligand-Enabled Pd(II)-Catalyzed Bromination and Iodination of C(sp^3)−H Bonds. *J. Am. Chem. Soc.* **2017**, *16*, 5724-5727.

(12) Aguilera, E. Y.; Sanford, M. S. Model Complexes for the Palladium-Catalyzed Transannular C−H Functionalization of Alicyclic Amines. *Organometallics* **2019**, *38*, 138-142.

(13) Other L-type ligands were also evaluated (e.g. bipyridine, PPh$_3$) and all gave poor yields of **γ-Br**.

(14) (a) Lapointe, D.; Fagnou, K. Overview of the Mechanistic Work on the Concerted Metallation-Deprotonation Pathway. *Chem. Lett.* **2010**, *39*, 1118-1126. (b) Gary, J. B.; Sanford, M. S. Participation of Carbonyl Oxygen in Carbon-Carboxylate Bond-Forming Reductive Elimination from Palladium. *Organometallics* **2011**, *30*, 6143-6149. (c) Ackermann, L. Carboxylate-Assisted Transition-Metal-Catalyzed C–H Bond Functionalizations: Mechanism and Scope. *Chem. Rev.* **2011**, *111*, 1315-1345. (d) Gorelsky, S. L.; Lapointe, D.; Fagnou, K. Analysis of the Palladium-Catalyzed (Aromatic) C–H Bond Metalation-Deprotonation Mechanism Spanning the Entire Spectrum of Arenes. *J. Org. Chem*. **2012**, *77*, 658-668. (e) Gorelsky, S. I. Origins of Regioselectivity of the Palladium-Catalyzed (Aromatic) C–H Bond Metalation-Deprotonation. *Coord. Chem. Rev.* **2013**, *257*, 153-164.

(15) Whitfield, S. R.; Sanford, M. S. Reactivity of Pd(II) Complexes with Electrophilic Chlorinating Reagents: Isolation of Pd(IV) Products and Observation of C–Cl Bond-Forming Reductive Elimination. *J. Am. Chem. Soc*. **2007**, *129*, 15142-15143.

(16) Racowski, J.; Sanford, M. S. Carbon-Heteroatom Bond Forming Reductive Elimination from Palladium (IV) Complexes, *In Topics in Organometallic Chemistry*, *Vol. 53*, Allan Canty, Ed., Springer, **2011**, 61-84.

(17) (a) Racowski, J. M.; Gary, B. J.; Sanford, M. S. Carbon(sp^3)–Fluorine Bond-Forming Reductive Elimination from Palladium(IV) Complexes. *Angew. Chem. Int. Ed.* **2012**, *51*, 3414-3417. (b) Chen, Y.-Q.; Singh, S.; Wu, Y.; Wang, Z.; Hao, W.; Verma, P.; Qiao, J. X.; Sunoj, R. B.; Yu, J.-Q. Pd-Catalzyed γ-C(sp^3)–H Fluorination of Free Amines. *J. Am. Chem. Soc.* **2020**, *142*, 9966-9974.

(18) Compound **α-N** was formed as a minor product (15% yield) with *N*-iodosuccinimide. With *N*-chlorosuccinimide, *N*-fluorobenzenesulfonimide, iodomesitylene diacetate, morpholino benzoate, B$_2$Pin$_2$, and S$_2$Ph$_2$, compound **α-N** was also detected but in <10% yield.

(19) (a)Larsen, M. A.; Hartwig, J. F. Iridium-Catalyzed C–H Borlyation of Heteroarenes: Scope, Regioselectivity, Application to Late-Stage Functionalization, and Mechanism. *J. Am. Chem. Soc.* **2014**, *136*, 4287-4299. (b) Fyfe, J. W. B.; Watson, A. J. B. Recent Developments in Organoboron Chemistry: Old Dogs, New Tricks. *Chem* **2017**, *3*, 31-55. (c) Xu, L.; Wang, G.; Zhang, S.; Wang, H.; Wang, L.; Liu, L.; Li, P. Recent Advances in Catalytic C–H Borylation Reactions. *Tetrahedron* **2017**, *73*, 7123-7157.

(20) Uehling, M. R.; King, R. P.; Krska, S. W.; Cernak, T.; Buchwald, S. L. Pharmaceutical Diversification via Palladium Oxidative Addition Complexes. *Science* **2019**, *363*, 405-408.

(21) Coe, J. W. Aryl Fused Azapolycyclic Compounds. WO1999055680A1, November 4, 1999.

(22) Tang, R.-J.; Milcent, T.; Crousse, B. Regioselective Halogenation of Arenes and Heterocycles in Hexafluoroisopropanol. *J. Org. Chem.* **2018**, *83*, 930–938.

(23) Foubelo, F.; Yus, M. Reduction/Hydrogenation of Aromatic Rings. In *Arene Chemistry*; John Wiley & Sons, Ltd, 2015; pp 337–364.

(24) Wagaw, S.; Buchwald, S. L. The Synthesis of Aminopyridines: A Method Employing Palladium-Catalyzed Carbon−Nitrogen Bond Formation. *J. Org. Chem.* **1996**, *61*, 7240–7241.

(25) Ji, Y.; Brueckl, T.; Baxter, R. D.; Fujiwara, Y.; Seiple, I. B.; Su, S.; Blackmond, D. G.; Baran, P. S. Innate C–H Trifluoromethylation of Heterocycles. *PNAS* **2011**, *108*, 14411–14415.

(26) Garbisch, E. W.; Griffith, M. G. Proton Couplings in Cyclohexane. *J. Am. Chem. Soc*. **1968**, *90*, 6543-6544.

Chapter 4 Leveraging Transient Alkenes for Divergent Functionalization at Multiple C−H Sites

Note: This work was performed in collaboration with Dr. Scott M. Thullen.

4.1 Introduction

Alicyclic amines appear in a wide variety of bioactive compounds.[1] In particular, six-membered alicyclic scaffolds are the single most common heterocyclic system observed in pharmaceutically relevant compounds.[2] In order to access these complex molecular architectures more efficiently, a diverse set of modular reactivity is required to rapidly diversify the core structure at multiple C−H sites.[3] Thus, it would be highly desirable to achieve the functionalization of multiple sites of these motifs in a single synthetic operation.

Scheme 4.1 (a) Our Goal (b) Previously Reported Pd-Catalyzed Transannular Arylation
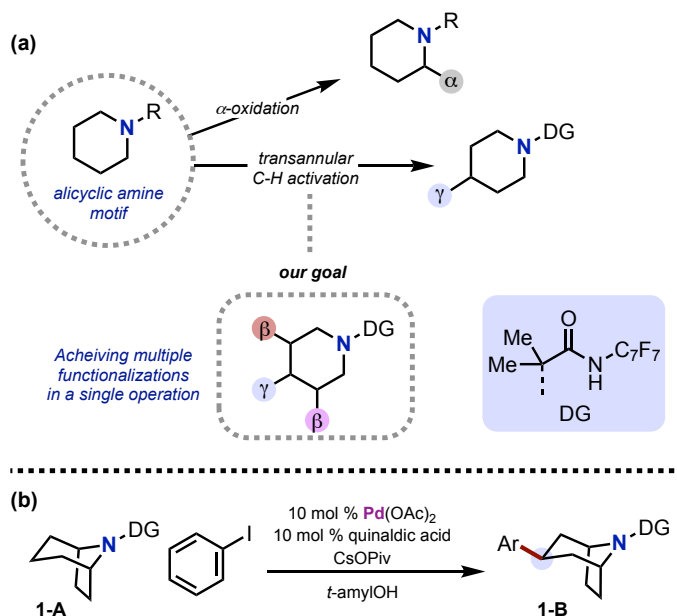
A desirable method for late-stage diversification is through C(sp^3)–H functionalization.[4] The majority of C–H functionalizations of alicyclic amines have focused on the functionalization of a single C–H bond. In particular, the highly activated C(sp^3)–H bond α to nitrogen is the most commonly activated and functionalized (Scheme 4.1a).[5] In contrast, the remote C$_\beta$–H and C$_\gamma$–H sites are relatively less activated and therefore are challenging to access. Recently, our group has addressed this challenge by developing a directed Pd-catalyzed transannular C–H activation sequence that enables selective C$_\gamma$–H arylation of alicyclic amines (Scheme 4.1b).[6-8] Of importance, by installing the directing group on the amine nitrogen, the alicyclic amine core remains available for other possible C–H functionalizations. As such, we were inspired to leverage this transannular C–H activation to achieve multi-site C–H functionalization of these motifs (Scheme 4.1).

Herein, we report a Pd-catalyzed remote functionalization at multiple C(sp^3)–H sites on alicyclic amines via transannular C–H activation in combination with traditionally overlooked Pd-mediated pathways to enable the rapid diversification of these cores. Moreover, we provide mechanistic insight into this transformation through isolation and study of a Pd$^\text{I}$–Pd$^\text{I}$ dimer.

4.2 Results and Discussion

Exploring Multiple C(sp^3)–H Site Functionalizations

We started these investigations with our previously reported Pd-catalyzed arylation reaction[7] of substrate **1-A** (Scheme 4.1b). By varying reaction additives (specifically bases and acids), we obtained mixtures of products including γ-arylation product **1-B** and allylic arylation product **1-C**. Notably, the generation of **1-C** involves the functionalization of three different unactivated C(sp^3)–H bonds. We confirmed the structure of **1-C** via ^{1}H NMR spectroscopic

analysis and X-ray crystallography. Both confirm that the aryl group is installed at the axial C_β position (Scheme 4.2). The optimal reaction conditions for allylic arylation were established to be 10 mol % of Pd(OAc)$_2$, 10 mol % of **L1**, 2 equiv of aryl iodide, 3 equiv of acetic acid, and Cs$_2$CO$_3$ in *tert*-amylOH for 18 h at 140 °C. Under these conditions, **1-C** is formed in 64% isolated yield. With this method in hand, the scope of this reaction with respect to the aryl iodide component was explored. Scheme 4.2 demonstrates that aryl iodides bearing both electron-withdrawing and electron-donating substituents affords products such as **2-C** and **3-C** in 71% and 45% isolated yield, respectively. Di-substituted aryl iodides also reacted to afford **5-C** in 69% yield. Sterically bulky *ortho*-substituted aryl iodides were also effective substrates, for instance, providing **8-C** in 56% yield. (Hetero)aryl iodides were also well tolerated, for example affording 60% of **9-C**.

Scheme 4.2 Scope of Aryl Iodides for Allylic Arylation
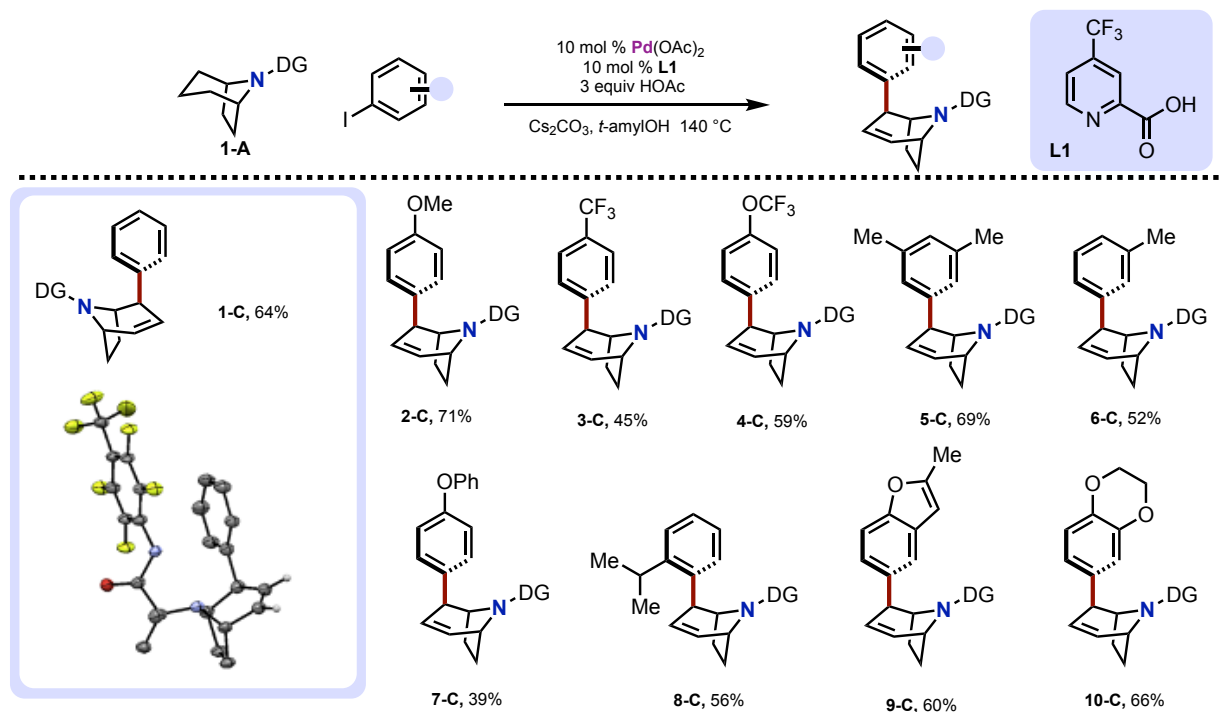
We hypothesized that potentially different allylic functionalizations could be achieved by replacing the ArI with an alternate oxidant. Indeed, in the absence of ArI with air as the terminal

oxidant, we observed allylic acetoxylation product **1-D** in <5% yield. Inspired by work from the White lab,[9] we explored alternative weakly nucleophilic oxidants, and ultimately identified benzoquinone as the optimal oxidant with acetic acid as the nucleophile. Under these conditions, product **1-D** was obtained in 55% isolated yield. Under these conditions, we found that the reaction worked with various carboxylic acids ranging in sterics from ethyl-, isopropyl-, and *tert*-butyl-affording moderate yields of **2-D**, **3-D**, **and 4-D**, respectively. Electronically diverse benzoic acid derivatives also reacted to afford **6-D**, **7-D**, and **8-D** in 64%, 39%, and 24% isolated yield, respectively. All products were characterized via ^{1}H and ^{13}C NMR spectroscopic analysis. In addition, the X-ray crystal structure of compound **2-D** further confirms the installation of the carboxylate at the β-site in the axial position.

Scheme 4.3 Scope of Allylic Acetoxylation Reaction

94
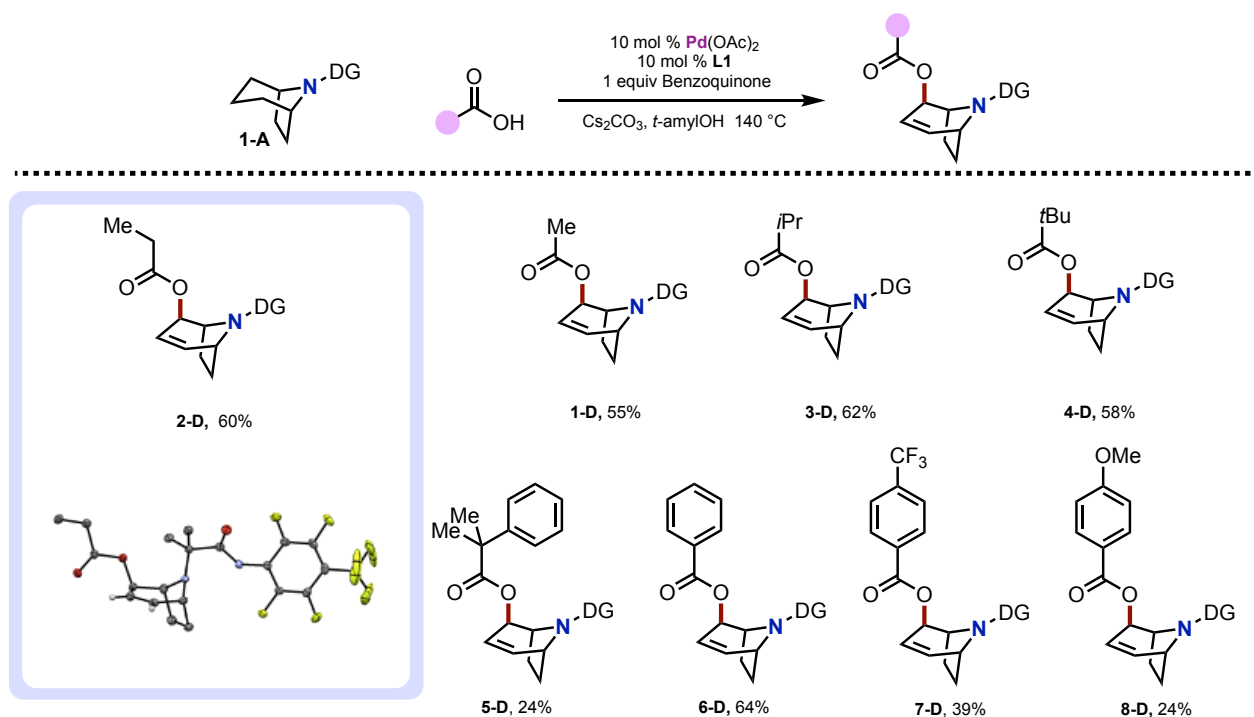
Mechanistic Investigations of Allylic Functionalization Transformations

        With optimal conditions and an established scope of allylic arylation and acetoxylation in hand, we sought to investigate the mechanism of their formation. As demonstrated in Chapters 2 and 3 of this thesis, we envisioned that we could gain insight into these transformations by isolation of a Pd^{II}–amine complex. Applying analogous conditions from our previously synthesized Pd^{II} complexes,[8] substrate **1-A** was stirred with Pd(OAc)$_2$ in the presence of 1 equiv of CsOPiv in MeCN at 60 °C. After 24 h, this reaction resulted in the formation of a bright orange solid (Figure 4.1a). ^{1}H NMR spectroscopic analysis and X-ray crystallography established that this orange solid is the Pd^I–Pd^I dimer **Dimer-1**. Each Pd^I center is coordinated to the two nitrogens of the directing group and then bridged by an alkene from the adjacent Pd center. The Pd-bound alkenes show diagnostic resonances between the 4.0 ppm to 5.5 ppm region via ^{1}H NMR spectroscopy.

**Figure 4.1** Mechanistic Studies with **Dimer-1**
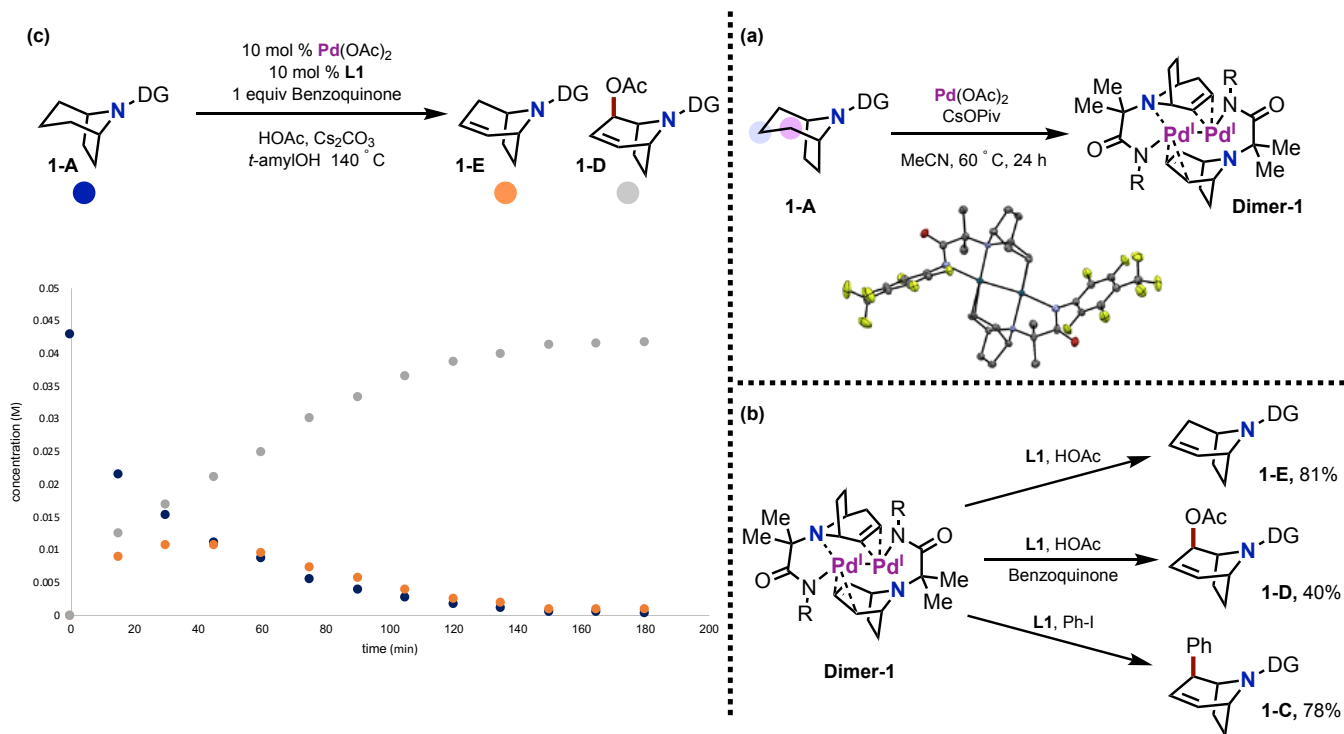
Dimer-1 was tested to see if it is a competent intermediate for allylic arylation and allylic acetoxylation (Figure 4.1b). Subjecting **Dimer-1** to the allylic arylation conditions (1 equiv of **L1**, 2 of equiv PhI in *t*-amylOH) resulted in the formation of **1-C** in 78% yield. Similarly, treating **Dimer-1** to the allylic acetoxylation conditions (1 equiv of **L1**, 1 equiv of Benzoquinone, and 5 equiv of HOAc in *t*-amylOH) afforded product **1-D** in 40% yield. Moreover, when **Dimer-1** was subjected to analogous conditions in the absence of an oxidant, the alkene **1-E** was released in 81% yield.

We next probed whether an alkene intermediate is detectable during allylic acetoxylation. As shown in Figure 4.1c, we observe the growth and then decay of alkene product, **1-E**, during the reaction. These data are consistent with dehydrogenated compound **1-E** serving as an intermediate en route to **1-D**.

A potential mechanism that accounts for the observed reactivity is shown in Scheme 4.4. A Pd^{II} catalyst binds to substrate **1-A** in a bidentate orientation between the substrate nitrogen atom and the deprotonated amide.[8] **1-A** undergoes a conformational change to the chair conformer, which places the γ-C–H bond in close proximity to the Pd^{II} center. The Pd center with a carboxylate ligand then participates in C–H activation via a concerted-metalation deprotonation (CMD) mechanism[8,10,11] to form **Int-1**. We propose a β-hydride elimination[12,13] event can occur to form a Pd-bound alkene followed by the loss of HOAc. The alkene can then be liberated from the Pd center via protonation or ligand exchange, generating the dehydrogenated product, **1-E**, and a Pd^0 center that can reenter the catalytic cycle upon re-oxidation.

Scheme 4.4 Proposed Mechanism of Transformations
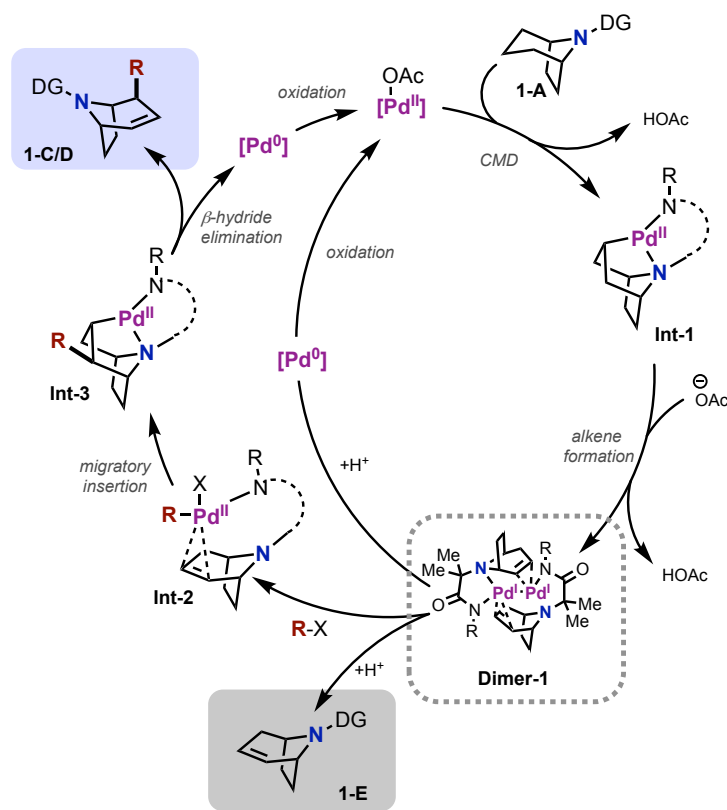
It is likely that **Dimer-1** forms via a comproportionation between Pd^0 and Pd^{II}.[14] When an oxidant, such as ArI, is present this can intercept the Pd^0 intermediate and undergo oxidative addition to afford an aryl Pd^{II}, **Int-2**.[15,16] Driven by complexation with the directing group, the Pd-bound alkene can undergo a migratory insertion into the Pd–aryl bond,[15,17] forging a new C–C bond at the β-position, **Int-3**. Similarly, as the reaction for forming the first alkene, the Pd center can then undergo β-hydride elimination in the opposite direction, forming the Pd-bound allylic-type product, which is liberated by protonation as the final product **1-C/D**. The Pd species can then re-enter the catalytic cycle after subsequent oxidation. Similarly, the allyl-acetate product likely is formed by similar means through a well-established allylic oxidation mechanism.[9,18]

4.3 Conclusions

In summary, we disclose Pd-catalyzed transannular C–H functionalization methodology that accesses multiple remote $C(sp^3)$–H sites of alicyclic amines in a single synthetic operation. In both allylic arylation and acetoxylation transformations, we achieve a wide scope of aryl iodides and carboxylic acids, respectively. Both transformations showed the oxidant/nucleophile selectively installed at the axial C_β position. Moreover, the alkene provides a handle for further reactivity allowing for facile access to highly decorated alicyclic amines.

Additionally, we showcase the use of isolated **Dimer-1** for mechanistic insight into these transformations. From our studies, it is revealed that our transformations occur via a transient alkene released from **Dimer-1**, in which the dimer allows for further Pd-mediated pathways to enable the rapid diversification of alicyclic amines.

4.4 Experimental Procedures

### 4.4.1 General Procedures, Materials and Methods

General Procedures

NMR spectra were obtained on a Varian VNMR 700 (699.76 MHz for ^1H; 175.95 MHz for ^{13}C) or a Varian VNMR 500 (500.09 MHz for ^1H; 470.56 MHz for ^{19}F) or a Varian NMR 400 (128.38 MHz for ^{11}B NMR) spectrometer. ^1H and ^{13}C chemical shifts are reported in parts per million (ppm) relative to TMS, with the residual solvent peak (most commonly $CDCl_3$) used as an internal reference. ^{19}F chemical shifts are reported in ppm and are referenced on a unified scale to the frequency of the residual solvent peak in the ^1H NMR spectrum. ^1H and ^{19}F multiplicities are reported as follows: singlet (s), doublet (d), doublet of doublets (dd), doublet of doublets of doublets (ddd), doublet of triplets (dt), triplet (t), quartet (q), and multiplet (m). High resolution

mass spectra were obtained at the University of Michigan core facility. X-ray crystallographic data were collected on a Bruker SMART APEX-I CCD-based X-ray diffractometer. Elemental analyses were conducted by Midwest Microlabs. Flash chromatography was conducted on a Biotage Isolera One chromatography system using preloaded high-performance silica gel columns (10 g, 25 g, 50 g, or 100 g as appropriate). GC-FID was conducted on a Shimadzu CG-17A system. Melting points were obtained on a OptiMelt automated melting point system.

Materials and Methods

All reagents were obtained from a commercial vendor (Aldrich, CombiBlocks, Oakwood, Synthonix, Enamine, Carbosynth, Pressure Chemicals, Matrix, SantaCruz Biotech, or Ontario Chemicals). 8-Azabicyclo[3.2.1]octane hydrochloride was purchased from PharmaBlock. $Pd(OAc)_2$ was purchased from Pressure Chemical Company. Acetonitrile and *tert*-amyl alcohol were purchased from Sigma-Aldrich. Hydrazine monohydrate was purchased from Alfa Aesar. All commercial reagents were used without further purification/drying unless explicitly stated in the experimental section. The manipulation of solid reagents was conducted on the benchtop unless otherwise stated. Reactions were conducted under ambient atmosphere unless otherwise stated. Reaction vessels were sealed with either a septum (flask) or a Teflon-lined cap (4 mL or 20 mL vial) with Teflon tape wrapped around the cap. Reactions conducted at elevated temperatures were heated on a hot plate using an aluminum block. Temperature was regulated using an external thermocouple.

4.4.2 Synthesis of Starting Materials

(A) + (B) → toluene, 140 °C, 18 h → (C)
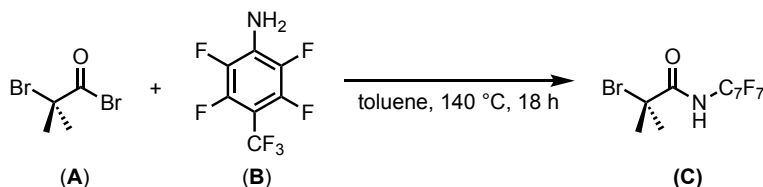
Synthesis of C: α-Bromo propanamide **C** was synthesized following a literature procedure[6,7] from starting materials **A** and **B**.

Directing Group Installation Procedures[6,7]

(D1) (C) → K$_2$CO$_3$, NaI / MeCN, 60 °C, 18 h → (S1)
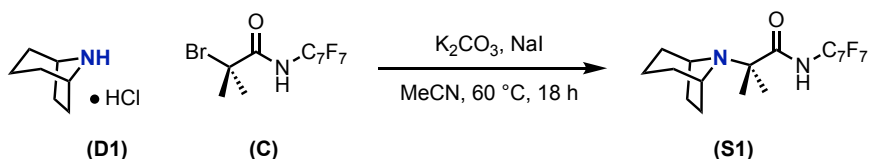
A 20 mL scintillation vial was charged with **D1** (250 mg, 1.70 mmol, 1.0 equiv), α-bromo propanamide **C** (650 mg, 1.70 mmol, 1.0 equiv), K$_2$CO$_3$ (752 mg, 5.44 mmol, 3.2 equiv), and NaI (127 mg, 0.85 mmol, 0.5 equiv). To the solids, anhydrous acetonitrile (15 mL) was added. The vial was sealed, and the reaction was stirred at an external temperature of 60 °C. After 18 h, the reaction was cooled to rt, diluted with EtOAc (~5 mL), and filtered through silica gel. The filtrate was concentrated under reduced pressure. Final purification via column chromatography (gradient elution from 0% to 5% EtOAc in hexanes) afforded product **S1** (450 mg, 64% yield) as a white solid.[2] Amine derivatives **S1–S3** were prepared in an analogous manner using the appropriate amine starting material.
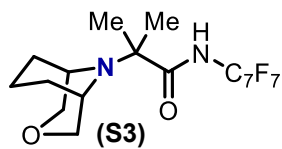
Characterization of Directing Group Installation Products (S1 *through* **S3)**

(S1)
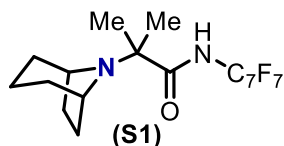
S1: The ^{1}H, ^{13}C, ^{19}F NMR spectral data for **S1** matched that reported in the literature.[6,7]
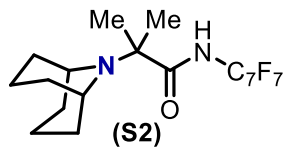
S2: The ^{1}H, ^{13}C, ^{19}F NMR spectral data for **S2** matched that reported in the literature.[6,7]

S3: Directing Group Installation Procedure was followed using 3-Oxa-9-azabicyclo[3.3.1]nonane hydrochloride as the substrate.
Isolated yield: 350 mg, 48% (white solid)

^{1}H NMR (700 MHz, CDCl$_3$, 23 ºC): δ 9.54 (br s, 1H), 3.98 (t, J = 2.6 Hz, 1H), 3.97 (t, J = 2.6 Hz, 1H), 3.89 (d, J = 1.2 Hz, 1H), 3.88 (d, J = 1.2 Hz, 1H), 3.00 (s, 2H), 2.60 (qt, J = 13.2, 6.4 Hz, 1H), 2.02 (tt, J = 13.6, 5.2 Hz, 2H), 1.82-1.70 (multiple peaks, 3H), 1.53 (s, 6H).

^{13}C NMR (176 MHz, CDCl$_3$, 23 ºC): δ 176.3, 72.3, 65.1, 50.0, 29.1, 25.7, 20.2. *Carbon resonances associated with perfluoroaryl group are not observed.*[6,7]

^{19}F NMR (470 MHz, CDCl$_3$, 23 ºC): δ –56.0 (t, 3F), –141.0 (m, 2F), –143.6 (m, 2F).

HRMS-electrospray (m/z): [M]$^+$ calcd. for C$_{18}$H$_{19}$F$_7$N$_2$O$_2$, 429.1408; found, 429.1407.

Melting point: 135-137°C

Chromatography conditions: 5% EtOAc in hexanes

4.4.3 Scope and Isolation of Allylic Arylation

General Procedure A: Under ambient conditions, a 0.02 M stock solution of Pd(OAc)$_2$ (22.5 mg Pd(OAc)$_2$ in 5 mL DCM) and 0.02 M stock solution of **L2** (19.1 mg of **L2** in 5 mL MeOH) were prepared. To a 4 mL vial, an aliquot of the **L2** solution (150 µL, 0.003 mmol, 10 mol%) was added and MeOH was removed at 70 °C for 5 min. To the same 4 mL vial, an aliquot of the Pd(OAc)$_2$ solution (150 µL, 0.003 mmol Pd, 10 mol%) was added and DCM was removed at 40 °C for 5 min. In the 4 mL vial with Pd(OAc)$_2$ and **L2**, substrate **S1** (12.37 mg, 0.03 mmol, 1.0 equiv) and Cs$_2$CO$_3$ (10.67 mg, 0.033 mmol, 1.1 equiv) were added. If the aryl iodide is a solid, it was added (0.06 mmol, 2.0 equiv) before solvent, if liquid, it was added after. The reaction mixture was then diluted with *t*-amylOH (0.30 mL). Acetic acid (5.1 µL, 0.09 mmol, 3 equiv). A stirbar was added to the vial and the vial was sealed with a Teflon-lined screw cap. The vial was heated to 140 °C for 18 h. After, the reaction was allowed to cool to room temperature and diluted with DCM (3.0 mL). The reaction solution was then filtered through a Celite pipette and washed with DCM. The

volatiles were removed under reduced pressure, and the residue was purified via column

chromatography to obtain the desired product **1-C** through **10-C**.
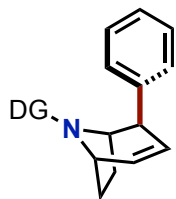
1-C: General Procedure A was followed using iodobenzene as the coupling partner.
Isolated yield: 9.3 mg, 64% (white solid). Procedures repeated with diphenyliodonium chloride (73%), potassium phenyltrifluoroborate (48%), and bromobenzene (23%)

^{1}H NMR (700 MHz, CDCl$_3$, 23 °C): δ 8.98 (br s, 1H), 7.25 (s, 2H), 7.17 (t, J = 7.6 Hz, 2H), 6.90 (t, J = 7.3 Hz, 1H), 6.34 (ddd, J = 9.5, 5.9, 1.5 Hz, 1H), 5.58 (ddd, J = 9.5, 4.0, 1.5 Hz, 1H), 3.71 (t, J = 5.5 Hz, 1H), 3.63 (d, J = 7.5 Hz, 1H), 3.34 (d, J = 4.0 Hz, 1H), 2.15 (tdd, J = 11.1, 7.5, 3.0 Hz, 1H), 2.02 (ddd, J = 12.2, 9.4, 3.1 Hz, 1H), 1.96 (tt, J = 11.6, 5.9 Hz, 1H), 1.89 (ddd, J = 15.5, 9.6, 6.1 Hz, 1H), 1.26 (s, 3H), 1.03 (s, 3H).

^{13}C NMR (176 MHz, CDCl$_3$, 23 °C): δ 175.4, 143.7, 136.5, 128.6, 128.0, 126.0, 124.4, 63.6, 63.3, 56.9, 53.0, 35.1, 31.1, 23.7, 23.6. *Carbon resonances associated with perfluoroaryl group are not observed* [6,7]

^{19}F NMR (470 MHz, CDCl$_3$, 23 °C): δ –56.0 (m, 3F), –142.0 (apparent s, 2F), –143.3 (apparent s, 2F).

HRMS-electrospray (m/z): [M]$^+$ calcd. for C$_{24}$H$_{21}$F$_7$N$_2$O, 487.1542; found, 487.1615.

Melting point: 97-100 °C

Chromatography conditions: Gradient elution from 2% to 5% EtOAc in hexanes
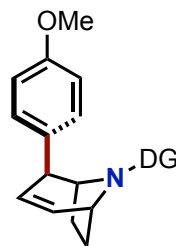
2-C: General Procedure A was followed using 1-iodo-4-methoxybenzene as the coupling partner.
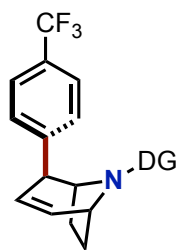Isolated yield: 11.0 mg, 71% (white solid)

^{1}H NMR (600 MHz, CDCl$_3$) δ 8.82 (s, 1H), 7.16 (m, 2H), 6.65 (m, 2H), 6.30 (ddd, J = 9.5, 6.0, 1.5 Hz, 1H), 5.54 (ddd, J = 9.5, 4.0, 1.4 Hz, 1H), 3.77 (t, J = 5.8 Hz, 1H), 3.58 (s, 3H), 3.55 (d, J = 7.5 Hz, 1H), 3.28 (d, J = 3.5 Hz, 1H), 2.14 (ddd, J = 12.9, 6.4, 3.5 Hz, 1H), 2.01 (ddd, J = 12.1, 9.3, 2.8 Hz, 1H), 1.94 (dd, J = 11.6, 5.8 Hz, 1H), 1.85 (m, 1H), 1.29 (s, 3H), 1.14 (s, 3H).

^{13}C NMR (151 MHz, CDCl$_3$) δ 175.1, 158.0, 136.0, 128.8, 124.3, 113.6, 64.1, 63.3, 56.2, 54.8, 52.0, 35.0, 30.6, 24.8, 22.1. *Carbon resonances associated with perfluoroaryl group are not observed.* [6,7]

^{19}F NMR (564 MHz, CDCl$_3$) δ –56.1 (dt, J = 74.8, 21.7 Hz, 3F), –142.2 (m, 2F), –143.2 (td, J = 13.6, 6.2 Hz, 2F).

Chromatography conditions: Gradient elution from 0% to 5% EtOAc in hexanes

3-C: General Procedure A was followed using 4-iodotrifluorotoluene as the coupling partner.

Isolated yield: 7.48 mg, 45% (white solid). Isolated with an impurity of alkene product of **N3**.

^{19}F NMR (564 MHz, CDCl$_3$) δ –56.3 (t, 3F), –62.6 (s, 3F), –141.5 (m, 2F), –144.1 (m, 2F).

Chromatography conditions: Gradient elution from 0% to 5% EtOAc in hexanes
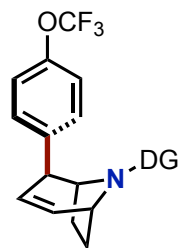
4-C: General Procedure A was followed using 1-iodo-4-trifluoromethoxybenzene as the coupling partner.
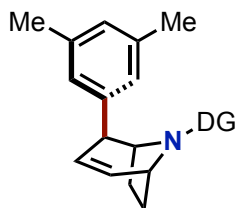
Isolated yield: 10.1 mg, 59% (white solid)

^{1}H NMR (600 MHz, CDCl$_3$) δ 8.88 (s, 1H), 7.28 (d, J = 8.6 Hz, 2H), 7.04 (d, J = 8.2 Hz, 2H), 6.36 (ddd, J = 9.4, 5.9, 1.4 Hz, 1H), 5.55 (ddd, J = 9.5, 4.0, 1.4 Hz, 1H), 3.71 (t, J = 5.7 Hz, 1H), 3.61 (d, J = 7.6 Hz, 1H), 3.34 (d, J = 3.5 Hz, 1H), 2.15 (m, 1H), 1.95 (m, 4H), 1.26 (s, 3H), 1.03 (s, 3H).

^{13}C NMR (151 MHz, CDCl$_3$) δ 175.0, 142.1, 136.8, 129.2, 123.8, 120.6, 63.3, 63.2, 56.8, 52.0, 34.8, 30.9, 23.5, 23.4. *Carbon resonances associated with perfluoroaryl group are not observed.*[6,7]

^{19}F NMR (564 MHz, CDCl$_3$) δ –56.3 (t, J = 21.7 Hz, 3F), –58.33 (s, 3F), –141.5 (qd, J = 21.7, 13.8 Hz), -143.7 (td, J = 13.4, 5.9 Hz, 2F).

Chromatography conditions: Gradient elution from 0% to 5% EtOAc in hexanes

5-C: General Procedure A was followed using 1-iodo-3,5-dimethylbenzene as the coupling partner.
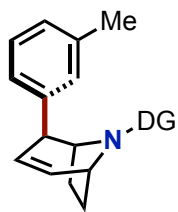
Isolated yield: 10.6 mg, 69% (white solid)

^{1}H NMR (600 MHz, CDCl$_3$) δ 8.81 (s, 1H), 6.84 (s, 2H), 6.33 (m, 2H), 5.55 (ddd, J = 9.5, 4.0, 1.4 Hz, 1H), 3.81 (t, J = 5.7 Hz, 1H), 3.59 (d, J = 7.5 Hz, 1H), 3.25 (d, J = 3.4 Hz, 1H), 2.16 (ddd, J = 13.0, 6.5, 3.7 Hz, 1H), 2.12 (s, 6H), 2.02 (ddd, J = 12.0, 9.3, 2.7 Hz, 1H), 1.94 (dt, J = 17.5, 5.9 Hz, 1H), 1.84 (m, 1H), 1.31 (s, 3H), 1.20 (s, 3H).

^{13}C NMR (151 MHz, CDCl$_3$) δ 175.00, 143.4, 138.3, 136.1, 126.9, 125.7, 124.1, 64.4, 63.4, 55.8, 52.5, 35.1, 30.8, 25.4, 21.4, 20.8. *Carbon resonances associated with perfluoroaryl group are not observed.*[6,7]

^{19}F NMR (564 MHz, CDCl$_3$) δ –56.0 (td, J = 21.7, 6.5 Hz, 3F), –142.4 (m, 2F), –143.2 (td, J = 13.8, 6.6 Hz, 2F).

Chromatography conditions: Gradient elution from 0% to 5% EtOAc in hexanes

6-C: General Procedure A was followed using 1-iodo-3-methylbenzene as the coupling partner.
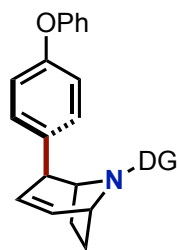
Isolated yield: 7.1 mg, 52% (white solid)

^{1}H NMR (600 MHz, CDCl$_3$) δ 8.88 (s, 1H), 7.08 – 6.97 (m, 3H), 6.60 (d, J = 7.3 Hz, 1H), 6.33 (ddd, J = 9.5, 6.0, 1.5 Hz, 1H), 5.56 (ddd, J = 9.5, 4.0, 1.4 Hz, 1H), 3.76 (t, J = 5.7 Hz, 1H), 3.61 (d, J = 7.6 Hz, 1H), 3.29 (d, J = 3.5 Hz, 1H), 2.18 (s, 3H), 2.16 (dd, J = 10.6, 2.2 Hz, 1H), 2.02 (ddd, J = 12.1, 9.4, 2.9 Hz, 1H), 1.94 (ddd, J = 17.4, 11.5, 5.9 Hz, 1H), 1.90 – 1.82 (m, 1H), 1.28 (s, 3H), 1.12 (s, 3H).

^{13}C NMR (151 MHz, CDCl$_3$) δ 175.1, 143.5, 138.3, 136.2, 128.7, 128.3, 126.3, 124.8, 124.1, 63.9, 63.2, 56.3, 52.7, 35.0, 30.8, 24.5, 22.3, 21.0. *Carbon resonances associated with perfluoroaryl group are not observed.*[6,7]

^{19}F NMR (564 MHz, CDCl$_3$) δ –56.0 (t, J = 21.7 Hz, 3F), –142.3 (m, 2F), –143.3 (td, J = 13.9, 6.6 Hz, 2F).

Chromatography conditions: Gradient elution from 0% to 5% EtOAc in hexanes

7-C: General Procedure A was followed using 1-iodo-4-phenoxybenzene as the coupling partner.
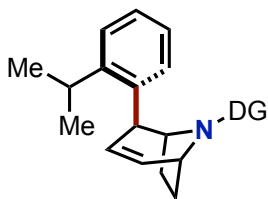
Isolated yield: 6.8 mg, 39% (white solid)

^{1}H NMR (600 MHz, CDCl$_3$) δ 8.99 (s, 1H), 7.28 (td, 2H), 7.23 (d, 2H), 7.06 (t, J = 7.4 Hz, 1H), 6.85 (m, 4H), 6.33 (ddd, J = 9.4, 5.9, 1.3 Hz, 1H), 5.57 (ddd, J = 9.5, 4.0, 1.3 Hz, 1H), 3.70 (t, J = 5.7 Hz, 1H), 3.62 (d, J = 7.6 Hz, 1H), 3.33 (d, J = 3.6 Hz, 1H), 2.14 (dd, J = 10.6, 2.0 Hz, 1H), 1.99 (m, 2H), 1.90 (dd, J = 11.1, 7.8 Hz, 1H), 1.27 (s, 3H), 1.06 (s, 3H).

^{13}C NMR (151 MHz, CDCl$_3$) δ 175.2, 157.4, 155.5, 138.6, 136.3, 129.6, 129.1, 124.2, 123.0, 119.3, 118.1, 63.4, 63.1, 56.9, 52.1, 34.9, 30.7, 23.7, 23.4. *Carbon resonances associated with perfluoroaryl group are not observed.* [6,7]

^{19}F NMR (564 MHz, cdcl$_3$) δ –55.94 (t, J = 21.7 Hz, 3F), –141.6 (m, 2F), –143.5 (td, J = 13.5, 6.0 Hz, 2F).

Chromatography conditions: Gradient elution from 0% to 5% EtOAc in hexanes

8-C: General Procedure A was followed using 1-iodo-2-isopropylbenzene as the coupling partner.

Isolated yield: 8.9 mg, 56% (white solid) Isolated with an 8% impurity of dehydrogenated product **1-E**.

^{1}H NMR (600 MHz, CDCl$_3$) δ 9.05 (s, 1H), 7.22 (m, 2H), 6.91 (dtd, J = 28.7, 7.4, 1.2 Hz, 2H), 6.35 (ddd, J = 9.4, 6.0, 1.6 Hz, 1H), 5.51 (ddd, J = 9.4, 4.0, 1.4 Hz, 1H), 3.74 (t, J = 5.7 Hz, 1H), 3.55 (d, J = 3.6 Hz, 1H), 3.48 (d, J = 7.5 Hz, 1H), 3.15 (m, 1H), 2.16 (m, 1H), 1.95 (m, 3H), 1.55 (s, 1H), 1.33 (d, J = 6.8 Hz, 3H), 1.27 (s, 3H), 1.18 (d, J = 6.8 Hz, 3H), 1.02 (s, 3H).
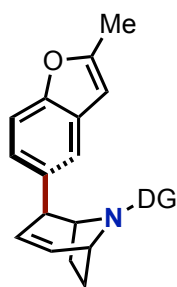
¹³C NMR (151 MHz, CDCl₃) δ 175.2, 146.7, 139.2, 136.0, 127.6, 126.4, 126.0, 125.32, 125.25, 63.1, 62.4, 56.7, 49.2, 35.0, 31.1, 28.3, 25.2, 23.7, 23.3, 22.9. *Carbon resonances associated with perfluoroaryl group are not observed.* [6,7]

¹⁹F NMR (564 MHz, CDCl₃) δ –56.0 (t, *J* = 21.7 Hz, 3F), –142.0 (m, 2F), –142.95 (td, *J* = 13.7, 6.3 Hz, 2F).

Chromatography conditions: Gradient elution from 0% to 5% EtOAc in hexanes

9-C: General Procedure A was followed using 5-iodo-2-methylbenzofuran as the coupling partner.
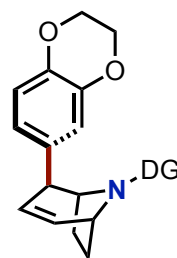
Isolated yield: 9.7 mg, 60% (white solid)

¹H NMR (600 MHz, cdcl₃) δ 8.64 (s, 1H), 7.33 (s, 1H), 7.09 (d, *J* = 1.6 Hz, 2H), 6.33 (ddd, *J* = 9.5, 6.0, 1.5 Hz, 1H), 6.22 (s, 1H), 5.60 (ddd, *J* = 9.5, 4.0, 1.5 Hz, 1H), 3.86 (t, *J* = 5.8 Hz, 1H), 3.60 (d, *J* = 7.5 Hz, 1H), 3.41 (d, *J* = 3.7 Hz, 1H), 2.33 (s, 3H), 2.18 (m, 1H), 2.04 (ddd, *J* = 11.8, 9.3, 2.6 Hz, 1H), 1.94 (dd, *J* = 11.5, 5.8 Hz, 1H), 1.91 – 1.83 (m, 1H), 1.30 (s, 3H), 1.21 (s, 3H).

¹³C NMR (151 MHz, CDCl₃) δ 174.9, 156.3, 153.1, 137.7, 136.1, 129.4, 124.3, 123.4, 119.1, 110.4, 102.0, 65.0, 63.4, 55.7, 52.6, 35.1, 30.6, 25.9, 20.9, 13.5. *Carbon resonances associated with perfluoroaryl group are not observed.* [6,7]

¹⁹F NMR (564 MHz, cdcl₃) δ –55.86 (t, *J* = 21.7 Hz, 3F), –142.55 (m, 2F), –142.91 (m, 2F).

Chromatography conditions: Gradient elution from 0% to 5% EtOAc in hexanes

10-C: General Procedure A was followed using 6-iodo-2,3-dihydrobenzo[1,4]dioxine as the coupling partner.

Isolated yield: 10.8 mg, 66% (white solid)

¹H NMR (600 MHz, CDCl₃) δ 9.07 (s, 1H), 6.75 (d, *J* = 2.1 Hz, 1H), 6.71 (dd, *J* = 8.2, 2.0 Hz, 1H), 6.61 (d, *J* = 8.2 Hz, 1H), 6.29 (ddd, *J* = 9.4, 5.9, 1.4 Hz, 1H), 5.51 (ddd, *J* = 9.5, 4.0, 1.4 Hz, 1H), 4.08 (ddd, *J* = 21.6, 7.7, 3.7 Hz, 4H), 3.71 (t, *J* = 5.7 Hz, 1H), 3.58 (d, *J* = 7.6 Hz, 1H), 3.22 (d, *J* = 3.6 Hz, 1H), 2.11 (m, 1H), 1.96 (m, 2H), 1.83 (m, 1H), 1.26 (s, 3H), 1.10 (s, 3H).

¹³C NMR (151 MHz, cdcl₃) δ 175.4, 143.5, 141.8, 136.9, 136.1, 124.3, 120.5, 117.0, 116.7, 64.0, 64.0, 63.6, 63.1, 56.5, 52.0, 34.9, 30.6, 24.0, 23.0. *Carbon resonances associated with perfluoroaryl group are not observed.* [6,7]

¹⁹F NMR (564 MHz, CDCl₃) δ –56.1 (t, *J* = 21.7 Hz, 3F), –141.9 (m, 2F), –143.1 (td, *J* = 13.9, 6.5 Hz, 2F).

Chromatography conditions: Gradient elution from 0% to 5% EtOAc in hexanes

4.4.4 Scope and Isolation of Allylic Acetoxylation

General Procedure B (*For isolations*): In a 4 mL vial, substrate **S1** (25.0 mg, 0.06 mmol, 1.0 equiv), Pd(OAc)$_2$ (1.4 mg, 0.006 mmol, 10 mol%), and **L2** (1.2 mg, 0.006 mmol, 10 mol%) was added. To the same 4 mL vial, Cs$_2$CO$_3$ (21.0 mg, 0.066 mmol, 1.1 equiv) and 1,4-Benzoquinone (6.5 mg, 0.06 mmol, 1.0 equiv) was added followed by the addition of the *desired carboxylic acid* (0.30 mmol, 5.0 equiv). The reaction mixture was then diluted with *t*-amylOH (0.60 mL). A stirbar was added to the vial and the vial was sealed with a Teflon-lined screw cap. The vial was heated to 140 °C for 4 h. During the 4 h reaction course for every 30 min, the vial was taken off heating, cooled, and the cap was open to expose the reaction to the air. The reaction vial would then be capped and sealed until the next time point. After, the reaction was allowed to cool to room temperature and diluted with DCM (3.0 mL). The reaction solution was then filtered through a Celite pipette and washed with DCM. The volatiles were removed under reduced pressure, and the residue was purified via column chromatography to obtain the desired product **1-D**.

General Procedure C (*Smaller scale*): Under ambient conditions, a 0.02 M stock solution of Pd(OAc)$_2$ (22.5 mg Pd(OAc)$_2$ in 5 mL DCM) and 0.02 M stock solution of **L2** (19.1 mg of **L2** in 5 mL MeOH) were prepared. To a 4 mL vial, an aliquot of the **L2** solution (150 μL, 0.003 mmol, 10 mol%) was added and MeOH was removed at 70 °C for 5 min. To the same 4 mL vial, an aliquot of the Pd(OAc)$_2$ solution (150 μL, 0.003 mmol Pd, 10 mol%) was added and DCM was removed at 40 °C for 5 min. In the 4 mL vial with Pd(OAc)$_2$ and **L2**, substrate **S1** (12.37 mg, 0.03 mmol, 1.0 equiv) and Cs$_2$CO$_3$ (10.67 mg, 0.033 mmol, 1.1 equiv) were added. Next, 1,4-Benzoquinone (3.3 mg, 0.03 mmol, 1.0 equiv) and the desired *carboxylic acid* (0.15 mmol, 5.0 equiv) were added. The reaction mixture was then diluted with *t*-amylOH (0.30 mL). A stirbar was added to the vial and the vial was sealed with a Teflon-lined screw cap. The vial was heated to 140

°C for 18 h. After, the reaction was allowed to cool to room temperature and diluted with DCM

(3.0 mL). The reaction solution was then filtered through a Celite pipette and washed with DCM.
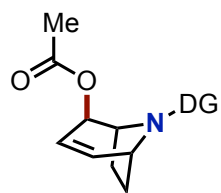
1-D: General Procedure B was followed using Acetic acid as the carboxylic acid.

Isolated yield: 15.4 mg, 55% (white solid)

^{1}H NMR (700 MHz, CDCl$_3$, 23 °C): δ 9.71 (br s, 1H), 6.38 (dd, J = 9.5, 5.9 Hz, 1H), 5.57 (ddd, J = 9.5, 4.3, 1.5 Hz, 1H), 4.88 (dd, J = 4.3, 2.0 Hz, 1H), 3.82 (d, J = 8.1 Hz, 1H), 3.71 (t, J = 5.9 Hz, 1H), 2.03 (m, 1H), 1.94 (s, 3H), 1.87 (ddt, J = 17.7, 11.8, 6.2 Hz, 1H), 1.75 (ddd, J = 12.3, 9.2, 3.0 Hz, 1H), 1.60 (m, 1H), 1.37 (s, 3H), 1.35 (s, 3H).

^{13}C NMR (176 MHz, CDCl$_3$, 23 °C): δ 176.1, 170.3, 140.2, 121.4, 73.5, 62.9, 58.4, 56.5, 31.3, 25.9, 24.9, 22.9, 21.1. *Carbon resonances associated with perfluoroaryl group are not observed.*[6,7]

^{19}F NMR (470 MHz, CDCl$_3$, 23 °C): δ –56.0 (t, 3F), –141.1 (m, 2F), –143.5 (m, 2F).

HRMS-electrospray (m/z): [M]$^+$ calcd. for C$_{20}$H$_{19}$F$_7$N$_2$O$_3$, 469.1357; found, 469.1358.

Melting point: 121-123 °C

Chromatography conditions: Gradient elution from 5% to 10% EtOAc in hexanes
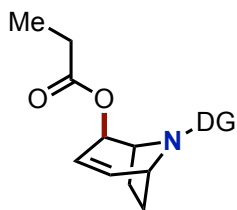
2-D: General Procedure B was followed using Propionic acid as the carboxylic acid.

Isolated yield: 17.4 mg, 60% (white solid)

^{1}H NMR (700 MHz, CDCl$_3$, 23 °C): δ 9.71 (br s, 1H), 6.38 (dd, J = 9.4, 5.9 Hz, 1H), 5.57 (m, 1H), 4.89 (dd, J = 4.4, 1.9 Hz, 1H), 3.82 (d, J = 8.2 Hz, 1H), 3.68 (t, J = 5.9 Hz, 1H), 2.19 (ddt, J = 37.0, 16.4, 8.2 Hz, 2H), 2.03 (m, 1H), 1.86 (tt, J = 11.7, 6.0 Hz, 1H), 1.75 (ddd, J = 12.3, 9.1, 3.0 Hz, 1H), 1.62 (m, 1H), 1.37 (s, 3H), 1.34 (s, 3H), 1.09 (t, J = 7.6 Hz, 3H).

^{13}C NMR (176 MHz, CDCl$_3$, 23 °C): δ 176.2, 173.8, 140.1, 121.6, 73.3, 62.9, 58.3, 56.6, 31.3, 27.7, 26.0, 25.2, 22.7, 9.2. *Carbon resonances associated with perfluoroaryl group are not observed.*[6,7]

^{19}F NMR (470 MHz, CDCl$_3$, 23 °C): δ –56.0 (m, 3F), –141.1 (m, 2F), –143.5 (m, 2F).

HRMS-electrospray (m/z): [M]$^+$ calcd. for C$_{21}$H$_{21}$F$_7$N$_2$O$_3$, 483.1513; found, 483.1514.

Melting point: 120-123 °C

Chromatography conditions: Gradient elution from 2% to 8% EtOAc in hexanes
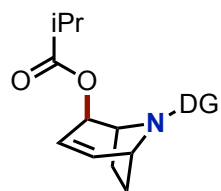
3-D: General Procedure B was followed using Isobutyric acid as the carboxylic acid.

Isolated yield: 18.2 mg, 62% (clear oil)

^{1}H NMR (700 MHz, CDCl$_3$, 23 °C): δ 9.71 (br s, 1H), 6.39 (dd, J = 9.5, 5.8 Hz, 1H), 5.57 (ddd, J = 9.5, 4.2, 1.4 Hz, 1H), 4.87 (dd, J = 4.2, 1.9 Hz, 1H), 3.85 (d, J = 8.1 Hz, 1H), 3.65 (t, J = 6.0 Hz, 1H), 2.39 (hept, J = 7.0 Hz, 1H), 2.03 (dddd, J = 13.7,

11.2, 8.1, 3.1 Hz, 1H), 1.88 (tt, J = 11.6, 5.7 Hz, 1H), 1.75 (ddd, J = 12.4, 9.0, 3.2 Hz, 1H), 1.63 (ddd, J = 14.5, 9.0, 5.7 Hz, 1H), 1.38 (s, 3H), 1.33 (s, 3H), 1.12 (dd, J = 7.0, 4.8 Hz, 6H).

^{13}C NMR (176 MHz, CDCl$_3$, 23 °C): δ 176.5, 176.2, 140.1, 121.7, 73.1, 62.8, 58.0, 56.8, 34.2, 31.3, 26.1, 25.7, 22.2, 19.1, 19.1. *Carbon resonances associated with perfluoroaryl group are not observed.*[6,7]

^{19}F NMR (470 MHz, CDCl$_3$, 23 °C): δ –56.0 (m, 3F), –141.1 (m, 2F), –143.5 (m, 2F).

HRMS-electrospray (m/z): [M]$^+$ calcd. for C$_{22}$H$_{23}$F$_7$N$_2$O$_3$, 497.1670; found, 497.1670.

Chromatography conditions: Gradient elution from 2% to 6% EtOAc in hexanes
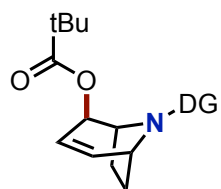
4-D: General Procedure B was followed using Pivalic acid as the carboxylic acid.

Isolated yield: 17.8 mg, 58% (white solid)

^{1}H NMR (700 MHz, CDCl$_3$, 23 °C): δ 9.68 (br s, 1H), 6.40 (dd, J = 9.4, 5.8 Hz, 1H), 5.57 (ddd, J = 9.4, 4.3, 1.4 Hz, 1H), 4.84 (dd, J = 4.3, 1.9 Hz, 1H), 3.89 (d, J = 8.0 Hz, 1H), 3.58 (t, J = 6.0 Hz, 1H), 2.02 (dddd, J = 13.6, 11.3, 8.0, 3.2 Hz, 1H), 1.89 (m,1H), 1.73 (m, 1H), 1.65 (m, 1H), 1.40 (s, 3H), 1.31 (s, 3H), 1.18 (s, 9H).

^{13}C NMR (176 MHz, CDCl$_3$, 23 °C): δ 178.0, 176.3, 140.1, 122.0, 73.1, 62.7, 57.4, 38.9, 34.9, 31.3, 29.8, 27.3, 26.6, 26.3, 23.8, 21.4. *Carbon resonances associated with perfluoroaryl group are not observed.*[6,7]

^{19}F NMR (470 MHz, CDCl$_3$, 23 °C): δ –56.0 (t, 3F), –141.1 (m, 2F), –143.7 (m, 2F).

HRMS-electrospray (m/z): [M]$^+$ calcd. for C$_{23}$H$_{25}$F$_7$N$_2$O$_3$, 511.1826; found, 511.1827.

Melting point: 102-105 °C

Chromatography conditions: Gradient elution from 2% to 6% EtOAc in hexanes
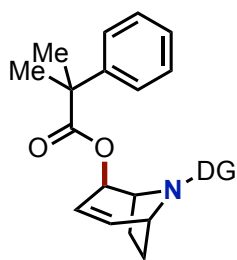
5-D: General Procedure B was followed using 2-Phenylisobutyric acid as the carboxylic acid.

Isolated yield: 8.2 mg, 24% (clear oil)

^{1}H NMR (700 MHz, CDCl$_3$, 23 °C): δ 9.28 (br s, 1H), 7.24-7.21 (multiple peaks, 2H), 7.13 (t, J = 7.8 Hz, 2H), 6.98 (t, J = 7.4 Hz, 1H), 6.34 (dd, J = 9.5, 5.9 Hz, 1H), 5.58 (ddd, J = 9.5, 4.2, 1.4 Hz, 1H), 4.86 (dd, J = 4.2, 1.9 Hz, 1H), 3.73 (d, J = 8.1 Hz, 1H), 3.46 (t, J = 5.9 Hz, 1H), 1.97 (dddd, J = 13.8, 11.3, 8.1, 3.1 Hz, 1H), 1.83 (tt, J = 11.6, 5.9 Hz, 1H), 1.69 (ddd, J = 12.3, 9.3, 3.1 Hz, 1H), 1.61 (s, 1H), 1.57 (s, 3H), 1.52 (s, 3H), 1.16 (s, 3H), 1.08 (s, 3H).

^{13}C NMR (176 MHz, CDCl$_3$, 23 °C): δ 176.2, 176.1, 144.6, 140.2, 128.6, 128.3, 126.5, 125.9, 125.4, 121.4, 73.5, 62.5, 57.2, 56.9, 46.6, 31.2, 26.8, 26.5, 26.1, 26.1, 21.2. *Carbon resonances associated with perfluoroaryl group are not observed.*[6,7]

^{19}F NMR (470 MHz, CDCl$_3$, 23 °C): δ –56.0 (t, 3F), –141.2 (m, 2F), –143.7 (m, 2F).

HRMS-electrospray (m/z): [M]$^+$ calcd. for C$_{28}$H$_{27}$F$_7$N$_2$O$_3$, 573.1983; found, 573.1980.

Chromatography conditions: Gradient elution from 2% to 8% EtOAc in hexanes
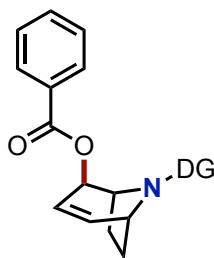
6-D: General Procedure B was followed using Benzoic acid as the carboxylic acid.

Isolated yield: 20.2 mg, 64% (white solid)

^{1}H NMR (700 MHz, CDCl$_3$, 23 ºC): δ 9.66 (br s, 1H), 7.84 (d, J = 6.9, 2H), 7.41 (tt, J = 7.4, 1.5 Hz, 1H), 7.25 (t, J = 7.8 Hz, 2H), 6.47 (dd, J = 9.4, 6.1 Hz, 1H), 5.63 (ddd, J = 9.4, 4.2, 1.5 Hz, 1H), 5.10 (dd, J = 4.2, 2.0 Hz, 1H), 3.96-3.84 (multiple peaks, 2H), 2.10 (dddd, J = 13.6, 10.8, 8.0, 3.0 Hz, 1H), 1.88 (tt, J = 11.6, 6.1 Hz, 1H), 1.82 (ddd, J = 12.1, 9.0, 3.0 Hz, 1H), 1.66 (m, 1H), 1.38 (s, 3H), 1.35 (s, 3H).

^{13}C NMR (176 MHz, CDCl$_3$, 23 ºC): δ 175.7, 165.8, 140.8, 133.4, 129.8, 129.2, 128.2, 120.9, 74.5, 63.3, 60.1, 55.9, 31.5, 25.6, 25.2, 22.2. *Carbon resonances associated with perfluoroaryl group are not observed.* [6,7]

^{19}F NMR (470 MHz, CDCl$_3$, 23 ºC): δ –56.2 (m, 3F), –141.0 (m, 2F), –143.9 (m, 2F).

HRMS-electrospray (m/z): [M]$^+$ calcd. for C$_{25}$H$_{21}$F$_7$N$_2$O$_3$, 531.1513; found, 531.1515.

Melting point: 135-137 °C

Chromatography conditions: Gradient elution from 2% to 6% EtOAc in hexanes
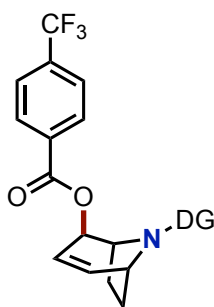
7-D: General Procedure B was followed using 4-(Trifluoromethyl)benzoic acid as the carboxylic acid.

Isolated yield: 13.9 mg, 39% (white solid)

^{1}H NMR (700 MHz, CDCl$_3$, 23 ºC): δ 9.60 (br s, 1H), 8.01 (d, J = 8.1 Hz, 2H), 7.58 (d, J = 8.1 Hz, 2H), 6.50 (dd, J = 9.5, 6.0 Hz, 1H), 5.66 (ddd, J = 9.5, 4.2, 1.5 Hz, 1H), 5.13 (dd, J = 4.4, 2.0 Hz, 1H), 3.96 (d, J = 8.0 Hz, 1H), 3.87 (t, J = 6.0 Hz, 1H), 2.12 (m, 1H), 1.91 (tq, J = 11.7, 6.0, 5.6 Hz, 1H), 1.83 (ddd, J = 12.1, 9.1, 2.9 Hz, 1H), 1.69 (m, 1H), 1.38 (s, 3H), 1.37 (s, 3H).

^{13}C NMR (176 MHz, CDCl$_3$, 23 ºC): δ 175.7, 164.7, 141.1, 135.0 (q, J = 32.7 Hz), 133.1, 129.8, 125.4 (q, J = 3.7 Hz), 123.5 (q, J = 274.0 Hz), 120.8, 75.0, 59.4, 56.3, 31.4, 29.9, 25.8, 24.2, 23.5. *Carbon resonances associated with perfluoroaryl group are not observed.*[6,7]

^{19}F NMR (470 MHz, CDCl$_3$, 23 ºC): δ –56.3 (app s, 3F), –63.5 (app s, 3F), –141.2 (m, 2F), –143.4 (m, 2F).

HRMS-electrospray (m/z): [M]$^+$ calcd. for C$_{26}$H$_{20}$F$_{10}$N$_2$O$_3$, 599.1314; found, 599.1389.

Melting point: 158-160 °C

Chromatography conditions: Gradient elution from 4% to 8% EtOAc in hexanes
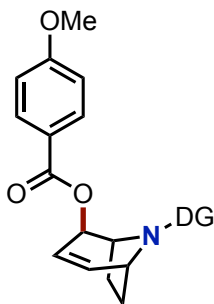
8-D: General Procedure B was followed using 4-Methoxybenzoic acid as the carboxylic acid.

Isolated yield: 4.0 mg, 24% (white solid)

^{1}H NMR (700 MHz, CDCl$_3$, 23 ºC): δ 9.68 (br s, 1H), 7.79 (d, J = 8.3 Hz, 2H), 6.71 (d, J = 8.8 Hz, 2H), 6.45 (dd, J = 9.4, 6.0 Hz, 1H), 5.62 (m, 1H), 5.06 (s, 1H), 3.97-3.83 (multiple peaks, 2H), 3.79 (s, 3H), 2.10 (d, J = 11.4 Hz, 1H), 1.84 (dt, J = 19.8, 12.4 Hz, 2H), 1.65 (dt, J = 14.6, 7.3 Hz, 1H), 1.39 (s, 3H),

1.35 (s, 3H).

^{13}C NMR (176 MHz, CDCl$_3$, 23 °C): δ 165.5, 163.3, 140.5, 131.3, 121.9, 121.1, 113.4, 106.5, 74.2, 60.3, 55.4, 31.6, 29.9, 25.6, 25.3, 22.1, 14.3. *Carbon resonances associated with perfluoroaryl group are not observed.* [6,7]
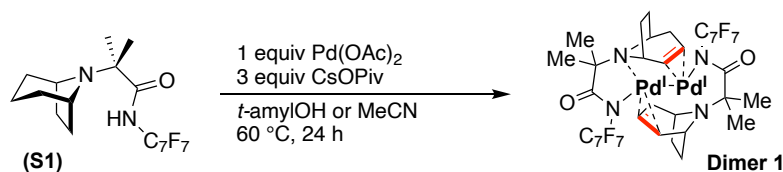
^{19}F NMR (470 MHz, CDCl$_3$, 23 °C): δ −56.2 (m, 3F), −141.8 (app s, 2F), −143.1 (app s, 2F).

HRMS-electrospray (m/z): [M]$^+$ calcd. for C$_{26}$H$_{23}$F$_7$N$_2$O$_4$, 561.1619; found, 561.1623.

Melting point: 117-119 °C

Chromatography conditions: Gradient elution from 2% to 8% EtOAc in hexanes

4.4.5 Synthesis and Isolation of Dimer-1

General Procedure for Synthesis of Dimer-1. A 4 mL vial was charged with substrate **S1** (20.6 mg, 0.05 mmol, 1.0 equiv), Pd(OAc)$_2$ (11.3 mg, 0.05 mmol, 1.0 equiv), CsOPiv (35.1 mg, 0.15 mmol, 3.0 equiv) and a stirbar. To this vial, *t*-amylOH or MeCN (1.0 mL) was added. The reaction was stirred at 60 °C forming a bright orange reaction mixture. After 24 h, the reaction was cooled to room temperature and the solvent was concentrated under reduced pressure. The reaction was then diluted with DCM (10 mL) and filtered through a Celite plug. The supernatant was kept and concentrated under reduced pressure. Minimal DCM (2 mL) was then added to dissolve the solid followed by the addition of pentanes (10 mL) allowing the formation of a bright orange precipitate. The mixture was filtered through a Celite plug where the supernatant was discarded, and the precipitate was collected at the top of the Celite plug. In a 20 mL vial, the precipitate was dissolved and flused through the Celite plug using DCM (5 mL). Volatiles were evaporated under reduced pressure. This step was repeated 2-3 more times to afford **Dimer-1** as a bright orange solid.
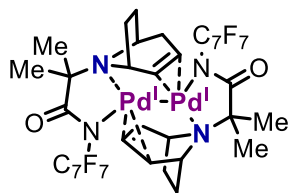
**Dimer-1:** Isolated yield: 18 mg, 35% (orange solid)

^{1}H NMR (700 MHz, CD$_3$CN, 23 ºC): δ 5.26 (ddd, J = 7.7, 3.9, 1.9 Hz, 2H), 4.87 (t, J = 3.9 Hz, 2H), 4.41 (t, J = 6.8 Hz, 2H), 3.99 (dd, J = 18.1, 4.8 Hz, 2H), 3.64 (t, J = 6.0 Hz, 2H), 2.54 (dd, J = 18.1, 6.0 Hz, 2H), 1.30 (s, 6H).

^{19}F NMR (470 MHz, CD$_3$CN $_3$, 23 ºC): δ –56.2 (t, 3F), –145.5 (m, 2F), –148.8 (m, 1F), –149.5 (m, 1F).

Elemental Analysis calcd for C$_{37}$H$_{36}$F$_{14}$N$_4$O$_3$Cl$_2$Pd$_2$, C:39.17; H: 3.20; N: 4.94; found, C: 39.75; H: 3.23; N: 4.72.

4.4.6 Scope and Isolation of Alkene

General Procedure D: Ligand Optimization with S1. Under ambient conditions, a 0.02 M stock solution of Pd(OAc)$_2$ (22.5 mg Pd(OAc)$_2$ in 5 mL DCM) and 0.02 M stock solution of **LX** (in MeOH) was prepared. To a 4 mL vial, an aliquot of the **LX** solution (0.003 mmol, 10 mol%) was added and MeOH was removed at 70 °C for 5 min. To the same 4 mL vial, an aliquot of the Pd(OAc)$_2$ solution (150 µL, 0.003 mmol Pd, 10 mol%) was added and DCM was removed at 40 °C for 5 min. In the 4 mL vial with Pd(OAc)$_2$ and **LX**, substrate **S1** (12.37 mg, 0.03 mmol, 1.0 equiv) and Cs$_2$CO$_3$ (10.67 mg, 0.033 mmol, 1.1 equiv) were added. The reaction mixture was then diluted with *t*-amylOH (0.30 mL) followed by the addition of acetic acid (18 µL, 0.30 mmol, 10 equiv). A stirbar was added to the vial and the vial was sealed with a Teflon-lined screw cap. The vial was heated to 140 °C for 18 h. After, the reaction was allowed to cool to room temperature and diluted with DCM (3.0 mL) followed by the addition of hydrazine monohydrate (50 µL). The reaction was then stirred at room temperature for 10-15 min. During this time, a 0.2 M stock solution of 1,3,5-methoxybenzene (168 mg, 1 mmol) dissolved in ethyl acetate (5 mL) was prepared. An aliquot of this solution (150 µL, 0.03 mmol) was added to the reaction as the GC standard. The reaction solution was then filtered through a Celite pipette and analyzed via GC-FID. Yields were determined based on a calibration curve. **Table 4.1** showcases the ligands screened.

Table 4.1 Ligand Optimization of 1-E
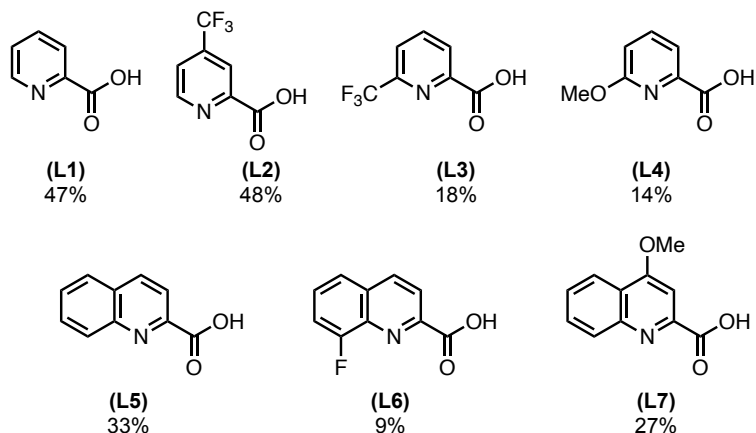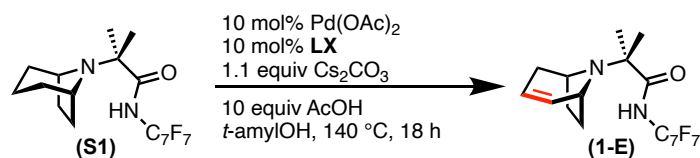
Variations of this procedure were used in all optimization reactions where the yield was determined by GC-FID. Ligand loading, solvent, acetic acid, base, and temperature were all parameters investigated.
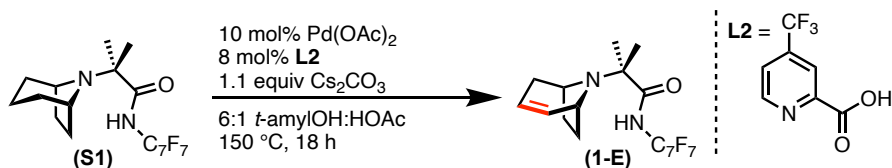
Optimized General Procedure E: Under ambient conditions, a 0.02 M stock solution of Pd(OAc)$_2$ (22.5 mg Pd(OAc)$_2$ in 5 mL DCM) and 0.02 M stock solution of **L2** (7.64 mg of **L2** in 2 mL MeOH) were prepared. To a 4 mL vial, an aliquot of the **L2** solution (100 μL, 0.002 mmol, 8 mol%) was added and MeOH was removed at 70 °C for 5 min. To the same 4 mL vial, an aliquot of the Pd(OAc)$_2$ solution (150 μL, 0.003 mmol Pd, 10 mol%) was added and DCM was removed at 40 °C for 5 min. In the 4 mL vial with Pd(OAc)$_2$ and **L2**, substrate **S1** (12.37 mg, 0.03 mmol, 1.0 equiv) and Cs$_2$CO$_3$ (10.67 mg, 0.033 mmol, 1.1 equiv) were added. The reaction mixture was

then diluted with *t*-amylOH (0.30 mL) followed by the addition of acetic acid (50 μL). A stirbar was added to the vial and the vial was sealed with a Teflon-lined screw cap. The vial was heated to 150 °C for 18 h. After, the reaction was allowed to cool to room temperature and diluted with DCM (3.0 mL) followed by the addition of hydrazine monohydrate (50 μL). The reaction was then stirred at room temperature for 10-15 min.

For GC-FID analysis: During this time, a 0.2 M stock solution of 1,3,5-methoxybenzene (168 mg, 1 mmol) dissolved in ethyl acetate (5 mL) was prepared. An aliquot of this solution (150 μL, 0.03 mmol) was added to the reaction as the GC standard. The reaction solution was then filtered through a Celite pipette and analyzed via GC-FID. Yields were determined based on a calibration curve.

For isolation: The reaction solution was then filtered through a Celite pipette and washed with DCM. The volatiles were removed under reduced pressure, and the residue was purified via column chromatography (0% to 5% EtOAc in hexanes) to afford the desired product **1-E**.
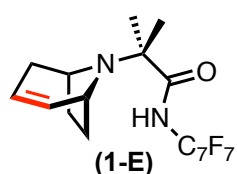
1-E: General Procedure E was followed using **S1** as the substrate.
Isolated yield: 7.8 mg, 63% (white solid)
^{1}H NMR (700 MHz, CD$_3$CN, 23 °C): δ 9.75 (br s, 1H), 6.05 (m, 1H), 5.53 (m, 1H), 3.66 (d, *J* = 6.9 Hz, 1H), 3.54 (t, *J* = 5.4 Hz, 1H), 2.66 (d, *J* = 17.7 Hz, 1H), 2.12 (d, *J* = 13.6 Hz, 3H), 1.91 (m, 1H), 1.68 (m, 1H), 1.42 (s, 3H), 1.37 (s, 3H).
^{13}C NMR (176 MHz, CD$_3$CN, 23 °C): δ 177.3, 135.5, 124.2, 63.5, 55.7, 55.2, 36.8, 36.3, 31.7, 25.0, 23.1. *Carbon resonances associated with perfluoroaryl group are not observed.*[6,7]
^{19}F NMR (470 MHz, CD$_3$CN, 23 °C): δ –56.8 (t, 3F), –144.1 (m, 2F), –145.3 (m, 2F).
HRMS-electrospray (m/z): [M]$^+$ calcd. for C$_{18}$H$_{17}$F$_7$N$_2$O, 411.1302; found, 411.1291.
Melting point: 101-104 °C
Chromatography conditions: Gradient elution from 0% to 4% EtOAc in hexanes
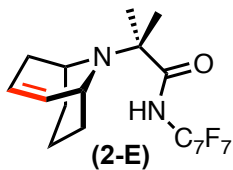
2-E: General Procedure E was followed using **S2** as the substrate. Isolated yield: 7.3 mg, 57% (white Solid)

^{1}H NMR (600 MHz, CDCl$_3$) δ 9.80 (s, 1H), 5.99 (m, 1H), 5.78 (m, 1H), 3.45 (m, 1H), 3.28 (s, 1H), 2.38 (m, 1H), 1.85 (m, 3H), 1.76 (ddd, J = 12.5, 8.4, 4.0 Hz, 1H), 1.68 (dd, J = 6.3, 2.6 Hz, 1H), 1.56 (m, 2H), 1.43 (s, 3H), 1.38 (s, 3H).

^{13}C NMR (151 MHz, CDCl$_3$) δ 176.6, 129.6, 128.3, 65.0, 50.3, 46.9, 35.8, 29.7, 28.5, 24.6, 22.9, 16.5. *Carbon resonances associated with perfluoroaryl group are not observed.* [6,7]

^{19}F NMR (564 MHz, cdcl$_3$) δ –56.0 (t, J = 21.7 Hz, 3F), –141.3 (m, 2F), –143.7 (td, J = 13.7, 6.2 Hz, 2F).

Chromatography conditions: 5% EtOAc in hexanes

3-E: General Procedure E was followed using **S3** as the substrate. Isolated yield: 11.5 mg, 90% (white solid)

^{1}H NMR (700 MHz, CDCl$_3$, 23 ºC): δ 9.59 (s, 1H), 6.10 (dt, J = 10.0, 3.5 Hz, 1H), 5.90 (ddt, J = 10.0, 4.8, 2.3 Hz, 1H), 3.92 (d, J = 2.2 Hz, 2H), 3.77 (dd, J = 10.7, 2.2 Hz, 1H), 3.64 (dd, J =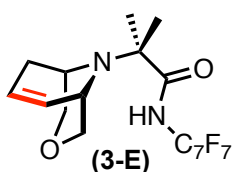 10.7, 1.7 Hz, 1H), 3.31 – 3.23 (m, 1H), 3.19 – 3.13 (m, 1H), 2.50 – 2.41 (m, 1H), 2.16 (ddd, J = 18.8, 4.2, 2.1 Hz, 1H), 1.46 (s, 3H), 1.41 (s, 3H).

^{13}C NMR (176 MHz, CDCl$_3$, 23 ºC): δ 175.8, 129.4, 127.4, 76.4, 89.8, 65.0, 51.8, 48.8, 28.1, 24.1, 22.9. *Carbon resonances associated with perfluoroaryl group are not observed.* [6,7]

^{19}F NMR (470 MHz, CDCl$_3$, 23 ºC): δ –56.9 (m, 3F), –141.0 (s, 2F), –143.9 (m, 2F).

HRMS-electrospray (m/z): [M]$^+$ calcd. for C$_{18}$H$_{17}$F$_7$N$_2$O$_2$, 427.1251; found, 427.1250.

Melting point: 150-152 °C

Chromatography conditions: Gradient elution from 8% to 12% EtOAc in hexanes

4.4.7 X-Ray Crystallography Data

Compound 1-C

Colorless needles of **1-C** were grown from a dichloromethane/hexanes solution of the compound at 22 deg. C. A crystal of dimensions 0.12 x 0.04 x 0.04 mm was mounted on a Rigaku AFC10K Saturn 944+ CCD-based X-ray diffractometer equipped with a low temperature device and Micromax-007HF Cu-target micro-focus rotating anode (λ = 1.54187 A) operated at 0.3 kW power (30 kV, 10 mA). The X-

1-C

ray intensities were measured at 85(1) K with the detector placed at a distance 42.00 mm from the crystal. A total of 2028 images were collected with an oscillation width of 1.0° in ω. The exposure times were 1 sec. for the low angle images, 3 sec. for high angle. Rigaku d*trek images were exported to CrysAlisPro for processing and corrected for absorption. The integration of the data yielded a total of 32406 reflections to a maximum 2θ value of 139.77° of which 3913 were independent and 3721 were greater than 2σ(I). The final cell constants were based on the xyz centroids of 17682 reflections above 10σ(I). Analysis of the data showed negligible decay during data collection. The structure was solved and refined with the Bruker SHELXTL (version 2018/3) software package, using the space group P2(1)/c with Z = 4 for the formula $C_{24}H_{21}N_2OF_7$. All non-hydrogen atoms were refined anisotropically with the hydrogen atoms placed in a combination of refined and idealized positions. The crystal was determined to be a pseudo-merohedral twin. Twin law [-1 0 0 0 -1 0 0 0 1], refined twin scale factor 0.235(3). Full matrix least-squares refinement based on F^2 converged at R1 = 0.0850 and wR2 = 0.2531 [based on I > 2sigma(I)], R1 = 0.0884 and wR2 = 0.2648 for all data. Additional details are presented in Table 4.2 and are given as Supporting Information in a CIF file. Acknowledgement is made for funding from NSF grant CHE-0840456 for X-ray instrumentation.

G.M. Sheldrick (2015) "Crystal structure refinement with SHELXL", Acta Cryst., C71, 3-8 (Open Access).

CrystalClear Expert 2.0 r16, Rigaku Americas and Rigaku Corporation (2014), Rigaku Americas, 9009, TX, USA 77381-5209, Rigaku Tokyo, 196-8666, Japan.

CrysAlisPro 1.171.40.53 (Rigaku Oxford Diffraction, 2019).

Table 4.2 Crystal Data and Structural Refinement for **1-C**

Empirical Formula	$C_{24}H_{21}F_7N_2O$

Formula Weight	486.43
Temperature	85 (2) K
Wavelength	1.54184 Å
Crystal System	Monoclinic
Space Group	P2(1)/c
Unit Cell Dimensions	a = 7.7054 (3) Å, α = 90 ° b = 12.5541 (4) Å, β = 90.196 (3)° c = 22.0120 (8) Å, γ = 90 °
Volume	2129.30 (13) Å^3
Z	4
Calculated Density	1.517 Mg/m^3
Absorption Coefficient	1.185 mm^{-1}
F(000)	1000
Crystal Size	0.120 x 0.040 x 0.040 mm
Theta Range for Data Collection	3.520 to 69.883 °
Limiting Indices	-8$\leq$h$\leq$8, -15$\leq$k$\leq$15, -26$\leq$l$\leq$25
Reflections Collected	32406
Independent Reflections	3913
Completeness to Theta	98.6%
Absorption Correction	Semi-empirical from equivalents
Max and Min Transmission	1.00000 to 0.54488
Refinement Method	Full-matrix least-squares on F^2
Data / Restraints / Parameters	3913 / 0 / 314

Goodness-of-Fit on F^2	1.138
Final R Indices [l>2σ(l)]	R1 = 0.0850, wR2 = 0.2531
R indices (all data)	R1 = 0.0884, wR2 = 0.2648
Extinction Coefficient	N/A
Largest Difference Peak and Hole	0.401 and -0.514 Å^{-3}

Compound 1-D

Colorless prisms of **1-D** were grown from a dichloromethane/hexanes solution of the compound at 22 deg. C. A crystal of dimensions

1-D
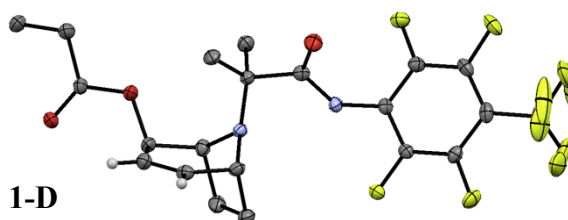
0.22 x 0.22 x 0.22 mm was mounted on a Rigaku AFC10K Saturn 944+ CCD-based X-ray diffractometer equipped with a low temperature device and Micromax-007HF Cu-target micro-focus rotating anode (λ = 1.54187 A) operated at 0.3 kW power (30 kV, 10 mA). The X-ray intensities were measured at 85(1) K with the detector placed at a distance 42.00 mm from the crystal. A total of 2028 images were collected with an oscillation width of 1.0° in ω. The exposure times were 1 sec. for all images. Rigaku d*trek images were exported to CrysAlisPro for processing and corrected for absorption. The integration of the data yielded a total of 30908 reflections to a maximum 2θ value of 138.62° of which 3800 were independent and 3722 were greater than 2σ(I). The final cell constants were based on the xyz centroids of 20201 reflections above 10σ(I). Analysis of the data showed negligible decay during data collection. The structure was solved and refined with the Bruker SHELXTL (version 2018/3) software package, using the space group P2(1)/n with Z = 4 for the formula $C_{21}H_{21}N_2O_3F_7$. All non-hydrogen atoms were refined anisotropically with the hydrogen atoms placed in a combination of refined and idealized

positions. Full matrix least-squares refinement based on F^2 converged at R1 = 0.0425 and wR2 = 0.1047 [based on I > 2sigma(I)], R1 = 0.0434 and wR2 = 0.1061 for all data. Additional details are presented in Table 4.3 and are given as Supporting Information in a CIF file.

G.M. Sheldrick (2015) "Crystal structure refinement with SHELXL", Acta Cryst., C71, 3-8 (Open Access).

CrystalClear Expert 2.0 r16, Rigaku Americas and Rigaku Corporation (2014), Rigaku Americas, 9009, TX, USA 77381-5209, Rigaku Tokyo, 196-8666, Japan.

CrysAlisPro 1.171.40.53 (Rigaku Oxford Diffraction, 2019).

Table 4.3 Crystal Data and Structural Refinement for **1-D**

Empirical Formula	$C_{21}H_{21}F_7N_2O_3$
Formula Weight	482.40
Temperature	85 (2) K
Wavelength	1.54184 Å
Crystal System	Monoclinic
Space Group	P2(1)/n
Unit Cell Dimensions	a = 11.17206 (13) Å, α = 90 °
	b = 16.78418 (16) Å, β = 100.8711 (9)°
	c = 11.27108 (10) Å, γ = 90 °
Volume	2075.55 (4) Å^3
Z	4
Calculated Density	1.544 Mg/m^3
Absorption Coefficient	1.281 mm^{-1}

F(000)	992
Crystal Size	0.220 x 0.220 x 0.220 mm
Theta Range for Data Collection	4.786 to 69.314 °
Limiting Indices	$-10 \leq h \leq 12$, $-20 \leq k \leq 20$, $-13 \leq l \leq 13$
Reflections Collected	30908
Independent Reflections	3800
Completeness to Theta	98.3%
Absorption Correction	Semi-empirical from equivalents
Max and Min Transmission	1.00000 to 0.81320
Refinement Method	Full-matrix least-squares on F^2
Data / Restraints / Parameters	3800 / 6 / 333
Goodness-of-Fit on F^2	1.048
Final R Indices [$l > 2\sigma(l)$]	R1 = 0.0425, wR2 = 0.1047
R indices (all data)	R1 = 0.0434, wR2 = 0.1061
Extinction Coefficient	0.0020 (2)
Largest Difference Peak and Hole	0.428 and -0.269 Å^{-3}

Dimer-1

Orange needles of **Dimer-1** were grown from a hexanes/dichloromethane solution of the compound at 23 deg. C. A crystal of dimensions 0.10 x 0.02 x 0.02 mm was
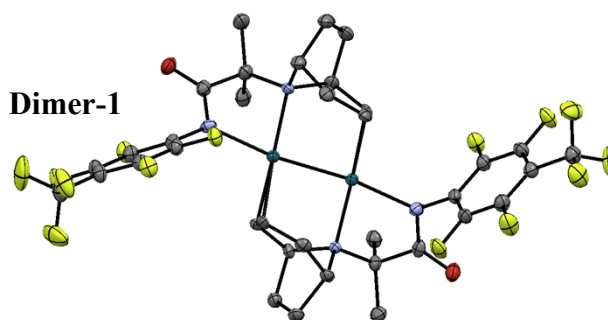
Dimer-1

mounted on a Rigaku AFC10K Saturn 944+ CCD-based X-ray diffractometer equipped with a low

temperature device and Micromax-007HF Cu-target micro-focus rotating anode (λ = 1.54187 A) operated at 1.2 kW power (40 kV, 30 mA). The X-ray intensities were measured at 85(1) K with the detector placed at a distance 42.00 mm from the crystal. A total of 2028 images were collected with an oscillation width of 1.0° in ω. The exposure times were 1 sec. for the low angle images, 3 sec. for high angle. Rigaku d*trek images were exported to CrysAlisPro for processing and corrected for absorption. The integration of the data yielded a total of 30119 reflections to a maximum 2θ value of 138.53° of which 7222 were independent and 6743 were greater than $2\sigma(I)$. The final cell constants were based on the xyz centroids of 14261 reflections above $10\sigma(I)$. Analysis of the data showed negligible decay during data collection. The structure was solved and refined with the Bruker SHELXTL (version 2016/6) software package, using the space group P1bar with Z = 2 for the formula $C_{37}H_{36}N_4O_3F_{14}Cl_2Pd_2$. All non-hydrogen atoms were refined anisotropically with the hydrogen atoms placed in a combination of idealized and refined positions. Full matrix least-squares refinement based on F^2 converged at R1 = 0.0406 and wR2 = 0.1129 [based on I > 2sigma(I)], R1 = 0.0429 and wR2 = 0.1164 for all data. Additional details are presented in Table 4.4 and are given as Supporting Information in a CIF file. Acknowledgement is made for funding from NSF grant CHE-0840456 for X-ray instrumentation.

G.M. Sheldrick (2015) "Crystal structure refinement with SHELXL", Acta Cryst., C71, 3-8 (Open Access).

CrystalClear Expert 2.0 r16, Rigaku Americas and Rigaku Corporation (2014), Rigaku Americas, 9009, TX, USA 77381-5209, Rigaku Tokyo, 196-8666, Japan.

CrysAlisPro 1.171.38.41 (Rigaku Oxford Diffraction, 2015).

Table 4.4 Crystal Data and Structural Refinement for **Dimer-1**

Empirical Formula	$C_{37}H_{36}Cl_2F_{14}N_4O_3Pd_2$

Formula Weight	1134.40
Temperature	85 (2) K
Wavelength	1.54184 Å
Crystal System	Triclinic
Space Group	P-1
Unit Cell Dimensions	a = 12.1394 (3) Å, α = 85.100(2)° b = 12.7800 (4) Å, β = 79.236 (2)° c = 13.9061 (3) Å, γ = 70.699 (2)°
Volume	1999.68 (9) Å^3
Z	2
Calculated Density	1.884 Mg/m^3
Absorption Coefficient	9.482 mm^{-1}
F(000)	1124
Crystal Size	0.100 x 0.020 x 0.020 mm
Theta Range for Data Collection	3.236 to 69.269 °
Limiting Indices	-14≤h≤14, -15≤k≤15, -14≤l≤16
Reflections Collected	30119
Independent Reflections	7222
Completeness to Theta	97.7%
Absorption Correction	Semi-empirical from equivalents
Max and Min Transmission	1.00000 to 0.46518
Refinement Method	Full-matrix least-squares on F^2
Data / Restraints / Parameters	7222 / 3 / 571

Goodness-of-Fit on F^2	1.070
Final R Indices [l>2σ(l)]	R1 = 0.0406, wR2 = 0.1129
R indices (all data)	R1 = 0.0429, wR2 = 0.1164
Extinction Coefficient	N/A
Largest Difference Peak and Hole	1.181 and -1.347 Å^{-3}

4.5 References

(1) (a) Taylor, R. D.; MacCoss, M.; Lawson, A. D. G. Rings in Drugs. *J. Med. Chem.* **2014**, *57,* 5845−5859. (b) Top 200 Pharmaceutical Products by Prescription in 2016; University of Arizona, **2016**. http://njardarson.lab.arizona.edu/sites/njardarson.lab.arizona.edu/files/ 2016Top200PharmaceuticalPrescriptionSalesPosterLowResV2.pdf (accessed March 1, 2021).

(2) Vitaku, E.; Smith, D. T.; Njardarson, J. T. Analysis of the Structural Diversity, Substitution Patterns, and Frequency of Nitrogen Heterocycles among U.S. FDA Approved Pharmaceuticals. *J. Med. Chem.* **2014**, *57*, 10257-10274.

(3) (a) Källström, S.; Leino, R. Synthesis of Pharmaceutically Active Compounds Containing a Disubstituted Piperidine Framework. *Bioorg. Med. Chem*. **2008**, *16*, 601-635. (b) Blakemore, D. C.; Castro, L.; Churcher, I.; Rees, D. C.; Thomas, A. W.; Wilson, D. M.; Wood, A. Organic Synthesis Provides Opportunities to Transform Drug Discovery. *Nature Chem* **2018**, *10*, 383–394. (c) Moir, M.; Danon, J. J.; Reekie, T. A.; Kassiou, M. An Overview of Late-Stage Functionalization in Today's Drug Discovery. *Expert Opinion on Drug Discovery* **2019**, *14*, 1137–1149. (d) Börgel, J.; Ritter, T. Late-Stage Functionalization. *Chem* **2020**, *6*, 1877–1887.

(4) (a) Wencel-Delord, J.; Glorius, F. C–H Bond Activation Enables the Rapid Construction and Late-Stage Diversification of Functional Molecules. *Nature Chem* **2013**, *5*, 369–375. (b) Cernak, T.; Dykstra, K. D.; Tyagarajan, S.; Vachal, P.; Krska, S. W. The Medicinal Chemist's Toolbox for Late Stage Functionalization of Drug-like Molecules. *Chem. Soc. Rev.* **2016**, *45,* 546–576.

(5) For examples of C$_{\alpha}$–H of alicyclic amines, see: (a) Pastine, S. J.; Gribkov, D. V.; Sames, D. sp^3 C−H Bond Arylation Directed by Amidine Protecting Groups: α-Arylation of Pyrrolidines and Piperidines. *J. Am. Chem. Soc*. **2006**, *128*, 14220−14221. (b) Campos, K. R. Direct sp^3 C−H Bond Activation Adjacent to Nitrogen in Heterocycles. *Chem. Soc. Rev.* **2007**, *36*, 1069−1084.(c) Mitchell, E. A.; Peschiulli, A.; Lefevre, N.; Meerpoel, L.; Maes, B. U. W. Direct α-Functionalization of Saturated Cyclic Amines. *Chem. - Eur. J.* **2012**, *18*, 10092−10142. (d) Shi, L.; Xia, W. Photoredox functionalization of C−H Bonds Adjacent to a Nitrogen Atom. *Chem. Soc. Rev*. **2012**, *41*, 7687−7697. (e) He, J.; Hamann, L. G.; Davies, H. M. L.; Beckwith, R. E. J. Late-Stage C−H Functionalization of Complex Alkaloids and Drugs Molecules via Intermolecular

Rhodium-Carbenoid Insertion. *Nat. Commun.* **2015**, *6*, 5943. (f) Spangler, J. E.; Kobayashi, Y.; Verma, P.; Wang, D.-H.; Yu, J.-Q. α-Arylation of Saturated Azacycles and N-methylamines via Palladium(II)-Catalyzed C(sp3) − H Coupling. *J. Am. Chem. Soc*. **2015**, *137*, 11876−11879. (g) Chen, W.; Ma, L.; Paul, A.; Seidel, D. Direct α-C−H Bond Functionalization of Unprotected Cyclic Amines. *Nat. Chem.* **2017**, *10*, 165−169.

(6) Topczewski, J. J.; Cabrera, P. J.; Saper, N. I.; Sanford, M. S. Palladium-Catalysed Transannular C−H Functionalization of Alicyclic Amines. *Nature* **2016**, *531*, 220−224.

(7) Cabrera, P. J.; Lee, M.; Sanford, M. S. Second-Generation Palladium Catalyst System for Transannular C−H Functionalization of Azabicycloalkanes. *J. Am. Chem. Soc*. **2018**, *140*, 5599–5606.

(8) Aguilera, E. Y.; Sanford, M. S. Model Complexes for the Palladium-Catalyzed Transannular C−H Functionalization of Alicyclic Amines. *Organometallics* **2019**, *38*, 138–142.

(9) (a) Chen, M. S.; White, M. C. A Sulfoxide-Promoted, Catalytic Method for the Regioselective Synthesis of Allylic Acetates from Monosubstituted Olefins via C−H Oxidation. *J. Am. Chem. Soc.* **2004**, *126*, 1346–1347. (b) Chen, M. S.; Prabagaran, N.; Labenz, N. A.; White, M. C. Serial Ligand Catalysis: A Highly Selective Allylic C−H Oxidation. *J. Am. Chem. Soc.* **2005**, *127*, 6970–6971. (c) Delcamp, J. H.; White, M. C. Sequential Hydrocarbon Functionalization: Allylic C−H Oxidation/Vinylic C−H Arylation. *J. Am. Chem. Soc.* **2006**, *128*, 15076–15077.

(10) Dewyer, A. L.; Zimmerman, P. M. Simulated Mechanism for Palladium-Catalyzed Directed γ-Arylation of Piperidine. *ACS Catal*. **2017**, *7*, 5466–5477.

(11) For examples of CMD pathway mechanistic work, see: (a) Lapointe, D.; Fagnou, K. Overview of the Mechanistic Work on the Concerted Metallation-Deprotonation Pathway. *Chem. Lett.* **2010**, *39*, 1118–1126. (b) Gary, J. B.; Sanford, M. S. Participation of Carbonyl Oxygen in Carbon-Carboxylate Bond-Forming Reductive Elimination from Palladium. *Organometallics* **2011**, *30*, 6143–6149. (c) Ackermann, L. Carboxylate-Assisted Transition-Metal-Catalyzed C–H Bond Functionalizations: Mechanism and Scope. *Chem. Rev.* **2011**, *111*, 1315–1345. (d) Gorelsky, S. L.; Lapointe, D.; Fagnou, K. Analysis of the Palladium-Catalyzed (Aromatic) C–H Bond Metalation-Deprotonation Mechanism Spanning the Entire Spectrum of Arenes. *J. Org. Chem*. **2012**, *77*, 658–668. (e) Gorelsky, S. I. Origins of Regioselectivity of the Palladium-Catalyzed (Aromatic) C–H Bond Metalation-Deprotonation. *Coord. Chem. Rev*. **2013**, *257*, 153–164.

(12) (a) Thorn, D. L.; Hoffmann, R. The Olefin Insertion Reaction. *J. Am. Chem. Soc.* **1978**, *100*, 2079–2090. (b) Huang, Q.; Larock, R. C. Synthesis of Substituted Naphthalenes and Carbazoles by the Palladium-Catalyzed Annulation of Internal Alkynes. *J. Org. Chem.* **2003**, *68*, 7342–7349.

(13) Cabri, W.; Candiani, I. Recent Developments and New Perspectives in the Heck Reaction. *Acc. Chem. Res.* **1995**, *28*, 2–7.

(14) (a) Stambuli, J. P.; Kuwano, R.; Hartwig, J. F. Unparalleled Rates for the Activation of Aryl Chlorides and Bromides: Coupling with Amines and Boronic Acids in Minutes at Room Temperature. *Angew. Chem. Int. Ed.* **2002**, *41*, 4746–4748. (b) Christmann, U.; Pantazis, D. A.; Benet-Buchholz, J.; McGrady, J. E.; Maseras, F.; Vilar, R. Experimental and Theoretical Investigations of New Dinuclear Palladium Complexes as Precatalysts for the Amination of Aryl

Chlorides. *J. Am. Chem. Soc.* **2006**, *128*, 6376–6390. (c) Durà-Vilà, V.; P. Mingos, D. M.; Vilar, R.; White, A. J. P.; Williams, D. J. Reactivity Studies of [Pd$_2$(μ-X)$_2$(PtBu$_3$)$_2$] (X = Br, I) with CNR (R = 2,6-Dimethylphenyl), H$_2$ and Alkynes. *Journal of Organometallic Chemistry* **2000**, *600*, 198–205. (d) Fricke, C.; Sperger, T.; Mendel, M.; Schoenebeck, F. Catalysis with Palladium(I) Dimers. *Angew. Chem.* **2021**, *133*, 3395–3406.

(15) Colman, J. P.; Hegedus, L. S.; Norton, J. R.; Finke, R. G. Principles and Applications of Organotransition Metal Chemistry, 2nd ed.; University Science Books: Mill Valley, CA, **1987**.

(16) Heck, R. F. Palladium-Catalyzed Reactions of Organic Halides with Olefins. *Acc. Chem. Res.* **1979**, *12*, 146–151.

(17) Heck, R. F. Mechanism of Arylation and Carbomethoxylation of Olefins with Organopalladium Compounds. *J. Am. Chem. Soc.* **1969**, *91*, 6707–6714.

(18) (a) Grennberg, H.; Bäckvall, J.-E. Mechanism of Palladium-Catalyzed Allylic Acetoxylation of Cyclohexene. *Chem. Eur. J.* **1998**, *4*, 1083–1087. (b) Liu, G.; Wu, Y. Palladium-Catalyzed Allylic C–H Bond Functionalization of Olefins. In *C-H Activation*; Yu, J.-Q., Shi, Z., Eds.; Topics in Current Chemistry; Springer Berlin Heidelberg: Berlin, Heidelberg, **2009**; Vol. 292, pp 195–209. (c) Fernandes, R. A.; Nallasivam, J. L. Catalytic Allylic Functionalization *via* π-Allyl Palladium Chemistry. *Org. Biomol. Chem.* **2019**, *17*, 8647–8672.

Chapter 5   Ni Aminoquinoline Complexes as Catalysts for Cross-Coupling Reactions

5.1 Introduction

Nickel has showcased an outstanding ability to catalyze challenging bond formations in the field of organic synthesis.[1] This is highlighted by the prominent achievements of Ni-catalyzed cross-couplings, such as the Kumada and Negishi couplings.[2] These cross-couplings typically proceed via two-electron redox pathways involving Ni^0/Ni^{II} catalytic cycles. Many of the Ni^{II} and Ni^0 intermediates have been well-characterized, thus providing a detailed mechanistic picture of their reaction mechanisms.[3]

Scheme 5.1 Reports of Dual Photoredox and Ni-Catalyzed Cross-Couplings
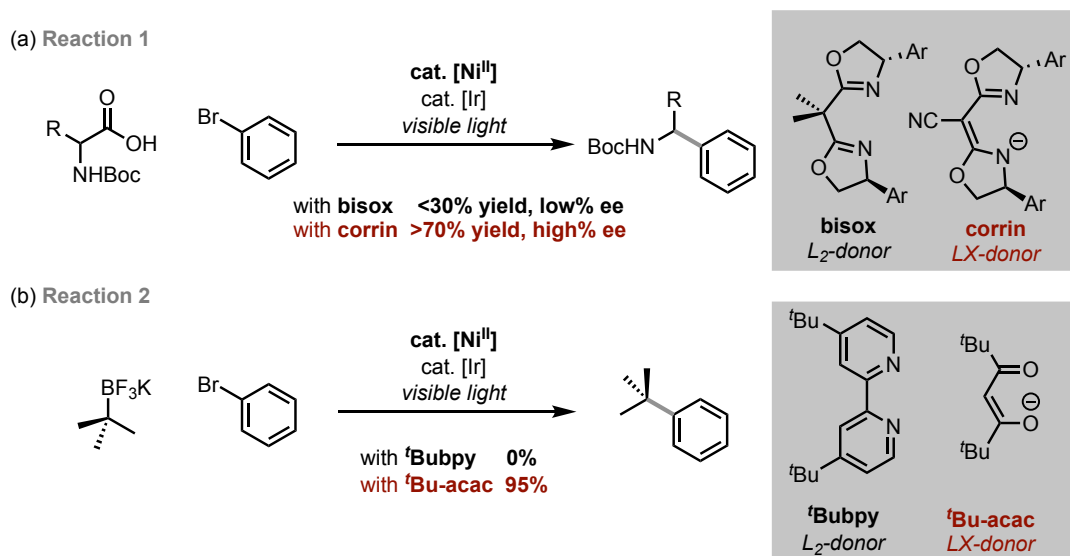
In addition to the two-electron methods mentioned above, organic chemists have also developed methods to leverage different combinations of one- and two-electron redox events that are feasible at Ni.[4] This is exemplified in the merger of photoredox and Ni-catalyzed cross-

coupling methodologies, in which $Ni^0/Ni^{II}/Ni^{III}$ and $Ni^0/Ni^I/Ni^{III}$ mechanistic manifolds have been proposed.[5,6] Due to the instability of the high-valent Ni^{III} and Ni^{IV} species, the isolation and characterization of these intermediates are rare.[7] As such, there is much less experimental insight into the mechanism of catalytic reactions invoking high-valent Ni, which results in poor understanding in the role of additives (*i.e.*, ligands, oxidants). Examples of photoredox/Ni-catalyzed cross-couplings that highlight this gap of knowledge are those developed by the Fu/MacMillan groups[8] (Scheme 5.1a) and the Molander group[9] (Scheme 5.1b). Both reports demonstrate challenging C–C cross-couplings that are enabled by anionic LX-donor ligands. In contrast, the use of related neutral L_2-donor ligands resulted in dramatically lower to trace yields of the desired cross-coupling products. These significant ligand effects demonstrate the need for mechanistic elucidation of high-valent Ni chemistry to understand the role of the ligands and to tune the catalyst system for a target transformation.

Herein, we propose the use of aminoquinoline (AQ) derived scaffolds as LX-donor supporting ligands to assist in the isolation and study of high-valent Ni species to gain mechanistic insight into the role of ligands in these transformations (Scheme 5.2). Isolation of a high-valent Ni–AQ species will give us the opportunity to study their reactivity and could thus lead to new method developments. We hypothesize AQs can provide sufficient stability for isolation of high-valent Ni species, as our lab has shown them to be effective supporting ligands for other Ni^{III} and Ni^{IV} complexes.[7d] Further impetus for examining AQs as ligands in these systems is provided by the numerous transition-metal catalyzed reactions employing these as both a substrate and ligand.[10]

**Scheme 5.2** Proposal of AQs to Study High-Valent Ni Intermediates
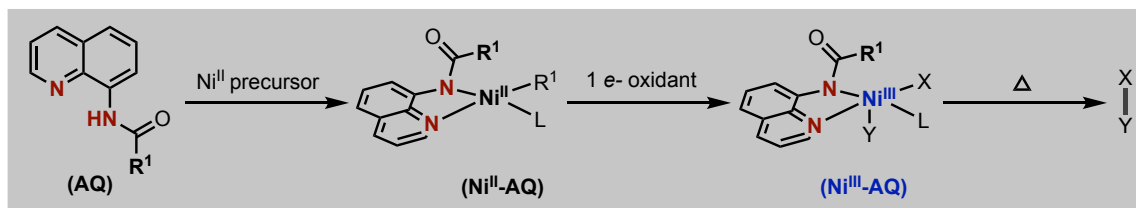
Moreover, the modular nature of the AQ scaffold allows for easy synthetic variations, including modifications preventing the AQ scaffold from acting as a substrate. This chapter will detail preliminary work towards these studies.

5.2 Results and Discussion

Synthesis of Aminoquinoline (AQ) ligand library

Initial electronic and steric modifications of AQ ligand scaffolds were performed by varying the R^1 group (Scheme 5.2). A series of ligands was synthesized in one-step from readily available starting materials (see Section 5.5.2). Table 5.1 shows the AQ ligands **AQ-1** through **AQ-13** synthesized, bearing ranging from alkyl (**AQ-1** through **AQ-7)** or aryl groups at R^1 (**AQ-8** through **AQ-13)**. Of note, ligand **AQ-9** differs in atom connectivity, and would be expected to form a 6-membered chelate with Ni as compared to the 5-membered chelate with the other shown AQ scaffolds.[11]

Table 5.1 Aminoquinoline (AQ) Ligands Synthesized

AQ-1   AQ-2   AQ-3   AQ-4   AQ-5   AQ-6   AQ-7

AQ-8   AQ-9   AQ-10   AQ-11   AQ-12   AQ-13
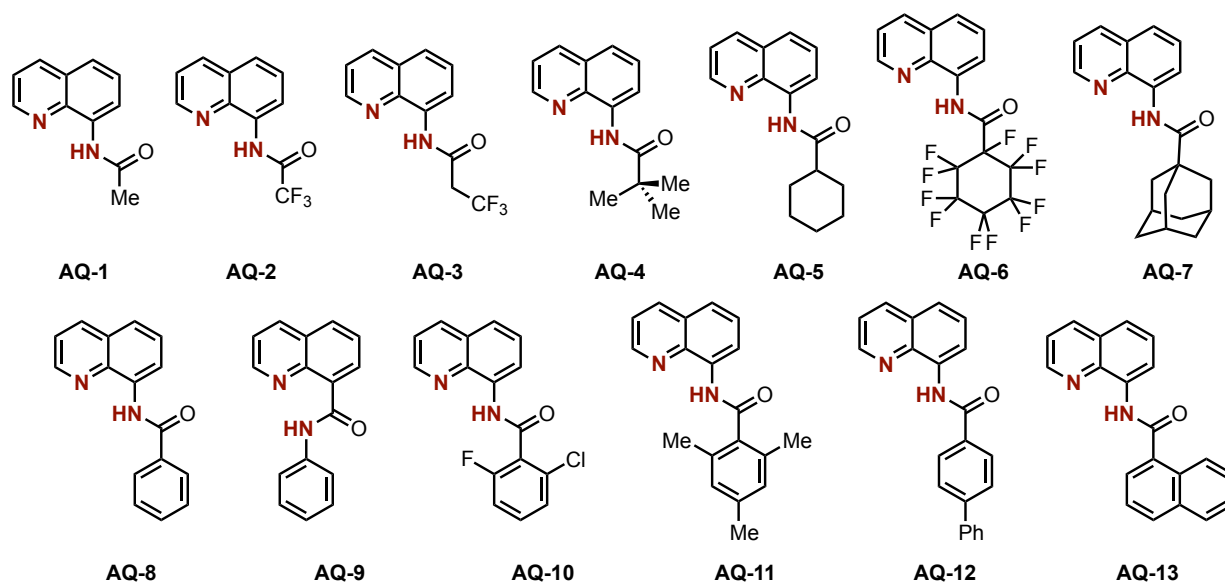
Evaluation of AQ Ligands in Ni-Catalyzed Cross-Couplings

Next, we sought out to test AQs as ligands for photoredox/Ni-catalyzed cross-couplings.

We selected the method established by the Fu and MacMillan groups (Scheme 5.1a, **Reaction 1**)

Table 5.2 Evaluation of Ligands **AQ-1** through **AQ-13** in Reaction 1
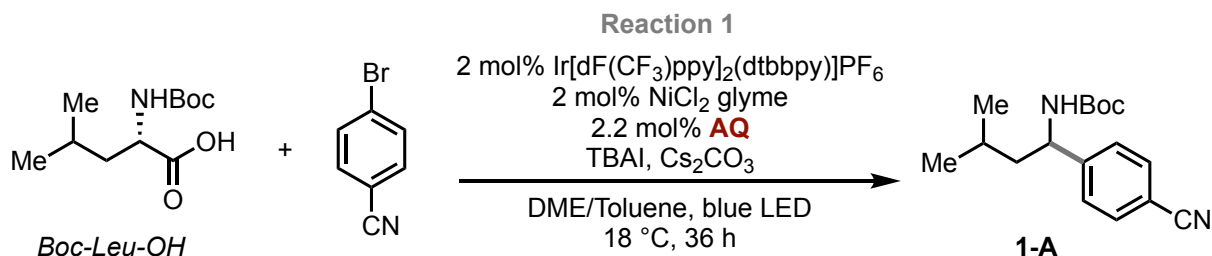
Ligand	1-A yield (%)
none	<1
corrin	24
AQ-1	7
AQ-2	0
AQ-3	9

AQ-4	11
AQ-5	2
AQ-6	3
AQ-7	<1
AQ-8	4
AQ-9	2
AQ-10	<1
AQ-11	14
AQ-12	8
AQ-13	0

to reproduce the reported transformation.[8] First, we performed the reaction with the reported LX-ligand, corrin, and obtained 24% yield of **1-A** (see Section 5.5.3). Notably, the literature reported yield with corrin of **1-A** is 70%. We continue to work on optimization to assess the origin of this significant difference. However, our yields are consistent and reproducible over four runs, which led us to explore the AQ derivatives, while comparing the yield to that with the corrin benchmark.

With the 24% yield as a benchmark, we assessed the synthesized AQ derivatives in Reaction 1 as shown in Table 5.2. Among the alkyl-substituted AQs, **AQ-1**, **AQ-3**, and **AQ-4** afforded similar yields of product **1-A** (7-11%). The aryl-substituted AQs **AQ-8** and **AQ-12** gave 4% and 8% yield of **1-A**, respectively. **AQ-11** provided the best yield of **1-A** at 14%. From these results, there is not a clear trend between R^1 and yield. However the data do show that AQs are viable LX-donor ligands for this Ni-catalyzed cross-coupling reaction. In addition, the data provide some guidance into which AQ ligands to initially explore for the synthesis of Ni^{II}–AQ complexes.

Synthesis of Ni^{II}–AQ Complexes

Based on the AQ ligand evaluation results in Table 5.2, we chose **AQ-1**, **AQ-7**, **AQ-8**, and **AQ-11** as the ligands for the synthesis of Ni^{II}–AQ complexes. The pairs of ligands **AQ-1** and **AQ-7**, and pair **AQ-8**, and **AQ-11** were selected as they have dramatic steric differences that can be compared and studied when bound to Ni. Dr. Abebu Kassie, a postdoctoral scholar in our lab, has focused on the synthesis and characterization of these Ni^{II}–AQ complexes. Currently, Ni^{II}–AQ complexes with **AQ-1** and **AQ-7** ligands have been synthesized and their structures have been established by X-ray crystallography and ^{1}H NMR spectroscopy analyses.

Complex **Ni-1** was synthesized from **AQ-1** in the presence of KOtBu followed by the addition of Ni(acac)$_2$ in THF at 25 °C (Scheme 5.3a). ^{1}H NMR spectroscopic analysis of the Ni product is inconclusive, but we tentatively assign this as the paramagnetic high spin Ni^{II} complex **Ni-1**. This is consistent with data obtained from previous studies using AQs in Ni catalysis.[11] Under analogous conditions using **AQ-7**, complex **Ni-2** was synthesized and isolated (Scheme 5.3b). Complex **Ni-2** was characterized by ^{1}H NMR spectroscopy (also a paramagnetic, high spin Ni^{II}) and X-ray crystallography confirming the bis-chelation of the AQ ligand.

Scheme 5.3 Synthesis of **Ni-1** and **Ni-2**

130
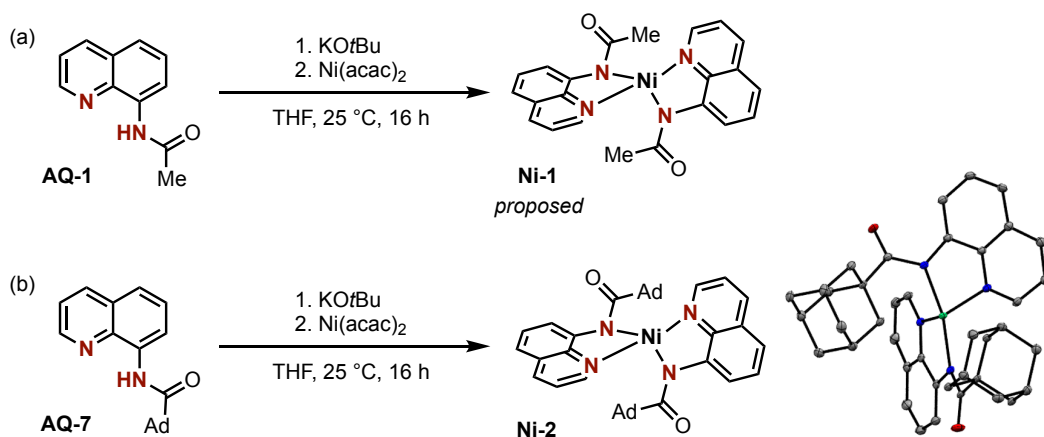
Evaluation of Ni^{II}–AQ Complexes in Dual Photoredox and Ni Catalysis Methods

With complexes **Ni-1** and **Ni-2** in hand, we evaluated their catalytic activity in the same reaction as described above. As shown in Table 5.3, complex **Ni-1** affords 42% of **1-A,** significant-

Table 5.3 Evaluation of Complexes **Ni-1** and **Ni-2**

Ni complex	1-A yield (%)
Ni(acac)$_2$	20
Ni-1	42
Ni-2	17
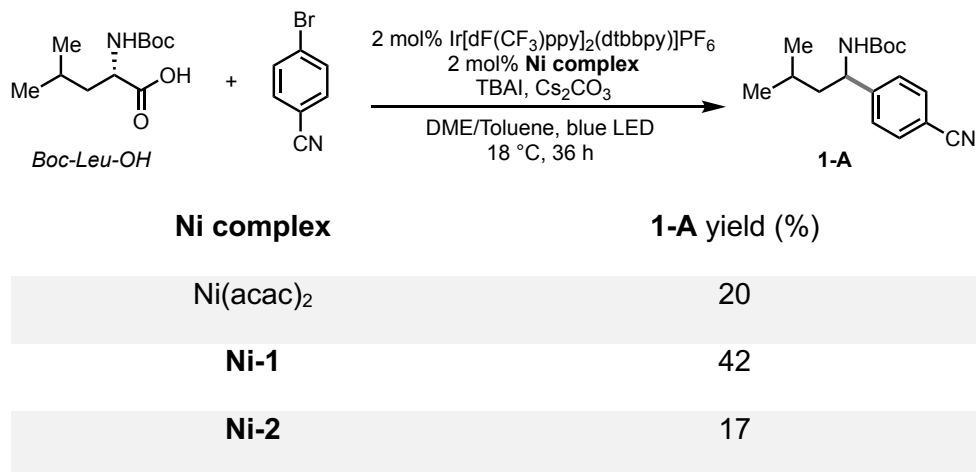
ly higher than that of complex **Ni-2**, which yielded 17% yield of **1-A**. Performing a control with Ni(acac)$_2$ (the Ni^{II} precursor of both complexes) we observed 20% yield of **1-A**, indicating it can catalyze the reaction and thus highlighting the requirement of highly pure Ni complexes. These preliminary results show that both **Ni-1** and **Ni-2** can catalyze this reaction, with **Ni-1** serving as the optimal catalyst. Again, this suggests that AQs serve as viable ligands for a Ni-catalyzed cross-coupling, therefore Ni^{II}–AQ complexes can be used for further mechanistic investigations of the reaction.

5.3 Conclusions

In summary, we describe the design and synthesis of AQ derivatives, and their corresponding Ni^{II}–AQ complexes for evaluation in photoredox and Ni-catalyzed cross-couplings. Our preliminary results suggest that AQs are viable ligands for Ni-catalyzed cross-couplings, in

particular for the Fu/MacMillan report (Reaction 1). As such, AQs and their complexes can be employed to gain mechanistic insight into the strong LX-donor ligand effects in these reactions.

5.4 Outlook

The preliminary results detailed in this chapter provide numerous directions for this work, in that an appropriate reaction, AQ ligands, and Ni^{II}–AQ complexes have been identified. The continuation of this work will focus on the synthesis of more Ni^{II}–AQ complexes with **AQ-1**, **AQ-7**, **AQ-8**, and **AQ-11**. From here, as outlined in Scheme 5.2, the reactivity of these Ni^{II}–AQ complexes towards one-electron oxidation will be studied to achieve an isolable high-valent Ni intermediate.

Meanwhile, all complexes will be tested in the Fu/MacMillan reaction to assess their viability as catalysts for the reaction. Moreover, with these complexes in hand, they will be evaluated in numerous other Ni-catalyzed cross-couplings[2b,9] that are known to demonstrate clear ligand effects (*e.g.,* Scheme 5.1b) as well as in improving the reaction yields and scope for difficult substrates in these cross-couplings. Overall, the stoichiometric studies with the isolated Ni complexes can allow us to generally study the mechanistic workings of Ni-catalyzed cross-coupling to understand the role of additives.

5.5 Experimental Procedures

5.5.1 General Procedures, Materials and Methods

General Procedures

NMR spectra were obtained on a Varian VNMR 700 (699.76 MHz for ^{1}H; 175.95 MHz for ^{13}C) or a Varian VNMR 500 (500.09 MHz for ^{1}H; 470.56 MHz for ^{19}F) or a Varian NMR 400 (128.38 MHz for ^{11}B NMR) spectrometer. ^{1}H and ^{13}C chemical shifts are reported in parts per million

(ppm) relative to TMS, with the residual solvent peak (most commonly CDCl$_3$) used as an internal reference. ^{19}F chemical shifts are reported in ppm and are referenced on a unified scale to the frequency of the residual solvent peak in the ^{1}H NMR spectrum. ^{1}H and ^{19}F multiplicities are reported as follows: singlet (s), doublet (d), doublet of doublets (dd), doublet of doublets of doublets (ddd), doublet of triplets (dt), triplet (t), quartet (q), and multiplet (m). High resolution mass spectra were obtained at the University of Michigan core facility. X-ray crystallographic data were collected on a Bruker SMART APEX-I CCD-based X-ray diffractometer. Flash chromatography was conducted on a Biotage Isolera One chromatography system using preloaded high-performance silica gel columns (10 g, 25 g, 50 g, or 100 g as appropriate). GC-FID was conducted on a Shimadzu CG-17A system. Melting points were obtained on a OptiMelt automated melting point system.

Materials and Methods

All commercial reagents were used as received without further purification unless otherwise noted. The following reagents were purchased from Aldrich: 8-aminoquinoline, NiCl$_2$·glyme (note: hygroscopic), ligand *(S,S)*-**6**, cesium carbonate (anhydrous), and DME (anhydrous). Other reagents were purchased from Aldrich, Alfa Aesar, ChemImpex, Combi-Blocks, Oakwood, and Strem. All other reaction solvents were purified by passage through columns of activated alumina. All glassware used in the glovebox was dried in an oven at 150 °C for at least 6 h and cooled under an inert atmosphere. Photoredox reactions were irradiated by blue LED lamps, and performed in a water bath and with a fan. Reaction vessels were sealed with either a septum (flask) or a Teflon-lined cap with Teflon tape wrapped around the cap. All experiments and synthetic procedures were carried out under an inert atmosphere of nitrogen unless otherwise noted.

5.5.2 Synthesis of Ligands

*All ligands were synthesized under General Procedure A expect **AQ-2** and **AQ-9**.*
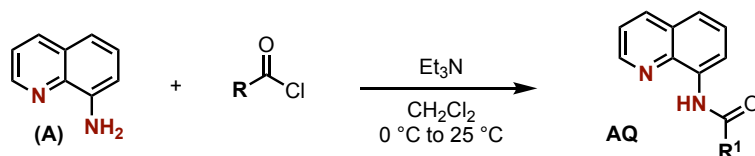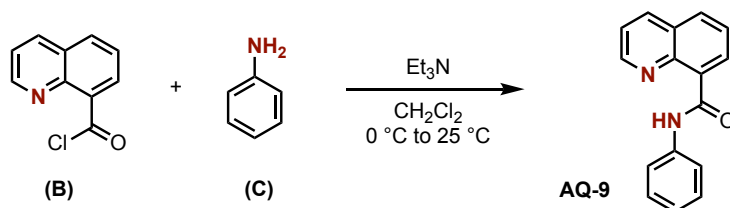

General Procedure A (*Performed under air*): A round bottomed flask was charged with the desired acid chloride (7.0 mmol, 1.0 equiv), CH_2Cl_2 (10 mL), and a magnetic stir bar. This flask was cooled down in an ice bath to 0 °C. In a 20 mL vial, **A** (1.0 g, 7 mmol, 1 equiv) and CH_2Cl_2 (10 mL) were added followed by the addition of Et_3N (2.3 mL, 16.8 mmol, 2.4 equiv). This solution was added to the round bottomed flask dropwise via syringe and was allowed warm to room temperature. After 16 h, the mixture was extracted with CH_2Cl_2 (20 mL) and aq. Na_2HCO_3 (15 mL). The combined organic phases were washed with 1M HCl aq. solution (20 mL), dried over anhydrous sodium sulfate, and concentrated *in vacuo*. The crude residue was dissolved in minimal CH_2Cl_2 and purified via flash chromatography using ethyl acetate/hexanes gradient elution. Removal of solvent afforded the desired **AQ**.
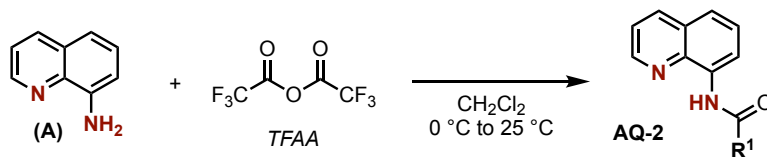
General Procedure B[12] (*Performed under air*): A round bottomed flask was charged with **A** (720 mg, 5 mmol, 1 equiv), CH_2Cl_2 (10 mL), and a magnetic stir bar. This flask was cooled down in an ice bath to 0 °C. to This flask, trifluoroacetic anhydride (TFAA) (755 uL, 5.5 mmol, 1.1 equiv) was added dropwise via syringe. Once added, the reaction was allowed warm to room temperature. After 16 h, the mixture was extracted with CH_2Cl_2 (15 mL) and aq. Na_2HCO_3 (10 mL). The combined organic phases were washed with a saturated NaCl aq. solution (15 mL) and water (15

mL). The combined organic phases were dried over anhydrous sodium sulfate and concentrated *in vacuo*. The crude residue was dissolved in minimal CH_2Cl_2 and purified via flash chromatography using ethyl acetate/hexanes gradient elution (5-10%). Removal of solvent afforded **AQ-2**.


General Procedure C (*Performed under air*): A round bottomed flask was charged with **C** (247 μL, 2.7 mmol, 1.0 equiv), Et_3N (1.0 mL, 5.6 mmol, 2.0 equiv), CH_2Cl_2 (7 mL), and a magnetic stir bar. This flask was cooled down in an ice bath to 0 °C. In a 20 mL vial, **B** (540 mg, 2.8 mmol, 1.1 equiv) and CH_2Cl_2 (10 mL) were added. This solution was added to the round bottomed flask dropwise via syringe and was allowed warm to room temperature. After 16 h, the reaction was concentrated *in vacuo*. The crude residue was dissolved in minimal CH_2Cl_2 and purified via flash chromatography using ethyl acetate/hexanes gradient elution. Removal of solvent afforded the desired **AQ-9**.
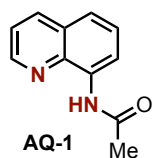
AQ-1: *General Procedure A was followed using Acetyl chloride.*
The ^1H, ^{13}C, and ^{19}F NMR spectral data for **AQ-1** matched that reported in the literature.[13]
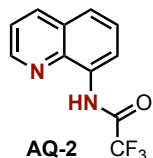
AQ-2: *General Procedure B was followed.*
The ^1H, ^{13}C, and ^{19}F NMR spectral data for **AQ-2** matched that reported in the literature.[12]
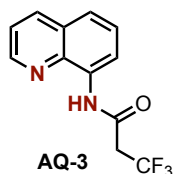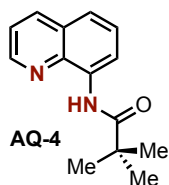
AQ-3: *General Procedure A was followed using 3,3,3-Trifluoropropionyl chloride.*

Isolated yield: 150 mg, 12% (yellow solid)

^{1}H NMR (700 MHz, CDCl$_3$, 23 ºC): δ 10.12 (br s, 1H), 8.82 (d, *J* = 4.3 Hz, 1H), 8.75 (dd, *J* = 6.5, 2.2 Hz, 1H), 8.19 (d, *J* = 8.4 Hz, 1H), 7.60-7.53 (multiple peaks, 2H), 7.49 (dd, *J* = 8.4, 4.3 Hz, 1H), 3.42 (q, *J* = 10.4 Hz, 2H).
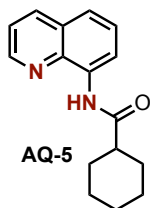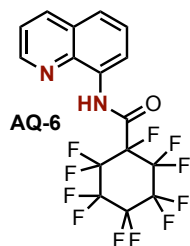
^{19}F NMR (470 MHz, CDCl$_3$, 23 ºC): δ – 62.9 (t, 3F).

Chromatography conditions: 15% EtOAc in hexanes

AQ-4: *General Procedure A was followed using Trimethyl acetyl chloride.*
The ^{1}H, ^{13}C, and ^{19}F NMR spectral data for **AQ-4** matched that reported in the literature.[14]

AQ-5: *General Procedure A was followed using Cyclohexane carbonyl chloride.*
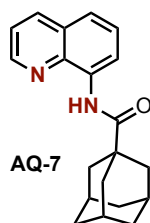The ^{1}H, ^{13}C, and ^{19}F NMR spectral data for **AQ-5** matched that reported in the literature.[15]

AQ-6: *General Procedure A was followed using Perfluorocyclohexane carbonyl chloride.*

Isolated yield: 160 mg, 12% (white solid)

^{1}H NMR (700 MHz, CDCl$_3$, 23 ºC): δ 11.05 (br s, 1H), 8.87 (dd, *J* = 4.2, 1.6 Hz, 1H), 8.75 (dd, *J* = 7.6, 1.3 Hz, 1H), 8.21 (dd, *J* = 8.3, 1.6 Hz, 1H), 7.66 (dd, *J* = 8.3, 1.3 Hz, 1H), 7.59 (t, *J* = 8.0 Hz, 1H), 7.52 (dd, *J* = 8.3, 4.2 Hz, 1H).

^{19}F NMR (470 MHz, CDCl$_3$, 23 ºC): δ –119.1 (dd, 2F), –122.2 (m, 1F), –122.9 (m, 2F), –131.3 (dd, 2F), –138.5 (dd, 2F), –141.0 (d, 1F), –178.8 (m, 1F).
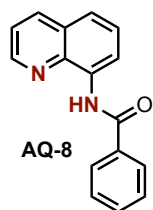
Chromatography conditions: 4% EtOAc in hexanes

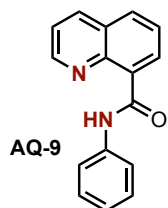**AQ-7:** *General Procedure A was followed using 1-Adamantanecarbonyl chloride.*
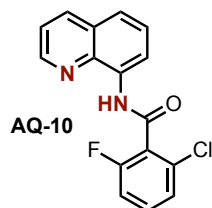The ^{1}H, ^{13}C, and ^{19}F NMR spectral data for **AQ-7** matched that reported in the literature.[16]

AQ-8: *General Procedure A was followed using Benzoyl chloride.*
The ^{1}H, ^{13}C, and ^{19}F NMR spectral data for **AQ-8** matched that reported in the literature.[14]

AQ-9: *General Procedure C was followed.*
The ^{1}H, ^{13}C, and ^{19}F NMR spectral data for **AQ-9** matched that reported in the literature.[17]

AQ-10: *General Procedure A was followed using 2-Chloro-6-Fluorobenzoyl chloride.*
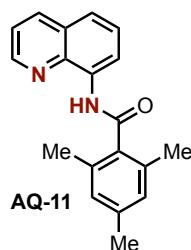Isolated yield: 280 mg, 41% (white solid)
^{1}H NMR (700 MHz, CDCl$_3$, 23 ºC): δ 10.15 (br s, 1H), 8.96 (dd, *J* = 6.6, 2.4 Hz, 1H), 8.78 (dd, *J* = 4.2, 1.7 Hz, 1H), 8.19 (dd, *J* = 8.3, 1.7 Hz, 1H), 7.66-7.56 (multiple peaks, 2H), 7.47 (dd, *J* = 8.3, 4.2 Hz, 1H), 7.39 (td, *J* = 8.2, 5.9 Hz, 1H), 7.31 (dt, *J* = 8.1, 1.1 Hz, 1H), 7.14 (td, *J* = 8.5, 1.1 Hz, 1H).
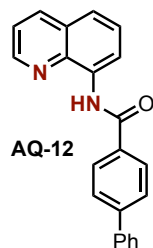^{19}F NMR (470 MHz, CDCl$_3$, 23 ºC): δ −112.3 (dd, 1F).
Chromatography conditions: 8% EtOAc in hexanes

AQ-11: *General Procedure A was followed using 2,4,6-Trimethyl benzoyl chloride.*
The ^{1}H, ^{13}C, and ^{19}F NMR spectral data for **AQ-11** matched that reported in the literature.[15]

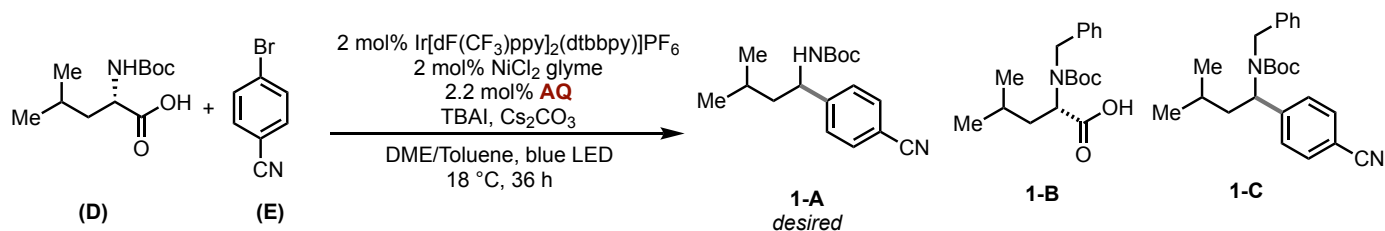**AQ-12:** *General Procedure A was followed using 4-phenylbenzoyl chloride.*
The ^{1}H, ^{13}C, and ^{19}F NMR spectral data for **AQ-12** matched that reported in the literature.[18]
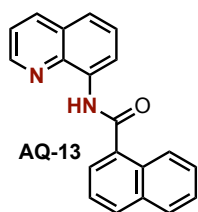
AQ-13: *General Procedure A was followed using 1-Naphthoyl chloride.* The ^{1}H, ^{13}C, and ^{19}F NMR spectral data for **AQ-13** matched that reported in the literature.[19]
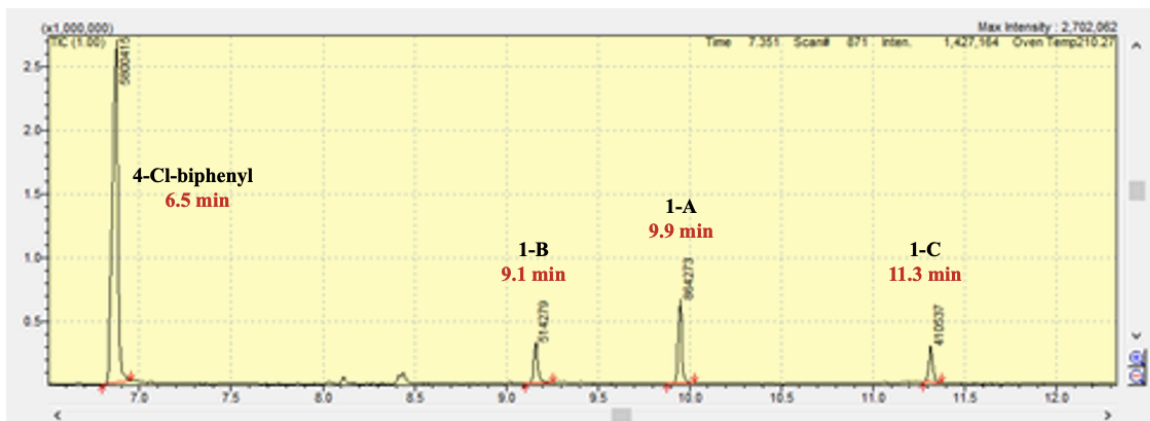
5.5.3 Reaction Procedures: Evaluation of Ligands

General Procedure D (Adapted from literature)[8]: In a glovebox, NiCl$_2$•glyme (1.1 mg, 0.0050 mmol, 2 mol %), **AQ** (0.0055 mmol, 2.2 mol %), and anhydrous 1,2-dimethoxyethane (DME, 1.0 mL) were added to a 4 mL vial equipped with a stir bar. The vial was sealed with a teflon-lined septum cap, and the mixture was stirred vigorously for 30 min. Meanwhile, to a 40 mL vial equipped with a stir bar, the following chemicals were added: Ir[dF(CF$_3$)ppy]$_2$(dtbbpy)(PF$_6$) (5.5 mg, 0.0050 mmol, 2 mol %); tetrabutylammonium iodide (9.2 mg, 0.025 mmol, 0.1 equiv); **D** (88.0 mg, 0.38 mmol, 1.5 equiv); anhydrous cesium carbonate (150 mg, 0.46 mmol, 1.85 equiv), **E** (46 mg, 0.25 mmol, 1.0 equiv), and anhydrous toluene (22.5 mL). Next, the Ni/ligand slurry was transferred via syringe to the 40 mL vial. The 4 mL vial that had contained the Ni/ligand slurry was rinsed with DME (1.5 mL), and the rinse was added to the 40 mL reaction vial via syringe. The vial was sealed with a teflon-lined septum cap, transferred out of the glovebox, and the reaction mixture was stirred vigorously under blue LED lights at 18 °C. The reaction time was 36 h. Next, the reaction mixture was transferred to a 250 mL separatory funnel, rinsed/diluted with 100 mL ether, and washed with 100 mL deionized water (twice) and finally 100 mL brine. The
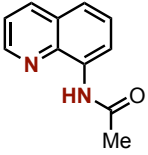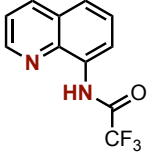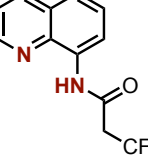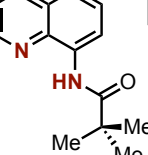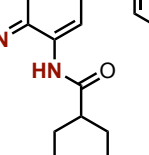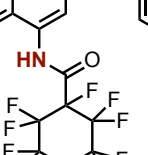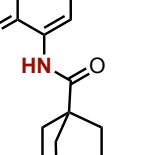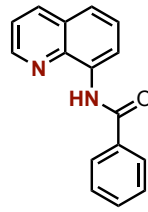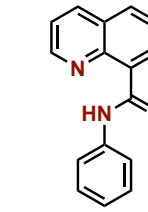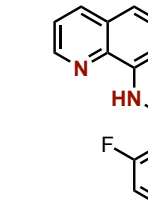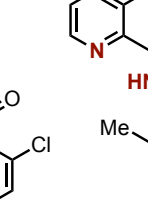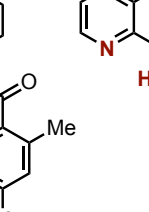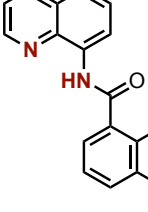
organic phase was concentrated under vacuum. Internal standard, 4-Chlorobiphenyl (47 mg, 0.25 mmol, 1.0 equiv) was used for GC analysis. The desired product **1-A** was observed as well as **1-B** and **1-C** as reported in Table 5.4. Please note product yields **1-A** and **1-C** have be combined for simplicity in Table 5.2.

1-A: The ^{1}H, ^{13}C, and ^{19}F NMR spectral data for **1-A** matched that reported in the literature.[8]

GC-MS Spectrum Analysis: Example of a GC-MS spectrum after reaction work-up

Table 5.4 General Procedure **D** Yields with **AQ** Ligands

	AQ-1	AQ-2	AQ-3	AQ-4	AQ-5	AQ-6	AQ-7
1-A	7%	0%	9%	7%	<1%	3%	<1%
1-B	0%	0%	9%	2%	3%	23%	3%
1-C	0%	0%	0%	4%	<1%	0%	0%

	AQ-8	AQ-9	AQ-10	AQ-11	AQ-12	AQ-13
1-A	4%	2%	<1%	14%	8%	0%
1-B	4%	<1%	<1%	7%	7%	0%
1-C	0%	0%	0%	0%	0%	0%

	no ligand	corrin	Ni-1	Ni-2	Ni(acac)$_2$
1-A	<1%	17%	13%	17%	20%
1-B	4%	8%	3%	15%	6%
1-C	0%	7%	29%	0%	0%

5.5.4 Synthesis of Ni-1 and Ni-2
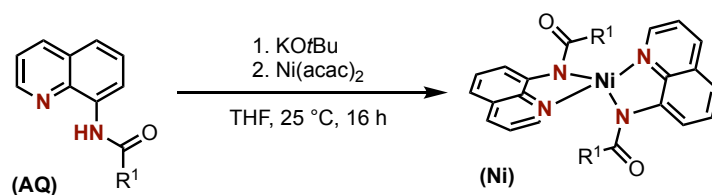
To a solution of the desired **AQ** (0.33 mmol, 1.0 equiv) in THF (3.0 mL) was added a solution of

KO*t*Bu (37.0 mg, 0.33 mmol, 1.0 equiv) in THF (2.0 mL). Upon addition of KO*t*Bu, a bright

yellow precipitate formed, which was added dropwise via syringe to a solution of Ni(acac)$_2$ (84.0

mg, 0.33 mmol, 1.0 equiv) in THF (3.0 mL). This solution was stirred at 25 °C. After 16 h, the

brown solution was filtered through a pad of celite, removed solvent *in vacuo*, and recrystallized from diethyl ether in the freezer to afford the desired **Ni** complex.

5.5.5 X-Ray Crystallography Data

X-Ray Crystallography Experimental Data of Ni-2

Orange plates of **Ni-2** were grown from a benzene-d_6/diethyl ether solution of the compound at 22 deg. C. A crystal of dimensions 0.22 x 0.14 x 0.14 mm was mounted on a Rigaku AFC10K Saturn 944+ CCD-based X-ray diffractometer equipped with a low temperature device and Micromax-007HF Cu-target micro-focus rotating anode (λ = 1.54187 A) operated at 1.2 kW power (40 kV, 30 mA). The X-ray intensities were measured at 85(1) K with the detector placed at a distance 42.00 mm from the crystal. A total of 2028 images were collected with an oscillation width of 1.0° in ω. The exposure times were 1 sec. for the low angle images, 3 sec. for high angle. Rigaku d*trek images were exported to CrysAlisPro for processing and corrected for absorption. The integration of the data yielded a total of 26767 reflections to a maximum 2θ value of 138.75° of which 6499 were independent and 6357 were greater than 2σ(I). The final cell constants (Table 1) were based on the xyz centroids of 20619 reflections above 10σ(I). Analysis of the data showed negligible decay during data collection. The structure was solved and refined with the Bruker SHELXTL (version 2018/3) software package, using the space group P1bar with Z = 2 for the formula $C_{44}H_{52}N_4O_3Ni$. All non-hydrogen atoms were refined anisotropically with the hydrogen atoms placed in idealized positions. Full matrix least-squares refinement based on F^2 converged at R1 = 0.0391 and wR2 = 0.1031 [based on I > 2sigma(I)], R1 = 0.0397 and wR2 = 0.1037 for all data. Additional details are presented in Table 1 and are given as Supporting Information in a CIF file.

G.M. Sheldrick (2015) "Crystal structure refinement with SHELXL", Acta Cryst., C71, 3-8 (Open Access).

CrystalClear Expert 2.0 r16, Rigaku Americas and Rigaku Corporation (2014), Rigaku Americas, 9009, TX, USA 77381-5209, Rigaku Tokyo, 196-8666, Japan.

CrysAlisPro 1.171.40.53 (Rigaku Oxford Diffraction, 2019).

Table 5.5 Crystal Data and Structural Refinement for **Ni-2**

Empirical Formula	$C_{44}H_{52}N_4NiO_3$
Formula Weight	743.60
Temperature	85 (2) K
Wavelength	1.54184 A
Crystal System	triclinic
Space Group	P-1
Unit Cell Dimensions	a = 10.5310(4) Å, α = 69.749(4) °
	b = 13.2916(5) Å, β = 87.584(4) °
	c = 13.7266(6) Å, γ = 87.504(3) °
Volume	1800.15(14) Å^3
Z	2
Calculated Density	1.372 Mg/m^3
Absorption Coefficient	1.150 mm^{-1}
F(000)	782
Crystal Size	0.220 x 0.140 x 0.140 mm
Theta Range for Data Collection	3.433 to 69.377 °

Limiting Indices	$-12 \leq h \leq 12$, $-16 \leq k \leq 15$, $-15 \leq l \leq 16$
Reflections Collected	26767
Independent Reflections	6499
Completeness to Theta	97.7%
Absorption Correction	Semi-empirical from equivalents
Max and Min Transmission	1.00000 to 0.68750
Refinement Method	Full-matrix least-squares on F^2
Data / Restraints / Parameters	6499 / 0 / 472
Goodness-of-Fit on F^2	1.084
Final R Indices [$l > 2\sigma(l)$]	R1 = 0.0391, wR2 = 0.1031
R indices (all data)	R1 = 0.0397, wR2 = 0.1037
Extinction Coefficient	0.0061(3)
Largest Difference Peak and Hole	0.383 and -0.536 $Å^{-3}$

5.6 References

(1) (a) Ananikov, V. P. Nickel: The "spirited horse" of transition metal catalysis. *ACS Catalysis* **2015**, *5*, 1964–1971. (b) Harry, N. A.; Saranya, S.; Ujwaldev, S. M.; Anilkumar, G. Recent Advances and Prospects in Nickel-Catalyzed C–H Activation. *Catal. Sci. Technol.* **2019**, *9*, 1726–1743.

(2) (a) Phapale, V. B.; Cárdenas, D. J. Nickel-Catalysed Negishi Cross-Coupling Reactions: Scope and Mechanisms. *Chem. Soc. Rev.* **2009**, *38*, 1598. (b) Ren, P.; Vechorkin, O.; Allmen, K. von; Scopelliti, R.; Hu, X. A Structure–Activity Study of Ni-Catalyzed Alkyl–Alkyl Kumada Coupling. Improved Catalysts for Coupling of Secondary Alkyl Halides. *J. Am. Chem. Soc.* **2011**, *133*, 7084–7095. (c) Tasker, S. Z.; Standley, E. A.; Jamison, T. F. Recent Advances in Homogeneous Nickel Catalysis. *Nature* **2014**, *509*, 299–309.

(3) (a) Tsou, T. T.; Kochi, J. K. Mechanism of Biaryl Synthesis with Nickel Complexes. *J. Am. Chem. Soc.* **1979**, *101*, 7547–7560. (b) Laskowski, C. A.; Bungum, D. J.; Baldwin, S. M.; Del Ciello, S. A.; Iluc, V. M.; Hillhouse, G. L. Synthesis and Reactivity of Two-Coordinate Ni(I) Alkyl and Aryl Complexes. *J. Am. Chem. Soc.* **2013**, *135*, 18272–18275. (c) Cornella, J.; Gomez-Bengoa, E; Martin, R. Combined Experimental and Theoretical Study on the Reductive Cleavage of Inert C–O Bonds with Silanes: Ruling out a Classical Ni(0)/Ni(II) Catalytic Couple and Evidence for Ni(I) Intermediates. *J. Am. Chem. Soc.* **2013**, 135, 1997–2009. (d) Montgomery, J.

"Organonickel Chemistry" in *Organometallics in Synthesis: Fourth Manual* Lipshutz, B. H. (Ed.) Wiley, Hoboken, N.J., **2013**, pp. 319-428. (e) Rosen, B. M.; Quasdorf, K. W.; Wilson, D. A.; Zhang, N.; Resmerita, A-M.; Garg, N. K.; Percec, V. Nickel-Catalyzed Cross-Couplings Involving Carbon–Oxygen Bonds. *Chem Rev.* **2011**, *111*, 1346.

(4) Zhu, C.; Yue, H.; Chu, L.; Rueping, M. Recent Advances in Photoredox and Nickel Dual-Catalyzed Cascade Reactions: Pushing the Boundaries of Complexity. *Chem. Sci.* **2020**, *11*, 4051–4064.

(5) (a) Jones, G. D.; Martin, J. L.; McFarland, C.; Allen, O. R.; Hall, R. E.; Haley, A. D.; Brandon, R. J.; Konovalova, T.; Desrochers, P. J.; Pulay, P.; Vicic, D. A. Ligand Redox Effects in the Synthesis, Electronic Structure, and Reactivity of an Alkyl−Alkyl Cross-Coupling Catalyst. *J. Am. Chem. Soc.* **2006**, *128*, 13175–13183. (b) Zultanski, S. L.; Fu, G. C. Catalytic Asymmetric γ-Alkylation of Carbonyl Compounds via Stereoconvergent Suzuki Cross-Couplings. *J. Am. Chem. Soc.* **2011**, *133*, 15362–15364. (c) Hu, X. Nickel-Catalyzed Cross Coupling of Non-Activated Alkyl Halides: A Mechanistic Perspective. *Chem. Sci.* **2011**, *2*, 1867. (d) Joshi-Pangu, A.; Wang, C.-Y.; Biscoe, M. R. Nickel-Catalyzed Kumada Cross-Coupling Reactions of Tertiary Alkylmagnesium Halides and Aryl Bromides/Triflates. *J. Am. Chem. Soc.* **2011**, *133*, 8478–8481. (e) Dudnik, A. S.; Fu, G. C. Nickel-Catalyzed Coupling Reactions of Alkyl Electrophiles, Including Unactivated Tertiary Halides, To Generate Carbon–Boron Bonds. *J. Am. Chem. Soc.* **2012**, *134*, 10693–10697. (f) Dai, Y. Wu, F.; Zang, Z. H.; You, H. Z.; Gong, H. G. Ni-Catalyzed Reductive Allylation of Unactivated Alkyl Halides with Allylic Carbonates. *Chem. Eur. J.* **2012** *18*, 808–812. (g) Schley, N. D.; Fu, G. C. Nickel-Catalyzed Negishi Arylations of Propargylic Bromides: A Mechanistic Investigation. *J. Am. Chem. Soc.* **2014**, *136*, 16588–16593. (h) Aihara, Y.; Tobisu, M.; Fukumoto, Y.; Chatani, N. Ni(II)-Catalyzed Oxidative Coupling between $C(sp^2)$–H in Benzamides and $C(sp^3)$–H in Toluene Derivatives. *J. Am. Chem. Soc.* **2014**, *136*, 15509–15512. (i) Wu, X.; Zhao, Y.; Ge, H. Nickel-Catalyzed Site-Selective Alkylation of Unactivated $C(sp^3)$–H Bonds. *J. Am. Chem. Soc.* **2014**, *136*, 1789–1792. (j) Tellis, J. C.; Primer, D. N.; Molander, G. A. Single-Electron Transmetalation in Organoboron Cross-Coupling by Photoredox/Nickel Dual Catalysis. *Science* **2014**, *345*, 433–436. (k) Zuo, Z.; Ahneman, D. T.; Chu, L.; Terrett, J. A.; Doyle, A. G.; MacMillan, D. W. C. Merging Photoredox with Nickel Catalysis: Coupling of -Carboxyl sp^3-Carbons with Aryl Halides. *Science* **2014**, *345*, 437–440. (l) Cornella, J.; Edwards, J. T.; Qin, T.; Kawamura, S.; Wang, J.; Pan, C.-M.; Gianatassio, R.; Schmidt, M.; Eastgate, M. D.; Baran, P. S. Practical Ni-Catalyzed Aryl–Alkyl Cross-Coupling of Secondary Redox-Active Esters. *J. Am. Chem. Soc.* **2016**, *138*, 2174–2177.

(6) (a) Semmelhack, M. F.; Helquist, P. M.; Jones, L. D. Synthesis with Zerovalent Nickel. Coupling of Aryl Halides with Bis(1,5-Cyclooctadiene)Nickel(0). *J. Am. Chem. Soc.* **1971**, *93*, 5908–5910. (b) Terao, J.; Kambe, N. Cross-Coupling Reaction of Alkyl Halides with Grignard Reagents Catalyzed by Ni, Pd, or Cu Complexes with π-Carbon Ligand(s). *Acc. Chem. Res.* **2008**, *41*, 1545–1554. (c) Aihara, Y.; Chatani, N. Nickel-Catalyzed Direct Alkylation of C–H Bonds in Benzamides and Acrylamides with Functionalized Alkyl Halides via Bidentate-Chelation Assistance. *J. Am. Chem. Soc.* **2013**, *135*, 5308–5311. (d) Aihara, Y.; Chatani, N. Nickel-Catalyzed Direct Arylation of $C(sp^3)$–H Bonds in Aliphatic Amides via Bidentate-Chelation Assistance. *J. Am. Chem. Soc.* **2014**, *136*, 898–901. (e) Iyanaga, M.; Aihara, Y.; Chatani, N. Direct Arylation of $C(sp^3)$–H Bonds in Aliphatic Amides with Diaryliodonium Salts in the Presence of a Nickel Catalyst. *J. Org. Chem.* **2014**, *79*, 11933–11939. (f) Castro, L. C. M.; Chatani, N. Nickel Catalysts/ *N*, *N* '-Bidentate Directing Groups: An Excellent Partnership in Directed C–H Activation Reactions. *Chem. Lett.* **2015**, *44*, 410–421. (g) Yan, S.-Y.; Liu, Y.-J.; Liu, B.; Liu, Y.-H.; Zhang,

Z.-Z.; Shi, B.-F. Nickel-Catalyzed Direct Thiolation of Unactivated C(sp^3)–H Bonds with Disulfides. *Chem. Commun.* **2015**, *51*, 7341–7344. (h) Yang, X.; Shan, G.; Wang, L.; Rao, Y. Recent Advances in Transition Metal (Pd, Ni)-Catalyzed C(sp^3)−H Bond Activation with Bidentate Directing Groups. *Tetrahedron Letters* **2016**, *57*, 819–836. (i) Ruan, Z.; Lackner, S.; Ackermann, L. A General Strategy for the Nickel-Catalyzed C−H Alkylation of Anilines. *Angew. Chem. Int. Ed.* **2016**, *55*, 3153–3157.

(7) (a) Camasso, N. M.; Sanford, M. S. Design, Synthesis, and Carbon-Heteroatom Coupling Reactions of Organometallic Nickel(IV) Complexes. *Science* **2015**, *347*, 1218–1220. (b) Bour, J. R.; Camasso, N. M.; Sanford, M. S. Oxidation of Ni(II) to Ni(IV) with Aryl Electrophiles Enables Ni-Mediated Aryl–CF$_3$ Coupling. *J. Am. Chem. Soc.* **2015**, *137*, 8034–8037. (c) Xu, H.; Diccianni, J. B.; Katigbak, J.; Hu, C.; Zhang, Y.; Diao, T. Bimetallic C–C Bond-Forming Reductive Elimination from Nickel. *J. Am. Chem. Soc.* **2016**, *138* (14), 4779–4786. (d) Roy, P.; Bour, J. R.; Kampf, J. W.; Sanford, M. S. Catalytically Relevant Intermediates in the Ni-Catalyzed C(sp^2)–H and C(sp^3)–H Functionalization of Aminoquinoline Substrates. *J. Am. Chem. Soc.* **2019**, *141*, 17382–17387.

(8) Zuo, Z.; Cong, H.; Li, W.; Choi, J.; Fu, G. C.; MacMillan, D. W. C. Enantioselective Decarboxylative Arylation of α-Amino Acids via the Merger of Photoredox and Nickel Catalysis. *J. Am. Chem. Soc.* **2016**, *138*, 1832–1835.

(9) Primer, D. N.; Molander, G. A. Enabling the Cross-Coupling of Tertiary Organoboron Nucleophiles through Radical-Mediated Alkyl Transfer. *J. Am. Chem. Soc.* **2017**, *139*, 9847–9850.

(10) (a) Daugulis, O.; Do, H.-Q.; Shabashov, D. Palladium- and Copper-Catalyzed Arylation of Carbon−Hydrogen Bonds. *Acc. Chem. Res.* **2009**, *42*, 1074–1086. (b) Aihara, Y.; Chatani, N. Nickel-Catalyzed Direct Alkylation of C–H Bonds in Benzamides and Acrylamides with Functionalized Alkyl Halides via Bidentate-Chelation Assistance. *J. Am. Chem. Soc.* **2013**, *135*, 5308–5311. (c) Aihara, Y.; Tobisu, M.; Fukumoto, Y.; Chatani, N. Ni(II)-Catalyzed Oxidative Coupling between C(sp^2)–H in Benzamides and C(sp^3)–H in Toluene Derivatives. *J. Am. Chem. Soc.* **2014**, *136*, 15509–15512. (d) Rej, S.; Ano, Y.; Chatani, N. Bidentate Directing Groups: An Efficient Tool in C–H Bond Functionalization Chemistry for the Expedient Construction of C–C Bonds. *Chem. Rev.* **2020**, *120*, 1788–1887.

(11) (a) He, Z.; Huang, Y. Diverting C–H Annulation Pathways: Nickel-Catalyzed Dehydrogenative Homologation of Aromatic Amides. *ACS Catal.* **2016**, *6*, 7814–7823. (b) Samanta, R. C.; Struwe, J.; Ackermann, L. Nickela-electrocatalyzed Mild C−H Alkylations at Room Temperature. *Angew. Chem. Int. Ed.* **2020**, *59*, 14154–14159.

(12) Liu, X.; Mao, G.; Qiao, J.; Xu, C.; Liu, H.; Ma, J.; Sun, Z.; Chu, W. Nickel-Catalyzed C–H Bond Trifluoromethylation of 8-Aminoquinoline Derivatives by Acyl-Directed Functionalization. *Org. Chem. Front.* **2019**, *6*, 1189–1193.

(13) Kathiravan, S.; Nicholls, I. A. Monoprotected L -Amino Acid (L -MPAA), Accelerated Bromination, Chlorination, and Iodination of C(sp^2)−H Bonds by Iridium(III) Catalysis. *Chem. Eur. J.* **2017**, *23*, 7031–7036.

(14) Hou, J.; Wang, K.; Zhang, C.; Wei, T.; Bai, R.; Xie, Y. Metal-Free Electrochemical Oxidative Dihalogenation of Quinolines on the C5 and C7 Positions Using *N* -Halosuccinimides. *Eur. J. Org. Chem.* **2020**, *2020*, 6382–6386.

(15) Liu, C.-K.; Chen, M.-Y.; Lin, X.-X.; Fang, Z.; Guo, K. Catalyst- and Oxidant-Free Electrochemical *Para* -Selective Hydroxylation of *N* -Arylamides in Batch and Continuous-Flow. *Green Chem.* **2020**, *22*, 6437–6443.

(16) Sun, B.; Li, D.; Zhuang, X.; Zhu, R.; Aisha, A.; Jin, C. Visible-Light-Triggered Decarboxylative Alkylation of 8-Acylaminoquinoline with N-Hydroxyphthalimide Ester. *Synlett* **2020**, *31*, 677–682.

(17) Carmellino, M. Insecticidal Activity of 6-Substituted 8-Quinolinecarboxylic Acids, 8-Quinolinecarboxylic Acid Esters and Amides, and 8-Quinolinecarboxaldehyde Derivatives. *Bollettino Chimico Farmaceutico*, **1990**, *129*, 190–194.

(18) Lv, N.; Chen, Z.; Yu, S.; Liu, Z.; Zhang, Y. Nickel-Catalyzed Dual C(sp^2)–H Activation of Arenes: A New Route to Diaryl Ethers. *Org. Chem. Front.* **2020**, *7*, 2224–2229.

(19) Yang, X.; Yang, Q.-L.; Wang, X.-Y.; Xu, H.-H.; Mei, T.-S.; Huang, Y.; Fang, P. Copper-Catalyzed Electrochemical Selective Bromination of 8-Aminoquinoline Amide Using NH$_4$Br as the Brominating Reagent. *J. Org. Chem.* **2020**, *85*, 3497–3507.